Research Report
Agreement No.T9903, Task 95
Geosynthetic Reinforcement III

INTERNAL STABILITY ANALYSES OF GEOSYNTHETIC REINFORCED RETAINING WALLS

by

Robert D. Holtz
Professor

Wei F. Lee
Research Assistant

Department of Civil and Environmental Engineering
University of Washington, Bx 352700
Seattle, Washington 98195

Washington State Transportation Center (TRAC)
University of Washington, Box 354802
University District Building
1107 NE 45th Street, Suite 535
Seattle, Washington 98105-4631

Washington State Department of Transportation
Technical Monitor
Tony Allen
Materials Laboratory Geotechnical Branch

Prepared for

Washington State Transportation Commission
Department of Transportation
and in cooperation with
U.S. Department of Transportation
Federal Highway Administration

January 2002

TECHNICAL REPORT STANDARD TITLE PAGE

1. REPORT NO.	2. GOVERNMENT ACCESSION NO.	3. RECIPIENT'S CATALOG NO.
WA-RD 532.1		

4. TITLE AND SUBTITLE	5. REPORT DATE
INTERNAL STABILITY ANALYSES OF GEOSYNTHETIC REINFORCED RETAINING WALLS	January 2002
	6. PERFORMING ORGANIZATION CODE
7. AUTHOR(S)	8. PERFORMING ORGANIZATION REPORT NO.
Robert D. Holtz, Wei F. Lee	
9. PERFORMING ORGANIZATION NAME AND ADDRESS	10. WORK UNIT NO.
Washington State Transportation Center (TRAC) University of Washington, Box 354802 University District Building; 1107 NE 45th Street, Suite 535 Seattle, Washington 98105-4631	11. CONTRACT OR GRANT NO. Agreement T9903, Task 95
12. SPONSORING AGENCY NAME AND ADDRESS	13. TYPE OF REPORT AND PERIOD COVERED
Research Office Washington State Department of Transportation Transportation Building, MS 47370 Olympia, Washington 98504-7370 Gary Ray, Project Manager, 360-709-7975	Final research report
	14. SPONSORING AGENCY CODE

15. SUPPLEMENTARY NOTES

This study was conducted in cooperation with the U.S. Department of Transportation, Federal Highway Administration.

16. ABSTRACT

This research project was an effort to improve our understanding of the internal stress-strain distribution in GRS retaining structures. Our numerical modelling techniques utilized a commercially available element program, FLAC (Fast Lagrangian Analysis of Continua). In this research, we investigated and appropriately considered the plane strain soil properties, the effect of low confining pressure on the soil dilation angle, and in-soil and low strain rate geosynthetic reinforcement properties.

Modeling techniques that are able to predict both the internal and external performance of GRS walls simultaneously were developed. Instrumentation measurements such as wall deflection and reinforcement strain distributions of a number of selected case histories were successfully reproduced by our numerical modeling techniques. Moreover, these techniques were verified by successfully performing true "Class A" predictions of three large-scale experimental walls.

An extensive parametric study that included more than 250 numerical models was then performed to investigate the influence of design factors such as soil properties, reinforcement stiffness, and reinforcement spacing on GRS wall performance. Moreover, effects of design options such as toe restraint and structural facing systems were examined.

An alternative method for internal stress-strain analysis based on the stress-strain behavior of GRS as a composite material was also developed. Finally, the modeling results were used to develop a new technique for predicting GRS wall face deformations and to make recommendations for the internal stability design of GRS walls.

17. KEY WORDS	18. DISTRIBUTION STATEMENT
Geosynthetic, reinforcement, retaining wall, FLAC	No restrictions. This document is available to the public through the National Technical Information Service, Springfield, VA 22616

19. SECURITY CLASSIF. (of this report)	20. SECURITY CLASSIF. (of this page)	21. NO. OF PAGES	22. PRICE

DISCLAIMER

The contents of this report reflect the views of the authors, who are responsible for the facts and the accuracy of the data presented herein. The contents do not necessarily reflect the official views or policies of the Washington State Transportation Commission, Department of Transportation, or the Federal Highway Administration. This report does not constitute a standard, specification, or regulation.

TABLE OF CONTENTS

LIST OF FIGURES

LIST OF TABLES

EXECUTIVE SUMMARY

Current internal stability analyses of geosynthetic reinforced soil (GRS) retaining structures, such as the common tie-back wedge method and other methods based on limiting equilibrium, are known to be very conservative. They have been found to over-predict the stress levels in the reinforcement, especially in the lower half of the wall, and because of that over-prediction, designs based on these methods are very uneconomical. Furthermore, current design methods do not provide useful performance information such as wall face deformations.

Previous research on this subject has had only limited success because (1) reliable information on the internal stress or strain distributions in real GRS structures was lacking; (2) numerical modeling techniques for analyzing the performance of GRS walls have been somewhat problematic; and (3) GRS material and interface properties were not well understood.

This research project was an effort to improve our understanding of the internal stress-strain distribution in GRS retaining structures. Our numerical modelling techniques utilized a commercially available element program, FLAC (Fast Lagrangian Analysis of Continua). FLAC solves the matrix equations by means of an efficient and stable finite difference approach. Large deformations are relatively easily handled, and in addition to the traditional constitutive models, FLAC also permits the use of project-specific stress-strain relations. In this research, we investigated and appropriately considered the plane strain soil properties, the effect of low confining pressure on the soil dilation angle, and in-soil and low strain rate geosynthetic reinforcement properties.

Modeling techniques that are able to predict both the internal and external performance of GRS walls simultaneously were also developed. Instrumentation measurements such as wall deflection and reinforcement strain distributions of a number of selected case histories were successfully reproduced by our numerical modeling techniques. Moreover, these techniques were verified by successfully performing true "Class A" predictions of three large-scale experimental walls.

An extensive parametric study that included more than 250 numerical models was then performed to investigate the influence of design factors such as soil properties, reinforcement stiffness, and reinforcement spacing on GRS wall performance. Moreover, effects of design options such as toe restraint and structural facing systems were examined.

An alternative method for internal stress-strain analysis based on the stress-strain behavior of GRS as a composite material was developed. Input properties for the composite numerical models of GRS retaining structures were obtained from an interpretation of tests performed in the unit cell device (UCD—Boyle, 1995), which was developed in earlier research sponsored by the Washington State Department of Transportation (WSDOT).

Finally, the modeling results were used to develop a new technique for predicting GRS wall face deformations and to make recommendations for the internal stability design of GRS walls.

This research has contributed to progress in the following six specific topic areas (chapters referred to below are in Lee, 2000, which is included as an appendix to this report):

1. Better understanding of the material properties of GRS retaining structures: plane strain soil properties and the effect of low confining pressure on the soil dilation angle were carefully investigated in this research (Chapter 7).
2. Improved modeling techniques for working stress analyses of GRS retaining structures: modeling techniques (Chapter 8) were developed to reproduce both the external and internal working stress information from selected case histories (Chapter 9), as well as to perform "Class A" predictions on three well instrumented laboratory test walls (Chapter 10). The results of this numerical modeling appeared to be successful.
3. Improved analytical models for analyzing the behavior of GRS: in this research, analytical models of the composite GRS modulus, lateral reinforced earth pressure distribution (Chapter 11), and the stress-strain relationship of a GRS composite element (Chapter 13) were developed to analyze the behavior of GRS and to validate the results of numerical modeling.
4. The results of an extensive parametric study of GRS walls: an extensive parametric study that included more than 250 numerical models was performed in this research. Influences of design factors such as soil properties, reinforcement stiffness, and reinforcement spacing on wall performance were carefully investigated. The effects of design options such as toe restraint and structural facing systems on the performance of the GRS walls were also examined (Chapter 12).

5. Development of a composite approach for the working stress analysis of GRS retaining structures: the developed analytical model of the GRS composite element was used to examine the effects of the geosynthetic on reinforced soil performance, as well as to develop composite numerical models for analyzing the performance of GRS retaining structures (Chapter 13).
6. Development of performance prediction methods and design recommendations for GRS retaining structures: performance prediction methods were developed on the basis of the results of the modeling and the parametric study. Finally, this research permitted reasonable but conservative recommendations for the internal stability design of GRS retaining structures to be made (Chapter 14).

1. INTRODUCTION

Geosynthetics were introduced as an alternative (to steel) reinforcement material for reinforced soil retaining structures in the early 1970s. Since then, the use of geosynthetic reinforced soil (GRS) retaining structures has rapidly increased for the following reasons:

1. Because of their flexibility, GRS retaining structures are more tolerant of differential movements than conventional retaining structures or even concrete-faced reinforced walls.
2. Geosynthetics are more resistant to corrosion and other chemical reactions than other reinforcement materials such as steel.
3. GRS retaining structures are cost effective because the reinforcement is cheaper than steel, and construction is more rapid in comparison to conventional retaining walls.

Reinforced wall design is very similar to conventional retaining wall design, but with the added consideration of internal stability of the reinforced section. External stability is calculated in the conventional way; the bearing capacity must be adequate, the reinforced section may not slide or overturn, and overall slope stability must be adequate. Surcharges (live and dead loads; distributed and point loads) are considered in the conventional manner. Settlement of the reinforced section also should be checked if the foundation is compressible.

A number of different approaches to internal design of geotextile reinforced retaining walls have been proposed, but the oldest and most common—and most

conservative—method is the tieback wedge analysis. It utilizes classical earth pressure theory combined with tensile resisting "tiebacks" that extend behind the assumed Rankine failure plane. The K_A (or K_o) is assumed, depending on the stiffness of the facing and the amount of yielding likely to occur during construction, and the earth pressure at each vertical section of the wall is calculated. This earth pressure must be resisted by the geosynthetic reinforcement at that section.

Thus, there are two possible limiting or failure conditions for reinforced walls: rupture and pullout of the geosynthetic. The corresponding reinforcement properties are the tensile strength of the geosynthetic and its pullout resistance. In the latter case, the geosynthetic reinforcement must extend some distance behind the assumed failure wedge so that it will not pull out of the backfill.

The tie-back wedge design procedure is based on an ultimate or limit state, and therefore it has the following disadvantages:

1. It tends to seriously over-predict the lateral earth pressure distribution within the reinforced section.
2. It is unable to accurately predict the magnitude and distribution of tensile stresses in the reinforcement.
3. It is unable to predict external (face) deformations under working stresses.

To improve predictions of the performance of GRS retaining structures and to increase our confidence in their use, especially for permanent or critical structures, reliable information on their face deformations and internal stress-strain distributions is necessary. Furthermore, overly conservative designs are also uneconomical, so considerable cost savings can result from improved design procedures.

2. RESEARCH OBJECTIVES

The objectives of this project were as follows:

1. Develop numerical techniques capable of analyzing the performance of GRS retaining structures. The numerical models should be able to provide useful information on the internal stress-strain distribution and external wall performance.
2. Verify the numerical modeling techniques by comparing the results of numerical models of GRS retaining structures with the results of instrumentation and other measurements from field and laboratory GRS wall tests.
3. Perform parametric studies on internal design factors such as layer spacing, the strength properties of geosynthetic reinforcement, and facing stiffnesses, and investigate their influence on the performance of GRS retaining structures.
4. Develop a method for internal stress-strain analysis based on the stress-strain behavior of GRS as a composite material. Composite modulus properties of GRS are obtained from the unit cell device (UCD—Boyle, 1995) and used as input properties for the composite numerical models of GRS retaining structures.
5. Provide recommendations for predicting the performance of and improving the internal design procedures for GRS retaining structures.

3. SCOPE OF WORK, TASKS, AND RESEARCH APPROACH

This section outlines our approach to accomplishing the above research objectives.

3.1 Development of Numerical Techniques for Analyzing GRS Retaining Structure Performance

In this task, numerical models of GRS retaining structures were developed by using the commercially available finite difference computer program FLAC (Fast Lagrangian Analysis of Continua). A numerical model was first created for the Rainier Avenue wall, a 12.6-m-high wrap-faced GRS wall designed and constructed by the Washington State Department of Transportation (WSDOT) in Seattle, Washington. Once the techniques of numerical modeling and FLAC programming were well understood, this FLAC model was able to accurately reproduce field instrumentation measurements, given properly determined input properties and realistic boundary conditions. Detailed modeling techniques developed in this research are summarized in Section 5 below and described in detail in Chapter 8 of Lee (2000)—See appendix.

3.2 Verification of the Developed Modeling Techniques

To verify the developed numerical modeling techniques, FLAC models of other GRS retaining structures were also created using the same modeling techniques developed for the Rainier Avenue wall. These models were developed to back-analyze the performance results of instrumented case histories, as well as to predict the performance of three large-scale instrumented model tests. Our approach was to (1) calibrate the modeling techniques by using instrumented case histories, (2) update the

modeling techniques, and (3) predict the performance of three large-scale GRS model wall tests.

3.2.1 Calibration of the Modeling Techniques by Using Case Histories

Performance data from five instrumented GRS retaining structures were obtained and reproduced with the developed modeling techniques. The walls were from the FHWA Reinforced Soil Project site at Algonquin, Illinois, and they included three concrete panel walls, a modular block faced wall, and a wrap-faced wall. The purpose of this task was to calibrate the developed modeling techniques so that they could be universally applicable.

3.2.2 Update of the Modeling Techniques

Additional modeling techniques were developed in this task for structures with different facings other than a wrapped face, with different boundary conditions, and with different types of surcharging utilized in the Algonquin test walls. Modeling techniques were updated during this task.

3.2.3 Prediction of the Performance of Large-Scale GRS Model Wall Tests

To further verify the developed modeling techniques, numerical models were created of three large-scale GRS model walls built and tested at the Royal Military College of Canada (RMCC). GRS walls tested in the laboratory provide advantages over field tests in that they tend to have more uniform material properties, better instrumentation measurements, incremental surcharge loadings, and simpler boundary conditions. The RMCC tests were designed to systematically change the internal stability design factors such as layer spacing and reinforcement stiffness. Appropriate adjustments were made to the modeling techniques, material and interface properties, wall

construction sequence, and boundary conditions to improve the utility and accuracy of the numerical models.

Although one wall was actually completed before modeling, true "Class A" predictions, predictions made before the completion of wall construction, were performed on two of the test walls to demonstrate the accuracy of the developed modeling techniques.

3.3 Performance of Parametric Study on the Internal Design Factors

Another important task of this research was to examine the influence of the internal design factors on the performance of GRS retaining structures. A parametric study was performed on internal design factors such as layer spacing, ratio of reinforcement length to wall height, soil properties, reinforcement properties, and facing types.

Two types of parametric analyses were performed in this research. In the first type, numerical models developed in previous tasks to model the performance of the Rainier Avenue wall and the Algonquin FHWA concrete panel test walls were used as the fundamental models of the parametric study. Major internal stability design factors were systematically introduced into these two models. The analyses were performed by varying only one design factor in each group at a time, while the other factors were fixed.

The second type of parametric study used a large number of GRS wall models with different internal stability design factors. Design factors such as layer spacing, soil strength properties, and reinforcement properties were systematically introduced into these models to observe the effects of combinations of design factors.

Hypothetical GRS wall performance factors such as internal stress-strain levels and face deformations were recorded and analyzed in both types of parametric analyses. The purpose of the parametric study was to obtain a thorough understanding of the influence of the major internal stability design factors on the performance of GRS retaining structures. With a better understanding of the internal design factors, the internal stability analysis and design of the GRS retaining structures can be improved.

3.4 Development of Composite Method for Working Stress-Strain Analysis

In this research, a composite method was developed to analyze the stress-strain behavior of a GRS element, as well as the performance of GRS retaining structures. The purpose of this part of the research was to evaluate the feasibility of using the composite approach to provide working stress-strain information about GRS retaining structures. Moreover, in a real design project, time and cost might limit the conduct of complicated numerical analyses. Thus, the composite method for a working stress analysis could quickly offer working stress-strain information for preliminary investigations and design, provided that sufficient composite GRS properties were available.

An analytical model that treats the GRS composite as a transversely isotropic homogenous material was developed and used to reduce GRS composite test data obtained from unit cell device test results (Boyle, 1995) to obtain the composite properties of GRS. Composite numerical models were then developed with composite GRS properties as the input properties. Since the composite GRS properties are the only inputs for the composite numerical models, less computation and iteration time were necessary. Moreover, information on the anisotropy of the internal stress distributions of

GRS retaining structures was obtained from the results of the composite numerical models.

3.5 Improvement of GRS Retaining Wall Design

The development of a practical and accurate design procedure for GRS retaining structure systems was the most important objective of this research. Knowledge of the influence of various design factors obtained from the previous tasks was used to develop an improved design procedure and performance prediction method for GRS retaining structures. Included was detailed information on modeling techniques, such as determination of soil and geosynthetic properties, determination of the properties of the interfaces between different materials, and FLAC programming.

4. MATERIAL PROPERTIES IN GRS RETAINING STRUCTURES

Successful working stress analyses rely very much on a good understanding of input material properties. Material properties under working conditions must be carefully investigated before working stress analyses are conducted. GRS retaining structures are constructed of backfill soil, geosynthetic reinforcement, and facing units, if any. Properties of these materials vary under different loading, deformation, or confinement conditions. For example, properties such as the friction angle and the modulus of a soil change when different loading conditions are applied. The stiffnesses of geosynthetics are affected by the strain rate as well as by confinement.

In Chapter 7 of Lee (2000), the properties of the GRS wall construction materials under loading conditions that occur inside these structures are discussed. Adjustments to convert soil and geosynthetic properties obtained from conventional tests into conditions inside the GRS walls are given, and the way to select these properties for numerical models is described in detail. These adjustments can be summarized as follows:

1. Convert triaxial or direct shear soil friction angles to plane strain soil friction angles using Equations 7.1.1 and 7.1.2 in Chapter 7.
2. Calculate the plane strain soil modulus using the modified hyperbolic soil modulus model.
3. Determine the appropriate dilation angles of the backfill material.
4. Investigate the effect of soil confinement on reinforcement tensile modulus.
5. Apply the appropriate modulus reduction on reinforcement tensile modulus to account for the low strain rate that occurs during wall construction.

Inaccurate input of material properties appears to be one of the major reasons that working stress analyses have not been successfully performed on GRS walls. The adjustments of material properties summarized above were utilized in this research to model the performance of GRS walls, and successful modeling results were obtained. Detailed descriptions of how these adjustments are implemented in the modeling techniques for GRS retaining structure performance prediction are presented in the next section and in Chapter 8 of Lee (2000).

5. DEVELOPING NUMERICAL MODELS OF GRS RETAINING STRUCTURES USING THE COMPUTER PROGRAM FLAC

In this research, numerical analyses were performed with the finite difference-based computer program FLAC (Fast Lagrangian Analysis of Continua). FLAC was selected because of its excellent capability to model geotechnical engineering related problems and its flexible programming capability. Although numerical analyses using the finite difference methods usually have much longer iteration times than finite element methods (FEM), with the general availability of high-speed digital personal computers, this is not a major shortcoming. Both discrete and composite models were developed with the FLAC program.

Details of the development of numerical models with the FLAC program are described in Chapter 8 of Lee (2000). After a general description of FLAC, the various stress-strain models provided by FLAC are briefly described. These include the isotropic elastic, transversely isotropic elastic, Mohr-Coulomb elasto-plastic, and a pressure dependent soil modulus models. Next is a description of the interface elements and cable elements used to model the reinforcement. The various techniques used to develop numerical models for analyzing the performance of GRS structures are described in some detail; these include a discussion of the model generation, boundary conditions, equilibrium criteria, and the hyperbolic soil modulus model specifically developed for this research. Next are discussions of how the reinforcement input properties are determined and how the arrangement of the reinforcement, facing systems, arrangement of interfaces, and wall construction are modeled. Finally, the chapter ends with a discussion of modeling results and data reduction.

In conclusion, the modeling techniques used to predict the performance of GRS retaining structures appear to be very complicated, especially when structural facing systems are involved. The modeling techniques described in this chapter were obtained from numerous trials and elaborate model calibrations. They provided the basic concepts and the specific procedures needed to improve the working stress analyses of GRS retaining structures with FLAC. A prerequisite for using these modeling techniques is a good understanding of the in-structure material properties. Recall that the properties of both soil and geosynthetic reinforcement have to be carefully determined, as described earlier and in Chapter 7 of Lee (2000).

6. VERIFICATION OF NUMERICAL MODELING TECHNIQUES – REPRODUCING THE PERFORMANCE OF EXISTING GRS WALLS

Performance data from four instrumented GRS retaining structures and two steel reinforced retaining structures were obtained and used to verify the numerical modeling techniques described above. These case histories were chosen because they were fully instrumented during construction, and the results of the instrumentation were well documented. These case histories included the WSDOT geotextile wall at the west-bound I-90 preload fill in Seattle, Washington, and five of the test walls constructed at the FHWA Reinforced Soil Project site at Algonquin, Illinois.

Development of reasonable numerical models for these case histories, as well as their proper calibration, required the development of numerous trial models and much arduous work. The modeling results are presented and compared to the field measurements from the six case histories in Chapter 9 of Lee (2000).

The results of the verification modeling of the six case histories led to the following conclusions:

1. Numerical models developed with modeling techniques summarized above in Section 5 and in detail in Chapter 8 of Lee (2000) were able to reproduce both the external and internal performance of GRS walls within reasonable ranges.
2. Accurate material properties are required to successfully model the performance of GRS walls. The material property determination procedures summarized above in Section 4 and in detail in Chapter 7 of Lee (2000) should be used.
3. For GRS walls with complicated facing systems such as modular blocks, accurate face deflection predictions require correct input properties of the soil, the

geosynthetic, the interfaces between the blocks, and the reinforcement inserted between the blocks. Interface properties can be determined with connection test data, if available.

4. The modeling results indicated that the soil elements adjacent to the reinforcement layers had smaller deformations than than soil elements located between the reinforcements. This local bulging phenomenon occurred especially in the lower half of the GRS walls or at the face of a wrap-faced wall where no structural facing units confined the bulges.
5. Significant differences were found between the modeling results and inclinometer measurements, especially above the locations of maximum wall deflections predicted by the numerical models. The inclinometer measurements indicated a maximum wall deflection at the top of the wall, while the modeling results indicated a maximum deflection at about two-thirds of the height of the wall. Both predicted and measured results of reinforcement strain distributions verified that the deflection predictions of the numerical models and optical face survey were more reasonable than the inclinometer measurements; i.e. only small deformation occurred at the top of the GRS walls.
6. Even when insufficient material properties information was available and input material properties had to be estimated from information on similar materials, the numerical models developed in this research were able to provide reasonable working strain information about the GRS walls
7. The results of one wrap-faced wall showed that the procedures used to determine the in-soil stiffness from in-isolation test data for nonwoven geosynthetics were

appropriate. On the basis of the unit cell device tests on this material reported by Boyle (1995), the input stiffness of the nonwoven geosynthetic reinforcement was obtained by multiplying the 2 percent strain in-isolation stiffness by 5.0.

8. Reinforcement tensions calculated by the tie-back wedge method appeared to be much higher, especially at the lower half of the wall, than those predicted by the numerical models that were able to reproduce both the external and internal performance of GRS walls. This observation confirms that the tie-back wedge design method over-predicts the reinforcement tensions, especially in the lower part of the wall. Possible reasons for this discrepancy are that the conventional lateral earth pressure distributions are not modified for soil-reinforcement interaction and toe restraint.
9. Modeling results showed that the actual locations of maximum reinforcement tensions in GRS walls occurred at heights of between 0.2H to 0.5H, and not at the bottom of the walls, as assumed by the tie-back wedge method.

7. PREDICTION OF THE PERFORMANCE OF FULL-SCALE GRS TEST WALLS

As part of a program to build and test large-scale GRS walls in the laboratory of the Royal Military College of Canada (RMCC), design factors such as reinforcement stiffness and spacing were systematically changed. We were able to obtain the results of instrumentation measurements of three of these walls from Dr. Richard Bathurst of RMCC. We developed FLAC models of these test walls in an attempt to predict performance before the walls were constructed (so-called "Class A" predictions). The purposes of this exercise were to (1) further examine and improve the developed modeling techniques, (2) investigate the effects of reinforcement stiffness and reinforcement spacing on wall performance under high surcharges, and (3) examine the feasibility of using the developed modeling techniques to perform parametric analyses of design factors such as reinforcement stiffness and spacing.

Chapter 10 of Lee (2000) briefly describes the RMCC test program, as well as the results of the Class A predictions. The differences between real walls and the experimental walls tested in the laboratory are also discussed. The following is a summary of the discussion and conclusions of this part of the research.

1. Numerical models tended to underpredict the wall face deflection at the end of the construction by only about 6 to 10mm. The most likely reason for this underestimation is that additional movement due to construction procedures such as soil compaction was not considered in the FLAC models.

2. Numerical models tended to overestimate the wall face deflection at the top of the wall after a surcharge had been applied. This result could be improved somewhat by decreasing the contact area of the surcharge pressure. Full contact between the airbag and backfill soil was assumed in the numerical models. During the tests of Walls 1 and 2, a decrease of the surcharge contact area (the area between the airbag and the backfill soil) behind the wall face due to inflation of the airbag was observed, however, the actual surcharge contact area was not reported, so the exact decrease in surcharge contact area could not be modeled.
3. Overall, the FLAC models tended to underpredict the reinforcement strains in the lower half of the test walls. A possible reason for this underestimation is that the FLAC models did not model the toe restraint of the test wall very well.
4. By comparing the results of the modeling after the fact, predictions of wall performance could be improved. For example, Test Wall 2 was constructed ith the same geogrid as that used for Walls 1 and 3, but with every second longitudinal member of the grid removed. This process was assumed to reduce the stiffness of the geogrid by 50 percent; however, the actual stiffness reduction of this modified geogrid was not measured, and no potential increase in stiffness of the geogrid due to soil confinement was considered. Performance predictions have been improved somewhat by increasing the reinforcement modulus to 70 percent of the original modulus of this geogrid.
5. Both numerical models and post-construction observations of the test walls indicated that large differential settlements occurred between the facing blocks and the backfill

soil. However, the strain gage measurements did not show any strain peaks near the blocks.

6. The stiff concrete foundation of the test walls affected both the face deflection profile and the reinforcement tension distribution, as shown in the normalized plots of figures 7.1 and 7.2 from Lee (2000, Chapter 10). These figures show the results of RMCC Wall 1 in comparison to the FHWA Algonquin modular block faced wall that was described in Chapter 9 of Lee (2000). Figure 7.1 indicates that the maximum face deflection of the wall with a stiff concrete foundation is located at top of the wall, while that of the wall with a less stiff soil foundation is located near the middle of the wall. Figure 7.2 also indicates that a stiff foundation has a similar effect on the reinforcement tension distributions. The maximum reinforcement tension of the test wall with a stiff concrete foundation occurred at a height of 0.8H, while the maximum reinforcement tension of the test wall with a soil foundation occurred at a height of 0.5H.

Note that the performance predictions presented in this chapter are Class A predictions, i.e., these modeling results were estimated before the construction of these test walls. Refinement is always possible after prediction. For example, face deflection predictions after surcharge could be further improved by decreasing the contact area of the surcharge. Moreover, the performance simulation of test Wall 2 could be improved by increasing the reinforcement modulus from 50 percent to 70 percent of the original modulus of the geogrid used in test Walls 1 and 3.

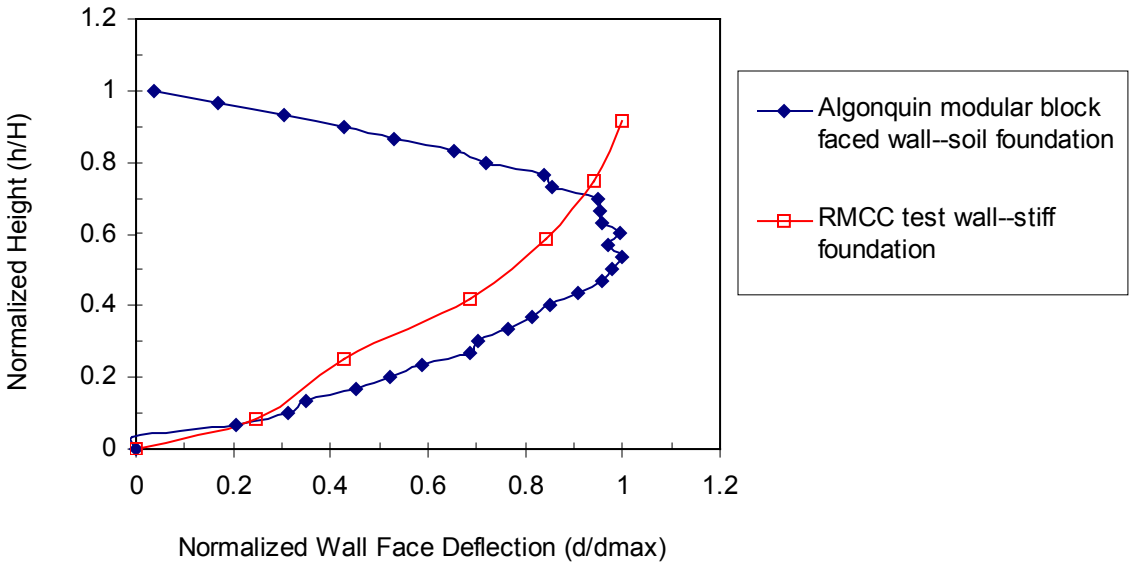

Figure 7.1 Normalized face deflections for GRS test walls with different foundations.

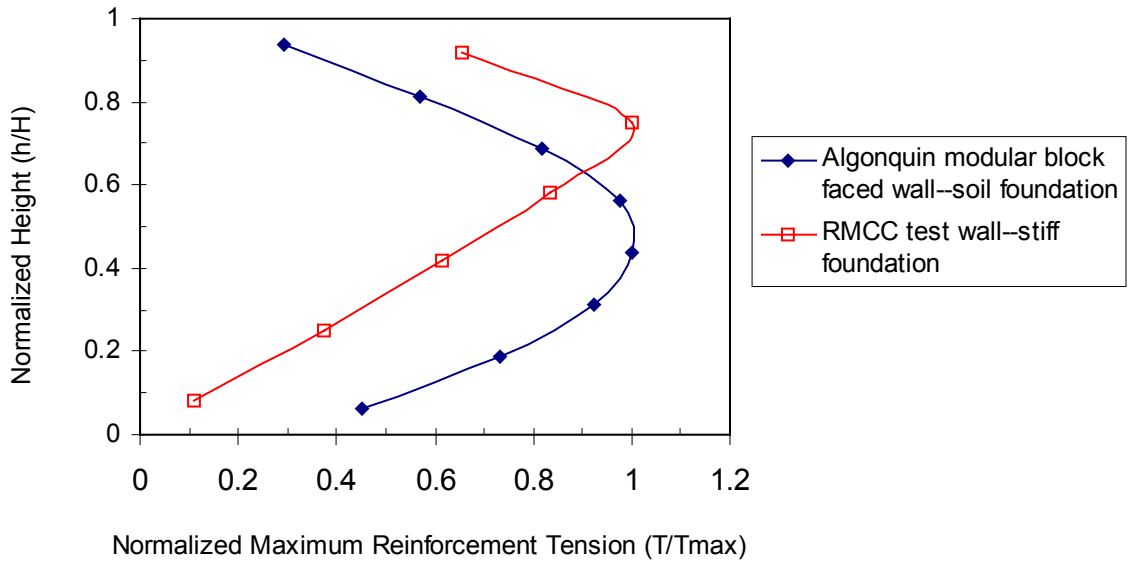

Figure 7.2 Normalized maximum reinforcement tension distributions for GRS test walls with different foundations.

8. ANALYTICAL MODELS OF LATERAL REINFORCED EARTH PRESSURE AND COMPOSITE MODULUS OF GEOSYNTHETIC REINFORCED SOIL

Two important design factors in current GRS wall design procedures are the distribution of lateral earth pressure and the reinforcement stiffness. The lateral earth pressure distribution is assumed, and the in-isolation stiffness of the geosynthetic reinforcement is usually used. Available evidence from full-scale and model GRS walls indicates that present design procedures tend to significantly overestimate the internal lateral stress distribution within the structure, probably because of errors in both these factors. The modeling results described in the section on verification also suggest that the soil-only coefficients of lateral earth pressure and the in-isolation stiffness of geosynthetics are not appropriate for characterizing the working stress or strain distribution inside GRS walls.

To analyze the composite GRS behavior, two new terms, the coefficient of lateral reinforced earth pressure, K_{comp}, and composite modulus of geosynthetic reinforced soil, E_{comp}, were proposed by Lee (2000). The analytical models, derivations, and applications of both K_{comp} and E_{comp} are described in Chapter 11 of Lee (2000).

Lee (2000) found that the GRS composite lateral earth pressure distribution is a function of the height of the wall, unit weight and the lateral earth pressure coefficient of the backfill soil, and the distribution of the reinforcement tension. He found that the horizontal modulus of the GRS composite is a function of the stiffness of the reinforcement, the vertical spacing of the reinforcement, and the soil modulus. Moduli thus calculated are only appropriate for characterizing the horizontal working stress or strain information of GRS walls. The in-soil and low strain rate adjustments discussed in

Chapter 7 of Lee (2000) have to be applied to the in-isolation reinforcement stiffness, and the plane strain soil modulus should be used when GRS retaining structures are analyzed. E_s, the soil modulus, can be obtained from strength test data or estimated by using a confining pressure dependent hyperbolic soil modulus model.

9. PARAMETRIC STUDY OF THE INTERNAL DESIGN FACTORS OF GRS WALLS

After the performance of the case histories and large-scale test walls had been successfully predicted, extensive parametric studies were performed to investigate the influence of internal design factors such as layer spacing, soil strength properties, reinforcement stiffness, and facing types. The results of the parametric analyses were recorded and analyzed in terms of GRS wall performance factors such as internal stress-strain levels and wall face deflections. The purposes of the parametric study were to (1) investigate the sensitivity of the modeling results to the input material properties, (2) examine the influence of the internal design factors on the performance of GRS retaining structures, and (3) improve the internal design of GRS walls on the basis of the working stress information obtained from the parametric study.

Two types of parametric analyses were performed in this research. In the first type, numerical models of the WSDOT Rainier Avenue wall and the FHWA Algonquin concrete panel test walls were used as the fundamental models of the parametric study. Internal design factors such as soil friction angle and reinforcement stiffness were systematically varied in the models. These analyses were performed by varying only one design factor at a time in each group while the other factors were fixed. The second type of parametric study was performed by using a large number of GRS wall models with different internal stability design factors. Design factors such as wall height, layer spacing, soil strength properties, and reinforcement properties were systematically introduced into GRS wall models to observe the effects of the interaction of these design

factors. The results of the parametric study are presented and discussed in detail Chapter 12 of Lee (2000); the summary and conclusions of this work follow.

1. Local failures were observed near the faces of GRS walls with larger vertical reinforcement spacings. For wrap-faced GRS walls that were designed with the same global stiffnesses but different vertical reinforcement spacings, the large spacing walls exhibited much higher face deflections than the small spacing ones.
2. Face deformation of GRS walls was affected by both the strength properties of the backfill and the global reinforcement stiffness. The parametric analysis results indicated that the face deflections of GRS walls increased as the soil strength decreased. Face deflections decreased as the global reinforcement stiffness increased. A good correlation was found between the GRS composite modulus (E_{comp}) and normalized maximum face deflection (d_{max}/H).
3. Reinforcement tensions in GRS walls were affected by both the strength properties of the backfill and the global reinforcement stiffness. The parametric analysis indicated that overall reinforcement tensions in the GRS walls increased as the soil strength properties decreased. Overall reinforcement tensions also increased as the global reinforcement stiffness increased. However, the reinforcement tensions started to increase when the walls were designed with very weak reinforcement because of the large strains exhibited.
4. Toe restraint was able to reduce the maximum face deflections and reinforcement tensions. Among three toe restraints investigated (0.05H embedment, 0.1H embedment, and fixed toe), the 0.1H embedment was found to be the most effective

toe condition for improving the performance of GRS walls, especially for walls designed with poor quality backfill.

5. For walls with large reinforcement spacings, secondary reinforcement was found to be effective at improving the performance of walls only with good quality backfill. Both the face deflections and reinforcement tensions of GRS walls with good quality backfill could be decreased by using secondary reinforcement.
6. Structural facing systems such as modular blocks and concrete panels were able to improve the stability and reduce the deformation of GRS walls, especially walls with large spacings. Using structural facing systems could reduce maximum face deflections, as well as the reinforcement tensions of wrap-faced walls with both large and small spacing.
7. In contrast to the results of the tie-back wedge method, which predicts a maximum reinforcement tension at the bottom of the wall, the parametric analyses indicated that the maximum overall (average) reinforcement tensions occurred between 0.25H when poor quality backfill was used to 0.5H when good quality backfill was used.

10. ANISOTROPIC MODEL FOR GEOSYNTHETIC REINFORCED SOIL COMPOSITE PROPERTIES

Instead of analyzing the geosynthetic reinforcement and soil separately, an effort was made in this research to develop numerical analyses based on composite material concepts. In the composite approach, the GRS element was considered to be a reinforced composite material. A theory of anisotropic material under plane strain loading conditions (described in Chapter 4 of Lee (2000) was used to analyze the different stress-strain behavior in the different principal directions of the GRS composite.

The principal conclusions of this work are as follows:

1. Analyzing GRS composite properties with the developed transversely isotropic elasticity model is feasible.
2. Different composite moduli of GRS elements were found in different principal directions by using the transversely isotropic elasticity model. Thus, the assumption that different reinforcing mechanisms exist in different principal directions inside a GRS wall was verified.
3. Because the input GRS composite properties were sampled at an average working strain found in the Rainier Avenue wall (1 percent), numerical models were able to predict quite well the field instrumentation measurements. To improve this approach so that it can be applied universally, the developed transversely isotropic elasticity model for GRS elements should be applied to additional unit cell device test results. The behavior of GRS composites sampled at different horizontal strains—for example, 0.5 percent, 1.5 percent, and 2 percent—should be analyzed. The stress-

strain distribution of GRS retaining structures can then be further analyzed by using composite property models with input of moduli sampled at these horizontal strains.

11. APPLICATIONS OF MODELING RESULTS: PERFORMANCE PREDICTION AND DESIGN RECOMMENDATIONS FOR GRS WALLS

In this section, methods for predicting GRS wall performance are presented. These methods were developed in an effort to provide preliminary working stress design information for GRS walls. The methods are based on the results of the parametric study presented previously, and the general conditions for using these methods are as follows:

1. The walls have a vertical face. This is conservative.
2. The walls are built on a firm foundation; thus bearing capacity failure of the foundation is not a concern.
3. The backfill extends behind the wall a distance equal to the embedded reinforcement length from the end of the reinforcement. The foundation soil in front of the wall also extends a distance equal to the embedded reinforcement length from the toe of the wall. The depth of the foundation soil is at least equal to the height of the wall.
4. All layers of reinforcement inside each model wall have the same stiffness and vertical spacing.
5. The ratio of reinforcement length to wall height is equal to 0.8.

The performance prediction methods summarized in the following sub-sections include prediction of (1) maximum face deflections, (2) maximum reinforcement tension, and (3) reinforcement tension distributions. The limitations of these prediction procedures are described in detail. Design recommendations for GRS walls are summarized at the end of this section. These recommendations are based on the results of case history modeling and the parametric study presented earlier.

Example problems the illustrate the performance prediction methods are presented in Lee (2000).

11.1 Maximum Face Deflection

A simplified method for predicting the maximum face deflection of GRS walls is presented in Figure 11.1 (from Lee, 2000, Chapter 14). GRS walls were categorized into three groups: (I) large spacing with a wrapped face, (II) large spacing with a structural facing or small spacing with a wrapped face, and (III) small spacing with a structural

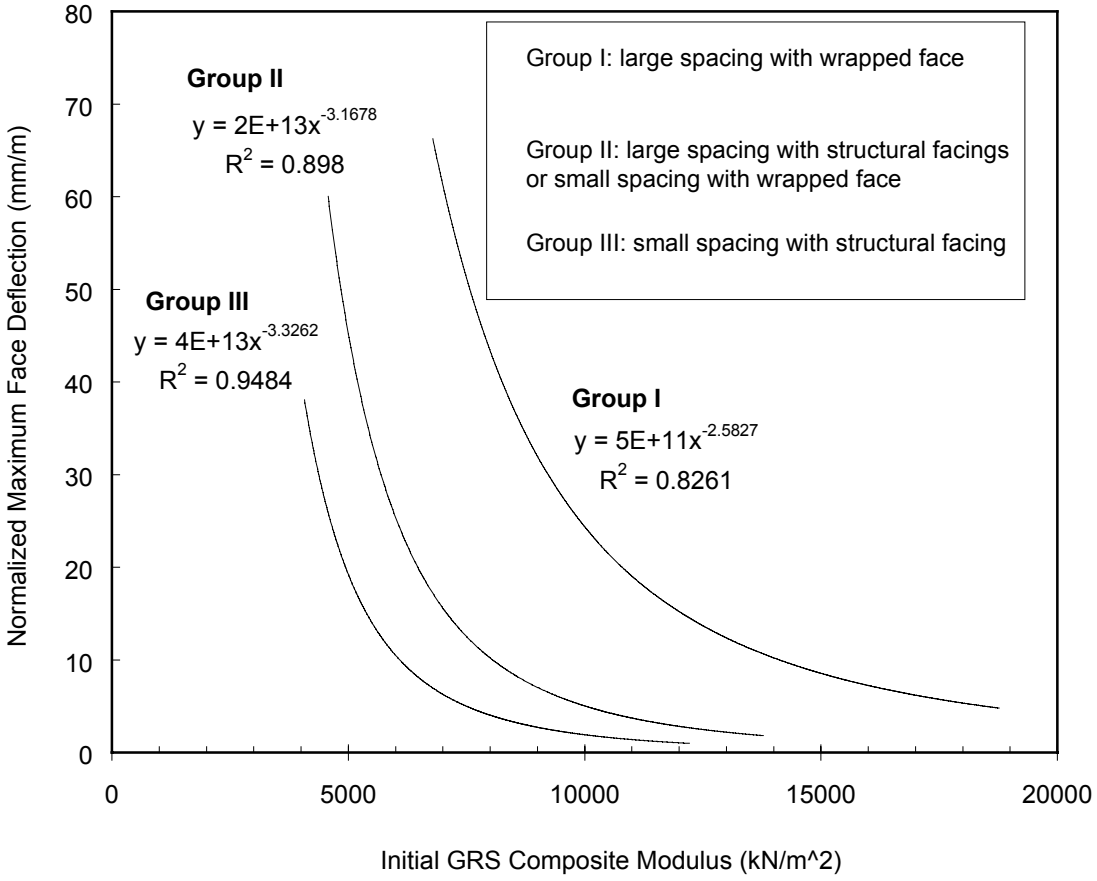

Figure 11.1 Maximum face deflection versus GRS composite modulus.

facing. The three curves in Figure 11.1 are the trend lines developed from the results of the parametric study presented earlier. The GRS walls were designed with typical soils (ϕ = 30 to 55 deg) and global reinforcement stiffnesses of between 500 to 5500 kN/m^2. The curves can be used to predict the face deflection if the material properties are known; or they can be used to estimate required reinforcement stiffness if the soil properties and tolerable deformation are known.

11.2 Reinforcement Tension

Maximum reinforcement tension can be estimated by using the analytical model presented in Section 8 above and in Lee (2000, Chapter 11). (For ease of cross-referencing, equation numbers in this report are the same as those in Lee, 2000). Equation 11.1.6 is the expression for the accumulated reinforcement tension at a given depth from the top of the wall. The reinforcement tension of an individual reinforcement layer (Equation 14.2.2) is obtained by subtracting Equation 14.2.1 (the accumulated reinforcement tension of layer n-1) from Equation 11.1.6.

$$\sum_{1}^{n} t_i(z) = \frac{\gamma \cdot z_n^{\,2}}{2} \cdot (K_{soil} - K_{comp}) \qquad (11.1.6)$$

$$\sum_{1}^{n-1} t_i(z) = \frac{\gamma \cdot z_{n-1}^{\,2}}{2} \cdot (K_{soil} - K_{comp}) \qquad (14.2.1)$$

$$t_n = \sum_{1}^{n} t_i - \sum_{1}^{n-1} t_i = \frac{\gamma}{2} \cdot (K_{soil} - K_{comp}) \cdot (z_n^2 - z_{n-1}^2) \qquad (14.2.2)$$

Equation 14.2.2 can be rearranged as Equation 14.2.3, where z_n - z_{n-1} = S_v, the reinforcement spacing, and $\frac{(z_n + z_{n-1})}{2} \approx z_n$. Reinforcement tension at a given layer can then be expressed in terms of S_v and z_n (Equation 14.2.4).

$$t_n = \frac{\gamma}{2} \cdot (K_{soil} - K_{comp}) \cdot (z_n - z_{n-1}) \cdot (z_n + z_{n-1}) \qquad (14.2.3)$$

$$t_n \approx (K_{soil} - K_{comp}) \cdot \gamma \cdot S_v \cdot z_n \qquad (14.2.4)$$

The maximum reinforcement tension can be expressed by using Equation 14.2.5:

$$T_{max} = (K_{soil} - K_{comp}) \cdot \gamma \cdot z_{t\,max} \cdot S_v$$

$$= \frac{(K_{soil} - K_{comp}) \cdot z_{t\,max}}{H} \cdot \gamma \cdot H \cdot S_v \qquad (14.2.5)$$

where z_{tmax} = depth of T_{max} from top of the wall, and
H = height of wall.

As discussed in Section 8 and Chapter 11 of Lee (2000), the soil properties, as well as the properties and arrangement of the reinforcement, control the values of K_{comp}. The results from the parametric study indicated that the locations of the maximum reinforcement tensions were also affected by the soil properties. To analyze the modeling results with Equation 14.2.5, two indices, a soil index and a geosynthetic index, were defined to represent the term $\frac{(K_{soil} - K_{comp}) \cdot z_{t\,max}}{H}$. Equation 14.2.5 can be rewritten as Equation 14.2.6 by introducing these two indices into it.

$$T_{max} = \Phi_s \cdot \Phi_g \cdot \gamma \cdot H \cdot S_v \qquad (14.2.6)$$

where Φ_s = soil index, and

Φ_g = geosynthetic index.

Numerical and statistical analyses were performed on the average reinforcement tension (T_{ave}) results obtained from all the group models of the parametric study in Chapter 12 of Lee (2000). The relationship between the soil index and soil properties, as well as the relationship between the geosynthetic index and geosynthetic properties was determined for GRS walls with different facing systems. Figure 11.2 (Lee, 2000, Chapter 14) shows the relation between the soil index and soil friction angles, and as shown in the figure, very good correlation was found. Figure 11.3 (Lee, 2000, Chapter 14) shows the relation between the geosynthetic index and the global reinforcement stiffnesses that were corrected for in-soil confinement and low strain rate effects. As shown in the figure, very good correlation was also found in this case for all models; however, the geosynthetic indices were not affected very much by the facing systems (Figure 11.3).

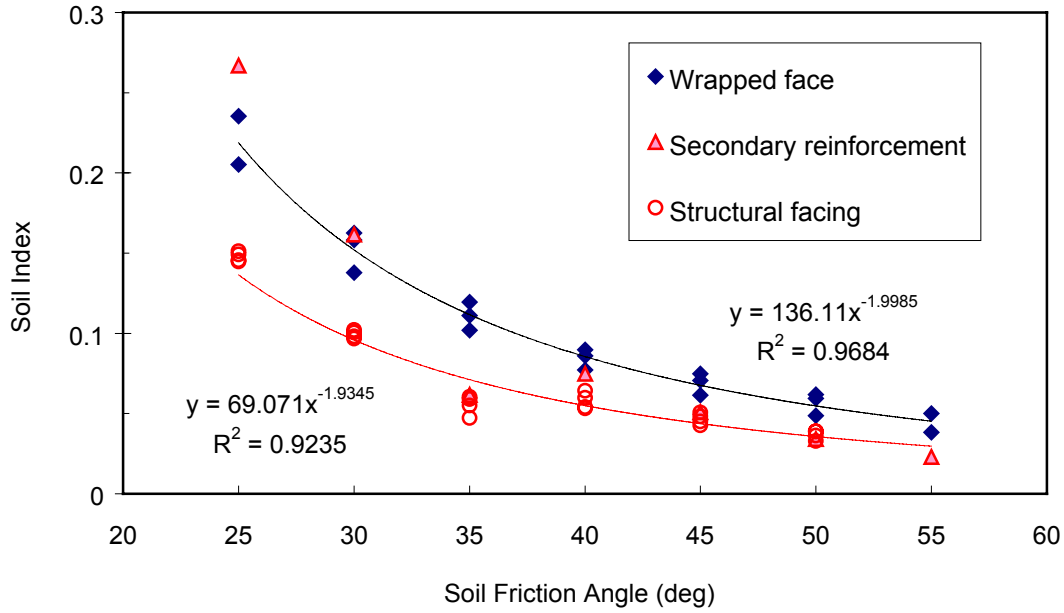

Figure 11.2. Soil index of walls with different facing systems.

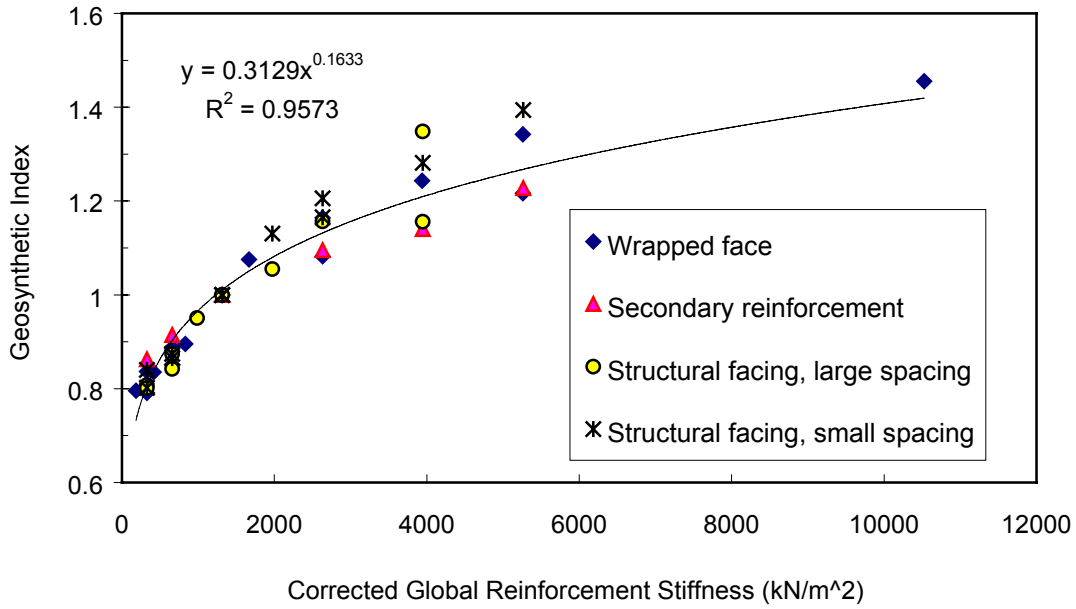

Figure 11.3. Geosynthetic index of walls with different facing systems.

Magnitudes of the maximum average reinforcement tensions (T_{ave_max}) can be estimated by using Equation 14.2.6. The soil and geosynthetic indices in this equation can be determined by using figures 11.2 and 11.3. The design curves shown in figures 11.4 and 11.5 are the trend lines of the modeling results shown in figures 11.2 and 11.3. Table 11.1 shows the average ratios (a_T) of the maximum average reinforcement tension to the maximum peak reinforcement tension (T_{peak_max} / T_{ave_max}) for all the models analyzed in this study. The maximum peak reinforcement tensions (T_{peak}) obtained from the numerical models tended to over-predict the actual peak reinforcement tensions in the GRS walls because the reinforcement elements were attached to the material element nodes. (Details of this over-estimation are described in Section 8.5.6 of Lee, 2000.) In comparison to the field measurements of the case histories analyzed in this research, T_{peak} obtained from the numerical models with reinforcement elements attached to the nodes tended to over-predict the actual peak reinforcement tension by about 20 percent.

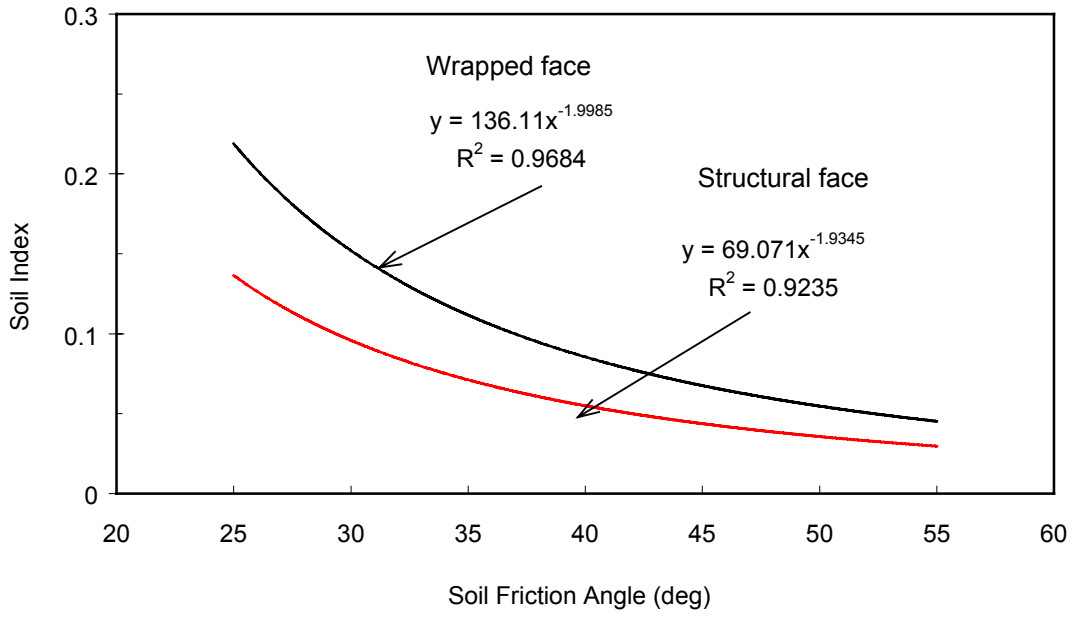

Figure 11.4. Design curves of soil index.

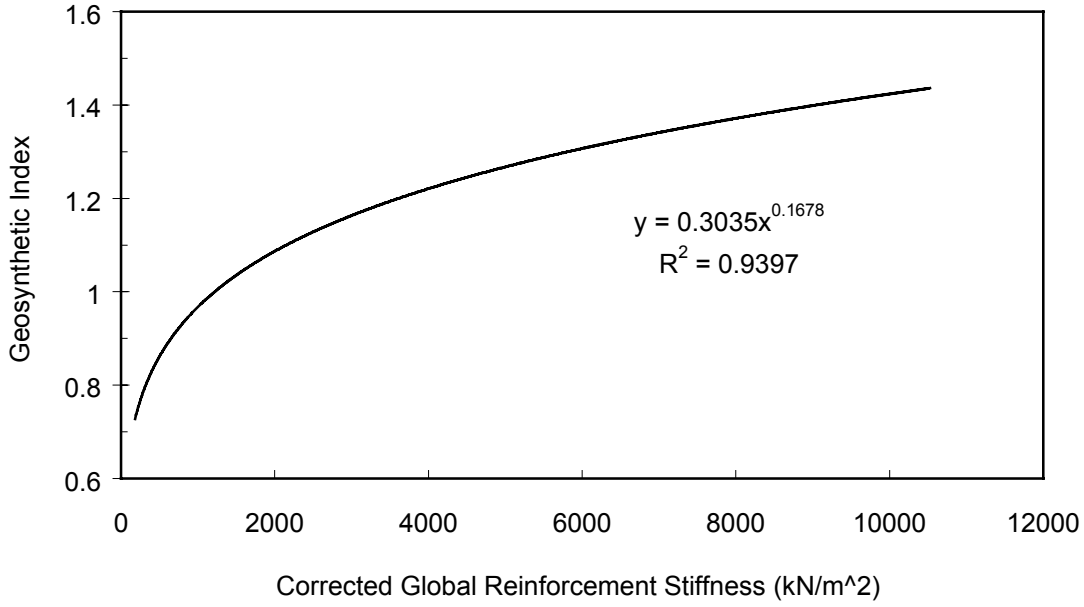

Figure 11.5. Design curve of geosynthetic index.

Maximum peak reinforcement tensions can be estimated by using a_T and Equation 14.2.6 (Equation 14.2.7).

$$T_{peak\_max} = a_T \cdot T_{ave\_max} = a_T \cdot \Phi_s \cdot \Phi_g \cdot \gamma \cdot H \cdot S_v \qquad (14.2.7)$$

where a_T = ratio of (T_{peak_max} / T_{ave_max}) (Table 14.2.1),

Φ_s = soil index, and

Φ_g = geosynthetic index.

Table 11.1 Values of a_T for different GRS walls.

Wall Types	a_T
Wrap faced, large spacing (S_v = 0.76m)	1.8
Wrap faced, small spacing (S_v = 0.38m)	1.5
Wrap faced, with secondary reinforcement, large spacing	1.7
Modular block faced, large spacing	1.7
Modular block faced, small spacing	1.5
Concrete panel faced, large spacing	2.2
Concrete panel faced, small spacing	1.8

11.3 Reinforcement Tension Distributions

The results of the case histories, laboratory test walls, and parametric studies indicated that the actual reinforcement tension distributions inside the GRS walls were very different from the reinforcement tension distributions calculated, for example, with the tie-back wedge method. The results of the parametric analysis indicated that the locations of maximum reinforcement tensions occurred between 0.25H for poor quality backfill to 0.5H for good quality backfill. The tie-back wedge method, of course, predicts maximum reinforcement tension at the bottom of the wall. Moreover, the modeling results presented in Section 6 and Chapter 9 of Lee (2000) also showed that the actual reinforcement tensions inside GRS walls were smaller than the maximum reinforcement tensions predicted by the tie-back wedge method.

Figure 11.6 shows a trapezoid reinforcement tension distribution for GRS walls. This distribution was developed to cover all the reinforcement tension distributions that were observed in the field measurements (Lee, 2000, Chapter 9) and the parametric study (Lee, 2000, Chapter 12). As shown in Figure 11.6, reinforcement tension increases from 0.2

T_{max} at the top of the wall to the maximum reinforcement tension (T_{max}) at a height equal to 0.6H. The reinforcement tension remains constant at T_{max} between 0.6H to 0.2H, and then it decreases from T_{max} to 0.2 T_{max} at the bottom of the wall.

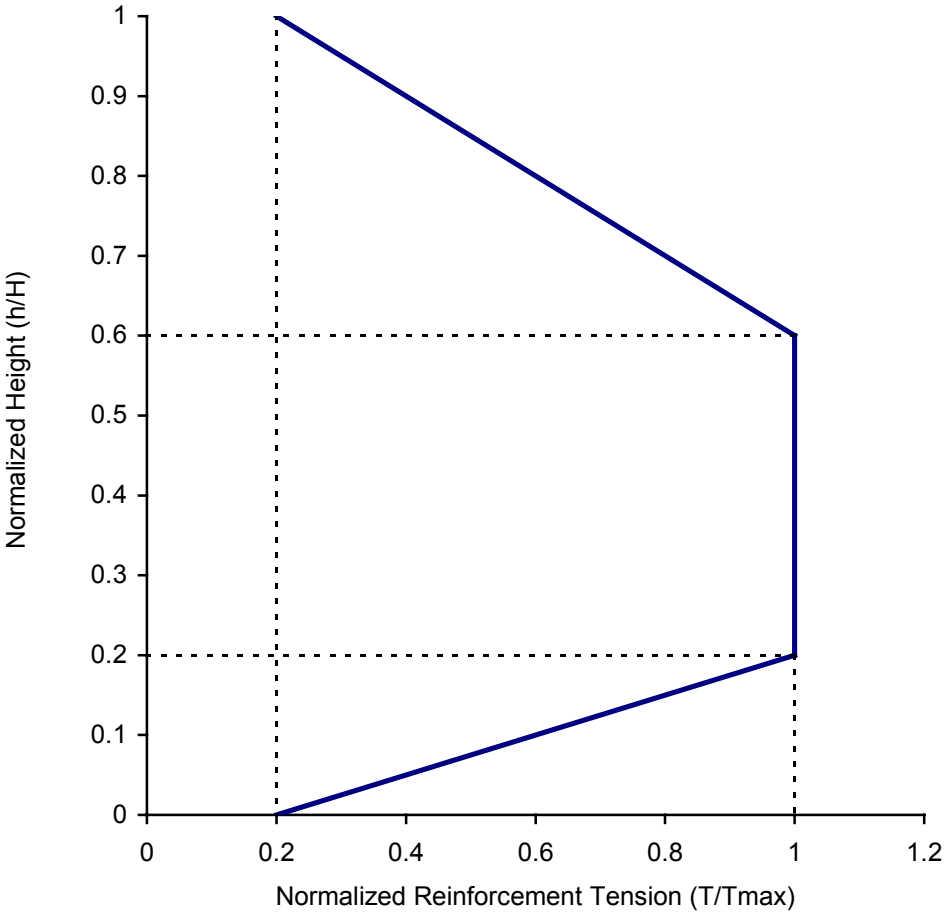

Figure 11.6. Reinforcement tension distribution of GRS walls.

Note that T_{max} can be determined by using equations 14.2.6 and 12.4.7 and the design curves shown in Figures 11.4 and 11.5, with modification to account for the over-prediction caused by attaching reinforcement elements to the material element nodes. An

example problem in Lee (2000) indicated that excellent prediction was obtained by using the method presented in this chapter.

11.4 Limitations of the Performance Prediction Methods

The performance prediction methods presented in this chapter were developed on the basis of the results of the extensive parametric study performed in this research (Section 9 and Chapter 12 of Lee, 2000). The limitations of using these methods to predict the performance of GRS walls include the wall geometry, boundary conditions, soil properties, and reinforcement properties and arrangement that are similar to the limitations for the numerical models of the parametric study. Details of these limitations are described in Lee (2000).

11.5 Design Recommendations for GRS Walls

1. The results of the parametric study indicate that reinforcement lengths equal to 0.8H (H is the height of the wall) seem to be adequate. Even models designed with very poor quality backfill material (ϕ = 25 deg) or very weak reinforcement (J = 55 kN/m) showed no failures in the backfill behind the reinforced zone. Only localized failures were found at the face of wrapped walls with large spacing.
2. Reinforcement spacings larger than 0.6m are not recommended for use in wrap-faced walls. Local failures were observed in the wrap-faced wall models with spacings larger than 0.6m. The face deflection profiles and reinforcement tension distributions of these large spacing wrap-faced wall models also indicated that these local failures can cause internal instability such as outward rotation of the wall face.
3. Material properties such as plane strain soil properties and in-soil low strain rate reinforcement stiffnesses have to be carefully investigated when GRS retaining

structures are designed. The modeling results in chapters 9 and 10 of Lee (2000) indicated that the performance of GRS walls can be accurately reproduced with correct material property information. To investigate the material properties inside GRS retaining structures, the property determination procedures summarized in Section 4 and detailed in Lee (2000, Chapter 7) can be used as a guideline.

4. If possible, good quality backfill (plane strain friction angle, ϕ_{ps}, larger than 35 deg) is recommended for the backfill material. The results of the parametric study indicated that GRS walls designed with poor quality backfill would experience very large wall face deflections as well as large reinforcement tensions.
5. Reinforcement stiffness was found to have less effect on the wall deflection and reinforcement tensions of GRS walls than the soil quality. However, a global stiffness (reinforcement stiffness divided by the spacing) of larger than 500 kN/m^2 is recommended for use in design.
6. Secondary reinforcement layers can only be used as an alternative facing system when the backfill quality is good (ϕ_{ps} > 35 deg). The wall deflections and reinforcement tensions of wrap-faced walls with secondary reinforcement layers and good quality backfill were very similarly to those of the small spacing wrap-faced wall.
7. Structural facing systems are able to improve both the performance and internal stability of the wrap-faced walls. As the parametric study indicated, both wall deflection and reinforcement tensions were reduced when structural facing systems were added in front of wrap-faced walls.

8. Preliminary design information such as maximum face deflection and reinforcement tension distributions can be obtained by using the prediction methods described in this section and Chapter 14 of Lee (2000).
9. With material properties and geometry known, the maximum face deflection of GRS walls can be reasonably predicted by using Figure 11.1. Figure 11.1 can also be used to determine the required reinforcement stiffness if soil properties and design geometry are known.
10. Maximum reinforcement tension inside the GRS walls can be estimated by using equations 14.2.6 and 14.2.7 and the design curves shown in figures 11.4 and 11.5.
11. Figure 11.6 shows a reinforcement tension distribution based on the working stress-strain information from the parametric study.
12. For critical cases, a numerical analysis is still recommended so that complete working stress-strain information can be obtained for internal stability. Determination of material properties and modeling techniques as described in Chapters 7 and 8 of Lee (2000) can be used as the "general rules" for performing the numerical analyses.

12. CONCLUSIONS

The main conclusions of this research are organized in terms of five subcategories: 1. material properties in GRS retaining structures; 2. performance modeling of GRS retaining structures; 3. parametric study; 4. anisotropic model for GRS composite properties; and 5. performance prediction and design recommendations for GRS retaining structures. The chapter references below refer to Lee (2000).

12.1 Material Properties in GRS Retaining Structures

1. The material properties inside the GRS retaining structures were found to be different than those obtained by using conventional properties tests. To design GRS retaining structures correctly, material properties such as plane strain strength properties of soil, low confining pressure soil dilation angles, in-soil properties of geosynthetic reinforcement, and low strain rate reinforcement stiffness need to be carefully determined.
2. The plane strain soil friction angles of rounded uniform sand such as Ottawa sand were found to be only slightly higher than triaxial friction angles. However, for angular material, the tendency of soils to posses a higher friction angle under plane strain conditions than under triaxial conditions is clear. The empirical equation proposed by Lade and Lee (1976, Equation 7.1.1) was able to predict the plane strain soil friction angle within a reasonable range.
3. The tendencies of plane strain soil moduli to be higher than triaxial soil moduli were clearly supported by test data presented in Chapter 7 (Tables 7.1.2 to 7.1.4). For uniform rounded material such as Ottawa sand, the plane strain 1 percent strain secant

moduli were only slightly higher than triaxial 1 percent strain secant moduli at low confining pressures (20 to 100 kPa). For angular material, in both dense and loose states, the plane strain 1 percent strain secant moduli were about twice as high as those obtained from triaxial tests at low confining pressures (20 to 100 kPa).

4. Granular soils at low confining pressures possess higher dilation angles than those tested under high confining pressures. For granular materials prepared in a dense state, the low confining pressure dilation angles were as high as 40 deg. Even for sands prepared in a loose state, the low confining pressure dilation angles were 26 deg. These dilation angles were determined on triaxial tests. Ideally, they should be determined in plane strain tests.
5. The stiffness of nonwoven geosynthetics increased when the geosynthetics were confined in soil. The increase of stiffness is controlled by the structure of the geotextile and the confining pressure. At present, because of the difficulty of testing geosynthetic reinforcement in soil, the magnitude of the increase in stiffness of the nonwoven geosynthetic reinforcement is not well characterized and therefore needs research.
6. For woven geotextiles, soil confinement seems to have less effect on stress-strain behavior. The in-isolation stiffness of the woven geosynthetic can be used as the in-soil reinforcement stiffness.
7. The strength properties of geosynthetic reinforcement were found to be affected by the strain rate. Wide width tensile and unit cell device tests conducted at low strain rates to simulate actual loading rates in full-scale structures have indicated that reductions in reinforcement stiffness are needed. For nonwoven geotextiles, because

of the random fabric filaments and very different index properties between different products, modulus reductions have not yet been clearly characterized. For woven reinforcement and geogrids made of polypropylene, a 50 percent reduction of the in-isolation modulus obtained from the wide width tensile test is recommended as the low strain rate adjustment. For woven reinforcement and geogrids made of polyester, a 20 percent reduction of modulus obtained from the wide width tensile test is recommended. However, further research on this point is recommended.

8. Adjustments that convert soil and geosynthetic properties obtained from conventional tests into those appropriate for GRS walls can be summarized as follows:
    - Convert triaxial or direct shear soil friction angles to plane strain soil friction angles using Equations 7.1.1 and 7.1.2.
    - Calculate the plane strain soil modulus by using the modified hyperbolic soil modulus model.
    - Determine the appropriate dilation angles of the backfill material.
    - Investigate the effect of soil confinement on reinforcement tensile modulus.
    - Apply the appropriate modulus reduction to reinforcement tensile modulus to account for the low strain rate that occurs during wall construction.

12.2 Performance Modeling of GRS Retaining Structures

1. Numerical models that were developed with the material property determination procedures described in Chapter 7 and modeling techniques described in Chapter 8 were able to reproduce both the external and internal performance of GRS walls within reasonable ranges.
2. Accurate and complete knowledge of material properties are the key to successfully

modeling the performance of GRS walls. Because information about the material properties of the Rainier Avenue wall, Algonquin concrete panel faced wall, and RMCC test walls was more complete, better predictions were made of those walls' deflections and reinforcement strain distributions than for the other cases.

3. For GRS walls with complicated facing systems such as modular block facing, accurate deflection predictions rely not only on the correct input properties of the soil and geosynthetic, but also on the correct input properties of the interfaces between the blocks and the reinforcement inserted between the blocks. The input properties of reinforcement inserted between the blocks can be determined by using connection test data, if available. More detailed modeling work is required to further refine the working stress predictions of GRS walls with structural facings.
4. The modeling results indicated that soil elements adjacent to reinforcement layers experienced smaller deformations than the elements in between the reinforcements. This reinforcing phenomenon becomes more obvious especially at the lower half of GRS walls or at the face of a wrap-faced wall,.
5. The inclinometer measurements indicated maximum wall deflection at the top of the wall, while the modeling results indicated maximum deflection at about two-thirds of the wall height. Both the predicted and measured results of reinforcement strain distributions verified that the deflection predictions of the numerical models and optical face survey were more reasonable than the inclinometer measurements, i.e., only small deformation occurred at top of the GRS walls.
6. The results of one wrap-faced wall showed that the procedures used to determine the in-soil stiffness from in-isolation test data for nonwoven geosynthetics were

appropriate. On the basis of the unit cell device tests on this material reported by Boyle (1995), the input stiffness of the nonwoven geosynthetic reinforcement was obtained by multiplying the 2 percent strain in-isolation stiffness by 5.0.

7. Reinforcement tensions calculated by the tie-back wedge method appeared to be much higher, especially at the lower half of the wall, than those predicted by the numerical models that were able to reproduce both the external and internal performance of GRS walls. This observation confirms that the tie-back wedge design method over predicts reinforcement tensions, especially in the lower part of the wall. A possible reason for this discrepancy is that the conventional lateral earth pressure distributions are not modified for soil-reinforcement interaction and toe restraint.
8. The modeling results showed that the actual locations of maximum reinforcement tensions in GRS walls occurred at heights of between 0.2H to 0.5H, and not at the bottom of the walls, as assumed by the tie-back wedge method.
9. The numerical models of the RMCC laboratory test walls tended to underpredict the wall face deflection at the end of the construction by only about 6 to 10mm. The most likely reason for this underestimation is that additional movement due to construction procedures such as soil compaction was not considered in the FLAC models.
10. The numerical models of the RMCC laboratory test walls also tended to overestimate the wall face deflection at the top of the wall after a surcharge had been applied. This result could be improved somewhat by decreasing the contact area of the surcharge pressure.
11. Overall, the FLAC models of the RMCC test walls tended to underpredict the reinforcement strains in the lower half of the test walls. A possible reason of this

underestimation is that the FLAC models did not model the toe restraint of the test wall very well. Other discrepancies between the modeling results and actual performance of the RMCC walls were described in Section 7 and Chapter 10 of Lee (2000).

12.3 Parametric Study

1. Local failures were observed near the faces of the GRS walls with larger vertical reinforcement spacings. For wrap-faced GRS walls that were designed with the same global stiffnesses but different vertical reinforcement spacings, the large spacing walls exhibited much higher face deflections than the small spacing ones.
2. Face deformation of the GRS walls was affected by both the strength properties of the backfill and the global reinforcement stiffness. Parametric analysis results indicated that the face deflections of the GRS walls increased as the soil strength decreased. Face deflections decreased as the global reinforcement stiffness increased. A good correlation was found between the GRS composite modulus (E_{comp}) and normalized maximum face deflection (d_{max}/H).
3. Reinforcement tensions in the GRS walls were affected by both the strength properties of the backfill and the global reinforcement stiffness. Parametric analysis indicated that overall reinforcement tensions in the GRS walls increased as the soil strength properties decreased. Overall reinforcement tensions also increased as the global reinforcement stiffness increased. However, the reinforcement tensions started to increase when the walls were designed with very weak reinforcement because of the large strains exhibited.

4. Toe restraints were able to reduce the maximum face deflections and reinforcement tensions. Among three toe restraints investigated (0.05H embedment, 0.1H embedment, and fixed toe), the 0.1H embedment was found to be the most effective toe condition to improve the performance of GRS walls, especially for walls designed with poor quality backfill.
5. For walls with large reinforcement spacings, secondary reinforcement was found to be effective at improving the performance of only the walls with good quality backfill. Both the face deflections and reinforcement tensions of GRS walls with good quality backfill could be decreased by using secondary reinforcement.
6. Structural facing systems such as modular blocks and concrete panels were able to improve the stability and reduce the deformation of GRS walls, especially walls with large spacings. Use of structural facing systems could reduce maximum face deflections, as well as the reinforcement tensions of wrap-faced walls with both large and small spacing.
7. In contrast to the tie-back wedge method that predicts a maximum reinforcement tension at the bottom of the wall, the results of the parametric analyses indicated that the the maximum overall (average) reinforcement tensions occurred between 0.25H where poor quality backfill was used to 0.5H when good quality backfill was used.

12.4 Anisotropic Model for Geosynthetic Reinforced Soil Composite Properties

1. Analysis of GRS composite properties with the developed transversely isotropic elasticity model was demonstrated to be feasible.
2. Different composite moduli of GRS elements were found in different principal directions by using the transversely isotropic elasticity model. Thus, the assumption

that different reinforcing mechanisms exist in different principal directions inside a GRS wall was verified.

3. Because the input GRS composite properties were sampled at an average working strain found in the Rainier Avenue wall (1 percent), numerical models were able to predict quite well the field instrumentation measurements. To improve this approach so that it can be more universally applicable, the developed transversely isotropic elasticity model for GRS elements should be applied to additional unit cell device test results. The behavior of GRS composites sampled at different horizontal strains—for example, 0.5 percent, 1.5 percent, and 2 percent—should be analyzed. The stress-strain distribution of GRS retaining structures can then be further analyzed by using composite property models with input of moduli sampled at these horizontal strains.

12.5 Performance Prediction and Design Recommendations of GRS Retaining Structures

1. The performance prediction methods developed on the basis of the modeling and analysis results are able to predict preliminary design information such as maximum face deflection and reinforcement tension distributions.
2. With material properties and design geometry known, maximum face deflection of GRS walls can be predicted by using Figure 11.1. The maximum face deflection that was calculated in Figure 11.1 showed an excellent agreement with the field measurements. Figure 11.1 can also be used to determine the required reinforcement stiffness if soil properties and design geometry are known.
3. Procedures were developed to determine the maximum reinforcement tension inside GRS walls.

4. Figure 11.6 describes a reinforcement tension distribution that was developed on the basis of the working stress-strain information from the extensive parametric study performed in this research.
5. Limitations to the performance prediction methods for GRS walls include the general boundary conditions, ranges of the design factors, and geometry limits that are similar to the limits of the numerical models of the parametric study.

13. REFERENCES

Boyle, S.R. (1995) "Deformation Prediction of Geosynthetic Reinforced Soil Retaining Walls," Ph.D. Dissertation, University of Washington, Seattle, 391p

Lade, P.V., and Lee, K.L. (1976) "Engineering Properties of Soils," Report UCLA-ENG-7652, 145pp.

Appendix A

Internal Stability Analyses of Geosynthetic Reinforced Retaining Walls

by

Wei F. Lee

A dissertation submitted in partial fulfillment of the
requirements for the degree of

Doctor of Philosophy
University of Washington

Civil and Environmental Engineering

2000

University of Washington

Abstract

Internal Stability Analyses of Geosynthetic Reinforced Retaining Walls

Wei Feng Lee

Chairperson of the Supervisory Committee:

Professor Robert D. Holtz
Department of Civil and Environmental Engineering

Present internal stability analyses of geosynthetic reinforced soil (GRS) retaining structures are based on the limit state approach. Design methods based on this approach, such as tie-back wedge method, do not provide performance information of GRS walls and also have been found to over-predict the stress levels inside the GRS retaining structures. Working stress analyses of GRS walls are needed to improve the internal stability design as well as the performance prediction of the GRS walls.

In this research, material properties such as plane strain soil properties, low confining pressure soil dilation angle, and in-soil and low strain rate geosynthetic reinforcement properties were carefully investigated. Modeling techniques that are able to predict both internal and external performance of GRS walls at the same time were also developed. Instrumentation measurements such as wall deflection and reinforcement strain distributions of the selected case histories were successfully reproduced by numerical models developed using these modeling techniques. Moreover, the developed modeling techniques were further verified by performing Class A predictions of three laboratory test walls. Results of the Class A predictions appear to be successful as well.

An extensive parametric study that included more than 250 numerical models was then performed in this research. Influences of design factors of GRS walls such as soil properties, reinforcement stiffness, and reinforcement spacing on the performance were carefully investigated. Moreover, effects of design options such as toe restraint and structural facing systems on the performance of the GRS walls were also examined in this parametric study. In addition, analytical models of the composite GRS modulus and lateral reinforced earth pressure distribution that analyze the

behavior of the geosynthetic reinforced soil were also developed in order to analyze the results of the parametric study.

In this research, effort was also made to develop the analytical model for the stress-strain relationship of a GRS composite element. The developed analytical model was used to examine the reinforcing effects of the geosynthetic reinforcement to the soil, as well as to develop composite numerical models for analyzing performance of GRS retaining structures.

Finally new performance prediction methods based on the result of the parametric study and design recommendations for the internal stability design of GRS walls were obtained.

TABLE OF CONTENTS

List of Figures

List of Table

Acknowledgments

Research work presented in this dissertation was funded by the Washington State Department of Transportation (WSDOT). This financial support is greatly appreciated.

I wish to express my greatest appreciation to Professor Robert D. Holtz not only for his guidance and full support during this research, but also for his invaluable advice and training that fulfilled my doctoral study.

This dissertation could not have been completed without the greatest supports and love from my wife, Yuan Ju, and our precious daughter, Madeleine. Encouragement and support from my parents (Mr. Lee, Mao Hsiung and Mrs. Lee Wu, Li Ching) throughout my graduate study are also another important factor of completion of this work.

Additional thanks to Professor Richard Bathurst at the Royal Military College of Canada, Professor Steven L. Kramer, and Professor Pedro Arduino at the University of Washington, for their many helpful discussions and for invaluable comments on the manuscript. Thanks also to Professors K. Y. Lin and G. R. Miller for serving on my Ph. D. committee. Special thanks to Mr. Tony Allen at WSDOT. Progress of this research would not be so distinguished without his enthusiasm for geosynthetics engineering.

Chapter 1
Introduction

1.1 The Need to Improve the Internal Stability Design of GRS Retaining Structures

Geosynthetics were first introduced as a reinforcement material for reinforced soil retaining structures in the 1970's. In last ten years, the use of geosynthetic reinforced soil (GRS) retaining structures has increased because:

1. GRS retaining structures are more tolerant of differential movements than conventional retaining structures because of the excellent flexibility and uniformity of geosynthetic materials.

2. Geosynthetics are more resistant to corrosion and other chemical reactions than other reinforcement materials like steel.

3. GRS retaining structures are cost effective because construction is quicker and less weather-dependent, and the volume of earthwork can often be reduced in comparison with conventional retaining structures.

In early applications, geosynthetic reinforcement was mainly used for temporary structures or projects that had a larger deformation tolerance. Recently, more and more evidence, including laboratory modeling tests, field instrumentation measurements, and

post event observations, have indicated that geosynthetic reinforced soil (GRS) structures are safe for use as permanent or critical structures.

The external (global) stability design of GRS retaining structures is the same as for conventional retaining structures. The most common internal stability design for GRS retaining structures is the tie-back wedge technique. This design procedure is based on limit state stress (ultimate or failure stress) analysis and has following disadvantages:

1. It tends to overestimate the reinforcement stresses within the GRS structure.

2. It is unable to predict external (face) deformations at working stresses.

3. It is unable to predict the internal stress distributions within GRS retaining structures, e.g., reinforcement tension and lateral earth pressure distributions, especially when different facing elements are used.

To improve the prediction of the performance of GRS retaining structures and to increase confidence in their use for permanent or critical structures, reliable information on their face deformations and internal stress-strain distributions is necessary.

1.2 Research Overview

This research project was an effort to improve our understanding of the internal stress-strain distribution in GRS retaining structures. The face deformations and internal stress-strain distributions were analyzed using numerical techniques. First numerical models were used to simulate the field instrumentation measurements in real walls. The same modeling techniques were then applied to develop numerical models for full scale test walls in order to predict their performance. Parametric studies were also carried out to investigate the influence of different internal stability design factors. Finally, improved techniques for analyzing the face deformations and internal stress-strain distributions as well as an improved internal stability design procedure were developed.

1.3 Thesis Organization

This thesis has four major sections:

1. Summaries of the fundamental theories and literature review (Chapters 2 to 4),
2. Research objectives (Chapter 5) and scope of work (Chapter 6),
3. Research results (Chapter 7 to 13), and
4. Working stress design recommendations (Chapter 14).

Chapter 15 contains a summary, conclusions, and suggestions for future research. References cited in this thesis are also listed at the end of this dissertation.

Chapter 2
Geosynthetic Reinforced Soil Retaining Structures

2.1 Retaining Structures

Mankind has been constructing soil retaining structures ever since they became sedentary; defensive walls and religious monuments were the earliest applications of soil retaining structures (Kerisel, 1992). As the needs of increasing size, especially the height, of soil retaining structures occurred, people soon learned that the earth pressure generated by the mass of the backfill soil was the most important stability concern. The first solution was to resist the pressure externally using materials such as rocks or huge stone blocks with a mass and volume larger than the backfill soil mass. Later on, people also learned that the earth pressure can be reduced by reinforcing the backfill soil. The earliest reference to reinforcing soil is found in Exodus 5, v. 6-9 of the Bible; reeds or straw were included in clay or bricks used for dwelling construction.

Evidence of applications of reinforced soil in retaining structures can be found in many historical structures. For example, ancient mideast people used woven reed mats as reinforcement when they constructed ziggurats more than 3000 years ago. The mats were laid horizontally inside the fill soil to provide planar tensile reinforcement, a similar concept to that which we use today (Jones, 1997).

2.2 Reinforced Soil Retaining Structures: Externally Stabilized vs. Internally Stabilized Systems

Soil retaining structures can be classified into two major categories: externally stabilized systems and internally stabilized systems (see Table 2.2.1). Externally stabilized soil retaining systems include conventional earth retaining systems in which backfill soils are retained by external structural walls composed of material with high stiffness and/or large unit weight in front of the backfill. Structural walls provide an external stabilizing force to the backfill soil when the outward earth pressure of the backfill soil is mobilized and acts against the structural walls. Figure 2.2.1a shows some examples of externally stabilized soil retaining systems.

Internally stabilized soil retaining systems are also known as reinforced soil systems. They stabilize the soil mass by introducing additional tensile reinforcing elements such as geosynthetics, steel straps, or soil nails into the backfill soil. Usually, layered (mostly horizontal) reinforcements are placed into and extending beyond the potential failure surface. Figures 2.2.1b and 2.2.1c show some examples of internally stabilized and hybrid soil retaining systems.

Table 2.1.1 Classification of earth retaining systems (after Jones, 1997).

Externally stabilized system

In-situ walls	Gravity walls
-timber	-masonry
-precast concrete	-concrete
-sheet piles	-cantilever
-soldier piles	-gabion
-cast in situ	-crib
-tie-back	-cellular cofferdam

Internally stabilized system

Reinforced soils	In-situ reinforcement
-anchored earth	-soil nailing
-organic reinforcing strips and grids	-reticulated micro piles
-metallic reinforcing strips and grids	-soil dowelling
-geosynthetics reinforcing strips and grids	

Hybrid system

-Geosynthetic reinforced masonry wall

-Geosynthetic reinforced gabion wall

-Geosynthetic reinforced precast concrete wall

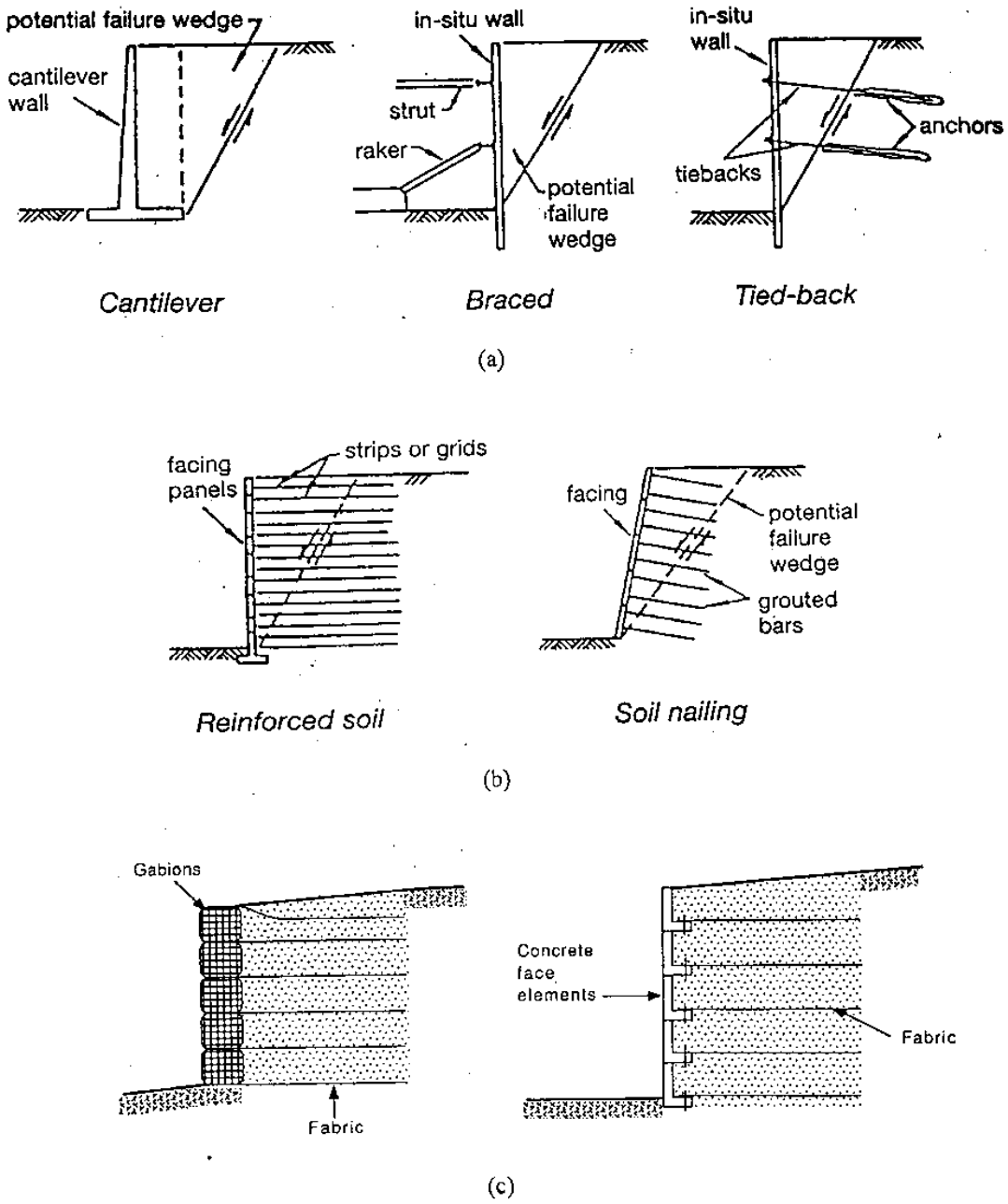

Figure 2.2.1 Examples of retaining wall systems: (a) externally stabilized, (b) internal stabilized, and (c) hybrid systems (after Jones, 1997; Hausmann, 1990).

The major difference between these two systems is the retaining mechanism. In an externally stabilized system, soil pressure is integrated to produce an overall driving force; external structures are placed in front of the soil to resist this driving force. The external structure only functions after the entire backfill soil starts yielding and reaches its critical state (active or passive states). Different from an externally stabilized system, the soil mass in an internally stabilized system is partitioned into layers by the planar reinforcement during construction. It receives local support (reinforcing) from the closest reinforcement as soon as any local yielding occurs; the local yielding is confined by the nearby reinforcement before it develops into major yielding of the entire backfill soil.

In this research project, work is concentrated on the internal stability analysis of the reinforced soil retaining (internally stabilized) systems, especially on soil structures reinforced using geosynthetic materials as the reinforcement.

2.3 Mechanism of Reinforced Soil Retaining Structures

In 1960s, Henri Vidal first illustrated the fundamental mechanism of reinforced soil and introduced Reinforced Earth as an alternative type of soil retaining structure (Vidal, 1969). The basic concept of Vidal's Reinforced Earth retaining system was to transfer shear forces occurring inside the soil mass to closely spaced reinforcements as yielding of the soil started (Mitchell and Villet, 1987). Two approaches have been used to explain the reinforcing mechanism: the discrete system and the composite material approach.

The discrete system, shown in Fig.2.3.1, indicates that the additional shear forces of the unstable soil mass are transferred to the reinforcement in two forms: friction and adhesion. Friction is the component of shear resistance that is proportional to the normal stress acting on the shear plane. Adhesion is the shear resistance between different materials (soil and reinforcements) and is independent of normal stress (Hausmann, 1990). As a result of this internal shear transformation, the soil mass is kept away from its critical state, and the lateral pressure that is generated by the reinforced soil mass is also reduced because of the existence of the reinforcements.

The other approach to explain the reinforcing mechanism of reinforced soil is to analyze it as a composite material. Schlosser and Long (1972) and Yang and Singh (1974) used an apparent cohesion concept. Hausmann (1976) and Hausmann and Lee (1976) also interpreted the reinforcing mechanism using similar concepts. Figure 2.3.2 summarizes the composite approach to the reinforcing mechanism using the Mohr-Coulomb failure criteria (after Hausmann, 1990). As shown in Fig. 2.3.2, Mohr circle 0 represents a reinforced soil composite element at its initial condition. Assume that this element has reinforcement inserted in the horizontal plane, and a pair of principal stresses (vertical and horizontal stresses, where vertical stress is the major principal stress) are applied to it. When the vertical stress increases, the Mohr circle moves to higher stress levels. Mohr circle 1 represents the failure condition if soil is not

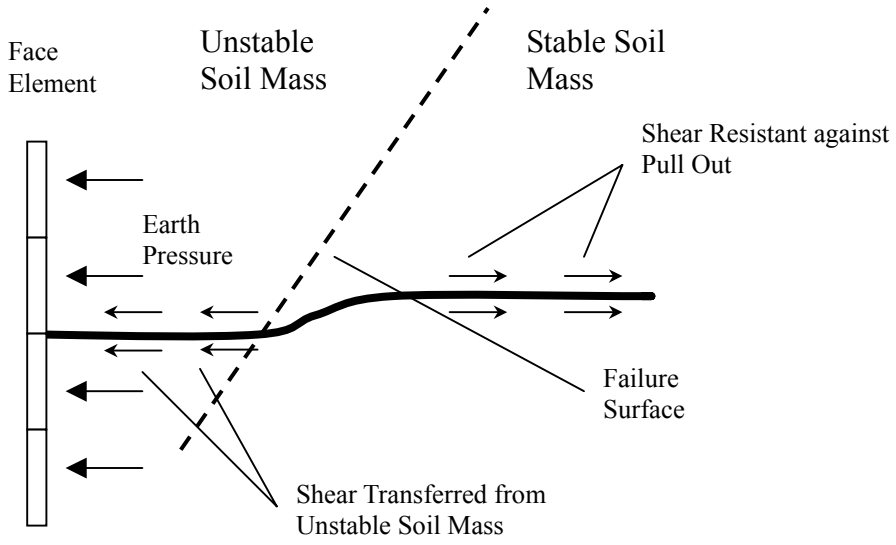

Figure 2.3.1 Reinforcing mechanism of reinforced soil retaining structures (after Huasmann, 1990).

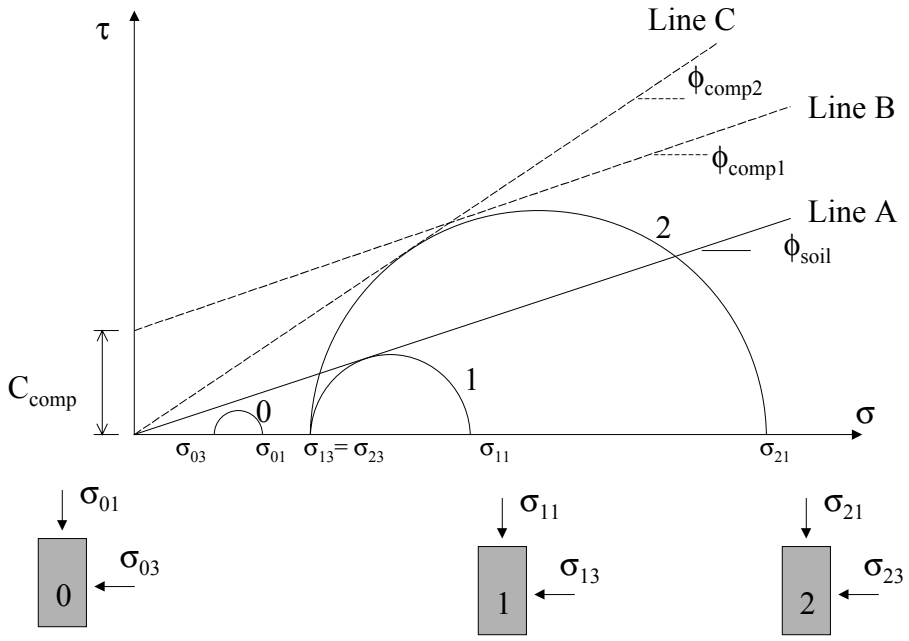

Figure 2.3.2 Principal stress conditions of reinforced soil.

reinforced, and Mohr circle 2 represents the failure condition of the reinforced soil composite. The difference between σ_{21} and σ_{11} is the additional vertical stresses that soil can take with the aid of the reinforcement. Line A is the failure envelope of the unreinforced soil. Lines B and C are two hypothetical failure envelopes that are used to define the failure of the reinforced soil composite. Line B represents the hypothesis that the reinforced soil composite has the same friction angle as the soil. What reinforcement provides is an additional cohesion C_{comp} to the composite. The hypothesis represented by Line C is that the reinforced soil composite has higher friction angle because of the existence of the reinforcement. Equations 2.3.1 and 2.3.2 are the equations of Lines B and C, or

$$\tau = C_{comp} + \sigma \cdot \tan\phi_{comp1} \quad \text{(Line B)} \qquad (2.3.1)$$

$$\tau = \sigma \cdot \tan\phi_{comp2} \qquad \text{(Line C)} \qquad (2.3.2)$$

Boyle (1995) verified that hypothesis presented by Line C (Equation 2.3.2) is more appropriate to explain the reinforcing mechanism of GRS with his Unit Cell Device (UCD) test data. The UCD was designed to test a GRS element under plane strain loading conditions to simulate the GRS element inside GRS soil structures. Both in-soil properties of geosynthetics and GRS composite properties are measured in the device (Boyle, 1995). Boyle found that the tension that develops in the reinforcements during straining of the GRS increased the lateral pressure acting on the soil, thus increasing the soil strength.

For failure mechanism of the GRS, Hausmann (1976), Hausmann and Lee (1976), and Gray and Ohashi (1983) found that at low confining pressures, failure of reinforced soil often occurred by slippage at the soil-reinforcement interface; and, at higher confining pressures, failure occurred due to the rupture of the reinforcement. However, this observation depends on the properties of the reinforcement material as well as the interface between reinforcement and soil. The discrete system approach is suitable for analyzing failure at both low and high confining pressures, although it involves complicated force transformation. On the contrary, the composite material approach, although less inter-layer force transformation is involved, will need a good constitutive stress-strain model to account the very different behaviors of GRS composite at different confining pressures.

2.4 Geosynthetic Reinforced Soil (GRS) Retaining Structures

Vidal's Reinforced Earth system was constructed using horizontally lying steel strips as reinforcement and with facing elements to locally retain the backfill soil. In addition, different materials such as steel bars, wire mats, and synthetic fabrics have been used as reinforcements for this system. Although its use as reinforcement did not start until the early 1970's, geosynthetics have become one of the most popular soil reinforcement materials. The usage of geosynthetics for soil reinforcing has increased dramatically in the past twenty years because (after Giroud, 1986):

1. Geosynthetic materials have excellent flexibility and uniformity, and therefore, they have better tolerance of differential movements,

2. Geosynthetic materials are more resistant to corrosion and other chemical reactions than steel reinforcement, and

3. Geosynthetic materials are able to provide the same (maybe even better) reinforcing effect than the steel reinforcement with easier and more cost effective construction procedures.

Despite considerable differences of reinforcing mechanisms, interaction with soil and geosynthetics, and property changes due to in-soil confinement and low strain rate conditions, stability analysis of GRS retaining walls is still performed in a similar manner to that of steel reinforced retaining walls. Internal design methods adopted from steel reinforced walls are based on limiting equilibrium concepts and require an assumption of the lateral earth pressure distribution against the face of the reinforced section in order to obtain the tensile stresses that must be resisted by the reinforcement. Available evidence from full-scale and model GRS walls indicates that these assumptions tend to significantly overestimate the internal stress distribution within the structure (Bell et al., 1983; Rowe and Ho, 1993; Allen et al., 1992; Christopher, 1993). These observations suggest that the assumptions of conventional lateral earth pressure theory used in steel reinforced wall design is not appropriate for estimating the lateral earth pressure distribution of GRS walls. To develop an appropriate internal stability

design for GRS walls, an alternate approach to obtain the internal distribution of lateral earth pressure behind the wall face is needed.

2.4.1 Reinforcing Mechanisms

The basic differences between steel and geosynthetic reinforcement are their stiffness, structures, and the interactions occurring at the interfaces between reinforcement and soil. Steel reinforcement is usually in the form of straps or mats (Fig. 2.4.1), while geosynthetic reinforcement is usually in the form of grids or planar sheets (Fig. 2.4.2). Because of the planar structure and flexibility of geosynthetics, the shear forces occurring inside the soil mass are transferred to geosynthetic reinforcement more uniformly and without interruptions; therefore, geosynthetic materials have a better ability to contain both local and global yielding of the soil mass than steel reinforcement. The limit equilibrium analysis assumes that reinforcement does not reinforce the soil until global failure occurs in the soil mass. Although this analysis provides satisfactory results for steel reinforced retaining structures, it tends to over-predict the internal stress distribution of GRS retaining structures.

2.4.2 Interaction with Surrounding Soil

In contrast to the smooth surfaces that steel reinforcements usually have, most geosynthetics have fabric-like surfaces (geotextiles) or grid structures (geogrids)

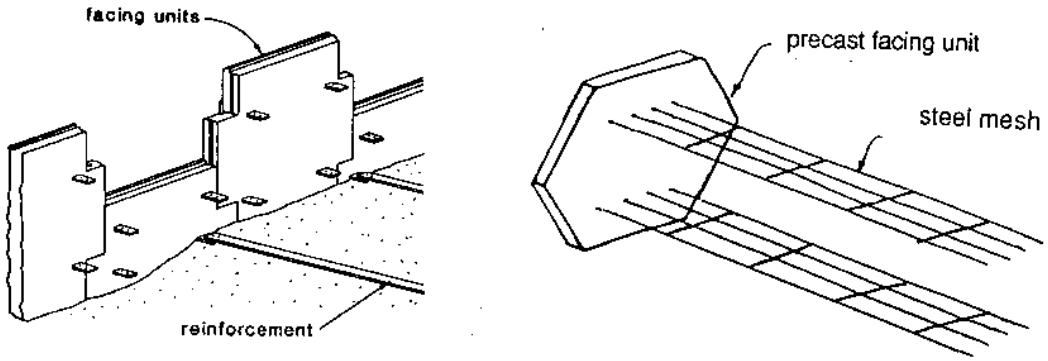

(a) (b)

Figure 2.4.1 Examples of steel reinforcement: (a) steel straps, and (b) steel mats (Jones, 1996).

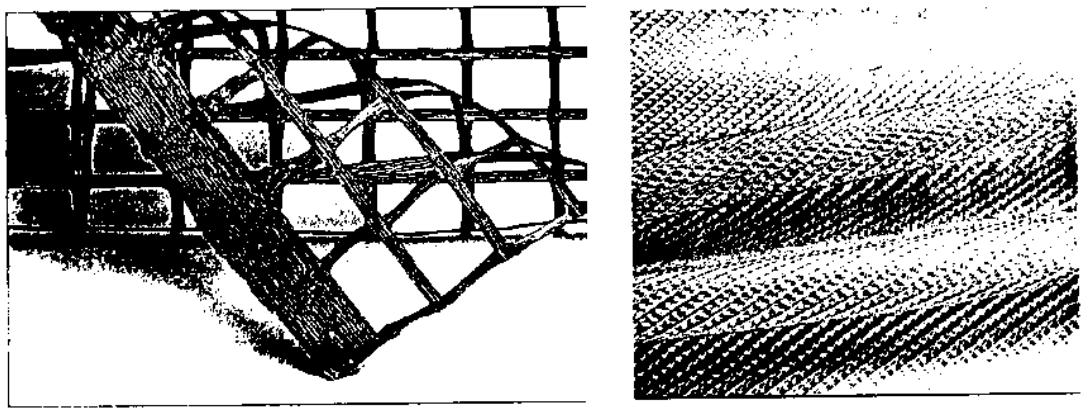

(a) (b)

Figure 2.4.2 Examples of geosynthetic reinforcement: (a) geogrids, and (b) woven geotextile (Koerner, 1998).

that produce much better bonding between soil and the reinforcement. In steel reinforced soil retaining systems, slippage occurs at the interface between soil and steel reinforcement, but in geosynthetic reinforced systems, the slipage surfaces were observed to occur inside the soil mass next to the reinforcement (Boyle, 1995). This observation is very important when using the discrete system approach to analyze the performance of the GRS retaining walls.

2.4.3 In-Soil and Low Strain Rate Reinforcement Stiffness

Research has shown that the strength of geosynthetics increases when it is confined (McGown et al., 1982; El-Fermaoui and Nowatzki, 1982; Leshchinsky and Field, 1987; Wu and Arabian, 1990; and Ling et al., 1992). Boyle (1995), based on UCD test results, reported that the apparent moduli of nonwoven geotextiles increased with confinement in soil, while the moduli of woven geotextiles and probably geogrids were not apparently influenced by soil confinement. However, Boyle et al. (1996) reported that the moduli of woven geotextiles decreased when a low strain rate was applied. Therefore, different from steel reinforcement, the influences of in-soil confinement and low strain rate conditions, probably the usual cases in construction, have to be carefully considered when performing stability analyses of GRS structures.

2.5 Stability of GRS Retaining Structures

2.5.1 External Stability

All reinforced soil retaining walls, whether reinforced by steel or geosynthetics, have the same external stability concerns as conventional retaining structures. Figure 2.5.1a shows the external failure modes of GRS retaining structures. External stability design of retaining structures basically includes analyses of:

1. Friction between retaining structures and foundation soil--possibility of base sliding failure,
2. Bearing capacity of foundation soil and creep of the foundation soil--possibility of overturning, and excessive settlement, and
3. Overall slope stability

2.5.2 Internal Stability

Figure 2.5.1b shows the internal failure modes and local stability failure modes of segmental facing units. Different from the conventional system in which backfill soil properties are the major internal stability design concern, the reinforced soil system has a much more complicated internal stability design. Internal stability design of the reinforced soil retaining structure involves consideration of:

1. The strength properties of backfill and reinforcement material,
2. The reinforcement arrangement,

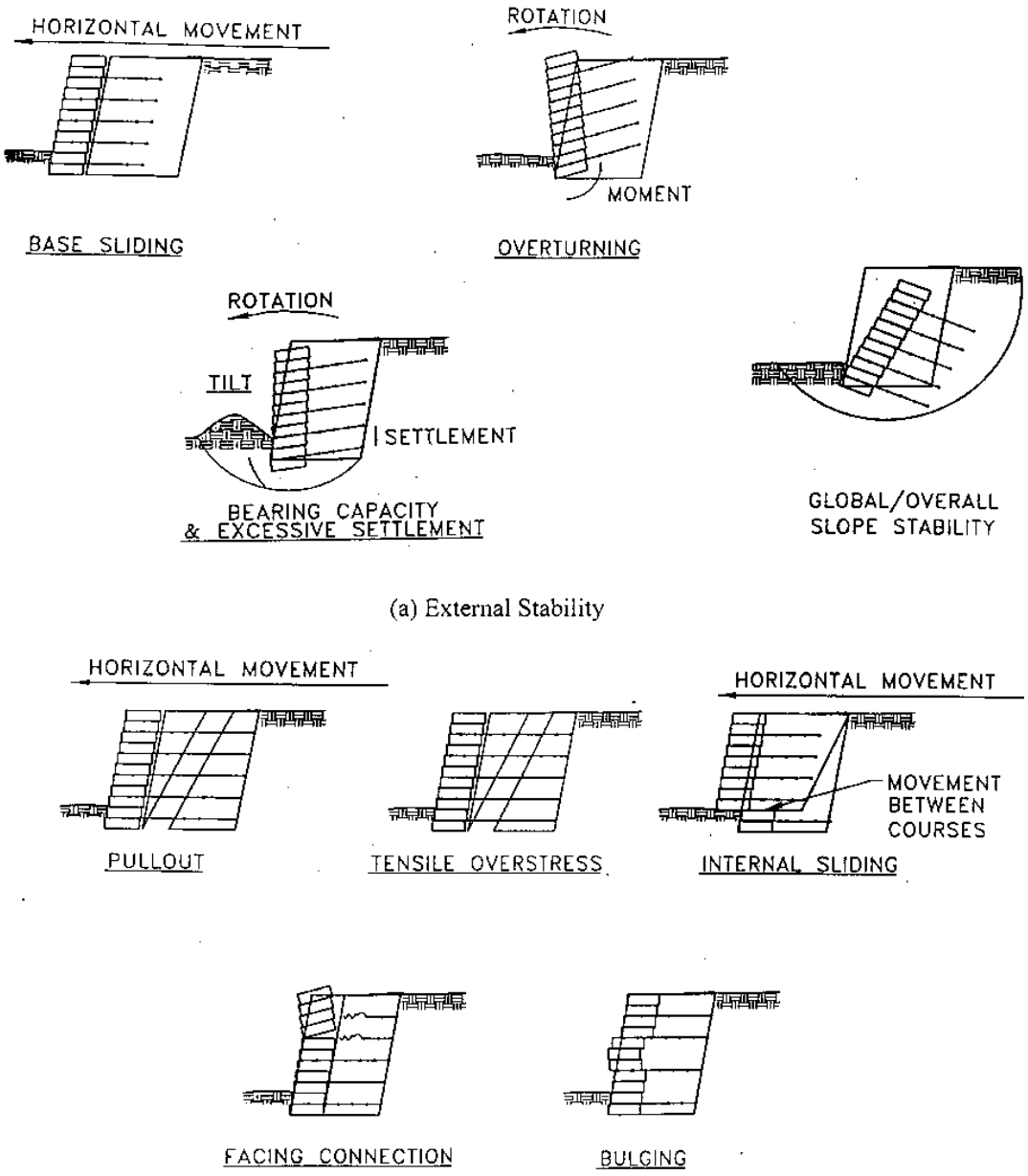

Figure 2.5.1 Failure modes of segmental GRS retaining structures (after NCMA 1996).

3. Interaction between soil and reinforcement,
4. Interaction between facing element and soil,
5. Durability of the reinforcement, and
6. Connection between facing units and reinforcement (especially for systems with segmental facing structures).

Present internal stability design methods of reinforced soil retaining structures are still based on a limit state analysis. This approach fails to provide internal working stress information as well as face deflections of the retaining structure. Furthermore, it tends to over-predict the internal stress distribution inside GRS retaining structures because of the considerable differences that were described in previous sections between steel and geosynthetic reinforcements.

Chapter 3
Internal Stability Analyses of GRS Retaining Structures

As summarized in Chapter 2, although improvement of the internal stability analyses of GRS retaining structures is needed, previous research on this subject has not made much progress because:

1. Minimal information on the internal stress or strain distributions in real GRS structures is available. Because of the difficulties in installing appropriate instrumentation to measure reinforcement strain and, most important, in interpreting strain measurements obtained from the field, only a few reliable internal stress or strain measurements are available.

2. Minimal calibration of numerical modeling techniques for analyzing the performance of GRS walls has been done. Most of the time, numerical models have been developed to simulate the performance of specific GRS retaining structure projects. Parametric studies of the effect of internal design factors have mostly been done by using models of hypothetical slopes or walls generated by computer programs. Although some computer programs have been used to perform numerical analyses on different GRS walls, procedures for interpreting input properties were found to be unclear, or sometimes even different procedures were used for models created using the same computer program.

3. Understanding of material and interface properties is not well developed. Within a GRS wall, material (both soil and geosynthetic) properties and the interactions between them vary when the loading and confining conditions are changed. Research on analyzing these material and interface changes has not progressed very much because of difficulties in designing laboratory tests and interpreting field measurements. Numerical analyses performed without appropriate interpretation of input properties may yield reasonable results for either external performance (face deflections) or internal performance (reinforcement strain distributions), but not both at the same time.

To overcome these drawbacks, numerical models that use clear and reasonable procedures to determine input material and interface properties as well as that are capable of reproducing both the internal and external performance of GRS retaining structures should be developed.

In this chapter, present internal stability design methods for GRS retaining structures are reviewed and commented upon. A general review of previous numerical modeling of GRS retaining structures is presented as well.

3.1 Concepts of Internal Stability Analyses of GRS Retaining Structures

Present internal stability analyses of GRS retaining structures basically consider two reinforcement failure modes:

1. Rupture or excessive elongation in the high stress zone within the reinforced backfill, and
2. Pull out or slippage from soil close to the end of the reinforced soil backfill.

However, stress or strain levels of the reinforced soil are not considered because most of these analyses are based on limiting equilibrium concepts. In limiting equilibrium analyses, the geosynthetic reinforcement is designed to be strong enough to take all the excess earth pressure within the backfill soil; yet interaction between soil and reinforcement, including force transformation, interlayer movements, and other working stress mechanisms, are not considered.

Different from limiting equilibrium analyses, working stress analyses can provide detailed internal and external stress-strain information of the structure. Information such as the development of reinforcement tension and strain compatibility under working conditions of the structure becomes available by performing working stress analyses. However, working stress analyses of GRS retaining structures are difficult to perform because limited calibration work of numerical modeling techniques has been done and understanding of material and interface properties is not well developed.

In the following sections, concepts of both limiting equilibrium and working stress analyses are described. The need for developing working stress based design methods will be further confirmed.

3.1.1 Ultimate Limit State Stress Analysis

The ultimate limit state stress analysis is the most commonly used analysis method for the stability of geotechnical projects such as retaining walls, slopes, excavations, as well as foundation bearing capacity. Basic procedures of this type of analysis include:

1. Assume a reasonable collapse mechanism for the foundation.
2. Calculate the demand forces or moments for satisfactory performance of the structure based on the assumed collapse mechanism. These forces or moments become the ultimate limit state requirements of the designed structure.
3. Design resistant components that would provide enough resistant forces or moments to the structure so that certain factors of safety (ratio of the resistant over the demand forces or moments) can be achieved.

Advantages of ultimate limit state analysis are: (1) only simple calculations are needed, and (2) results of the design tend to be on the conservative side, as long as the assumed collapse mechanism is close to what really happens if the designed structure collapses. However, the performance as well as the internal stress and strain levels of the designed structure cannot be obtained from this type of analysis. For geotechnical structures, such as GRS retaining walls with complicated interactions between construction materials, as the difficulty of assuming a reasonable collapse mechanism increases, the accuracy of calculating demand forces for design decreases. Therefore, a

working stress analysis that can provide internal stress distribution as well as structure performance becomes necessary.

3.1.2 Working Stress Analysis

Different from the ultimate limit state analysis, a working stress analysis analyzes the actual stress levels within the designed structure. Basic procedures of a working stress analysis include:

1. Develop analytical models for the elements (materials) that form the designed structure and the interactions between them.
2. Calculate the stress and strain levels within the designed structure using developed material and interface models based on laws of strain compatibility and stress equilibrium.
3. Repeat the stress-strain calculation for each working stress condition that the structure might experience.

Advantages of the working stress analysis are: (1) no assumption of a collapse mechanism needs to be made, (2) the actual stress levels within the designed structure can be obtained, and (3) the performance of the structure can also be observed. However, analytical models for materials and interfaces between them are not always easy to develop, and these types of analyses always involve complex equations and numerous calculations. Numerical analysis methods such as finite element method or

finite difference method are commonly used as tools to perform these types of analyses.

In the remaining sections of this chapter, internal stability design methods of GRS retaining structures based on both limit state analysis and working stress analysis are reviewed. Technical problems of these methods and needs for developing general rules and practical calculation methods for the working stress analysis of GRS retaining structures will be summarized as well.

3.2 Internal Stability Analyses of GRS Retaining Structures I--Limit State Design Methods

Allen and Holtz (1991), and Holtz et al. (1997) have summarized various internal stability design methods. These methods are mostly based on ultimate limit state stress analysis. General procedures for these methods include:

1. Assume a lateral stress (lateral earth pressure) distribution behind the wall face.
2. Calculate reinforcement tension to avoid tensile failure of reinforcement based on the assumed lateral earth pressure distribution with a certain factor of safety applied.
3. Calculate required reinforcement length to avoid pull-out failure of the reinforcement, based on the assumed lateral earth pressure distribution, failure

plane orientation, and interlayer friction angle (soil-reinforcement) with certain factor of safety applied.

A summary of these methods will be discussed in terms of assumed lateral earth pressure distributions, determination of reinforcement tensile forces, and determination of reinforcement embedment lengths required to resist pullout forces. Only theoretical concepts are discussed in the following sections.

3.2.1 Lateral Earth Pressure Distributions

Several lateral earth pressure distributions have been proposed for internal stability design for GRS retaining structures (Figures 3.2.1a to 3.2.1d). The most commonly used is the classical Rankine earth pressure distribution, which assumes a triangular shape lateral earth pressure distribution (Figure 3.2.1a). Use of the Rankine earth pressure distribution was proposed by Steward et al. (1977), and is still extensively used in many popular design methods such as FHWA (Federal Highway Administration) (Holtz et al., 1997) and NCMA (National Concrete and Masonry Association) (NCMA, 1996) methods.

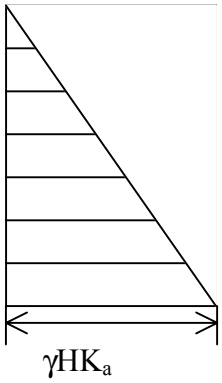

(a) Rankine (Triangular)

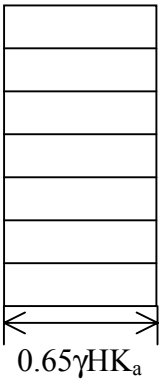

(b) Rectilinear

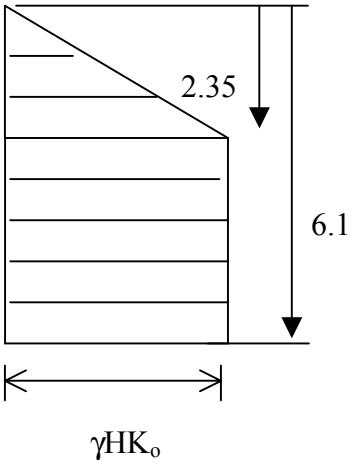

(c) Bilinear

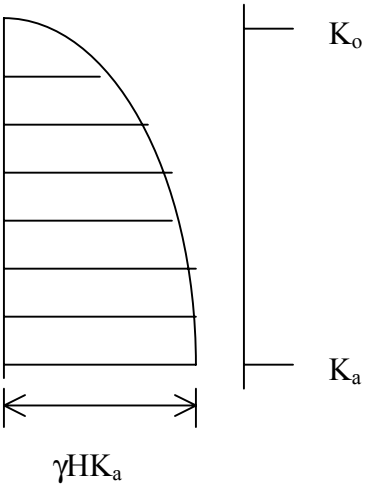

(d) Coherent gravity

Figure 3.2.1 Various lateral earth pressure distributions: (a) Classical Rankine (Triangular), (b) Rectilinear (Broms, 1978), (c) Bilinear (Christopher et. Al., 1989), and (d) Coherent gravity (Christopher et al. 1989, Simac et al. 1990).

Other lateral earth pressure distributions such as rectilinear (Figure 3.2.1b, Broms, 1978), bilinear (Figure 3.2.1c, Christopher et al. 1989), and coherent gravity (Figure 3.2.1d, Christopher et al. 1989, Simac et al. 1990) distributions have been proposed. These distributions were developed mostly based on field observations or experiences to account for the soil-reinforcement composite effects. Leshchinsky and his colleagues (Leshchinsky and Boedeker, 1989, Shiwakoti et al., 1998) also assumed a triangular lateral earth pressure distribution for reinforcement tension calculations; however, a logarithmic spiral failure surface was used to describe the failure mechanism within the reinforced soil.

3.2.2 Reinforcement Tensile Forces

The Rankine earth pressure distribution does not take existing reinforcement material properties into account when calculating the reinforcement tension at certain heights of the wall. Additional adjustments of the lateral earth pressure coefficients were made based on empirical experience when calculating the reinforcement tensions (NCMA, 1996, Holtz et al, 1997).

In most of the limit state stress-based GRS internal stability analyses, concepts of the tie-back wedge design method were adopted to calculate the reinforcement tensile forces. In the tie-back method, the reinforcement was designed to resist the thrust that resulted from the lateral earth pressure acting on the wall face in between the

reinforcement layers. General procedures of this method are described in the following sections.

Reinforcement tensile force at a certain depth from top of the wall is determined by calculating the horizontal force at the same depth based on the assumed lateral earth distribution (Equation 3.2.1). σ_h in Equation 3.2.1 is determined based on the lateral earth pressure distribution used.

$$T_{reinf}(z) = \sigma_h(z) \cdot S_v \qquad \text{(Eq. 3.2.1)}$$

where $T_{reinf}(z)$ = reinforcement tensile force at depth z from top of the wall.
$\sigma_h(z)$ = horizontal pressure at depth z from top of the wall.
S_v = vertical spacing of the reinforcement.

The calculated reinforcement tensile forces are then multiplied by a factor of safety to use as the design reinforcement tensions (Equation 3.2.2). Different factors of safety are used by different design methods because different lateral earth pressure distributions or adjustments for existing reinforcement are used.

$$T_{design}(z) = T_{reinf}(z) \cdot FS \qquad \text{(Eq. 3.2.2)}$$

where $T_{design}(z)$ = designed reinforcement tension at depth z from top of the wall.
FS = factor of safety.

3.2.3 Reinforcement embedment length

The embedment length required to prevent pullout failure of the reinforcement is calculated from force equilibrium at the depths where the reinforcement layers are located. The resistant force against pullout failure is the friction developed on both surfaces of the reinforcement, and the driving force is equal to horizontal force acting on the plane where the reinforcement lies (Equation 3.2.3).

$$\sigma_v \cdot f^* \cdot 2 \cdot L_{e,required} \cdot w = \sigma_h \cdot 1 \cdot w \qquad \text{(Eq. 3.2.3)}$$

where σ_v = vertical earth pressure acting on the reinforcement.

f^* = interlayer friction coefficient between soil and reinforcement.

$L_{e,\ required}$ = required embedment length of reinforcement.

w = unit width of the designed wall.

σ_h = horizontal earth pressure acting on the reinforcement.

σ_v in Equation 3.2.3 usually equals γ (unit weight) times z (depth) plus additional surcharge loads, and σ_h can be determined using the assumed lateral earth pressure distribution. By solving the force equilibrium described in Equation 3.2.3, the designed reinforcement embedment length can be determined with an appropriate factor of safety (Equation 3.2.4).

$$L_{e,design} = \frac{FS}{2} \cdot \frac{\sigma_h}{\sigma_v} \cdot \frac{1}{f^*} \qquad \text{(Eq. 3.2.4)}$$

where $L_{e,\ design}$ = design embedment length of reinforcement.

Values of minimum embedment length were also recommended in most of the methods to prevent internal sliding between the geosynthetics and soil.

3.3 Analytical Models of Reinforced Soil

As described in Section 3.1.2, an important part of working stress analyses is to develop analytical models for the materials used in GRS walls and the interfaces between them. As described in Section 2.3, behavior of reinforced soil can be analyzed using two approaches: the discrete soil reinforcement system and the composite material model. Both approaches have been utilized to develop analytical models for numerical analyses of GRS walls. Figure 3.3.1 describes the material properties involved in both types of analytical models. The discrete element model considers individual structural elements in the reinforced soil and the interfaces between them, and the composite element model treats the reinforced soil as an anisotropic homogeneous material. In the following sections, a review of these analytical models and the numerical analyses developed based on them are described. The progress and shortcomings of present research are summarized as well.

3.3.1 Discrete Element Model

The discrete element model analyzes individual structural elements of the reinforced soil and interfaces between them (Figure 3.3.1a). Properties of the soil, reinforcement, facing units, and interfaces between different materials are necessary to develop this type of numerical model. An advantage of using the discrete soil-reinforcement approach is that the stress levels in individual structural elements can be determined within this model. Especially for segmental faced GRS retaining structures, important design information such as friction between facing units and backfill, as well as reinforcement stresses at the connections, can be estimated using this approach. Disadvantages of this model are (after Rowe and Ho, 1988; Bathurst and Koerner, 1988):

1. Difficulty in developing numerical models--numerical models developed based on this approach usually have many different material and interface elements representing different materials and interfaces.

2. Difficulty of characterizing the interactions between soil, reinforcement and other structural elements--input properties of interfaces between different materials in the system are difficult to determine.

3. Large computation time required for the numerical analyses--numerical models based on this approach usually require a large number of computation units (elements), and the time required for numerical iterations is fairly large.

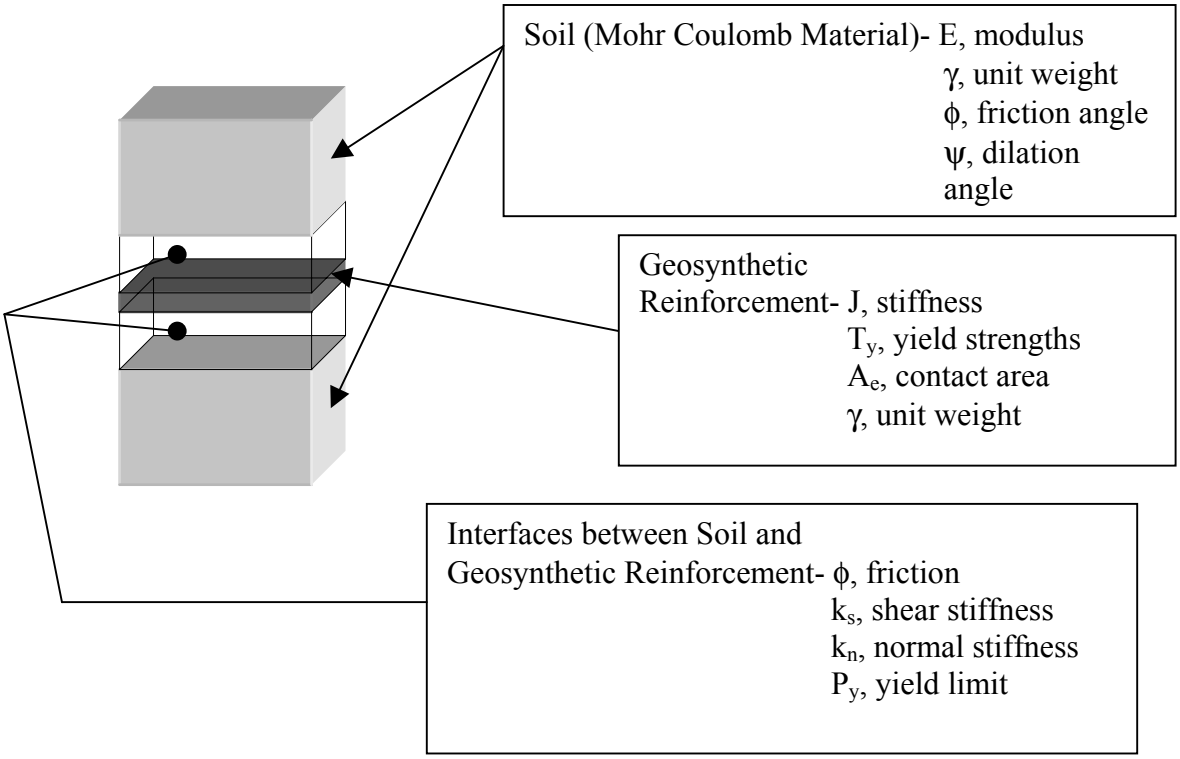

(a) discrete soil reinforcement model

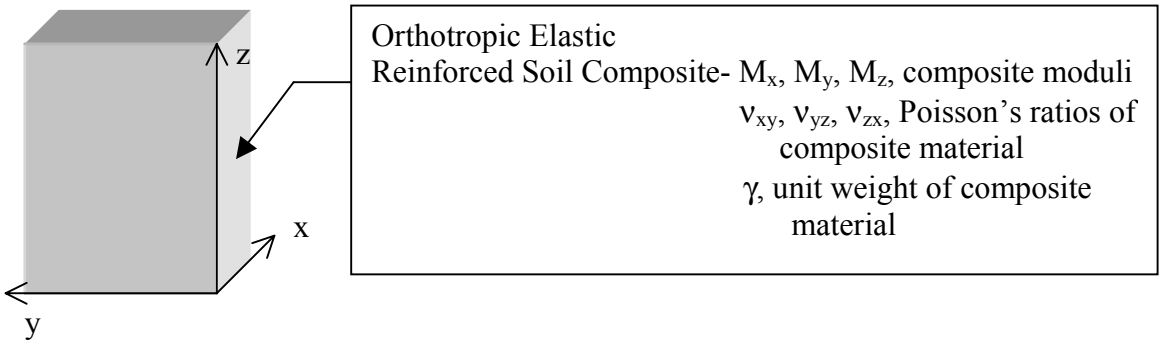

(b) orthotropic elastic reinforced soil composite model.

Figure 3.3.1 Material properties involved in the development of the analytical models.

So far, most of the working stress analyses for GRS retaining structures have been performed using the discrete soil reinforcement system. Research progress and difficulties encountered are summarized in Section 3.4.

3.3.2 Composite Element Model

The reinforced soil composite element model considers the reinforced soil to be an anisotropic homogeneous material. As shown in Fig. 3.3.1b, only orthotropic elastic composite material properties are needed to develop this type of numerical model. Advantages of using the reinforced soil composite model are:

1. Less effort required to develop numerical models--by using composite material concepts, only composite elements of reinforced soil are used in numerical models; therefore construction of numerical models is much easier than using discrete elements.

2. Less time needed for iterations--computation units (elements) of numerical models are dramatically decreased by using the composite elements instead of different material and interface elements, and the iteration time of a composite model is expected to be much less than a discrete model that is modeling the same object.

Although the composite approach offers simpler and time saving numerical analyses, yet it has following disadvantages (after Rowe and Ho, 1988):

1. Stress levels of individual structural materials are not available--the internal stress or strain distribution is presented in a composite sense.

2. Interactions between different materials cannot be modeled--the composite model assumes that reinforced soil has perfect bonding at the interfaces between soil and reinforcement, interlayer movement such as slipages between soil and reinforcement cannot be modeled.

3. Localized failure cannot be modeled--because no individual material elements are used, localized failures such as connection failure of the segmental GRS walls cannot be simulated.

Treating construction materials as composites has been proposed by, for example, Westergaard (1938), Salamon (1968), Harrison and Gerrard (1972), Romstad et al. (1976), and Shen et al. (1976). Among these researchers, Harrison and Gerrard (1972) first applied the elasticity to analyze reinforced soil. They developed a series of equations to convert individual elastic material properties into the elastic composite material properties. The elasto-plastic model of reinforced soil composite was not developed until 1980's. Sawicki and Lesniewska (1988, 1991, 1993), and Sawicki and Kulczykowski (1994) updated the elastic formulations to include plastic yielding of the material. Effort has also been made to simulate the slip between soil and reinforcement by adding extra yielding criteria into the composite elements (Hermann and Al-Yassin, 1978; Naylor, 1978; Naylor and Richards, 1978).

The major difficulty in performing numerical analyses using composite elements is obtaining the composite properties of the reinforced soil. In the present research, composite material properties were first interpreted from individual material properties using developed elasticity models; thus numerical analyses were performed using the interpreted composite material properties. Boyle (1995) developed the Unit Cell Device (UCD) to test reinforced soil composites under plane strain loading conditions. Anisotropic composite properties were obtained by reducing the UCD test data (Lee and Holtz, 1998). These composite properties were also used as the input properties of numerical models that were developed to simulate the WSDOT Rainier Avenue wall performance. These models were able to predict the wall performance reasonably well (Lee and Holtz, 1998).

3.4 Internal Stability Analyses of GRS Retaining Structures II--Working Stress Design Methods and Numerical Analyses

3.4.1 Present Working Stress Design Methods

So far, working stress analyses for both performance and internal stability designs of GRS retaining structures are not well developed. Existing case histories utilizing working stress analyses were done by numerical techniques. Numerical models were created using various finite element or finite difference computer programs to either examine designs for critical structures or reproduce instrumentation measurement for research purposes. However, performance prediction of any large-scale test walls or

real walls has not previously succeeded using working stress analyses. Major reasons for this is the lack of knowledge of in-soil geosynthetic properties, strain rate-dependent geosynthetic properties, and soil-geosynthetic interface mechanisms. Arbitrary assumptions of material properties were involved in most of these models; i.e. determination of input properties often changed when different objects were analyzed.

Recently, a commercial finite difference method (FDM) based computer program FLAC has become popular for analyzing geotechnical stability problems. Numerical models of GRS retaining structures have been developed using FLAC by several researchers, including the author. With aid of recent progress in understanding of material properties, these models were able to reproduce the performance of different GRS retaining structures even using the same procedures to determine material properties and to model the interaction between soil and geosynthetic.

3.4.2 Summary of Numerical Analysis Methods

Both the finite element method (FEM) and the finite difference method (FDM) were used to perform working stress analyses to predict performance of GRS retaining structures. Various computer programs have been developed using both the discrete and composite approaches. In this section, both FEM and FDM methods are reviewed, and problems encountered and progress are summarized.

3.4.2.1 Finite Element Method

Table 3.4.1 summarizes some of the popular FEM computer programs and researchers that have used these programs as tools to perform numerical analyses on GRS retaining structures. Although a lot of FEM computer programs have been used to model the performance of GRS retaining structures, none of them have really succeeded because of the difficulties described at the beginning of this chapter. Problems in modeling GRS retaining structures include:

1. Both internal and external performance cannot be accurately predicted at the same time.--Because of inadequate consideration of in-soil and low strain rate strength properties of geosynthetic reinforcement, results of these FEM analyses could often only match either wall deflections or reinforcement stress/strain levels, and not both at the same time.

2. Adjustments to input material properties were made without a clear explanation or consistent rules.--In order to make an accurate prediction of both internal and external performance, some of these analyses had to apply different “in-soil” stiffness adjustments for geosynthetic reinforcement for different modeling projects.

3. The result of parametric analyses cannot be correlated to real wall performance.--Although some parametric studies of design factors of GRS retaining structures have been performed using these FEM programs, results of

these studies did not correlate very well to real wall performance. One of the major reasons for this poor agreement is that most of the parametric studies were done using hypothetical models that were still having the problems described above.

4. Another problem of using the FEM programs to model GRS retaining structures is that most of these programs were developed for research purposes. Modeling techniques such as the determinations of input material or interface properties were often changed when different projects were analyzed.

Table 3.4.2 summarizes the problems found in modeling performance of GRS retaining structures using the FEM computer programs listed in Table 3.4.1.

3.4.2.2 Finite Difference Method

Recently, the FDM program FLAC has become popular for modeling the performance of GRS walls because of its excellent capability to model geotechnical engineering stability problems and its extended programming ability (Itasca, 1995). Besides research results presented in this thesis, Bathurst and Hatami (1998a and b) have used the FLAC program to analyze the seismic response of GRS walls. They also

Table 3.4.1 FEM programs used to analyze performance of GRS retaining structures.

Program Names	References
REA	Herrmann and Al-Yassin (1978) Xi (1992)
SSCOMP	Seed and Duncan (1984) Collin (1986) Adib (1988) Schmertmann, et al. (1989) Chew, et al. (1989) Jaber, et al. (1992) Zornberg and Mitchell (1993) Chew and Mitchell (1994) Pinto, et al. (1998)
AFENA	Ho and Rowe (1993) Ho and Rowe (1994)
DACSAR	Chou (1992) Helwany (1992) Chou and Wu (1993)
SOILSTRUCT	Ebling, et al. (1992a) Ebling, et al. (1992b) Ebling, et al. (1993)
GEOFEM	Karpurapu and Bathurst (1992) Karpurapu and Bathurst (1994) Bathurst, et al. (1997)
CRISP	Yeo, et al. (1992) Andrawes and Saad (1994) Yogarajah and Andrawes (1994) Ghinelli and Sacchetti (1998)
M-CANDE	Ling and Tatsuoka (1992) Porbaha and Kobayashi (1997)

Table 3.4.2 Problems found in modeling performance of GRS retaining structures using FEM computer programs listed in Table 3.4.1.

	Computer Programs							
Problems found	REA	SSCOMP[1]	AFENA	DACSAR	SOILSTRUCT	GEOFEM	CRISP	MCANDE
Internal and external performance can not be accurately predicted at the same time.	X	X	X	X	X	X	X	X
Adjustments of input material properties were made without a clear explanation or consistent rules.		X	X			X		
Parametric study result can not be correlated to real wall performance.	X	X	X	X			X	

X indicates that the problem described on left was found.

[1] Procedures using SSCOMP in modeling GRS retaining structures have been found inconsistent in different references. Problems indicated are not all applicable to any individual application.

performed parametric studies to examine the influence of various internal design factors. The numerical interpretation models that Bathurst and Hatami (1998a and b) used were hypothetical models. These models were not calibrated using any actual wall performance or large-scale test results. Lindquist (1998) also used FLAC to analyze the seismic response of GRS slopes. A parametric study of seismic design factors was performed using the developed model, and test results of centrifuge model tests under dynamic shaking were reproduced (Lindquist, 1998). Adjustments to soil and in-soil reinforcement properties without a clear explanation and verification were found in the models developed by Lindquist (1998). Different values of soil friction angle and reinforcement stiffness had to be systematically introduced into his models in order to match the results of centrifuge and shaking table tests. FLAC models described in these references were all created using discrete elements.

3.5 Conclusions

3.5.1 Problems of Present Numerical Analysis Applications

1. Present FEM programs have difficulties to predict both external and internal performance data of GRS retaining structures at the same time. Although some of them reported that successful modeling results had been obtained for both internal and external performance, adjustments of the input material properties had to be made, often without clear explanation.

2. Input properties used in some numerical methods are still decided based on personal experience or, most of the time, arbitrary assumptions. Present numerical analyses are usually performed by systematically introducing different values of soil friction angles, soil dilation angles, or reinforcement stiffnesses. Specific procedures that take material properties from laboratory test results and convert to input parameters for numerical analyses are not well developed yet.

3. Numerical models developed using FLAC program have not been well calibrated with real wall performance.

3.5.2 Research Needs for Internal Stability Analyses of GRS Retaining Structures

To improve the numerical analyses of internal stability of GRS retaining structures, research is needed to:

1. Develop simple and straightforward procedures for converting material properties that are obtained from ordinary laboratory tests to properties of materials that are really present inside GRS retaining structures. Two examples are to convert a triaxial soil friction angle into a plane strain soil friction angle, and to convert in-isolation tensile properties to in-soil tensile properties of reinforcements.

2. Develop general rules (techniques) for numerical modeling that are capable of predicting both internal and external performance using input properties that have real physical meaning.

3. Perform parametric studies on these internal design factors using well calibrated numerical models to obtain a better understanding of the influence of these design factors.

Chapter 4
Elasticity Theory and Stress-Strain Interpretation Used to Develop the GRS Composite Model

4.1 Elasticity

This chapter describes the fundamental elasticity theory and stress-strain interpretation used to develop the GRS composite model.

4.1.1 Transversely Isotropic Elasticity

Real soil is seldom an isotropic material. In most cases, soil responds in the same way if it is loaded in any horizontal direction, and may respond differently if it is loaded in the vertical direction. The behavior of soil is similar to the behavior of a transversely isotropic material (Wood, 1990). Transversely isotropic materials have the same stress-strain relationships in two of the three principal directions. Especially for the reinforced backfill of retaining structures, horizontally layered reinforcements and uniform backfill material make this soil-reinforcement "composite" a typical transversely isotropic material.

Equation 4.1.1 shows the complete description of an orthotropic elastic material. In Eq.4.1.1, $\mathbf{E}_1$, $\mathbf{E}_2$, $\mathbf{E}_3$, μ_{12}, μ_{23}, μ_{31}, ν_{32}, ν_{23}, ν_{13}, ν_{12}, ν_{21}, and ν_{31} are defined as the elastic moduli, shear moduli and Poisson's ratios of the anisotropic elastic material in its three principal directions (Figure 4.1.1).

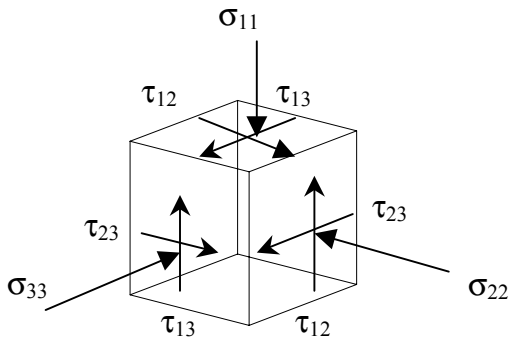

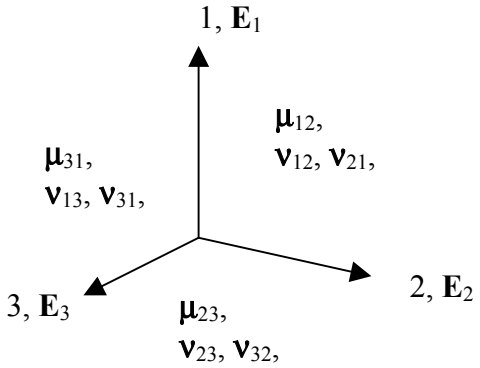

Figure 4.1.1 A schematic sketch of Equation 4.1. 1.

$$\begin{bmatrix} \varepsilon_{11} \\ \varepsilon_{22} \\ \varepsilon_{33} \\ \gamma_{12} \\ \gamma_{23} \\ \gamma_{31} \end{bmatrix} = \begin{bmatrix} \frac{1}{E_1} & \frac{-\nu_{21}}{E_2} & \frac{-\nu_{31}}{E_3} & 0 & 0 & 0 \\ \frac{-\nu_{12}}{E_1} & \frac{1}{E_2} & \frac{-\nu_{32}}{E_3} & 0 & 0 & 0 \\ \frac{-\nu_{13}}{E_1} & \frac{-\nu_{23}}{E_2} & \frac{1}{E_3} & 0 & 0 & 0 \\ 0 & 0 & 0 & \frac{1}{\mu_{12}} & 0 & 0 \\ 0 & 0 & 0 & 0 & \frac{1}{\mu_{23}} & 0 \\ 0 & 0 & 0 & 0 & 0 & \frac{1}{\mu_{31}} \end{bmatrix} \times \begin{bmatrix} \sigma_{11} \\ \sigma_{22} \\ \sigma_{33} \\ \tau_{12} \\ \tau_{23} \\ \tau_{31} \end{bmatrix} \qquad \text{(Eq. 4.1.1)}$$

Shear moduli of the anisotropic elastic material can be obtained by Equation 4.1.2a. To obtain the elastic moduli of the anisotropic elastic material, only Equation 4.1.2b, the normal part of Eq.4.1.1, needs to be solved.

$$\mu_{ij} = \frac{\tau_{ij}}{\gamma_{ij}} \qquad \text{(Eq. 4.1.2a)}$$

$$\begin{bmatrix} \varepsilon_{11} \\ \varepsilon_{22} \\ \varepsilon_{33} \end{bmatrix} = \begin{bmatrix} \frac{1}{E_1} & \frac{-\nu_{21}}{E_2} & \frac{-\nu_{31}}{E_3} \\ \frac{-\nu_{21}}{E_1} & \frac{1}{E_2} & \frac{-\nu_{32}}{E_3} \\ \frac{-\nu_{31}}{E_1} & \frac{-\nu_{23}}{E_2} & \frac{1}{E_3} \end{bmatrix} \cdot \begin{bmatrix} \sigma_{11} \\ \sigma_{22} \\ \sigma_{33} \end{bmatrix} \qquad \text{(Eq. 4.1.2b)}$$

By assuming the material transversely isotropic, and the major principal stress acts in the vertical direction, $\mathbf{E}_1 = \mathbf{E}_v$, $\mathbf{E}_2 = \mathbf{E}_3 = \mathbf{E}_h$, $\nu_{32} = \nu_{23} = \nu_{hh}$, $\nu_{31} = \nu_{21} = \nu_{hv}$, and $\nu_{13} = \nu_{12.} = \nu_{vh}$ into Equation 4.1.2b, it can be further simplified as Equation 4.1.3.

$$\begin{bmatrix} \varepsilon_{11} \\ \varepsilon_{22} \\ \varepsilon_{33} \end{bmatrix} = \begin{bmatrix} \frac{1}{\mathbf{E}_v} & \frac{-\nu_{hv}}{\mathbf{E}_h} & \frac{-\nu_{hv}}{\mathbf{E}_h} \\ \frac{-\nu_{vh}}{\mathbf{E}_v} & \frac{1}{\mathbf{E}_h} & \frac{-\nu_{hh}}{\mathbf{E}_h} \\ \frac{-\nu_{vh}}{\mathbf{E}_v} & \frac{-\nu_{hh}}{\mathbf{E}_h} & \frac{1}{\mathbf{E}_h} \end{bmatrix} \cdot \begin{bmatrix} \sigma_{11} \\ \sigma_{22} \\ \sigma_{33} \end{bmatrix} \qquad \text{(Eq. 4.1.3)}$$

4.1.2 Plane Strain Loading Conditions

For the material elements inside soil structures like retaining walls, long embankments, or slopes, it is appropriate to apply plane strain loading conditions to analyze their stress-strain behavior. Plane strain conditions indicate that there is no strain in one of the horizontal direction, for example, if direction 2 is the plane strain direction, then $\varepsilon_{22} = \gamma_{12} = \gamma_{23} = 0$. Figure 4.1.2 shows a material element under plane strain loading condition. Equations 4.1.4 and 4.1.5 are expanded from Equation 4.1.3 for plane strain. These two equations and Equation 4.1.6, the shear part, therefore represent the transversely isotropic elasticity model for a material element under plane strain loading conditions.

$$\varepsilon_{22} = 0 = -\nu_{vh}\frac{\sigma_{11}}{\mathbf{E}_v} + \frac{\sigma_{22}}{\mathbf{E}_h} - \nu_{hh}\frac{\sigma_{33}}{\mathbf{E}_h} \qquad \text{(Eq. 4.1.4)}$$

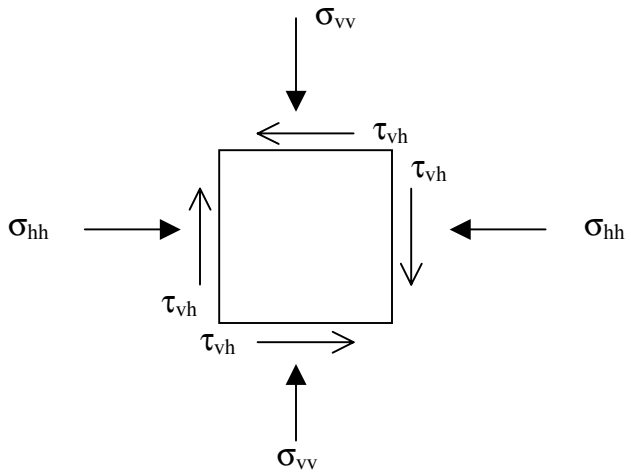

Figure 4.1.2 A material element under plane strain loading condition.

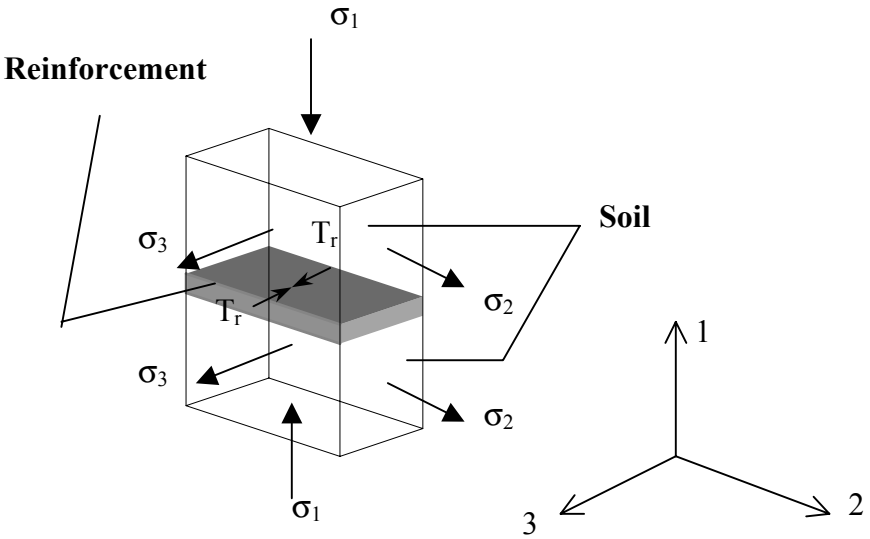

Figure 4.2.1 Stress condition of a reinforced soil composite.

$$\begin{bmatrix} \varepsilon_{11} \\ \varepsilon_{33} \end{bmatrix} = \begin{bmatrix} \left(\frac{1}{E_v} - \frac{\nu_{hv}^{\,2}}{E_h}\right) & \left(\frac{-\nu_{hv} - \nu_{hv}\nu_{hh}}{E_h}\right) \\ \left(\frac{-\nu_{hv} - \nu_{hv}\nu_{hh}}{E_h}\right) & \left(\frac{1}{E_h} - \frac{\nu_{hh}^{\,2}}{E_h}\right) \end{bmatrix} \cdot \begin{bmatrix} \sigma_{11} \\ \sigma_{33} \end{bmatrix} \qquad \text{(Eq. 4.1.5)}$$

$$\mu_{31} = \frac{\tau_{31}}{\gamma_{31}} \qquad \text{(Eq. 4.1.6)}$$

4.2 Stress-Strain Interpretations of a GRS Composite Element

The elasticity theories described in the previous section are only for homogeneous materials. To apply them to obtain moduli of composite materials, composite stresses and strains have to be used in Eqs. 4.1.4 and 4.1.5. In this research, the developed GRS composite model was applied to the UCD test data. A UCD specimen is exactly a reinforced soil composite element under plane strain loading condition (Fig. 4.2.1). In order to obtain the reinforced soil composite moduli, measurements of stresses σ_1, σ_2, and σ_3, and reinforcement tension, T_r have to be interpreted into composite stresses.

As shown in Fig. 4.2.1, pressure σ_1 is the stress applied to the composite element in direction 1. Instrumentation was used to measure the soil stresses σ_2 and σ_3, and the reinforcement tension, T_r. Pressure σ_1 and strain in direction 1 are the stress and strain that the reinforced soil composite element has in direction 1 (Eq. 4.2.1).

$$\sigma_{1comp} = \sigma_1 , \ \varepsilon_{1comp} = \varepsilon_1 \qquad \text{(Eq. 4.2.1)}$$

where ε_1 = the strain of the composite element in direction 1

Direction 2 is the direction that controls the plane strain condition; i.e. there is no strain in direction 2 and the reinforcement tension in that direction is negligible. Therefore, measured pressure σ_2 and strain in direction 2 also can be used as the stress and strain of reinforced soil composite element in direction 2 (Eq.4.2.2).

$$\sigma_{2comp} = \sigma_2 , \ \varepsilon_{2comp} = \varepsilon_2 \qquad \text{(Eq. 4.2.1)}$$

where ε_2 = the strain of the composite element in direction 2

In direction 3, because uniform deformation is controlled, the composite stress can be defined as:

$$\sigma_{3comp} = \frac{F_3}{A_3}$$

where $A_3 = A_{3S} + A_{3G}$, A_{3G} and A_{3S} are the areas of the reinforcement and the soil element in direction 3, and

$F_3 = \sigma_3 \cdot A_{3S} + T_r$, total force in direction 3

Because $A_{3S} >> A_{3G}$, $A_3 \approx A_{3S}$. Therefore stress and strain in direction 3 for the reinforced soil composite are:

$$\sigma_{3comp} = \sigma_3 + \frac{T_r}{A_3} \qquad \text{(Eq. 4.2.3)}$$

$$\varepsilon_{3comp} = \varepsilon_3 \qquad \text{(Eq. 4.2.4)}$$

where A_3 = the area of the composite element in direction 3

ε_3 = the strain of the composite element in direction 3

Equations 4.2.1 to 4.2.4 were used in this research to convert the UCD test data into composite stress and strain information. The composite stress and strain information were introduced into the transversely isotropic material model to solve the composite strength properties of reinforced soil composite (Lee and Holtz, 1998).

Chapter 5
Research Objectives

Objectives of this research include:

1. Develop numerical techniques that are capable of analyzing the performance of GRS retaining structures--Numerical GRS wall models that are able to provide information on the internal stress-strain distribution and external wall performance will be developed.

2. Verify the numerical modeling techniques--To verify the developed numerical modeling techniques, numerical models of GRS retaining structures will be created, and results will be compared to the field instrumentation measurements.

3. Perform parametric studies on internal design factors--The internal stability design factors such as layer spacing, strength properties of geosynthetic reinforcement, and facing stiffnesses will be used as the controlling factors in the parametric studies. The parametric studies will investigate the influence of these design factors on the performance GRS retaining structures.

4. Develop a composite method for internal stress-strain analysis--A composite analytical method that analyzes the stress-strain behavior of GRS in a composite

material concept. Composite strength properties will be obtained by reducing UCD test data and then used as input properties for the composite numerical models of GRS retaining structures.

5. Provide recommendations for improving internal design procedures for GRS retaining structures--At the end of this research, recommendations for improving the internal stability design procedures of GRS retaining structures will be provided.

Chapter 6
Scope of Work

Specific tasks to accomplish the research objectives are outlined in the following paragraphs.

6.1 Development of Numerical Techniques for Analyzing GRS Retaining Structure Performance

The first task of this research was to develop general "rules" (modeling techniques) for performing working stress analyses when utilizing numerical techniques to analyze the performance of GRS retaining structures. In this research, numerical techniques were developed to create models of GRS retaining structures. By using these numerical models, the performance of GRS retaining structures was analyzed. The finite difference computer program, FLAC, was used to develop the numerical models of GRS retaining structures. Numerical models were first created for a 12.6 m high wrapped face GRS wall, the Rainier Avenue wall built in Seattle, Washington. This FLAC model was able to accurately reproduce field instrumentation measurements, and techniques of numerical modeling such as determination of input properties, installation of boundary conditions, and FLAC programming were also developed. Detailed modeling techniques developed in this research are described in Chapter 8. Results of this modeling work are given in Chapter 9.

6.2 Verification of the Developed Modeling Techniques

In order to verify the developed numerical modeling techniques, FLAC models of other GRS retaining structures were also created using the same modeling techniques developed in the previous task. These models were developed to predict performance of other case histories and large scale model tests as well. Purpose of this task was to:

1. Calibrate the modeling techniques using case histories,
2. Update the modeling techniques, and
3. Predict the performance of large scale GRS model wall tests.

6.2.1 Calibration of the Modeling Techniques Using Case Histories

Performance data from a few instrumented GRS retaining structures, including three concrete panel walls, a modular block faced wall, and a wrapped faced wall of the test walls constructed at the FHWA Reinforced Soil Project site at Algonquin, Illinois, were obtained for this task. These performance data were reproduced using the developed modeling techniques. Purpose of this task was to calibrate the developed modeling techniques so that they can be universally applicable.

6.2.2 Update of the Modeling Techniques

Additional modeling techniques were developed when different structures were analyzed, such as those with different facings, different boundary conditions, and different types of surcharging. Models of Algonquin test walls were developed in this

task for developing modeling techniques of wall cases other than wrapped face walls. Modeling techniques have been updated during this task.

6.2.3 Predict the Performance of Large Scale GRS Model Wall Tests

To further verify the developed modeling techniques, numerical models of some large-scale GRS model walls were created. These large-scale GRS model walls were built and tested at the Royal Military College of Canada (RMCC). Large-scale GRS walls tested in laboratory provide advantages of more uniform material properties, better instrumentation measurements, incremental surcharge loading, and simpler boundary conditions. Instrumentation measurements of three large-scale model test walls that were designed to systematically change the internal stability design factors such as layer spacing and reinforcement stiffness were modeled. Class A predictions, predictions made before the completion of wall construction, were performed on two of the test walls to demonstrate the feasibility of the developed modeling techniques. Modeling techniques for determination of material and interfaces properties, and installation of boundary conditions, were further examined. Appropriate adjustments to the modeling techniques and material properties were again made to improve the utility and accuracy of the numerical models of GRS retaining structures.

6.3 Parametric Study on the Internal Design Factors

Another important task of this research was to examine the influence of the internal design factors on the performance of GRS retaining structures. A parametric study was performed on the internal design factors such as layer spacing, ratio of reinforcement length to wall height, soil strength properties, reinforcement strength properties, and facing types.

Two types of parametric analyses were performed in this research. In first type, numerical models developed in previous tasks for modeling the performance of the Rainier Avenue wall and the Algonquin FHWA concrete panel test walls were used as the fundamental models of the parametric study. Major internal stability design factors were systematically introduced into the models. The analyses were performed by varying only one design factor in each group while the other factors were fixed.

The second type of parametric study was performed using a large amount of GRS wall models with different internal stability design factors. Design factors such as layer spacing, soil strength properties, and reinforcement properties were systematically introduced into these models to observe combination effects of design factors.

Hypothetical GRS wall performance factors such as internal stress-strain levels and face deformations were recorded and analyzed in both types of parametric

analyses. The purpose of the parametric study was to obtain a thorough understanding of the influence of the major internal stability design factors on the performance of GRS retaining structures. With a better understanding of the internal design factors, the internal stability analysis and design of the GRS retaining structures are expected to be improved.

6.4 Composite Method for Working Stress-Strain Analysis

In this research, effort was also made to develop a composite method to analyze the stress-strain behavior of the GRS element as well as the performance of GRS retaining structures. The purpose of this part of research was to evaluate the feasibility of using the composite approach to access the working stress-strain information in GRS retaining structures. Moreover, in a real design project, time and cost might limit performing complicated numerical analyses such as developing discrete numerical models. The composite method for a working stress analysis could offer a time saving access to working stress-strain information for preliminary investigations and design if sufficient composite GRS properties were available.

An analytical model that treats the GRS composite as a transversely isotropic homogenous material was developed. This analytical model was then used to reduce GRS composite test data obtained from UCD test results (Boyle, 1995) to obtain the composite properties of GRS. Composite numerical models were then developed using composite GRS properties as the input properties. Since the composite GRS

properties are the only inputs for the composite numerical models, less computation time and iteration processes are expected. Moreover, information on the anisotropy of internal stress distributions of GRS retaining structures was obtained from the results of the composite numerical models as well.

6.5 Improvement of GRS Retaining Wall Design

The development of a practical and accurate design procedure for GRS retaining structure systems was the most important objective of this research. Improved knowledge of the influence of various design factors obtained from the previous tasks was utilized to develop an improved design procedure and performance prediction method for GRS retaining structures. Included was detailed information on modeling techniques, which include determination of soil and geosynthetic properties, determination of properties of interfaces between different materials, and FLAC programming as well.

In the following chapters, the results of the research conducted to meet the stated objectives are presented. Chapter 7 describes the determination of the material properties of GRS retaining structures, while Chapter 8 describes the FLAC techniques used for modeling the performance of GRS retaining structures. Chapter 9 describes the modeling results of existing GRS wall case histories, and Chapter 10 presents the predictions of the performance of the large scale walls tested in the laboratory.

Analytical models used in the parametric analyses are given in Chapter 11, while Chapter 12 presents the results of an extensive parametric study of the internal design factors of GRS walls. Chapter 13 gives a new anisotropic model of GRS composites and its application to perform prediction of GRS retaining structures. Performance prediction methods and design recommendation for GRS retaining structures are presented in Chapter 14, and finally the summary, conclusions, and future research suggestions are presented in Chapter 15.

Chapter 7
Material Properties in GRS Retaining Structures

Successful working stress analyses rely very much on a good understanding of input material properties. Material properties under working conditions must be carefully investigated before performing working stress analyses. Construction materials of GRS retaining structures include backfill soil, geosynthetic reinforcement, and facing units, if any. Properties of these materials vary when different loading, deformation, or confinement conditions are applied. For example, properties such as the friction angle and the elastic modulus of a soil change when different loading conditions are applied; stiffnesses of geosynthetics are affected by the strain rate as well as by confinement.

In this chapter, properties of construction materials under loading conditions that occur inside GRS retaining structures are discussed, and the appropriate selection of these properties for numerical models is described.

7.1 Soil Properties

For soil structures such as retaining walls, long embankments, or slopes, it is appropriate to represent the conditions inside these structures using plane strain loading conditions. Recent GRS retaining structure analyses has also suggested that plane strain soil properties should be used when analyzing the behavior of geosynthetic reinforced walls (Rowe and Ho, 1993; Bathurst, 1993; and Zornberg et

al., 1998). Plane strain strength properties of soil such as friction angle and elastic modulus are different from those properties obtained from traditional soil strength tests such as triaxial and direct shear tests.

Another major concern of soil properties inside GRS retaining structures is the confining pressure. The lateral earth pressure range for retaining walls is relatively low compared to the range of confining pressures that has been commonly reported in soil strength test data. As shown in Table 7.1.1, the typical lateral earth pressure range for walls with heights lower than 10m is only 0 to 100 kPa. Yet very few soil tests have been conducted with confining pressures less than 100kPa.

Effort has been made in this research to characterize the low confining pressure plane strain soil properties, in order to perform accurate working stress analyses of GRS retaining structures. In the following sections, the differences between plane strain loading conditions and triaxial loading conditions are first described. Results of both plane strain and triaxial tests that were performed at low confining pressures are compared. Applications of low confining pressure plane strain soil properties will be discussed as well.

Table 7.1.1 Typical earth pressure range for walls with heights less than 10m.

Depth from top of the wall (m)	Overburden pressure[a] (kPa)	Lateral earth pressure, at rest[b] (kPa)	Active lateral earth pressure[c] (kPa)
1	20	10	6
2	40	20	12
3	60	30	18
4	80	40	24
5	100	50	30
6	120	60	36
7	140	70	42
8	160	80	48
9	180	90	54
10	200	100	60

[a] unit weight of soil was assumed to be 20 kN/m^3.

[b] lateral earth pressure coefficient at rest was assumed to be 0.5 (ϕ = 30 deg)

[c] active lateral earth pressure coefficient was assumed to be 0.3 (ϕ = 30 deg)

7.1.1 Plane Strain Loading Conditions

Plane strain conditions mean that there is no strain in one of the principal directions. For retaining walls, usually the direction parallel to the wall face is assumed to be the direction without strain (or displacement).

Figure 7.1.1 shows a material element under plane strain loading conditions. Compared to a material element under triaxial loading conditions, one of the common loading conditions of soil testing (Figure 7.1.2), there is more confinement in the horizontal directions in plane strain. Plane strain strength properties of soil such as friction angle, cohesion, and elastic modulus should be investigated in order to have accurate material information when performing working stress analyses.

7.1.2 Plane Strain Soil Test Results

In this section, plane strain test results for Ottawa sand and two different granular soils that were the backfill materials of the GRS wall case histories analyzed in this research are presented. Table 7.1.2 presents the prepared density, relative density, and plane strain test device used with these three test materials. Figure 7.1.3 shows the grain size distributions of these three soils.

The plane strain test results of these three soils were also compared to their triaxial test results. The comparison is concentrated on cases in which confining pressures are lower than 100 kPa because, as stated in the beginning of this section, 0 to 100 kPa

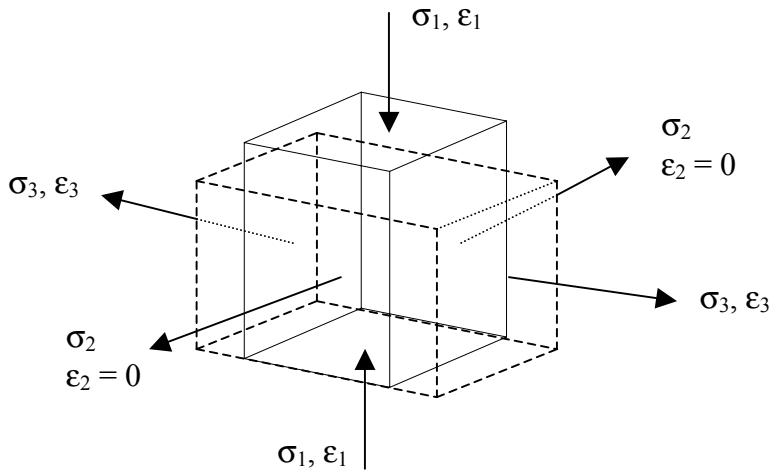

Figure 7.1.1 A material element under plane strain loading conditions.

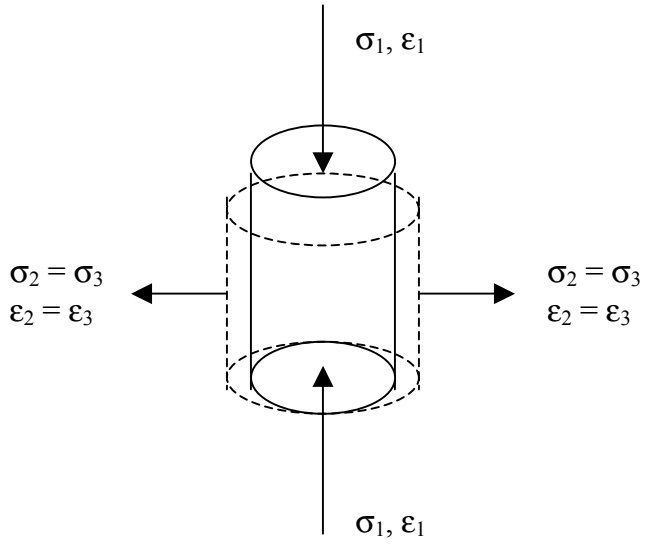

Figure 7.1.2 A material element under typical triaxial loading conditions.

Table 7.1.2 Descriptions of soils tested under plane strain loading conditions.

Name	Description	Tested Density[a] (Relative density)	Plane Strain Test Device
Ottawa Sand	Rounded, uniformly graded,	17.0 kN/m^3 (90%)	UCD (Boyle, 1995)
Rainier Sand	Angular, poorly graded, (Backfill material of the WSDOT Rainier Avenue geotextile wall, Seattle, Washington)	18.0 kN/m^3 (90%)	UCD (Boyle, 1995)
RMC sand	Sub-angular to angular, poorly graded, (Backfill material of large scale test walls tested at Royal Military College of Canada, Kingston, Ontario)	16.4 kN/m^3 (50%)	UC Berkeley plane strain test device (Riemer, 1999)

[a] average density of all specimens tested

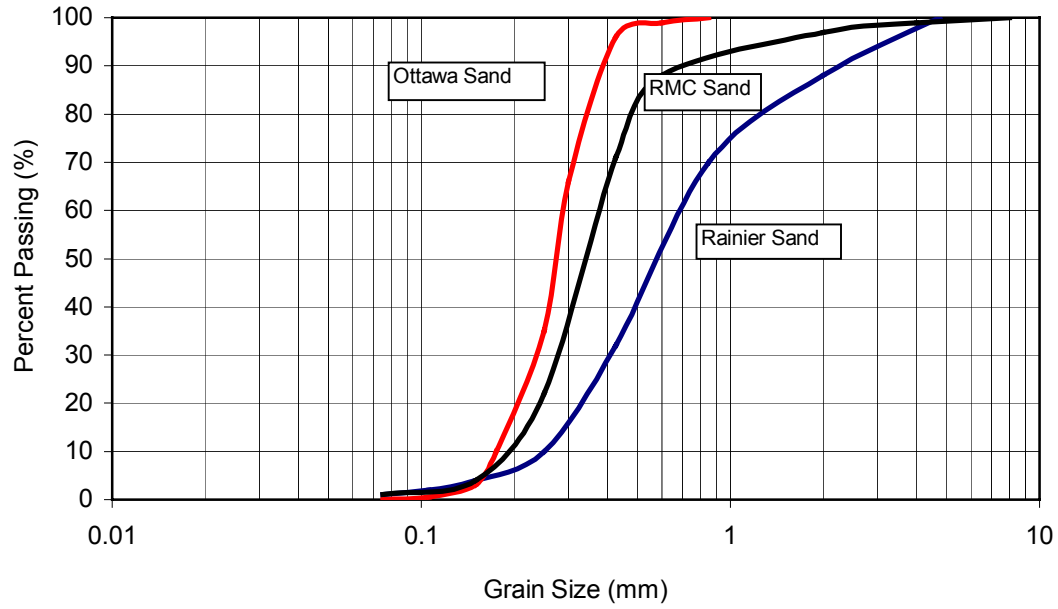

Figure 7.1.3 Grain size distributions of three tested soils.

would be the appropriate lateral earth pressure range for common retaining walls (with heights lower than 10m). Initial moduli, 1% strain secant moduli, and friction angles obtained from both plane strain and triaxial tests were evaluated. The 1% strain secant moduli were chosen because most of the analyzed cases histories showed an average working strain about 1%. Values of the soil initial moduli, 1% strain secant moduli, and friction angles were obtained by analyzing the test data.

Figure 7.1.4 shows the plane strain test results of Ottawa sand (Boyle, 1995). Compared to the triaxial test results shown in Figure 7.1.5a, the plane strain initial moduli were higher about 40% to 80% than the triaxial initial moduli at the confining pressure range tested (less than 100 kPa); yet much less difference was found in the 1% secant moduli for 25 and 50 kPa (Table 7.1.3). Soil friction angles obtained from both plane strain and triaxial tests were very similar (Table 7.1.3).

Figures 7.1.6 and 7.1.7 show the plane strain and triaxial test results respectively of Rainier sand. This sand is more angular than Ottawa sand and was prepared at a high relative density of 90%. Initial moduli obtained from plane strain tests were found to be about seven to eight times the initial moduli obtained from triaxial tests. The 1% strain secant moduli obtained from plane strain tests were about 100% higher than those obtained from triaxial tests at confining pressures lower than 75kPa. Soil friction angles obtained from plane strain tests were also higher than those obtained

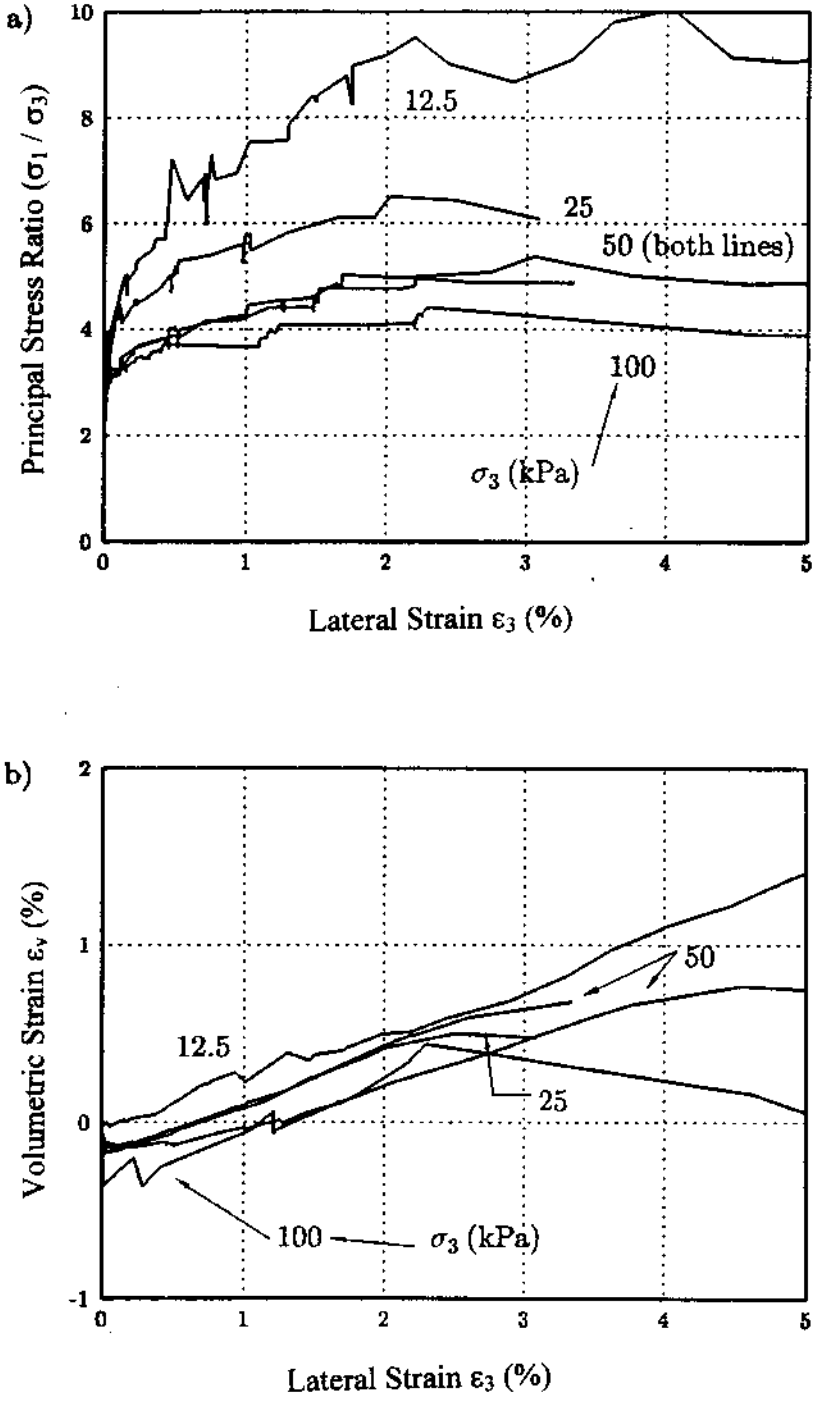

Figure 7.1.4 Plane strain test results for Ottawa sand (Boyle, 1995).

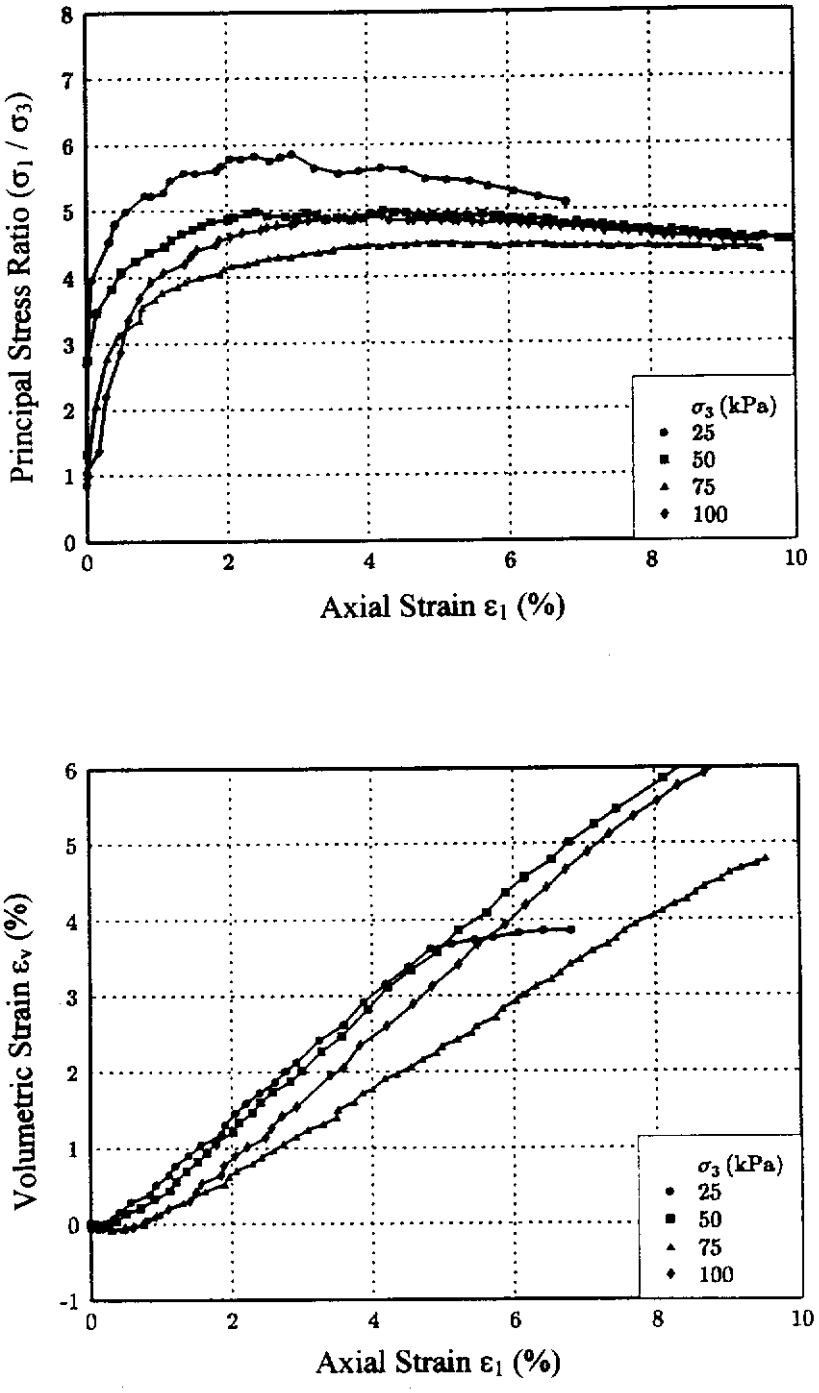

Figure 7.1.5 Triaxial test results for Ottawa sand (Boyle, 1995).

Table 7.1.3 Summary of strength properties of Ottawa sand.

Test Condition (confining pressures)		Initial Modulus, (kN/m^2)	1% Strain Secant Modulus, (kN/m^2)	Friction Angle[1], (deg)
Plane Strain	25 kPa	3.5E+4	1.45E+4	47
	50 kPa	4.0E+4	2.2E+4	42
Triaxial	25 kPa	2.0E+4	1.3E+4	45
	50 kPa	2.8E+4	2.2E+4	42

[1] Calculated using equation $\phi = \mathrm{Sin}^{-1}[(S_r-1)/(S_r+1)]$, where $S_r = (\sigma_1/\sigma_3)$ at peak.

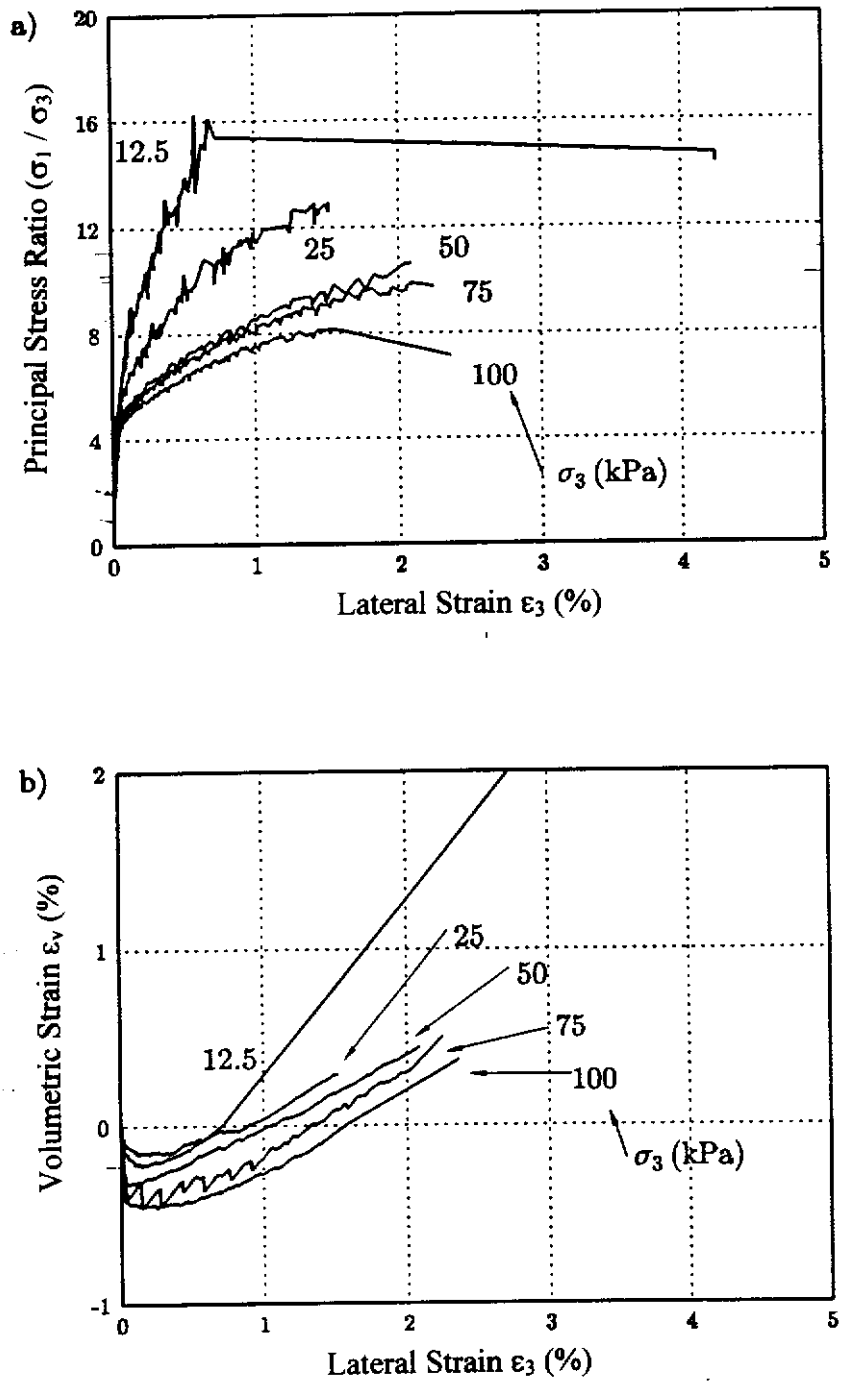

Figure 7.1.6 Plane strain test results for Rainier sand (Boyle, 1995).

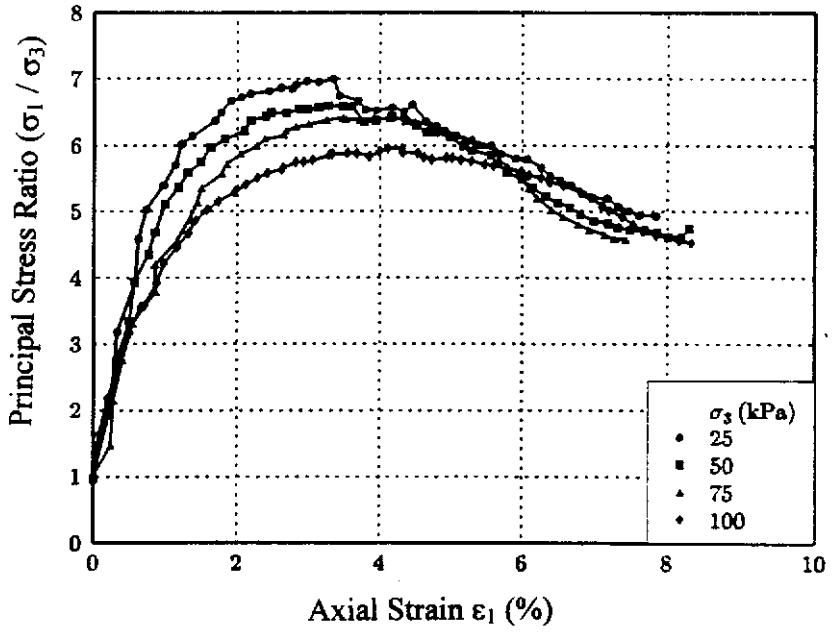

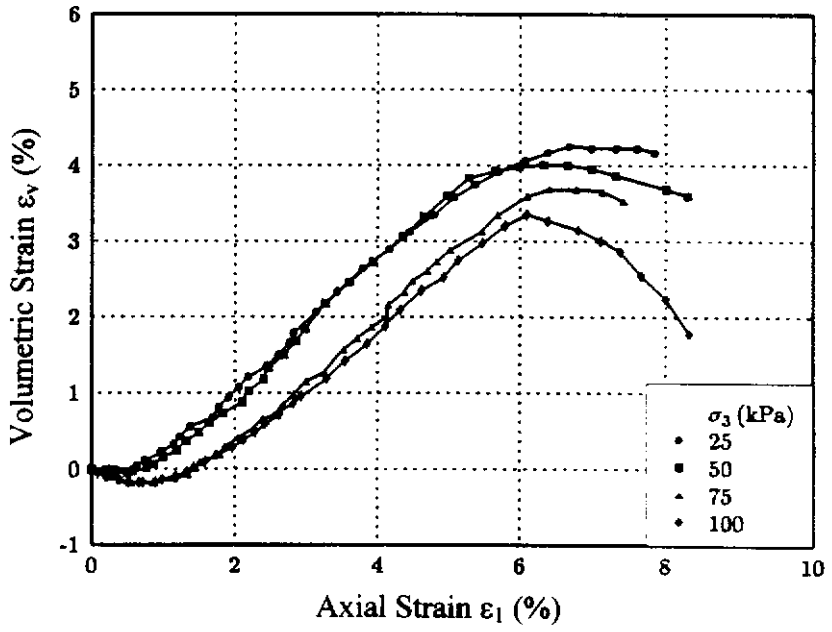

Figure 7.1.7 Triaxial test results for Rainier sand (STS, 1990).

Table 7.1.4 Summary of strength properties of Rainier sand.

Test Condition (confining pressures)		Initial Modulus, (kN/m^2)	1% Strain Secant Modulus, (kN/m^2)	Friction Angle[1], (deg)
Plane Strain	25 kPa	1.2E+5	3.0 E+4	59
	50 kPa	2.5 E+5	4.25 E+4	56
	75 kPa	3.5 E+5	6.0 E+4	55
Triaxial	25 kPa	1.8 E+4	1.4 E+4	49
	50 kPa	3.0E+4	2.5 E+4	47
	75 kPa	4.2 E+4	3.3 E+4	47

[1] Calculated using equation $\phi = \mathrm{Sin}^{-1}[(S_r-1)/(S_r+1)]$, where $S_r = (\sigma_1/\sigma_3)$ at peak.

from triaxial tests (Table 7.1.4). Test results shown in Figures 7.1.6 and 7.1.7 also indicated that, for dense angular materials, the soils tested under plane strain loading conditions tended to reach their peak strength at smaller strains than soils under triaxial loading conditions. Rainier sand reached its peak strength at 0.5% to 1.5% axial strain when plane strain loading conditions were applied, but it did not reach its peak strength until 3% to 4% axial strain when triaxial loading conditions were applied.

Both Ottawa sand and Rainier sand test specimens were prepared at 90% relative density. In order to investigate the plane strain properties of angular material at looser conditions, both plane strain and triaxial tests were performed on RMC sand at a relative density of 50%. As shown in Figures 7.1.8 (plane strain test result) and 7.1.9 (triaxial test result), for angular material at a loose state, the tendency that plane strain soil moduli are higher than triaxial moduli is still observed (Table 7.1.5). The plane strain soil friction angles were also found to be higher than triaxial friction angles at a loose state (Table 7.1.5). Test results shown in Figures 7.1.8 and 7.1.9 also indicated that, even at a loose state, soil under plane strain loading conditions tended to reach its peak strength at a smaller strain than soil under triaxial loading conditions. RMC sand reached its peak strength at 1.5% axial strain for low confining pressures (20 and 30 kPa) and 3% for higher confining pressure (80 kPa) when plane strain loading conditions were applied. However, it did not reach its peak strength until 5% axial strain when triaxial loading conditions were applied.

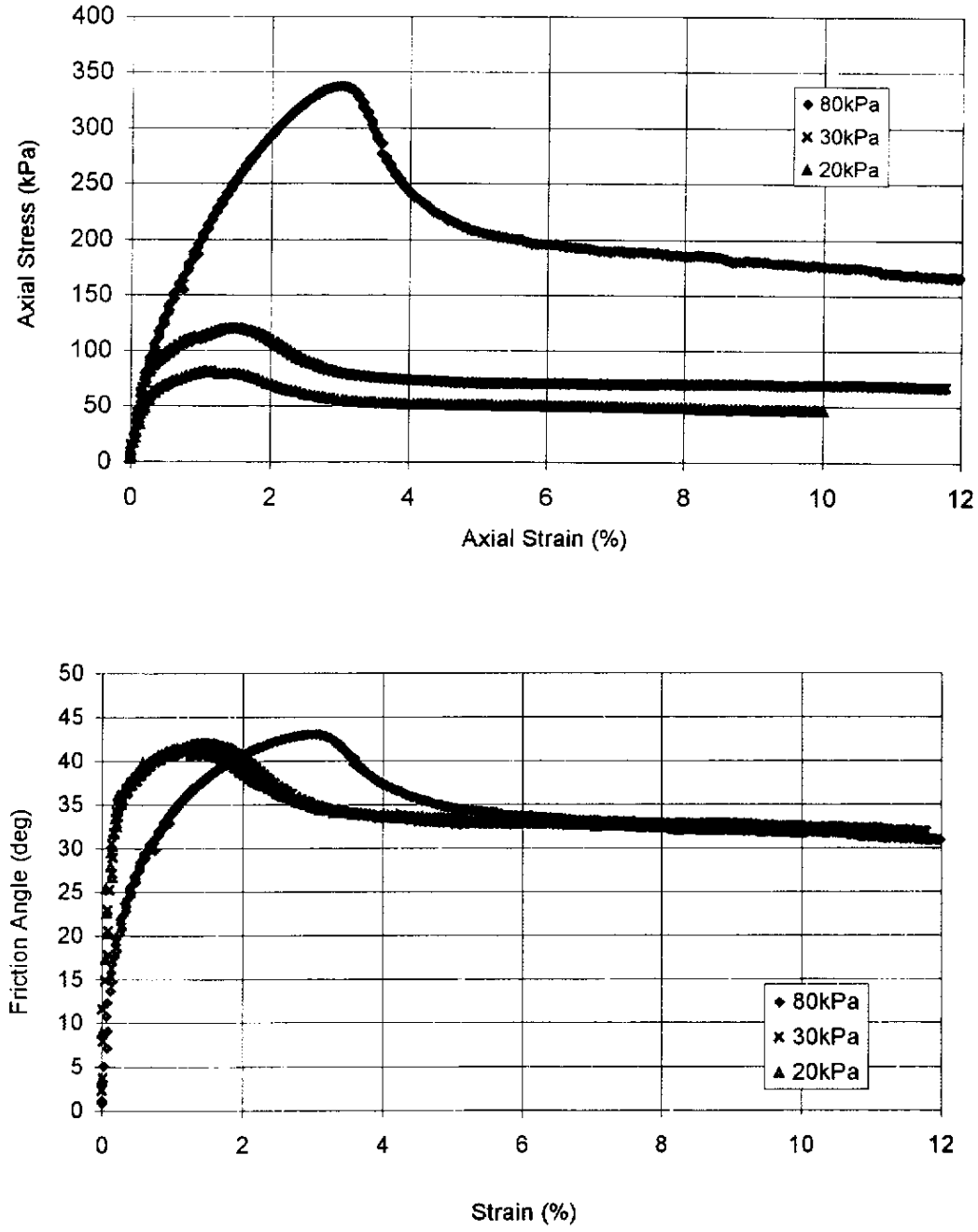

Figure 7.1.8 Plane strain test results for RMC sand (After Riemer, 1999).

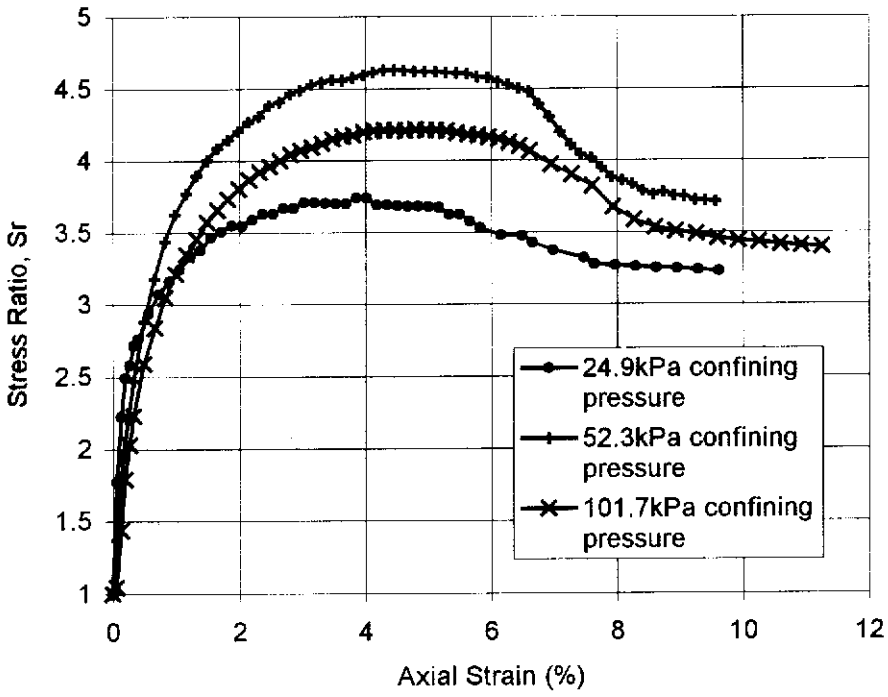

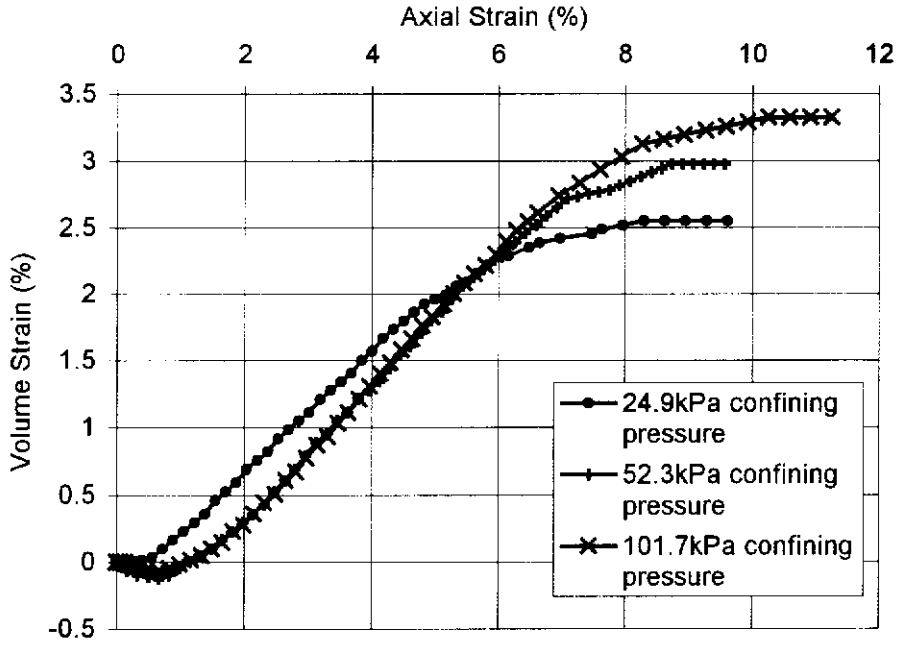

Figure 7.1.9 Triaxial test results for RMC sand (conducted by the author).

Table 7.1.5 Summary of strength properties of RMC sand.

Test Condition (confining pressures)		Initial Modulus, (kN/m^2)	1% Strain Secant Modulus, (kN/m^2)	Friction Angle[1], (deg)
Plane Strain	20 kPa	3.5 E+4	1.5 E+4	41
	30 kPa	4.0 E+4	2.0 E+4	42
	80 kPa	4.0 E+4	3.8 E+4	43
Triaxial	25 kPa	1.3 E+4	0.8 E+4	37
	50 kPa	2.3 E+4	1.8 E+4	38
	100 kPa	3.6 E+4	3.2 E+4	39

[1] Calculated using equation $\phi = \mathrm{Sin}^{-1}[(S_r-1)/(S_r+1)]$, where $S_r = (\sigma_1/\sigma_3)$ at peak.

7.1.3 Summary of Plane Strain Soil Properties

In the following sections, plane strain soil properties of three tested granular soils are summarized. Because testing soils under plane strain conditions is not very common, these test data were also used to examine some empirical relationships that have been proposed to convert conventional triaxial test results to plane strain soil properties.

The plane strain soil friction angles of rounded uniform sand such as Ottawa sand were found to be only slightly higher than triaxial friction angles at low confining pressures. However, for angular material such as the Rainier and RMC sands, the tendency that soils posses a higher friction angle under plane strain conditions than under triaxial conditions is clear. For granular material, Lade and Lee (1976) proposed an empirical equation (Equation 7.1.1) to convert the triaxial friction angle to a plane strain friction angle. Equation 7.1.1 was able to predict the low confining pressure plane strain soil friction angles within a reasonable range (Table 7.1.6). It tends to over-predict the plane strain friction angles of Ottawa sand (rounded sand), and under-predict the plane strain friction angles of Rainier Sand and RMC sand (angular sands) at low confining pressures.

$$\phi_{ps} = 1.5\phi_{tx} - 17^{o} \quad (\phi_{tx} > 34^{o})$$
$$\phi_{ps} = \phi_{tx} \quad (\phi_{tx} \leq 34^{o}) \qquad (7.1.1)$$

where ϕ_{ps} = plane strain soil friction angle, and

ϕ_{tx} = soil friction angle obtained from triaxial tests.

The tendency that plane strain soil moduli are higher than triaxial soil moduli is clearly supported by test data presented in Tables 7.1.3 to 7.1.5. For uniform rounded material like Ottawa sand, its plane strain initial moduli were about 70% higher than triaxial initial moduli. However, its plane strain 1% strain secant moduli were only slightly higher than triaxial 1% strain secant moduli (Table 7.1.3). For angular material in dense state, results of Rainier sand tests indicated that the plane strain initial moduli can be as high as seven times the triaxial initial moduli. Even for the 1% strain secant moduli, the plane strain moduli were still about twice as high as the triaxial moduli (Table 7.1.4). For angular material in loose state, results of RMC sand tests indicated that both initial and 1% strain secant moduli obtained from plane strain tests were about twice as high as those obtained from triaxial tests at low confining pressure range (Table 7.1.5). However, when high confining pressures were applied to RMC sand at a low relative density, a similar tendency could not be found.

To further characterize the plane strain soil moduli, the hyperbolic soil modulus model developed by Duncan and his co-workers (Duncan and Chang, 1970; Duncan et al., 1980) was used in the following section to analyze RMC sand plane strain test data.

7.1.4 Effects of Confining Pressure – Corrected Hyperbolic Soil Modulus Models for Plane Strain Conditions

For geological materials such as soil, stiffness (modulus) is found to increase with increasing confining pressure. Duncan and Chang (1970) developed a hyperbolic soil

Table 7.1.6 Summary of calculated and tested plane strain soil friction angles.

Soil	Confining Pressure (kPa)	Predicted Plane Strain Soil Friction Angle[a] (deg)	Test Results of Plane Strain Soil Friction Angle (deg)
Ottawa Sand	25	50.5	47 [b]
	50	46	42 [b]
Rainier Sand	25	57	59 [b]
	50	54	56 [b]
	75	54	55 [b]
RMC Sand	25/20	39	41 [c]
	50/30	40	42 [c]
	100/80	42	43 [c]

[a] calculated using Equation 7.1.1 (Lade and Lee, 1976).
[b] obtained from soil-only UCD tests (Boyle, 1995).
[c] obtained from plane strain tests (Riemer, 1999).

modulus model for characterizing nonlinear (hyperbolic) stress-strain behavior of soil under different confining stresses. Equation 7.1.3 is the mathematical expression of hyperbolic model of soil tangent modulus (Duncan et al. 1980). It has been extensively used in numerical analyses to simulate the confining stress dependent modulus change of soil. In this research, Eq. 7.1.3 was also programmed by the author into FLAC code to improve the modeling results.

$$E_t = \left[1 - \frac{R_f (1-\sin\phi)(\sigma_1 - \sigma_3)}{2c \cdot \cos\phi + 2\sigma_3 \cdot \sin\phi}\right]^2 \cdot K \cdot P_{atm} \cdot \left(\frac{\sigma_3}{P_{atm}}\right)^n \qquad \text{(Eq. 7.1.3)}$$

where E_t = Young's modulus,

R_f, K, n = model parameters,

P_{atm} = atmospheric pressure,

ϕ = soil friction angle,

c = soil cohesion,

σ_1 = effective vertical (overburden) pressure, and

σ_3 = effective confining pressure

In Equation 7.1.3, model parameters R_f and n are the failure ratio and modulus exponent that define the hyperbolic relation between the soil modulus and confining pressure. K is the modulus number that determines the scale of the soil modulus. The values of R_f, K and n can be determined using stress-strain data obtained from strength tests (Duncan et al., 1980), mostly obtained from triaxial test data. For soil under plane strain loading conditions, the stress-strain relationship is different from that of soil

under triaxial conditions. Therefore, different model parameters should be used to describe the pressure dependent soil modulus under plane strain loading conditions.

Figure 7.1.10 shows the curve fitting result of the triaxial test data of RMC sand (where $R_f = 0.73$, $K = 850$, and $n = 0.5$). Plane strain test data of RMC sand tested at low confining pressures showed a stress-strain curve similar to triaxial test data. To curve fit the plane strain test data, the model parameter K had to be increased to 2000 for best curve fitting result while the other parameters, R_f and n, remained constant (Figure 7.1.11).

Because most of the case histories analyzed in this research (Chapter 9) had only triaxial test data available, the following adjustments to the hyperbolic soil modulus model were used to convert triaxial soil moduli to plane strain soil moduli:

1. Increase the modulus number K obtained from triaxial test data by 100% to account for the large values of the plane strain soil moduli, and

2. Use the same failure ratio (R_f) and modulus exponent (n) obtained from triaxial test. This procedure is based on the observation that plane strain stress-strain curves of soils analyzed in this research had similar shapes as the triaxial stress-strain curves at strain levels less than the peak strain.

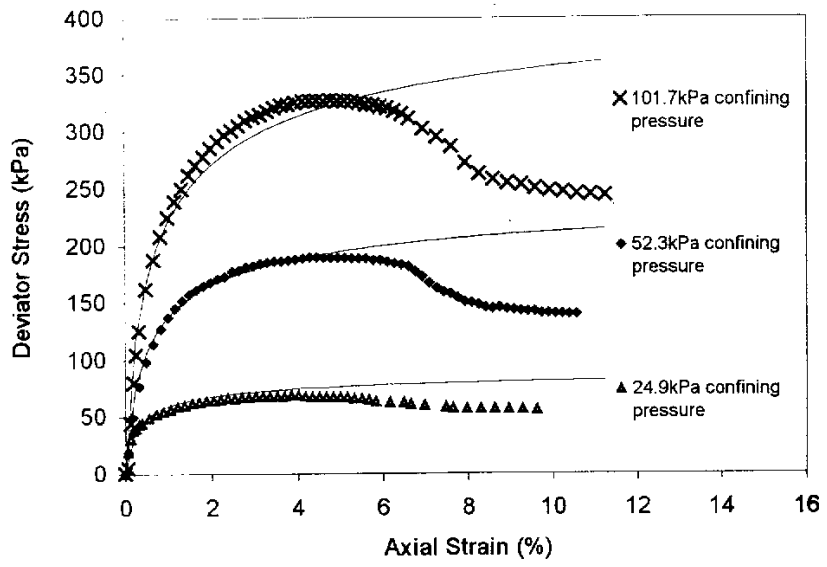

Figure 7.1.10 Hyperbolic curve fitting for triaxial test data of RMC sand (K = 850, R_f = 0.73, n = 0.5).

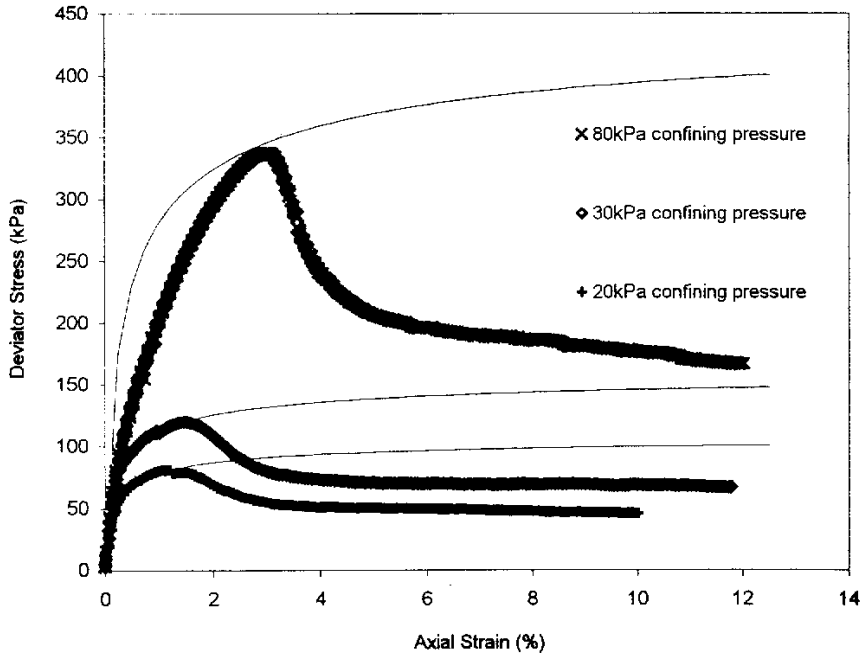

Figure 7.1.11 Hyperbolic curve fitting for plane strain test data of RMC sand(K = 2000, R_f = 0.73, n = 0.5).

7.1.5 Dilation Angle at Low Confining Pressure

Dilation angle is used to describe the change of angle between the failure planes of frictional material to the horizontal plane. The peak shear stresses of dense granular soil will increase with increase of the dilation angle due to their dilative behavior. For performance modeling of poorly designed structures or structures under high surcharge loads, dilation angle of the backfill soil becomes very important, especially when significant yielding occurs in the backfill material.

The definition of dilation angle is given by Equation 7.1.4. Dilation angle of soil can be obtained by performing drained stress-strain tests with volume change measurements.

$$\tan\psi = \frac{\delta\varepsilon_v}{\delta\gamma} \qquad \text{(Eq. 7.1.4)}$$

where ψ = angle of dilation,

ε_v = volumetric strain, and

γ = shear strain.

The dilation angle is often obtained by measuring the slope angles of the linear portion of the volumetric strain versus axial strain curves of drained triaxial test data, for example, in Figures 7.1.5b, 7.1.7b, and 7.1.9b. It can be also estimated from direct shear test data by measuring the maximum upward angle of the vertical displacement versus horizontal displacement curve. Range of typical values of dilation angles were

reported as 10 to 20 deg for granular soil tested at confining pressures higher than 100 kPa (Bolton, 1986). However, dilation angles of granular soil at confining pressures less than 100kPa have apparently not yet been investigated. Table 7.1.7 lists the soil dilation angles of Ottawa sand, Rainier sand and RMC sand at low confining pressures. These values were determined by reducing results shown in Figures 7.1.5b, 7.1.7b and 7.1.9b. Values of soil dilation angles shown in Table 7.1.7 indicated that granular soil at low confining pressures possesses higher dilation angles than those under high confining pressures. For material prepared in a dense state, the low confining pressure dilation angles were as high as 40 degrees. Even for material prepared in loose state, the low confining pressure dilation angles were 26 deg. This observation is very important to working stress analyses of GRS retaining structure analyses because the major portion of wall deflections were observed during the construction stage when confining pressures of backfill soil are very low. Values of soil dilation angles shown in Table 7.1.7 were used as the inputs of the developed numerical models of GRS walls developed in this research.

Table 7.1.7 Summary of low confining pressure dilation angles of granular material.

Soil	Confining Pressure, (kPa)	Dilation Angle, (deg)
Ottawa Sand	25	39
	50	42
	75	39
Rainier Sand	25	34
	50	39
	75	45
RMC Sand	25	26
	50	26
	100	26

7.2 Geosynthetic Reinforcement Properties

7.2.1 Material Types and Structures

Most geosynthetic reinforcements are manufactured using polypropylene, polyester, and polyethylene polymers. Table 7.2.1 lists the index properties of these polymers. Due to these basic polymer differences, geosynthetic reinforcements that are manufactured using different polymers have different mechanical properties, especially, when different loading conditions or environmental conditions such as strain rate and temperature exist.

Fabric structure is another important factor that affects the mechanical properties of various geosynthetic reinforcements. Common geosynthetic structures include nonwoven and woven geotextiles and geogrid structures.

Most of the geotextiles are manufactured using polypropylene and polyester polymers (Table 7.2.1). The woven fabrics are made on conventional textile-weaving machinery into a wide variety of fabric weaves. In contrast, nonwoven fabrics are usually manufactured by heat-bonding or needle-punching the fibers (continuous filaments or long staple fibers) into the geotextile sheets. Details on manufacturing processes and basic properties of geotextiles can be found in Koerner (1998). Generally speaking, woven geotextiles have higher strengths than nonwoven geotextiles because of their structures. For woven geotextiles, multifilament geotextiles have higher tensile strengths than monofilament geotextiles, and monofilament geotextiles have higher tensile strengths than the slit film geotextiles.

Table 7.2.1 Index properties of various polymers used to manufacture geosynthetic reinforcement. (after Koerner, 1998).

Fiber	Breaking Tenacity, g/denier[1]	Specific Gravity	Coefficient of Thermal Expansion, $^{o}F^{-1}$	Melting Temperature, ^{o}F
Polyethylene (High Density)	--	0.96	12.5	230-285
Polypropylene	4.8-7.0	0.91	6.2E-5	325-335
Polyester Regular-Tenacity	4.0-5.0	1.22 or 1.38	4.2E-5 to 4.8E-5	480-550
Polyester High-Tenacity	6.3-9.4	1.22 or 1.38	4.2E-5 to 4.8E-5	480-550

[1] Denier is the equivalent to the grams per 9000 m in the fiber used to make synthetic fabrics.

For nonwoven geotextiles, heat-bonded geotextiles usually have a higher strength than needle punched geotextiles for the same mass per unit area.

The polymer materials used in the manufacture of oriented geogrids are high-density polyethylene, polypropylene or polyester. There are two types of geogrids. Stiff geogrids are made by punching patterned holes into heavy gauge sheets of polyethylene or polypropylene and then drawing the sheets at controlled temperature and strain rate. Flexible geogrids are made by weaving high-tenacity polyester yarns into an open structure with the junctions being knitted together or physically interwined into transverse and longitudinal ribs. Additional information about geogrid types, manufacture, and basic properties can be found in Koerner (1998).

When geosynthetic reinforcement is buried in soil, different types tend to have different interactions with the surrounding soil. Therefore, in-soil properties of geosynthetic reinforcement are often different from their in-isolation properties. Similarly, reinforcement-soil interfaces also are different between different geosynthetic reinforcement.

In the following sections, two important factors that influence the in-soil performance of geosynthetic reinforcement, soil confinement and strain rate, are described. Their effects on the properties of geosynthetic reinforcement inside GRS

structures, as well as appropriate property adjustments to account for these factors, are discussed.

7.2.2 Effect of Soil Confinement

As noted above, when buried in soil, geosynthetic reinforcement may have a very different behavior than it has in isolation. The interactions between the geosynthetics and soil also affect the properties of the geosynthetic reinforcement.

When buried in soil, the loose filament structure of nonwoven geosynthetics tends to be compressed by the soil and also allowes soil particles to enter the spaces in between the filaments. The apparent stiffness of this filament-soil composite then becomes the in-soil stiffness of the nonwoven geotextile. There is strong evidence that nonwoven geotextiles do in fact have greater moduli and strengths when they are confined in soil (McGown et al., 1982; El-Fermaoui and Nowatzki, 1982; Leshchinsky and Field, 1987; Wu and Arabian, 1990; Ling et al., 1992). Results of the UCD tests also indicated that the tensile moduli of nonwoven geosynthetics increased when the geosynthetics were confined in soil (Boyle, 1995). Thus the increase of stiffness of nonwoven geotextiles is controlled by the structure of the geotextile and the confining pressure.

At present, because of difficulty of testing geosynthetic reinforcement in soil, the magnitude of stiffness increase of nonwoven geosynthetic reinforcement has not yet

been well characterized. However, the soil confining effect has to be considered when selecting the tensile modulus for the nonwoven geosynthetic reinforcement.

Soil confinement seems to have minimal effect on the stress-strain behavior of woven geosynthetic or geogrid reinforcements. Boyle (1995) found that the tensile moduli of woven geotextiles were not significantly influenced by confinement in the UCD device. The in-isolation tensile modulus of the woven geosynthetic reinforcement can be used as the in-soil tensile modulus.

No specific in-soil properties of geogrids have been measured. Koerner (1998) commented that the tensile moduli of geogrids are probably not affected very much by confinement based on the in-soil tests of nonwoven and woven geotextiles.

Interaction between soil and geosynthetic reinforcement is another important issue beside the in-soil confinement that needs to be characterized for performing working stress analyses of GRS walls. Holtz (1977) and Jewell (1984) both concluded that the interaction between soil and geosynthetic reinforcement is controlled by the particle size of the surrounding soil and the apertures of the geotextiles or geogrids. For cases that the soil particle is small enough to enter the fabric apertures, the interlocks between soil and geosynthetics allow pullout resistance close to the full shearing resistance of the soil to develop. Results of UCD tests (Boyle, 1995) indicated that the shear surfaces did occur in the soil next to the reinforcement when loading GRS

specimens in the UCD. For GRS wall case histories collected in this research, all backfill soils had a D_{50} less than 1mm (Figure 7.1.3), i.e. most particles of these backfill soils has sizes smaller than the apertures of the reinforcements used in these case histories. Complete interlock between soil particles and geosynthetic reinforcement is assumed. Properties of backfill (internal friction angle and elastic modulus) were used as the interface properties of the geosynthetic reinforcements in this research.

7.2.3 Effect of Strain Rate

Mechanical properties of geosynthetic reinforcement were also found to be affected by the strain rate. Boyle et al. (1996) reported that the moduli of woven geotextiles decreased when they were tested at a low strain rate. Strength properties of geosynthetic reinforcement are often obtained by performing ASTM D 4595 wide width tensile tests. However, the actual rate of loading of the reinforcement in the field during wall construction may be five or six orders of magnitude slower than the standard ASTM D 4595 wide width testing rate of 10%/min. In order to model the working stress conditions inside GRS retaining structures, the moduli of geosynthetic reinforcement had to be adjusted for the low strain rate conditions that really existed during wall construction. Wide width tensile and UCD tests conducted at low strain rates to simulate actual loading rates in full scale structures have indicated that reductions in tensile moduli are needed to account for the slow loading of the reinforcement (Boyle 1995; Boyle at al., 1996; Holtz and Lee, 1998). However,

magnitudes of these modulus reductions are found to be dependent upon following factors:

1. The actual strain rate (rate of loading),
2. The properties of the polymer fibers used in the reinforcement,
3. Structure of the reinforcement,
4. Unit weight of the reinforcement,
5. In-isolation stiffness of the reinforcement, and
6. Temperature.

For nonwoven geotextiles, because of the random filaments and very different index properties between different products, modulus reductions have not yet been clearly characterized. For woven reinforcement made of polypropylene, a 50% reduction of the in-isolation modulus obtained from the wide width tensile test (ASTM D 4595) is recommended as the low strain rate adjustment (Holtz and Lee, 1998). For woven reinforcement made of polyester, a 20% reduction of modulus obtained from the wide width tensile test (ASTM D 4595) is recommended (Holtz and Lee, 1998). For HDPE geogrids, 50% modulus reduction on wide width tensile modulus is recommended (Lee, Holtz, and Allen, 1999).

7.3 Conclusions

In this chapter, soil and geosynthetic properties inside the GRS walls were discussed. Adjustments that convert soil and geosynthetic properties obtained from conventional tests into those inside the GRS walls were also presented. These adjustments can be summarized as:

1. Convert triaxial or direct shear soil friction angles to plane strain soil friction angles using Equations 7.1.1 and 7.1.2;
2. Calculate plane strain soil modulus using the modified hyperbolic soil modulus model;
3. Investigate the appropriate dilation angles of the backfill material;
4. Investigate the effect of soil confinement on reinforcement tensile modulus; and
5. Apply appropriate modulus reduction on reinforcement tensile modulus to account for the low strain rate that occurs during wall construction.

As described in Section 3.4, inaccurate input of material properties was one of the major reasons why no working stress analyses have been successfully performed on GRS walls in the past. Adjustments of material properties summarized above were utilized in this research to model the performance of GRS walls. Successful modeling results were obtained. Detailed descriptions of how these adjustments are implemented in the modeling techniques used for GRS retaining structure performance prediction are presented in Chapter 8.

Chapter 8

Developing Numerical Models of GRS Retaining Structures Using the Computer Program FLAC

In this research, numerical techniques were used to perform the internal stability analyses of GRS retaining structures. A finite difference method based computer program, FLAC (Fast Lagrangian Analysis of Continua), was used to perform working stress analyses for GRS retaining structures. FLAC was selected for this research because of its excellent capability of modeling geotechnical engineering related stability problems and its extended programming ability. Although numerical analyses using FDM usually have longer iteration times than FEM, with the development of high-speed computers, this is not a major shortcoming. Both discrete and composite models were developed using the FLAC program. Moreover, a practical (simplified) calculation method of working stress analyses for GRS retaining structures was also developed after a detailed parametric study was performed on the design factors of GRS retaining structures using FLAC. Details of the development of numerical models using FLAC program are described in this Chapter.

8.1 General Description of FLAC

The FLAC program is a two-dimensional explicit finite difference program developed for mining and civil engineering projects. Large strain behavior such as plastic collapse and flow of structures can be modeled using the explicit, Lagrangian, calculation scheme and the mixed-discretization zoning technique of FLAC (Itasca,

1995). The FLAC program was originally developed for geotechnical and mining engineers. In FLAC, materials are represented by elements whose behavior follows a prescribed linear or non-linear stress/strain law when external forces or boundary restraints are applied. Users can form these material elements into a grid to represent the shape of the modeled object. FLAC also provides a FISH programming code to allow users to define their own constitutive material models. Besides the material models, FLAC also provides some built-in structural elements that can be used as reinforcement or structural supports. These structural elements can be embedded into the grid mesh without any geometric restrictions, and they can be fully incorporated with the surrounding material elements according to their specified built-in interface properties. Another special feature that FLAC provides is interface elements. Interface elements allow FLAC to simulate distinct planes along which slip and/or separation can occur.

Figure 8.1.1 shows a typical section of a GRS retaining structure that was modeled using FLAC. As shown in the figure, elements of elastic material, Mohr-Coulomb material, cable, and interfaces can be used to develop FLAC models of GRS retaining structures. In this research, the transversely isotropic elastic material model within FLAC was also used to develop the composite material approach for GRS retaining structures. In the following sections, specific input properties as well as modeling guidelines for different material models are described. Detailed formulation of these material and structural elements can be found in the FLAC manuals (Itasca, 1995).

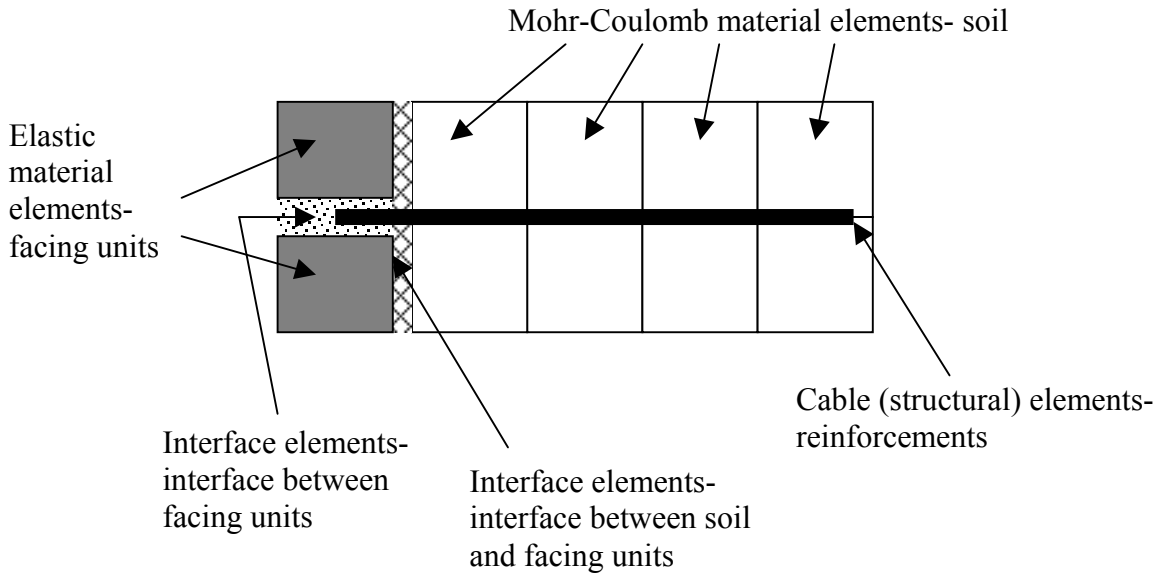

Figure 8.1.1 Typical section of a GRS retaining structure modeled using FLAC.

8.2 Built-in Material Models

In the following sections, the built-in constitutive material models of FLAC program that were used to assemble the numerical models of GRS retaining structures are summarized according to their basic stress-strain behavior, applications in model development, and input properties.

8.2.1 Elastic Material Model

The elastic material model is the model with a linear stress-strain relationship. Elastic material elements were usually used to represent the facing as well as the reaction wall and concrete foundation plate of large scale test walls. Input properties of the elastic material elements were the material density, and the bulk and shear moduli of the material.

8.2.2 Transversely Isotropic Elastic Material Model

Besides the elastic and Mohr-Coulomb material models, the transversely isotropic elastic material model was also used to develop composite GRS retaining structure models. The transversely isotropic elastic material elements allow the user to specify the stress-strain properties (elastic modulus and Poisson's ratio) in two principal directions rather than assign isotropic stress-strain properties. In this research, transversely isotropic elastic material elements were used to describe the transversely isotropic behavior of the GRS composite material.

8.2.3 Mohr-Coulomb Material Model

The Mohr-Coulomb material model is actually an elasto-plastic material model. The Mohr-Coulomb elements are mainly used for the backfill soil of the GRS retaining structures. By adding three more input properties, the friction angle, cohesion and dilation angle, onto the elastic material, the shear failure (plastic yielding) of material can be simulated.

The soil friction angle and cohesion (if any) can be obtained from laboratory soil strength tests such as direct shear tests, triaxial tests, or other appropriate soil strength tests. However, each of these laboratory tests simulates different loading conditions and therefore provides different values of friction angle and cohesion even when the same material is tested. Test results have to be carefully converted to input properties that can accurately represent the real loading conditions inside GRS retaining structures.

Another important input property of Mohr-Coulomb material elements is the dilation angle. The physical meaning of the dilation angle was described in Chapter 7. This input property is very important when larger strain situations are modeled such as structures with large surcharges, structures designed with a low factor of safety, and structures under dynamic loading. The value of the dilation angle can be determined from triaxial or direct shear test data with volumetric measurements. Table 7.1.6 listed values of dilation angles of backfill material analyzed in this research.

Advantages of using the Mohr-Coulomb material model for the backfill includ:

1. The model provids a yielding criteria (failure envelope) similar to the backfill material (soil), and

2. The input properties of Mohr-Coulomb material model can be obtained from regular soil strength tests such as direct shear test and triaxial test.

8.2.4 Pressure Dependent Soil Modulus Model

Because face deflections and other movements have been observed during the construction of real and test GRS walls, it is very important to simulate the wall construction in order to have an accurate prediction of wall performance. During GRS wall construction, the backfill material is placed and compacted layer by layer. The confining pressure of the backfill material is of course very small when each lift is first placed. As the height of the wall increases, the confining pressures in the finished lifts increase. At the end of construction, the lower part of the wall has a higher confining pressure, and the upper part of the wall has lower confining pressure. This confining pressure change of the backfill has a very important effect on the performance of the GRS walls, because moduli of soil are actually pressure dependent, especially for granular soils. Moduli of granular soil increase as the confining pressures increase. In order to include the confining pressure effects on soil modulus during construction, the modified hyperbolic soil modulus model described in Section 7.1.4 was also introduced into the FLAC Mohr-Coulomb material model. Equation 7.1.3 (Duncan et

al., 1980) was programmed as a FISH subroutine that updates the soil moduli according to the stress conditions of the soil elements. Details of the development of this subroutine are described in Section 8.5.4.

8.3 Interface Elements

The FLAC program also provided interface elements to enable the simulation of the contacts between different materials. As shown in Figure 8.1.1, two different types of interfaces were used in a GRS retaining structure model: the interfaces between facing units and the interfaces between soil and structural objects like the wall face. The interface elements were also used to simulate the contacts between the backfill and reaction wall or concrete foundation of the in-laboratory large-scale test walls. Figure 8.3.1 shows the mechanical representation of the interface (Itasca, 1995). In FLAC, the interface element is characterized by Coulomb sliding and/or tensile separation elements. Input properties for the interface elements include friction, cohesion, normal and shear stiffness, and tensile strength. Determination of these input properties for GRS retaining structures is described in Section 8.5.7.

8.4 Cable Element—Structural Elements for Modeling Reinforcements

There are four different forms of structural elements in FLAC: beam, cable, pile, and support elements. Both beam and cable elements can be used to model reinforcements.

Cable elements were chosen in this research to represent the geosynthetic reinforcement because of their ability to provide sufficient information on the

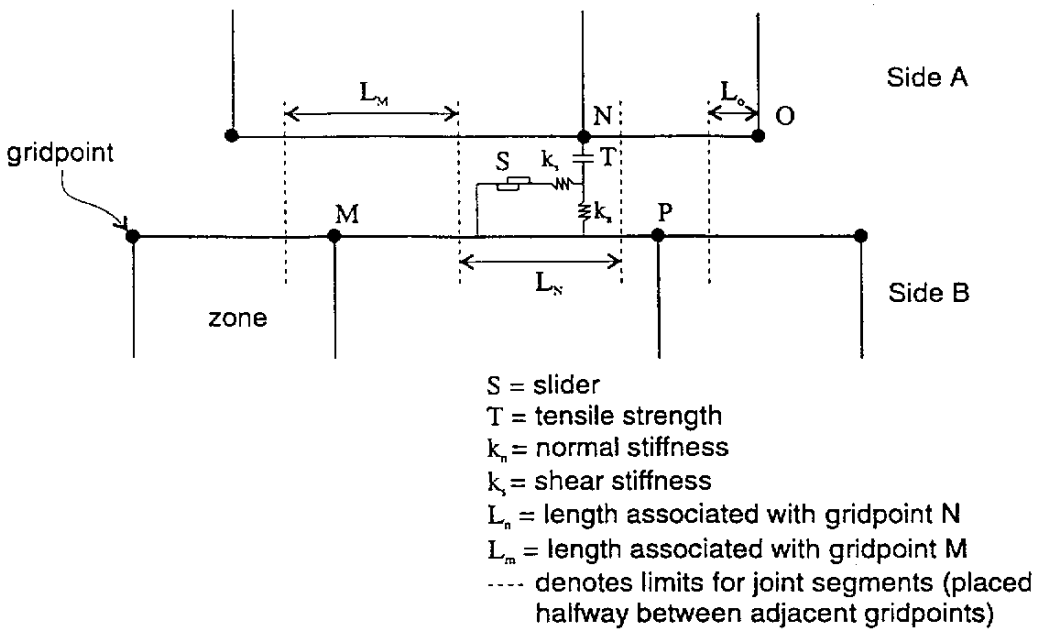

Figure 8.3.1 Mechanical representation of the interface (After Itasca, 1995).

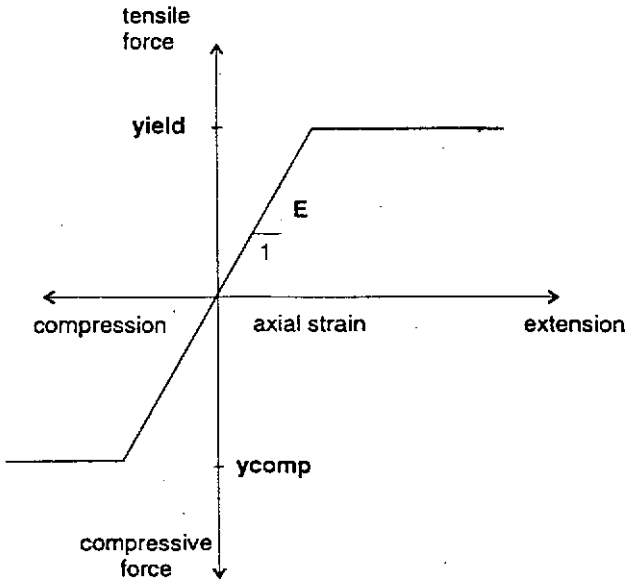

Figure 8.4.1 Material behavior of the cable element.

reinforcement stress-strain distribution, as well as simpler interface input properties and better computational time efficiency than the beam elements. Basically a cable element is made of an axial elastic material element (cable) with interface elements (grout) around it. Yielding limits of both tensile and compressive forces can be assigned to the cable element (Figure 8.4.1). When utilizing the cable element to simulate the geosynthetic reinforcement, properties of the interfaces between soil and reinforcement were used as interface properties that were originally used to describe the bonding of in-situ reinforcements such as soil nails or grouted rock bolts. Although, by definition, the cable elements are one-dimensional axial elements, they can still be used to represent planar reinforcement such as geosynthetic reinforcement when they are used in a two-dimensional analysis. The advantages of using cable elements are a simple geometry, direct axial stress-strain information, and computational time savings. Details of input property determination for cable elements are described in Section 8.5.5.

8.5 Techniques Used to Develop Numerical Models for Analyzing the Performance of GRS Retaining Structures

One of the major tasks of this research was to develop "general rules" or universal modeling techniques for the working stress analysis of GRS retaining structures. Throughout this project, techniques for model generation, boundary condition setup, determination and arrangement of construction materials and interfaces, and data reduction were developed. Key technical aspects of these modeling techniques are

summarized in this section. These comments were described in terms familiar to a FLAC program user; therefore, terminology and programming techniques of FLAC are used. Detailed information on the terminology and basic programming commands of FLAC are described in the FLAC manuals (Itasca, 1995).

8.5.1 Model Generation

1. Four kinds of material elements described in the previous sections, elastic material elements, Mohr-Coulomb material elements, structure (cable) elements, and interface elements, were used to create models of GRS retaining structures.
   1.1 Elastic material elements were used to represent the material with higher strength and a linear stress-strain behavior under working stresses. They were used to represent different facing materials such as precast concrete panels, modular blocks, or rock-filled gabion baskets. They were also used to represent the concrete foundation and the reaction wall of the large-scale test walls built in the laboratory (Chapter 10).
   1.2 Mohr-Coulomb material elements were used to represent the soil, including the backfill and foundations of GRS retaining structures.
   1.3 Cable elements were used to represent the geosynthetic reinforcement.
   1.4 Interface elements were used to describe the interaction between different materials or the discontinuities between the same materials such as interfaces between backfill soil and structural facing, and interfaces between structural facing units.

2. When setting up the grids for FLAC models of GRS retaining structures, at least three rows of soil elements should be inserted in between reinforcement layers. This technique allows users to observe the interaction between the reinforced composite layer (soil elements with reinforcement elements attaching to their nodes) and the soil-only layer.

3. An aspect ratio of 0.5 to 2 is recommended for elements within the reinforced zone (the aspect ratio is the ratio of the height to the length of the element). In FLAC, the aspect ratio is limited to a range of 0.2 to 5. Having an aspect ratio close to a value of one helps not only to reduce the iteration time, but it also ensures stress or strain equilibrium inside the elements when the stress ratio limit is set for the equilibrium criteria. The disadvantage of using aspect ratios close to one is that the number of total elements increases considerably when the size of the modeling object is large or when the reinforcement layout of the modeling project is complicated.

4. The program command that allows large strain calculations has to be used in order to allow for post-yielding behavior to occur in material elements, especially in the backfill material. This technique helps the designer to identify the high stress-strain zones, including a failure surface, if any, inside the modeling structure

especially when the structure is poorly designed. FLAC program command to allow large strains to occur is "**set large**" [1].

8.5.2 Boundary Conditions

In numerical analyses, the boundary conditions have to be carefully set up to avoid any artificial reaction forces or deformations to occur. The following recommendations are for static analyses of GRS retaining structures only. Boundary condition criteria must be carefully investigated if dynamic analyses are performed.

1. The unreinforced backfill of the GRS retaining structure models should be extended a distance equal to at least the length of "reinforced zone" to eliminate boundary effects. For cases in which the reinforced backfill has an irregular shape or intersects bedrock, the actual boundary conditions should be modeled.

2. To eliminate boundary effects, the foundation part of the GRS retaining structure models should be extended to a depth at least equal to the height of the GRS wall or to bedrock. However, when the settlement of the GRS retaining structure is a major issue, the foundation soil should be extended to a depth that would cover all the compressible soil layers that might contribute to the total settlement of the structure.

[1] Bold words are the commands or symbols used in FLAC

3. For the portion in front of the wall face, as with the unreinforced backfill, an irregular shape or shorter length boundary has to be modeled. Otherwise, the horizontal boundary in front of the wall face should be extended at least equal to the length of reinforcement to eliminate boundary effects.

4. When developing numerical models of laboratory-scale test walls, the boundary conditions of the test facilities such as the reaction wall, the concrete foundation, and any toe restraints have to be carefully set up. (In Chapter 10, the difference between laboratory test walls and real walls is discussed and summarized, based on results of numerical models with different boundary conditions.)

8.5.3 Equilibrium Criteria

With FLAC. to ensure that the results of the numerical analysis have converged and that the unbalanced forces within individual material elements have been minimized, it is necessary to set up equilibrium criteria.

Within FLAC, users can set limits on the unbalanced force and/or stress ratio of the material elements as the equilibrium criteria. Each grid point in the FLAC model is surrounded by up to four material elements. The algebraic sum of forces contributed by these surrounding elements at any specific grid point should converge to zero when the model reaches equilibrium. This algebraic sum of forces acting on the grid point is defined as the unbalanced force. In FLAC analyses, users can define equilibrium

criteria by setting limits on the unbalance forces. However, these forces are calculated by multiplying the stresses within the elements by the element lengths perpendicular to the forces. Small values of unbalanced forces might not indicate a converging equilibrium result when models have very small grid sizes.

The stress ratio is defined as the ratio of maximum unbalanced force to the representative internal force. The grid size is no longer a factor that affects the equilibrium convergence when stress ratio is used to set up the equilibrium criteria. In this research, a stress ratio less than 0.01 was used as the equilibrium criteria for intermediate stages (during wall construction) and stress ratio less than 0.001 was used as the equilibrium criteria for final stages (after construction, and after surcharges).

8.5.4 Hyperbolic Soil Modulus Model

As described in Section 8.2.3, the hyperbolic soil modulus model was used to simulate the change of soil modulus due to confining pressure change during wall construction. In this research, a FISH subroutine was developed to update the moduli of Mohr-Coulomb material (soil) elements automatically according to the change of the confining pressure. This subroutine was edited based on the hyperbolic soil modulus model (Equation 7.1.3). Example 8.5.1 shows the FLAC code of this subroutine. In Example 8.5.1, the area that needs this modulus adjustment is defined by parameters vi, vf, hi, and hf. **Bulk_mod(i,j)** and **Shear_mod(i,j)** are bulk and shear moduli of the element defined by horizontal grid number **i** and vertical grid number **j**. **nu** is the

Example 8.5.1 FISH subroutine for updating soil modulus according the confining pressure – Hyperbolic soil modulus model.

```
*************************************************************************
        def janbu2
          loop j (vi,vf)
            loop i (hi,hf)
              temp1=-0.5*(sxx(i,j)+syy(i,j))
              temp2=sqrt(sxy(i,j)^2+0.25*(sxx(i,j)-syy(i,j))^2)
              sigma3=min(temp1-temp2, -szz(i,j))
              if sigma3<0 then
                sigma3=0.0
              end_if
              sl=max(temp1+temp2, -szz(i,j))
              sl=0.5*(sl-sigma3)*(1-sin(fri*degrad))
              sl=sl/(coh*cos(fri*degrad)+sigma3*sin(fri*degrad))
              ela=(1-rf*sl)^2*k1*pat*(sigma3/pat)^nd
              bulk_mod(i,j)=ela/(3*(1-2*nu))
              shear_mod(i,j)=ela/(2*(1.0+nu))
            end_loop
          end_loop
        end
*************************************************************************
        def supstep
          janbu
          command
            step 100
          end_command
        end
*************************************************************************
        def supsolve
          loop kk(1,10)
          supstep
          end_loop
        end
*************************************************************************
        set fric=45 coh=0 nu=0.25
        set k1=2000 rf=0.73 nd=0.5
        set pat=101.3
*************************************************************************
```

Poisson's ratio of the backfill material. As described in Section 7.1.4, the model parameters **k1**, **rf**, and **nd** have to be modified for plane strain loading conditions when using this subroutine to model structures like GRS retaining walls.

8.5.5 Determination of Reinforcement Input Properties

Input properties of cable elements can be divided into two categories: the strength properties and geometric properties. The strength properties include:

1. Elastic modulus (**e**),
2. Tensile (**yield**) and compressive (**ycomp**) yield strengths, and
3. Stiffness (**kbond**), cohesive strength (**sbond**), and friction resistance (**sfric**) of the interface.

The geometric properties include:

1. Cross-sectional area (**a**), and
2. Exposed perimeter (**peri**).

Input properties of the cable elements were computed by assuming the cable elements have an out-of-plane depth of unity. This interpretation was verified when the model was able to reproduce the shear resistance developed along the reinforcement of real GRS walls. The FLAC models were not sensitive to the in-soil thickness of the cable elements. To convert the planar strength properties of geosynthetics, an arbitrary yet reasonable in-soil thickness was assumed. In this research, the in-soil thickness of

geosynthetic reinforcements was set to an arbitrary and convenient 5 mm. However, once the in-soil thickness has been decided, the cross sectional area, elastic modulus, and perimeter of the cable element has to be calculated using the same in-soil thickness. Example 8.5.2 is an example of input property determination of cable elements (geosynthetic reinforcement).

In this research, the assumption was made that no slippage occurred between the soil and the geosynthetic reinforcement, because almost no pullout failures were observed in any of the analyzed case histories. Therefore, cable elements were fixed to the nodes of the Mohr-Coulomb material elements to avoid violation of compatibility. Experiences from previous modeling studies indicated that soil elements tend to "penetrate" the cable element and cause inaccurate stress and strain information when the model had large deformations and the cable elements were not fixed to the nodes of the material elements. There is no need to input values of **kbond**, **sbond**, and **sfric** (properties of the interface) when cable elements are fixed to the nodes of the material elements because perfect bonding between cable and soil is assumed.

8.5.6 Arrangement of Reinforcement

In all the numerical models presented in this dissertation, the reinforcement (cable) elements were attached to the nodes of the material elements. This technique was used to avoid the violation of strain compatibility, such as when soil elements penetrate the cable elements at large strains (Figure 8.5.1). However, this technique (attaching the

Example 8.5.2 Input property determination of cable elements.

****

Given: Geosynthetic (geogrid) reinforcement stiffness obtained from wide width tensile test at 2% strain, $J_{wwt,2\%}$ =100 kN/m, and ultimate tensile strength T_{ult} = 12 kN/m.

Calculation:

Low strain rate reinforcement stiffness ($J_{2\%}$) for geogrid:

$$J_{2\%} = 50\% \cdot J_{wwt,2\%} = 50 \text{ kN/m}$$

where 50% reduction is the low strain rate stiffness reduction for geogrid (Chapter 7)

Assume in-soil thickness of reinforcement, t = 0.005m

$$\mathbf{e} = \frac{J_{2\%}}{t} = 10{,}000 \text{ kN/m}^2$$

Tensile and compression yielding limits are:

$$\mathbf{yield} = T_{ult} \cdot 1\text{m} = 12 \text{ kN}$$

A small value, for example, 10Pa, is suggested as the compression limit (**ycomp**) when cable elements are used to model geosynthetic reinforcement.

Area and exposed perimeter of cable elements are:

$$\mathbf{a} = t \cdot 1 = 0.005\text{m}^2$$

$$\mathbf{peri} = 2 \cdot (1 + t) \approx 2\text{m}$$

****

cable elements to the nodes of the material) tended to over-predict the reinforcement tension near the faces of the GRS walls because no relative movements were allowed to occur in between the material and cable elements (Figure 8.5.1). For example, numerical models of wrapped face walls tended to predict the peak reinforcement tension at the wall face because soil elements near the wall face had high deflections; however, very small reinforcement strains (tensions) were observed at the face of the wrapped face wall in the field.

Moreover, reinforcement tensions at connections of GRS walls with structural facing systems were also over-predicted by using this technique because the cable elements moved with soil element without any slippage (Figure 8.5.1).

GRS wall models without fixing cable elements to the material element nodes were also developed in this research. Properties of the backfill soil at the same levels of the modeled reinforcement layer were used as interface properties of the reinforcement element when the cable elements were not attached to the material element nodes. Results of these models tended to predict smaller reinforcement tensions than when cable elements were attached to material element nodes. For the cases studied in this research, prediction of these (unfixed) models appears to be closer to the instrumentation measurements. Equation 8.5.1 shows the general relations between reinforcement tension predictions made by models with different cable element arrangements. Values of coefficient a in Equation 8.5.1 were the average

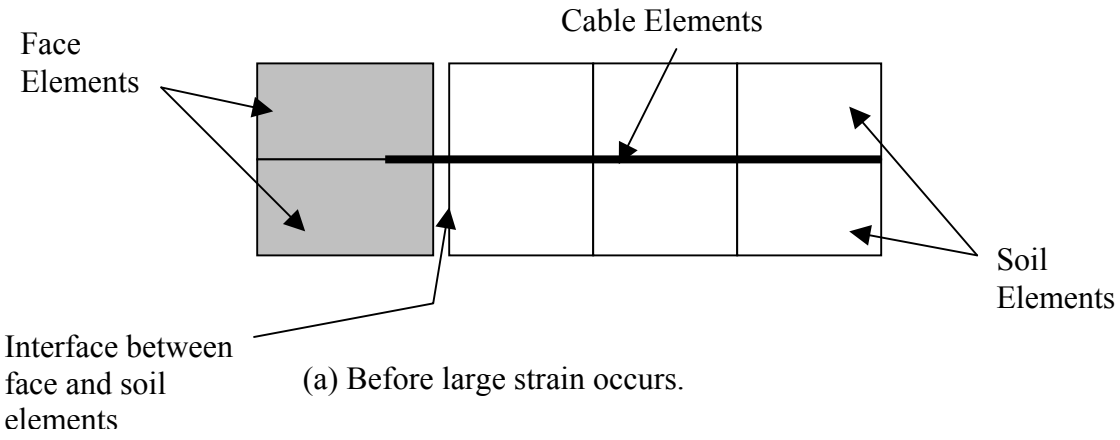

(a) Before large strain occurs.

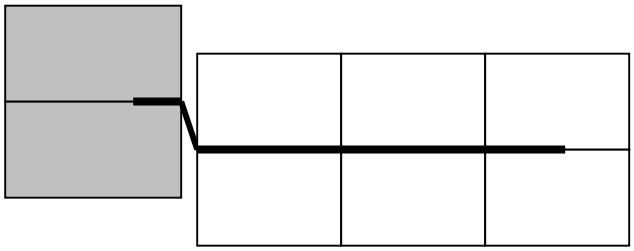

(b) After large strain occurred.

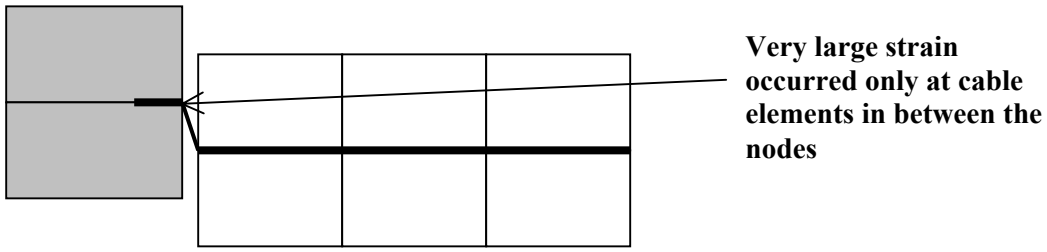

(c) Cable elements were attached to the nodes.

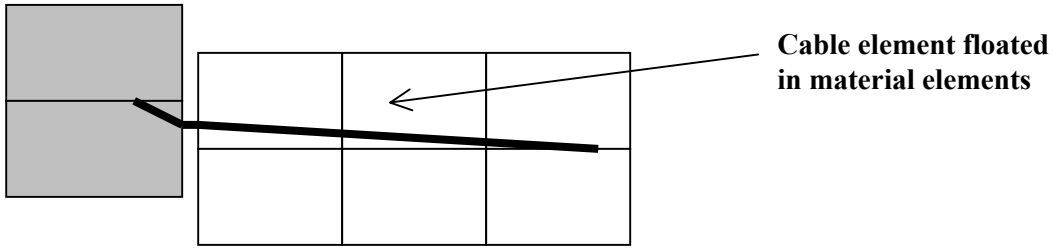

(d) Cable elements were not attached to the nodes.

Figure 8.5.1 Effects of attaching cable elements to the material element nodes.

ratios of reinforcement tensions predicted by models in which cable elements were not attached to material element nodes to reinforcement tensions predicted by models in which cable elements were attached to material element nodes. Equation 8.5.1 was used to adjust the prediction of the model developed to predict the performance of the GRS walls (Chapter 14).

$$T_{uf} = a \cdot T_f \qquad \text{(Eq. 8.5.1)}$$

where T_{uf} = reinforcement tensions were obtained from models in which cable elements were not attached to material element nodes,

a = 0.6 at the connections of walls with structural facing systems or at the face of the wrapped face walls,

= 0.8 reinforcement elements inside the backfill, and

T_f = reinforcement tensions were obtained from models in which cable elements were attached to material element nodes.

Example 8.5.4 shows two FISH subroutines **Hrein** and **Vrein** that can automatically attach cable elements to the material element nodes. **Hrein** is used to assign the horizontal member of the reinforcement elements, and **Vrein** is used to assign the vertical member. Users only have to input the beginning node (**Rbeg**) and the ending node (**Rend**) of the cable elements; these two subroutines will attach the cable elements to every material element node in between the beginning and ending nodes. Input parameters **v0** and **h0** are the location nodes for vertical and horizontal

Example 8.5.4 FISH subroutines for attaching cable elements to material element nodes.

```
**********************************************************************
        def Hrein
          h1=Rbeg
          Rend=Rend-1
          f1=f1
          v0=v0
          loop i (Rbeg,Rend)
            h2=h1+1
            command
            struct cable begin grid h1,v0 end grid h2,v0 seg=1 pr=f1
            end_command
            h1=h2
          end_loop
        end
**********************************************************************
        set vo= Rbeg= Rend=
**********************************************************************
        def Vrein
          v1=Rbeg
          Rend=Rend-1
          f1=f1
          h0=h0
          loop j (Rbeg,Rend)
            v2=v1+1
            command
            struct cable begin grid h0,v1 end grid h0,v2 seg=1 pr=f1
            end_command
            v1=v2
          end_loop
        end
**********************************************************************
        set ho= Rbeg= Rend=
**********************************************************************
```

members of the reinforcement elements.

8.5.7 Facing Systems

Three common facing systems were modeled in this research:

1. Fabric wrapped face--Geosynthetic reinforcement is wrapped around and tucked back into the backfill at the wall face. No structural facing units are used.
2. Concrete panel face--Pre-cast concrete panels are used as the structural facing units for wall face. The concrete panels and reinforcement are connected by pre-casting a small portion of the reinforcement in the concrete panels and then connecting this portion to the main reinforcement when the concrete panels are placed in position.

3. Modular block facing--Modular (pre-cast concrete) blocks are used as the structural facing units of wall face. Geosynthetic reinforcement is inserted and fixed in between the blocks by steel or polymer pins, clamping in block wedges or lips, or just relying on the friction between blocks and friction of the gravel material filled in the block units.

The fabric wrapped faced GRS retaining walls were the least complicated systems modeled in this research, because no elastic material elements or the interface elements were necessary to model this type of GRS wall. For GRS walls with

structural facing systems such as concrete panels and modular block facings, additional elastic material elements were used to represent these structural units; interface elements were also used to simulate the interaction between elements of different materials.

Figure 8.5.2 shows a typical section of concrete panel GRS walls modeled using FLAC. Elastic material elements were used to represent the concrete panel facing units. Interfaces were also inserted between the Mohr-Coulomb material elements (soil) and the elastic material elements. Properties of the concrete panel facing units were determined using properties of typical concrete material if manufacturing information was not available. Properties of concrete were also assigned as the interface properties (**kbond**, **sbond**, and **sfric**) of cable elements that were cast inside the elastic material elements to simulate the bonding between the geosynthetic reinforcements and the concrete panels. Details of property determination and arrangement of interface elements that were inserted in between elastic and Mohr-Coulomb material elements are described in the following section. The concrete panels can be either large panels cast to full wall height or discrete panels assembled to full wall height. Additional support member elements, which are structural elements used to connect two separate material elements, were inserted in between some elastic material elements to represent the mechanical joints of the discrete panel system.

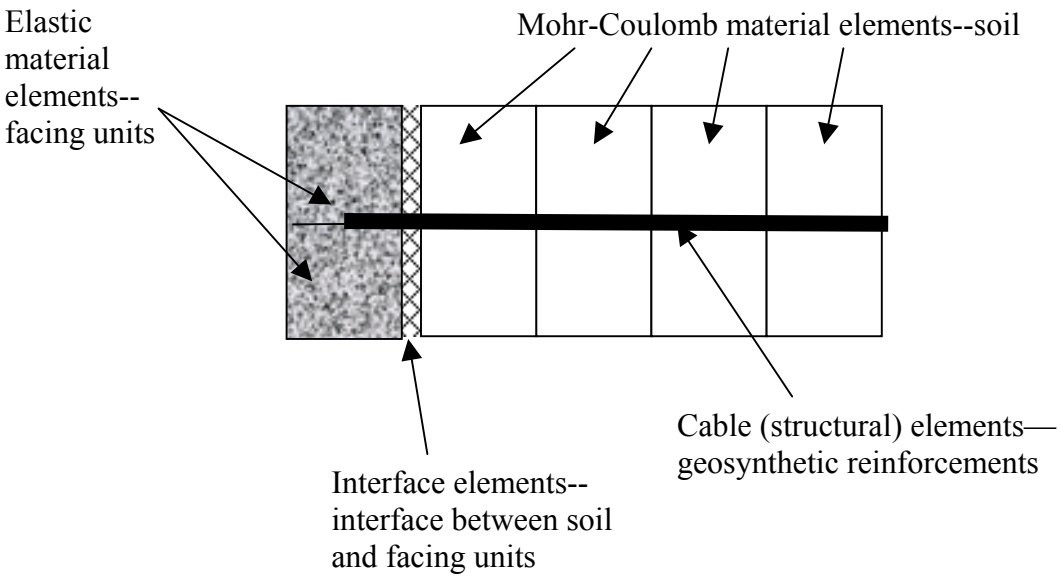

Figure 8.5.2 Typical section of concrete panel GRS walls modeled using FLAC.

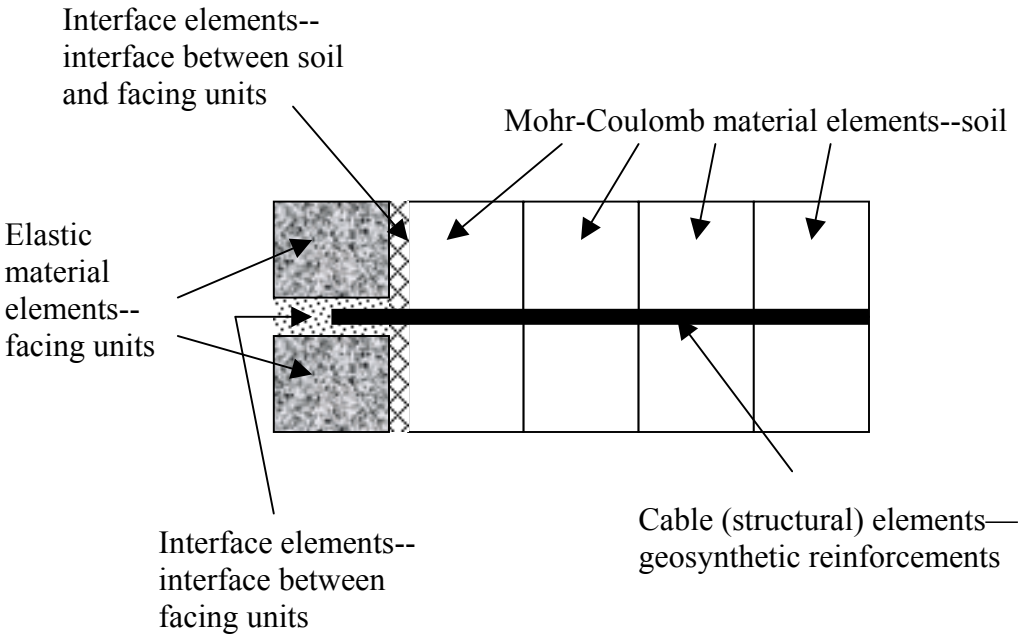

Figure 8.5.3 Typical section of modular block GRS walls modeled using FLAC.

Similar techniques to those used in models of concrete panel GRS walls were also used to develop modular block GRS walls. As shown in Figure 8.5.3, a similar material and interface element set up was used to develop models of modular block GRS walls. Additional interface elements were inserted between every elastic material element to simulate the interactions between individual blocks. Interface properties of cable elements that were placed between the elastic material elements (modular blocks) were determined based on how the reinforcement was fixed in between the blocks. In this research, the connection strength of each block system obtained from the manufacturing information or laboratory connection test results were used to interpret the interface properties of cable elements located in the area between blocks. Details of property determination and arrangement of interface elements that were inserted in between elastic and Mohr-Coulomb material elements are described in the following section.

8.5.8 Input Property Determination and Arrangement of Interfaces

As described in the previous section, three different interfaces were used when developing FLAC models for GRS walls with different structural facing systems:

1. Interface between concrete material and soil – this type of interface was used at the boundaries of soil and concrete panels, or soil and the concrete reaction wall of test walls;
2. Interface between modular block facing and soil; and

3. Interface between modular block and block.

The input properties of interface elements in FLAC include:

1. Normal stiffness, **kn**
2. Shearing stiffness, **ks**
3. Friction, **fric**
4. Cohesion, **coh**

In this research, the normal stiffness of all interfaces were assigned with a value at least ten times the stiffness of the materials that were connected by the interfaces. This modeling technique was used to avoid material elements penetrating the interfaces and causing numerical instability. Cohesion was not assigned to the interfaces between the facing units and backfill soil because backfill materials analyzed in this research were all cohesionless.

For the interface elements between soil and concrete material, such as concrete panels and the reaction wall of test walls, a friction angle equal to two-thirds of the plane strain soil friction angle and moduli equal to the moduli of the soil at the same stress level were used. The determination of wall friction angle (two-thirds of the plane strain soil friction angle) was based on the typical wall friction angle between concrete wall and coarse sand (Fang, 1991, Chapter 12). In this research, numerical models that had interfaces with friction angles equal to the full plane strain soil friction angles were also analyzed. Results of these models were found to be very

similar to models that used two-thirds of the plane strain soil friction angles as the interface friction angles.

Modular block facing systems are more flexible than concrete panel systems. Moreover, modular block facing systems have increased interaction with the backfill because the blocks are usually set up with a certain setback between blocks that forms a stepped contact surface between blocks and the backfill soil. Therefore properties of interfaces between modular blocks and soil are expected to be different than the interface properties of concrete panel facing systems. Burgess (1999) back-calculated the vertical drag forces measured at the bottom of large scale GRS test walls and found that the soil friction was fully mobilized behind the modular block facing. For the interfaces between soil and modular block facing, a full friction angle equal to the plane strain soil friction angle and moduli equal to the moduli of the soil at the same stress level were used.

Properties of interface between block and block are really not easy to characterize because different manufacturers develop different connection systems for their products. Interface characteristics of blocks are also affected by the geosynthetic reinforcements inserted between the blocks. There are three basic types of the block connections:

1. Friction connection – the connection relies on the friction between the block material and gravel material filled in the blocks. Interface properties of this type of connection are assumed to be the friction angle and shearing stiffness of the gravel material.

2. Steel pin connection – steel pins are inserted in between the blocks to help maintain the alignment of the blocks as well as to attach the reinforcement to the facing units. Interface properties of this type of connection are assumed to be the friction angle and shearing stiffness of the gravel infill material. The existence of the steel pin of this type of connection can be simulated by cohesion at the interface. The cohesion value can be obtained by dividing the yield strength of the steel pin by the area of the blocks. However, the difference between models with and without cohesion was found to be very minor. This observation indicates that because the cross sectional area of the pins is small, this type of block facing system still relies mainly on the friction of the block material and the gravel material filled in the blocks.

3. Wedge connection – blocks of this type of connection system are made with a convex wedge at one contact face and a compatible concave groove at the other. This wedge design provides a very stiff connection because the connection not only relies on the friction of the infill gravel material but also on the strength of the block material. Friction of this type of connection is assumed to be the friction angle of the gravel material. The shearing stiffness

of the interface is calculated using Equation 8.5.1. The cohesion of the interface is assumed to be the apparent cohesion of the block material.

$$ks = E_g \cdot R_g + E_b \cdot R_b \qquad \text{(Eq. 8.5.1)}$$

where ks = shearing stiffness of the interface,

E_g = stiffness of the gravel material,

R_g = coverage ratio of the gravel material = $\frac{A_g}{A_{total}}$,

A_g = cross sectional area occupied by the gravel material,

A_{total} = total cross sectional area of the block unit,

E_b = stiffness of the block material,

R_b = coverage ratio of the block material = $\frac{A_b}{A_{total}}$, and

A_b = cross sectional area occupied by the block material.

8.5.9 Wall Construction

Field observations (instrumentation measurements) obtained from the case histories analyzed in this research (Chapter 9), as well as the excellent performance of GRS walls built as early as 1970s, indicate that most of the wall deflection occurs during the wall construction, especially in well-designed GRS walls. Due to the conservative nature of present design methods, these walls are so strong that almost no additional deflections have been observed after construction. Deflections mostly occurred during construction because soil moduli are relatively small when soil is first placed on each lift of construction. Soil moduli increase as the confining pressure increases, i.e. as the

height of the wall increases. Therefore, modeling the construction procedures and the change of soil moduli caused by this confining pressure change are very important. Modeling techniques used to account for the change of soil moduli due to confining pressure change have been described in Section 8.5.4. GRS wall construction procedures can be modeled as follows (Figure 8.5.4):

1. Place backfill soil (Mohr-Coulomb) and facing (elastic) elements of first layer.
2. Insert the interface between the soil and facing elements.
3. Place reinforcement (cable) elements.
4. Place backfill soil (Mohr-Coulomb) and facing (elastic) elements of next layer.
5. Insert the interface between the soil and facing elements, including interfaces between facing elements of different layers, if any.
6. Solve the model to intermediate equilibrium state (intermediate equilibrium criteria: **srat=0.01**), and
7. Repeat steps 3 to 6 until the wall is completed.

It is strongly recommended that the iteration result of construction of each lift be saved, i.e. save each immediate and final stages, so that the development of the working stress and strain of the modeling object can be monitored throughout the construction simulations.

Step 1:

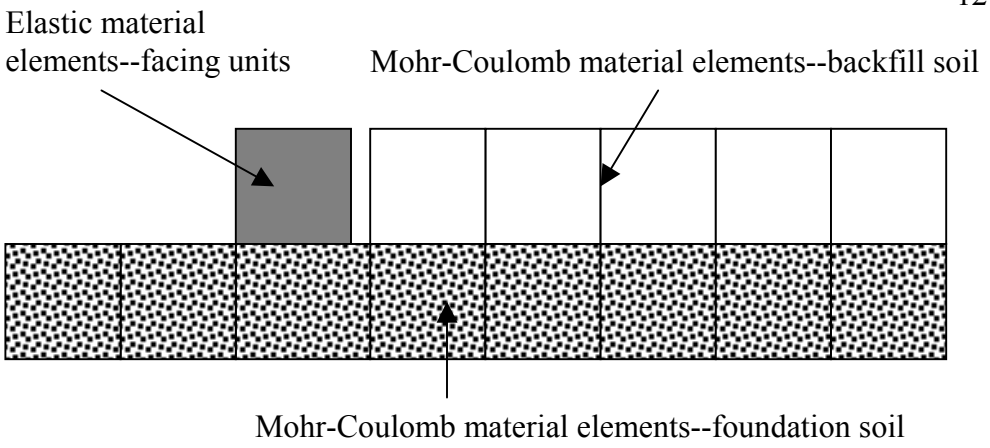

Steps 2 and 3:

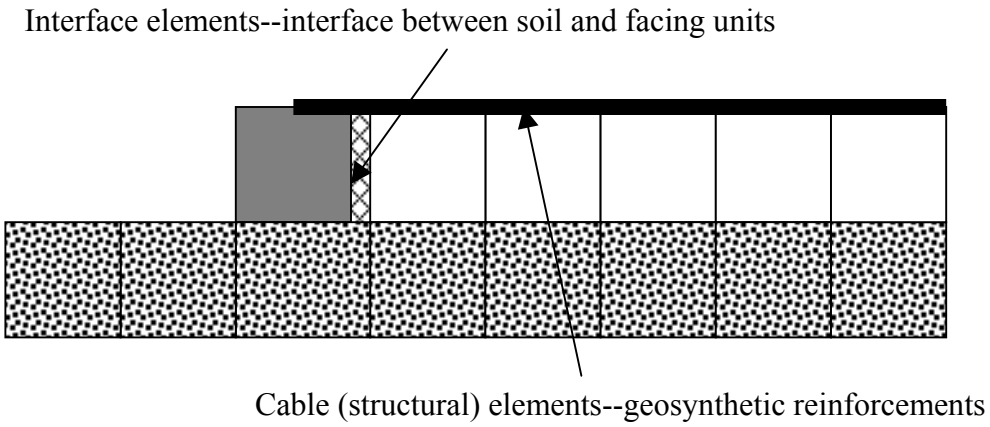

Steps 4 and 5:

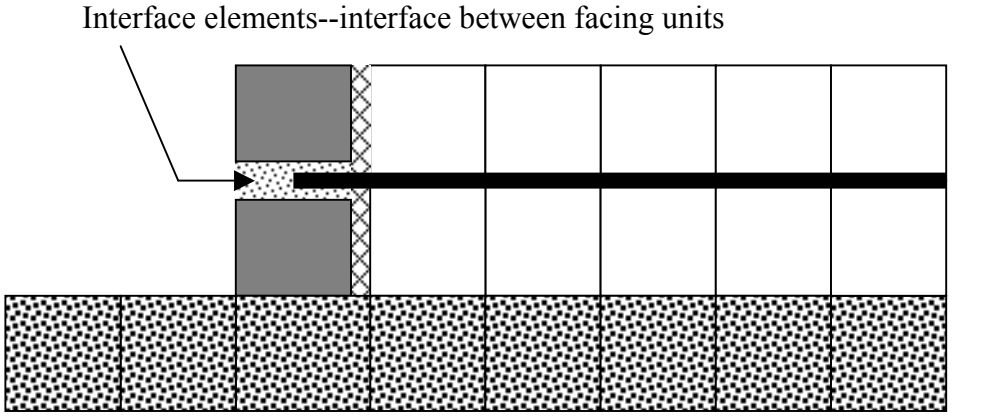

Figure 8.5.4 Construction procedures of a GRS wall modeled in FLAC.

8.5.10 Modeling Result and Data Reduction

When FLAC models reach equilibrium at their final stages, displacement, stress and strain of each material element as well as the axial forces of reinforcement element are obtained directly from the saved result files. This information is either printed out as data files or shown on the screen directly. The high stress-strain zone of the analyzed walls can be located by showing the yielding (elastic or plastic) states of the material elements. To ensure accuracy of the modeling results, the following issues were checked:

1. That the equilibrium criteria were actually reached. Sometimes the iteration process was stopped because the limit of the number of iterations was reached before the stress ratio limit, but the modeling result had not converged.
2. That there were no notable displacements or reaction forces at the boundaries.
3. That strain compatibility is satisfied at every material element, i.e. that there is no overlap or penetration of any adjacent material elements.

The horizontal displacement of the first column of material elements was used to represent the wall face deflections. The horizontal stress distribution of this column was also used to represent the distribution of the lateral reinforced earth pressures. Strain distribution along the reinforcements was obtained by dividing the axial loads of reinforcement with the tensile moduli of the reinforcements.

8.6 Conclusions

Modeling techniques used to predict performance of the GRS retaining structures appear to be very complicated, especially when structural facing systems are involved. Modeling techniques described in Section 8.5 were obtained from numerous trials and elaborate model calibrations. They provided the basic concepts and the specific procedures to improve the working stress analyses of GRS retaining structures using FLAC. Prerequisites for using these modeling techniques are a good understanding of the in-structure material properties. Properties of both soil and geosynthetic reinforcement have to be carefully determined as described in Chapter 7.

Chapter 9
Verification of Numerical Modeling Techniques – Reproducing the Performance of Existing GRS walls

9.1 Introduction

Performance data from four instrumented GRS retaining structures and two steel reinforced retaining structures were collected to verify the numerical modeling techniques described in Chapter 8. These case histories were chosen because they were fully instrumented during construction and the results of the instrumentation were well documented. These case histories include the WSDOT geotextile wall at the west-bound I-90 preload fill in Seattle, Washington, and five of the test walls constructed at the FHWA Reinforced Soil Project site at Algonquin, Illinois (Table 9.1.1).

Numerous trial models and much arduous work were done to develop models for these case histories, as well as to calibrate these models to the latest modeling techniques. In this chapter, results of six FLAC models that were developed to model the performance of the case histories are presented and compared to the field measurements. These FLAC models were developed following the same property determination procedures and numerical modeling techniques described in Chapters 7 and 8, and they were able to reproduce the field performance of the analyzed case histories within a reasonable range.

Table 9.1.1 Summary of the numerical models of case histories.

Case History	Model Name
WSDOT Rainier Avenue Geotextile Wall Seattle, Washington (Allen et al., 1992) (12.6m high with 32 woven geotextile reinforcement layers)	RAING
FHWA Algonquin Precast Concrete Panel Faced Test Walls Algonquin, Illinois (Christopher, 1993) (6.1m high with 8 reinforcement layers)	ALGPC1 (Wall 1: steel strips)
	ALGPC2 (Wall 2: geogrid)
	ALGPC3 (Wall 3: steel bar mats)
FHWA Algonquin Modular Block Faced Test Wall Algonquin, Illinois (Christopher, 1993) (6.1m high with 8 geogrid reinforcement layers, uneven vertical spacing)	ALGMB1
FHWA Algonquin Geotextile Wrapped Faced Test Wall Algonquin, Illinois (Christopher, 1993) (6.1m high with 7 primary and 6 secondary nonwoven reinforcement layers)	ALGWF1

9.2 Summary of the Case Histories and Their Numerical Models

9.2.1 WSDOT Rainier Avenue Geotextile Wall

The first FLAC GRS wall model of this research was developed to predict the instrumentation measurements of the WSDOT Rainier Avenue wall built in Seattle, Washington. It was the highest GRS wall in the world at the time it was constructed. The wall was 12.6 m high and had a surcharge of 5.3 m high with 1V: 1.8H slope. No structural facing system was used for this wall; geotextiles were wrapped around the wall face. Four different kinds of woven geotextiles were used to reinforce the backfill of this wall (Christopher et al., 1990, Allen et al., 1992).

Figure 9.2.1 shows a typical cross-section with material properties of this wall. Deflections of the wall were measured using optical surveys, photogrammetry, and mechanical extensometer plate surveys at the wall face and inclinometers at the wall face and 2.75 m behind the wall face. The internal strain distribution was measured using strain gages and extensometers attached to the geosynthetic reinforcement. Figure 9.2.2 shows the instrumented wall section of the Rainier Avenue wall (from Allen et al., 1992).

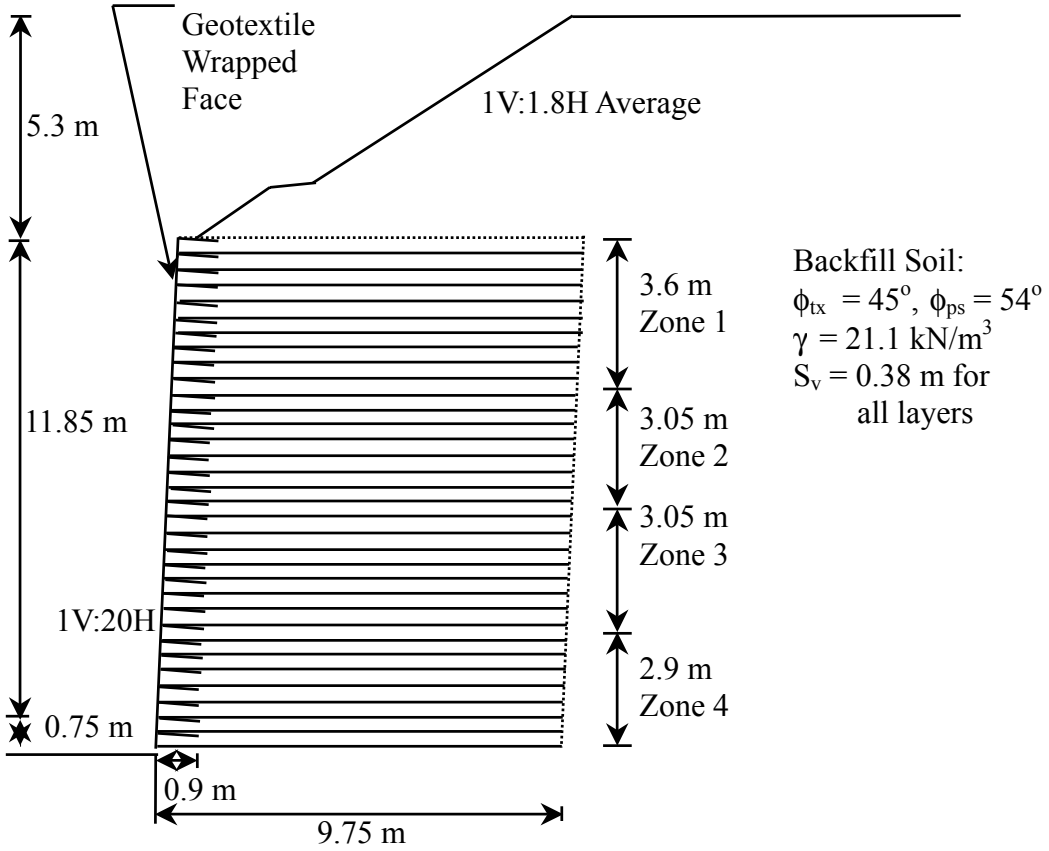

Foundation soil consists of 6m of dense gravelly sand underlain by 1 to 3 m of soft clayey silt, which is underlain by very dense gravelly sand

Reinforcement:

Zone	Geotextile	T_{ult} (kN/m)	J (kN/m)
1	GTF200 (PP)	31	102
2	GTF375 (PP)	62	204
3	GTF5500 (PP)	92	357
4	GTF1225T (PET)	186	1125

PP: Polypropylene
PET: Polyester

Figure 9.2.1 Typical cross section of Rainier Avenue Geotextile wall (After Allen, 1999).

The FLAC model, Model RAING, was developed for simulating the performance of the Rainier Avenue Wall. In Model RAING, the soil moduli were determined using the modified hyperbolic soil modulus model. Model parameters were determined based on the triaxial test data with plane strain modifications, as described in Chapter 7. During the iteration process, soil moduli were automatically updated by the FISH subroutine that was embedded in the FLAC model. Details of the FISH subroutine were presented in Section 8.5.1. Input properties of the reinforcement were determined using procedures described in Example 8.5.2 with an assumption of in-soil reinforcement thickness equal to 5mm. The reinforcement (cable) elements were hard tied onto the material element nodes, i.e. perfect bonding between the reinforcement (cable) and soil (Mohr-Coulomb) elements was imposed. As described in Chapter 8, this technique was used to avoid the violation of strain compatibility when large deformations occurred in the models. Table 9.2.1 lists the input properties of Model RAING.

9.2.2 Algonquin Precast Concrete Panel Faced Walls

The second set of FLAC wall models were developed to predict the performance data of the Federal Highway Administration (FHWA) test walls built at Algonquin, Illinois. These test walls were constructed as part of a FHWA study to investigate the behavior of mechanically stabilized earth (MSE) walls (Christopher, 1993). Three of these walls used the same type of wall facing, the cruciform precast concrete panels of the

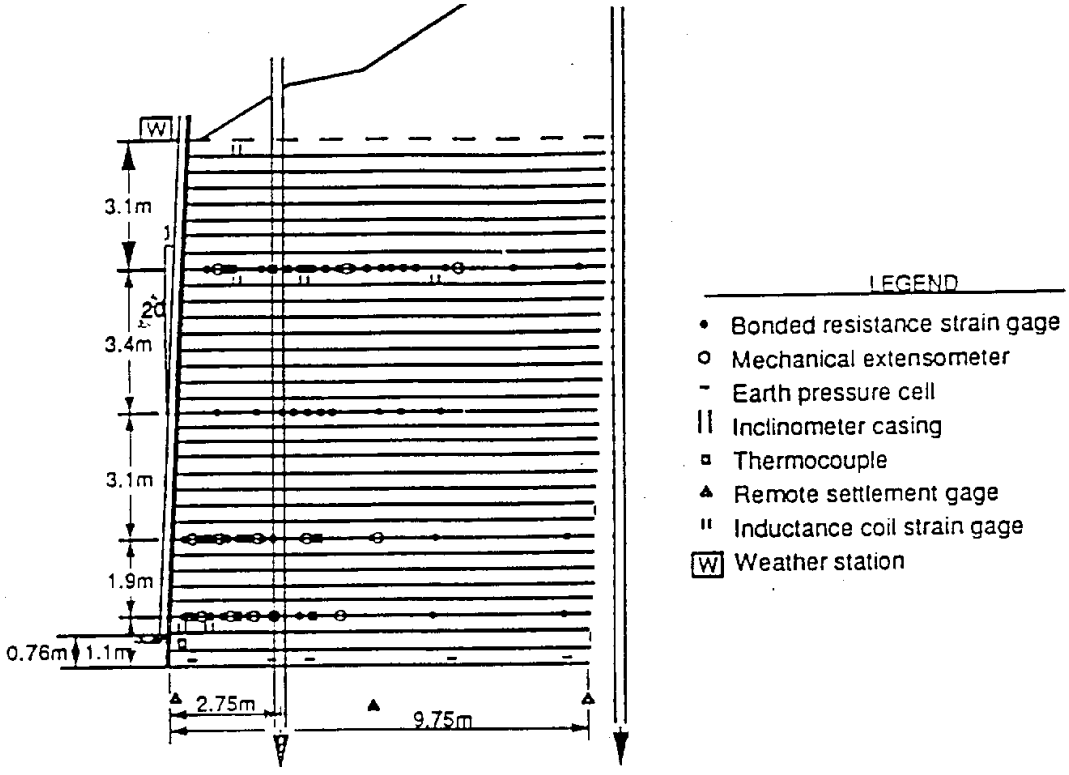

Figure 9.2.2 Instrumented wall section of Rainier Avenue wall (after Allen et al., 1992).

Reinforced Earth Company design, and each was reinforced with different reinforcement materials. Two were reinforced using steel reinforcements and the other was reinforced with geogrids. Table 9.2.2 summarizes the reinforcement types and properties used in each wall. Figure 9.2.3 shows the wall geometry, material properties, and instrumentation details for the geogrid wall (Wall 2). The wall geometry was identical for Walls 1, 2 and 3, and the instrumentation details were similar. Backfill material was a well-graded sand and gravel (Figure 9.2.3). The performance of all three concrete panel walls was measured using inclinometers and surface optical surveys for deflections, and strain gages and extensometers for internal strain distributions. In this research, numerical models were first developed to simulate the instrumentation measurements of the geogrid reinforced wall, Wall 2. Walls 1 and 3 were used as verifying cases in the parametric study. Results of the parametric study are described in Chapter 12.

Models ALGPC1, ALGPC2, and ALGPC3 are the final models that were developed by following the modeling techniques described in Chapter 8. Similar to Model RAING, soil moduli for these models were also updated automatically using the hyperbolic soil modulus model and the reinforcement elements were also attached to the material element nodes. Input properties of the reinforcement were determined by using procedures described in Example 8.5.2 with a assumption of in-soil reinforcement thickness equal to 5 mm. Interface elements were inserted in between the concrete panel (elastic material elements) and the backfill soil (Mohr-Coulomb

Table 9.2.1 Input properties of Model RAING.

Input Property	Model RAING
Soil Friction Angle	50 deg
Soil Dilation Angle	15 deg
Soil Cohesion	0 kPa
Soil Moduli	Automatically updated using modified hyperbolic soil modulus model (K=1800, R_f=0.73, n=0.5)
Reinforcement – GTF 200	**E** = 20300 kN/m^2 **Yield** = 31 kN, **Ycomp** = 0
Reinforcement – GTF 375	**E** = 40800 kN/m^2 **Yield** = 62 kN, **Ycomp** = 0
Reinforcement – GTF 500	**E** = 71300 kN/m^2 **Yield** = 92 kN, **Ycomp** = 0
Reinforcement – GTF 1225T	**E** = 225000 kN/m^2 **Yield** = 186 kN, **Ycomp** = 0

Table 9.2.2 Construction and reinforcement information of the Algonquin concrete panel faced walls (Christopher, 1993).

Wall Names	Wall 1	Wall 2	Wall 3
Reinforcement Name and Type	Reinforced Earth Company—Ribbed Steel Strips	Tensar SR2—Polyethylene Extruded Geogrids	VSL—Steel Bar Mats using W11 Bars
Reinforcement Strength, Strain, and Stiffness	T_{yield}= 67.9kN/m [a] ε_{yield}=0.12% J=54690kN/m [a]	T_{peak}= 67.7kN/m [b] ε_{peak}=16.0% J=2040kN/m [b]	T_{yield}= 44.4kN/m [a] ε_{yield}=0.12% J=37860kN/m [a]

[a] per meter of wall, calculated based on the coverage ratio (the width of the reinforcement divided by the center to center horizontal spacing).

[b] from wide width strip tensile tests (ASTM D 4595)

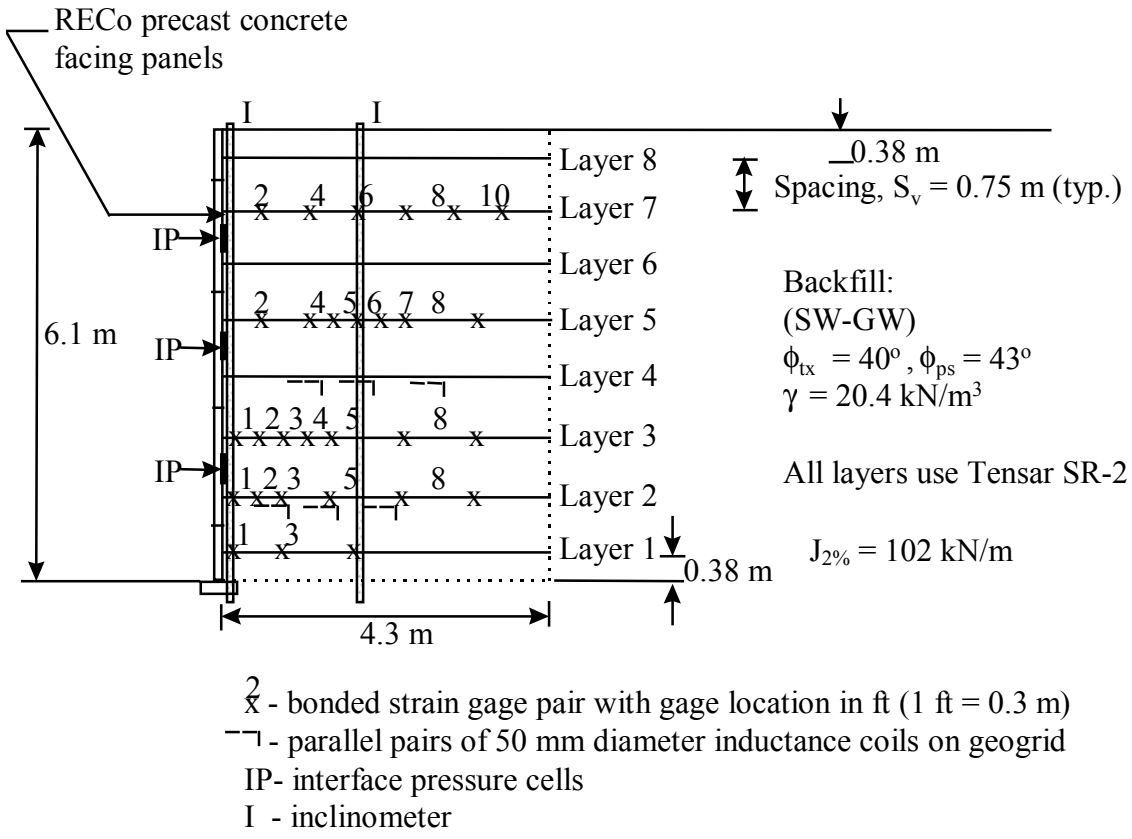

Figure 9.2.3 Wall geometry and instrumentation plan for Wall 2 (After Lee, Holtz, and Allen, 1999).

material elements). As stated in Chapter 8, for the interface elements between soil and concrete panels, a friction angle equal to two-thirds of the plane strain soil friction angle and stiffness equal to the average stiffness of the soil behind the wall face were used. Table 9.2.3 lists the input properties of these models.

9.2.3 Algonquin Modular Block Faced Wall

FLAC models were also developed to simulate the performance of the geogrid reinforced modular block faced wall of the FHWA Algonquin test walls, in order to calibrate the developed modeling techniques for different MSE wall facing systems. Figure 9.2.4 shows the typical cross section and material properties of the modular block faced wall. As shown in Figure 9.2.4, vertical spacings of the reinforcement layers were varied throughout the wall height in an attempt to “amplify” the face deformation as well as the internal strain levels of the wall. wall (after Bathurst et. al., 1993). The wall was designed to have the largest spacing at two-thirds of the wall height where the maximum wall deflection was expected to occur. Deflections of the wall were measured using inclinometers at the wall face and 2.7 m behind the wall face. The internal strain distribution was measured using strain gages attached to the geogrids reinforcements. Figure 9.2.5 shows the instrumentation wall section of this wall (Bathurst et al., 1993).

Table 9.2.3 Input properties of Models ALGPC1, ALGPC2, and CLGPC3.

Input Property	Model ALGPC1 Model ALGPC2 Model ALGPC3
Soil Friction Angle	43 deg
Soil Dilation Angle	15 deg
Soil Cohesion	0 kPa
Soil Moduli	Automatically updated using hyperbolic soil modulus model (K=1100, R_f=0.73, n=0.5)
Interface	**kn** = 373000 kN/m^2, **ks** = 187000 kN/m^2, **fric** = 28.7, **coh** = 0,
Ribbed Steel Strip Wall 1 Model ALGPC1	**E** = 1.2E7 kN/m^2 **Yield** = 1E6 kN, **Ycomp** = 1E6 kN.
Geogrid Wall 2 Model ALGPC2	**E** = 204000 kN/m^2 **Yield** = 67.8 kN, **Ycomp** = 0.
Steel Bar Mat Wall 3 Model ALGPC3	**E** = 8.0E6 kN/m^2 **Yield** = 1E6 kN, **Ycomp** = 1E6kN.

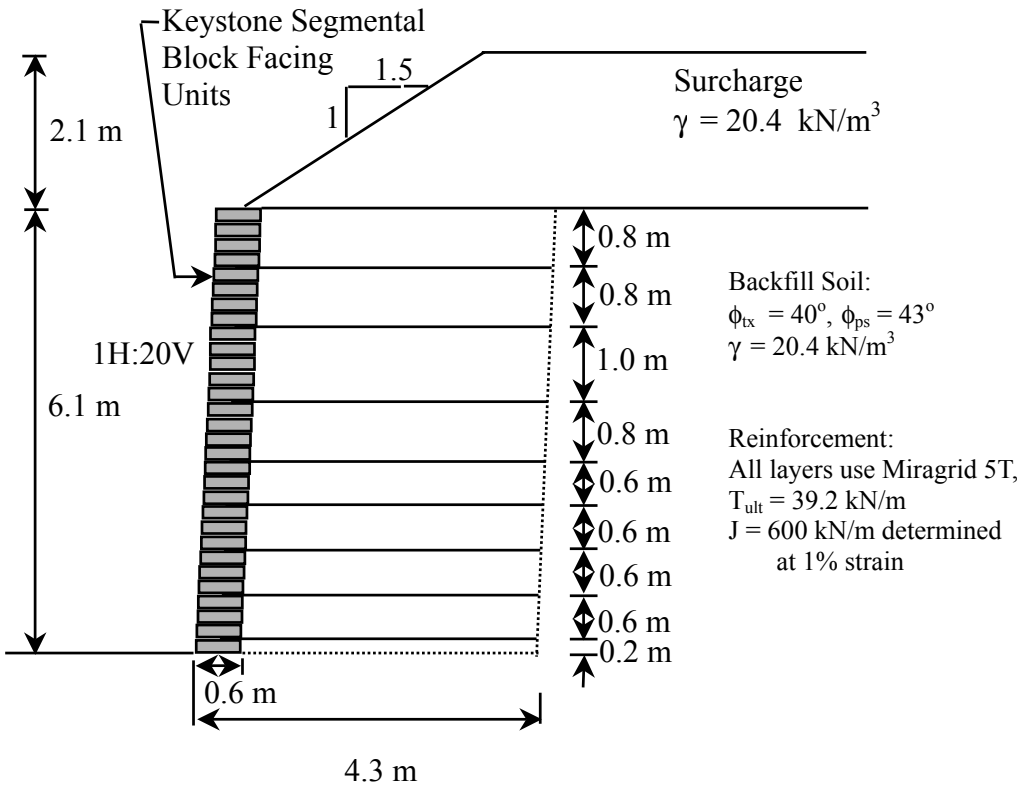

Foundation soil is 5 m of dense gravelly sand or fine to medium sand underlain by very dense sandy silt

Figure 9.2.4 Cross section and material properties of Algonquin modular block faced test wall (after Allen, 1999)

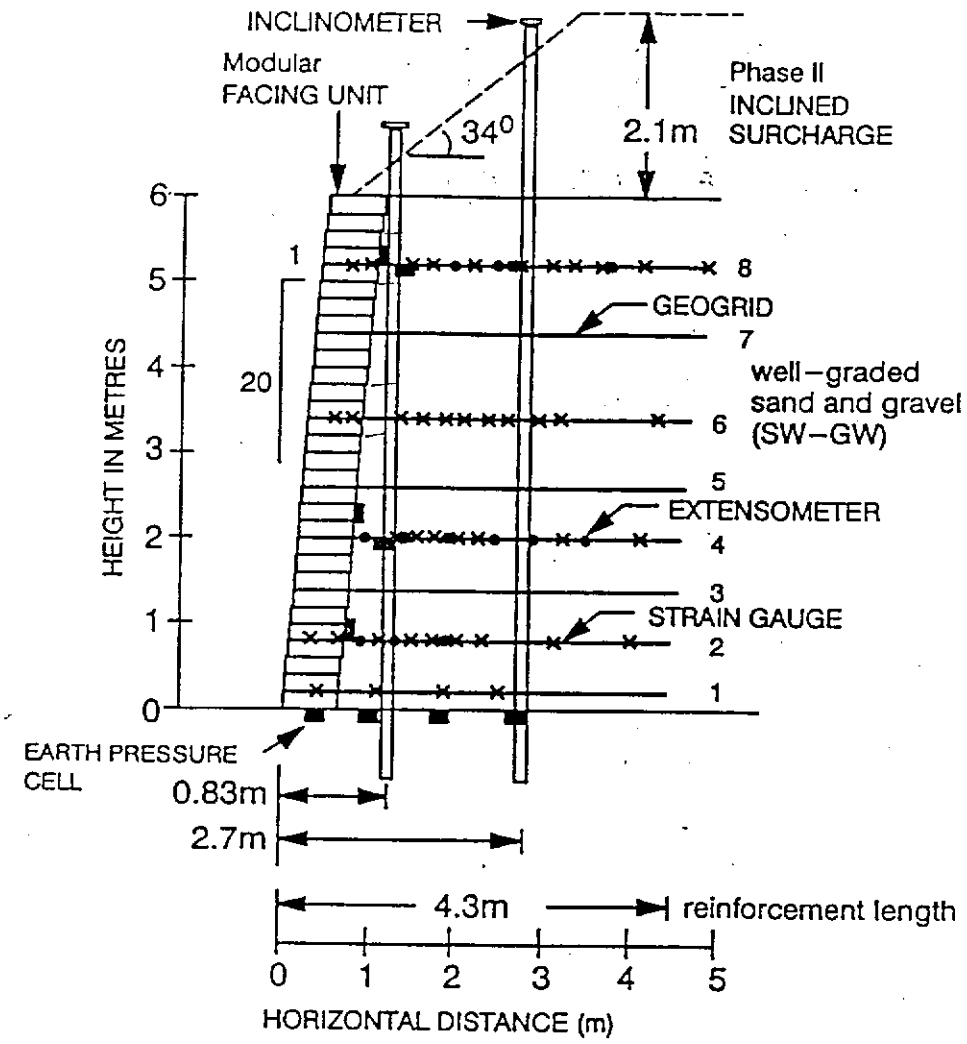

Figure 9.2.5 Instrumentation section of the Algonquin modular block faced geogrid

FLAC model ALGMB1 was developed to model the performance of this wall. Model ALGMB1 was developed utilizing the modeling techniques described in Chapter 8, such as using the hyperbolic soil modulus models and attaching reinforcement elements to the material element nodes. In Model ALGMB1, the modulus of the geogrid reinforcement was the tangent modulus determined at 1% strain with in-soil and low strain rate modification because the average reinforcement strain measured by the strain gages was less than 1%. The in-soil reinforcement thickness was assumed to be 5 mm similar to other cases. Moreover, the stiffness that was determined from connection test data (Bathurst, 1999) was used as the modulus of the reinforcement located inside the blocks. In Model ALGMB1, effort was also made to model the block facing system including the interfaces between blocks as well as the gravel column behind the modular block face. The purpose of placing this gravel column was to maintain good drainage and thus reduce excessive water pressure on the wall face. However, properties of the interfaces between blocks and the gravel material were not clearly described in the documentation (Bathurst et al, 1993). Table 9.2.4 lists the input properties of Model ALGMB1, most of which were determined from manufacturer's information.

9.2.4 Algonquin Wrapped Face Wall

FLAC models were also developed to reproduce the performance of the wrapped face wall of FHWA Algonquin test walls because the poor design of this wall allowed large strains to occur. The test wall was designed with a very weak nonwoven geosynthetic

as reinforcement and a 1 m high surcharge on the top. Secondary reinforcement layers, additional horizontal reinforcement, were inserted near the face of the wall to increase the stability of the face. A water pond built with an impermeable membrane was also placed in front of the wall to help maintain the stability of the wall during surcharge construction. Figure 9.2.6 shows the typical cross section and material properties of the wrapped face wall. This retaining water pond was then removed after the wall was completed to observe the possible failure of this GRS wall. Similar instrumentation to the other Algonquin test walls was used to monitor the performance of this wrapped face wall. Figure 9.2.7 shows the instrumentation section of this wall. However, optical survey and inclinometer measurements of wall deflection were not available because of the retaining water pond in front of the wall and the gabion basket surcharge on the top of the wall (Christopher 1993).

FLAC model ALGWF1 was developed using similar modeling techniques to those used in Model RAING. The average measured reinforcement strain inside the wrapped face wall was less than 2%. However, there was only an in-soil stiffness obtained from pull-out test at 12% strain available in the documentation (Christopher, 1993). In Model ALGWF1, the reinforcement stiffness was determined using in-isolation test data of reinforcing material similar to what was used in this test wall. The input stiffness of the reinforcement was determined by multiplying the 2% strain in-isolation stiffness by five, a modification based on the UCD test results reported by Boyle (1995). Additional effort was also made to model the completed boundary conditions

Table 9.2.4 Input properties of Model ALGMB1.

Input Property	Model ALGMB1 (final model)
Soil Friction Angle	43 deg
Soil Dilation Angle	15 deg
Soil Cohesion	0 kPa
Soil Moduli	Automatically updated using hyperbolic soil modulus model (K=1100, R_f=0.73, n=0.5)
Gravel Column	Friction angle = 55 degrees Dilation angle = 20 degrees Hyperbolic model parameters (K=4000, R_f=0.73, n=0.5)
Interface (block – block)	**Kn** = 1.095E8 kN/m^2, **ks** = 1E7 kN/m^2, **fric** = 55, **coh** = 10000,
Interface (block – soil)	**Kn** = 373000 kN/m^2, **ks** = 187000 kN/m^2, **fric** = 28.67, **coh** = 0,
Reinforcement inside the blocks	**E** = 5E5 kN/m^2 **Yield** = 1E7 kN, **Ycomp** = 1E7 kN, (**kbond** = 1.2E5 kN/m^2, **sbond** = 0 kN/m^2, **sfric** = 55).
Reinforcement inside the backfill	**E** = 1.2E5 kN/m^2 **Yield** = 39.2 kN, **Ycomp** = 0.

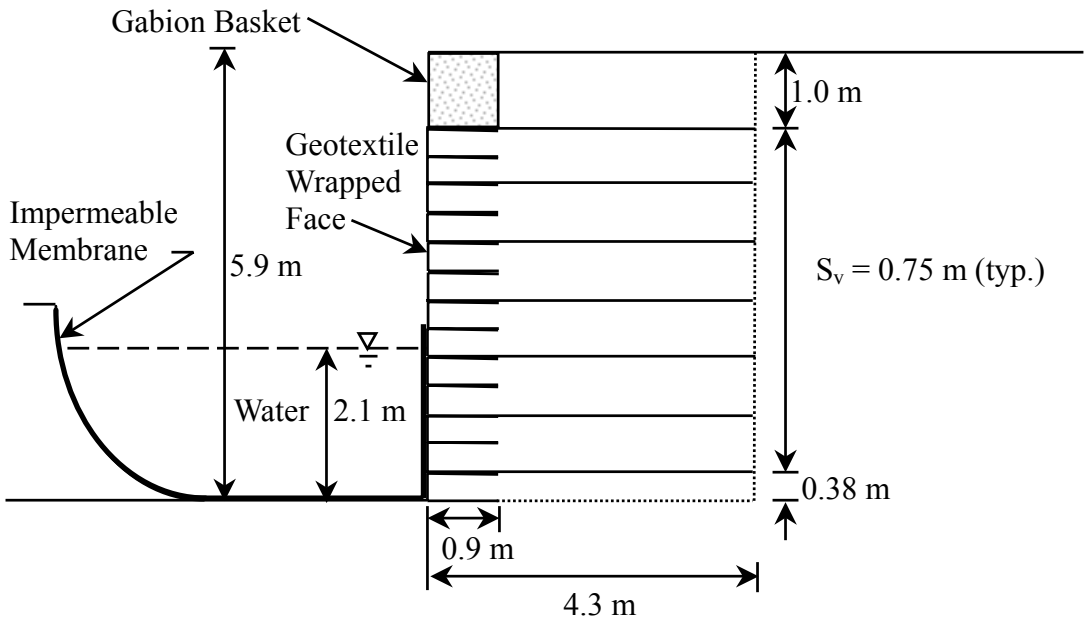

Foundation soil is 5 m of dense gravelly sand or fine to medium sand underlain by very dense sandy silt

Figure 9.2.6 Typical cross section and material properties of Algonquin wrapped faced wall (after Allen, 1999).

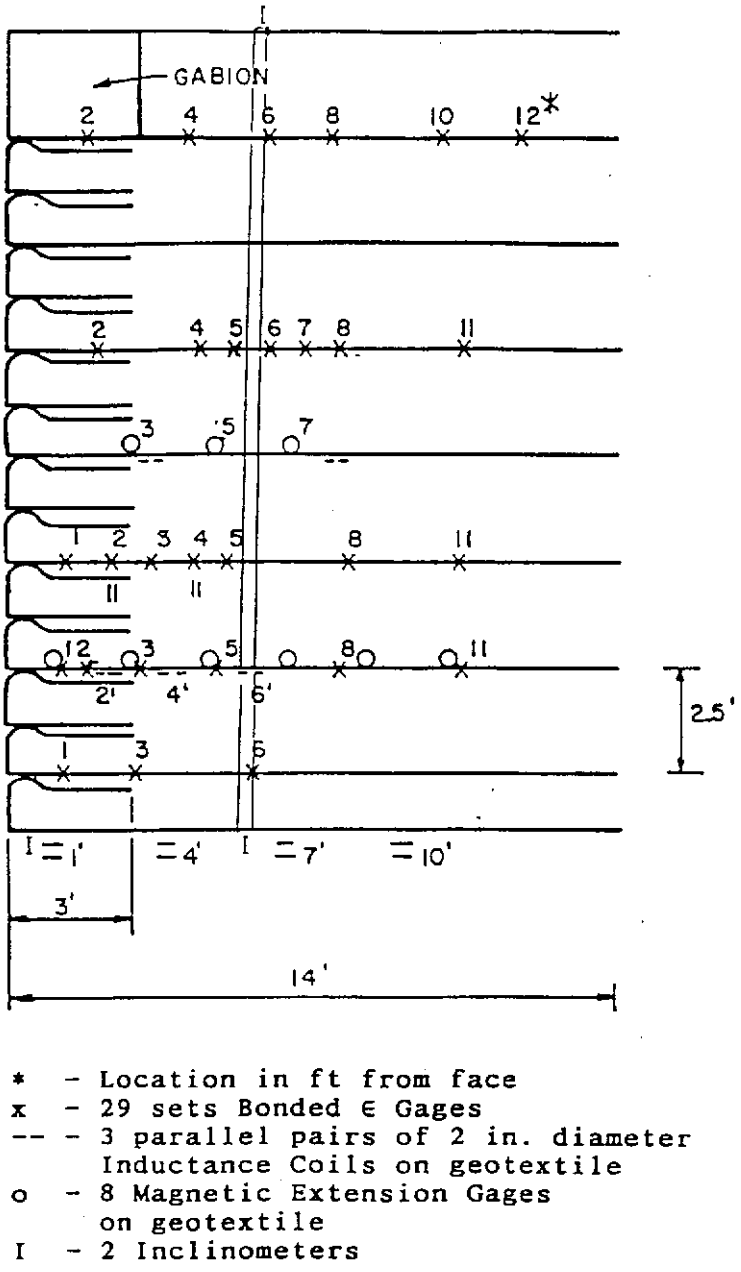

Figure 9.2.7 Instrumentation section of the Algonquin wrapped faced wall (After Christopher, 1993).

of this wall. The retaining water pond was modeled using elastic material elements with density equal to 1 and Poisson's ratio equal to 0.5. The gabion baskets were modeled by wrapping the Mohr-Coulomb material element (properties of gravel were assigned) with cable elements with properties of steel wires. Table 9.2.5 lists the input properties of Model ALGWF1.

In the following sections, performance predictions of the developed models of the case histories described above are presented. In Section 9.3, deflection predictions of the developed wall models are presented and compared to the optical survey or inclinometer measurements. In Section 9.4, predictions of the reinforcement strain distributions of these models are also presented and compared to the strain gage measurement as well as the extensometer measurements if available. Finally, the reinforcement tension distributions obtained from the numerical models are presented in Section 9.5 to compare with the predictions made by the tie-back wedge method.

Table 9.2.5 Input properties of Model ALGWF1.

Input Property	Model ALGWF1
Soil Friction Angle	43 deg
Soil Dilation Angle	15 deg
Soil Cohesion	0 kPa
Soil Moduli	Automatically updated using hyperbolic soil modulus model (K=1100, R_f=0.73, n=0.5)
Gabion Basket	Gravel: **Den**=2.4 **fric**=50 **di**=10 **coh**=35 Steel wire: **E**=175e3 **yield**=200 kN **ycomp**=200 kN **sbond**=0 **kbond**=175e3 **sfric**=50
Reinforcement At face (in-isolation)	**E** = 1.6E4 kN/m^2 **Yield** = 19.3 kN, **Ycomp** = 0
Reinforcement In backfill (in soil)	**E** = 8E4 kN/m^2 **Yield** = 19.3 kN, **Ycomp** = 0,

9.3 Modeling Results I—Wall Deflection

9.3.1 WSDOT Rainier Avenue Wall

Figures 9.3.1a and 9.3.1b show the face deflection results of Model RAING compared with the average survey measurements of the WSDOT Rainier Avenue wall at end of the construction and after surcharge. Average deflection survey measurements were used to eliminate errors between different survey measurements. Model RAING was able to predict reasonable face deflections and the locations where the maximum deflection was observed. As shown in Figure 9.3.1, Result of Model RAING under-predicts the wall face deflection by only about 20 mm at end of construction and over-predicts the wall deflection by only about 10 mm after surcharge applied for the 12.6 m high wrapped face wall.

Similar tendencies were also found when comparing the modeling results to the measurements of the inclinometer located at 2.75 m behind the wall face (Figures 9.3.2a and 9.3.2b). As shown in Figure 9.3.2a, Model RAING under-predicted the wall deformation by less than 10 mm at the elevation where maximum face deformation was observed (Figure 9.3.1) at end of construction. After surcharge is applied, result of Model RAING also had a very good agreement to the inclinometer measurements below the elevation where maximum wall face deflection was observed. It only slightly under-predicts the deformation by 10 mm at the elevation where maximum face deflection was observed.

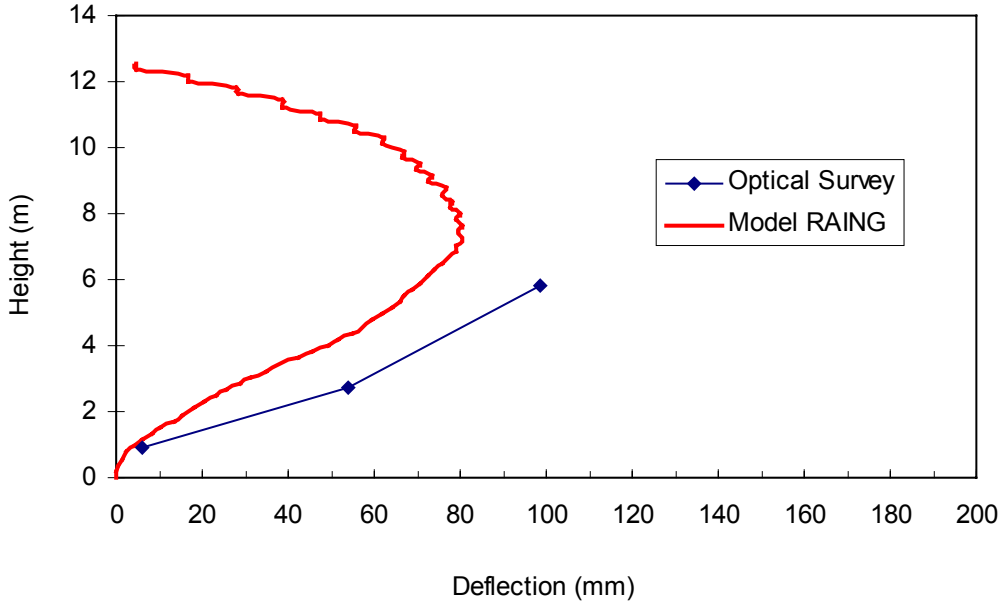

(a)

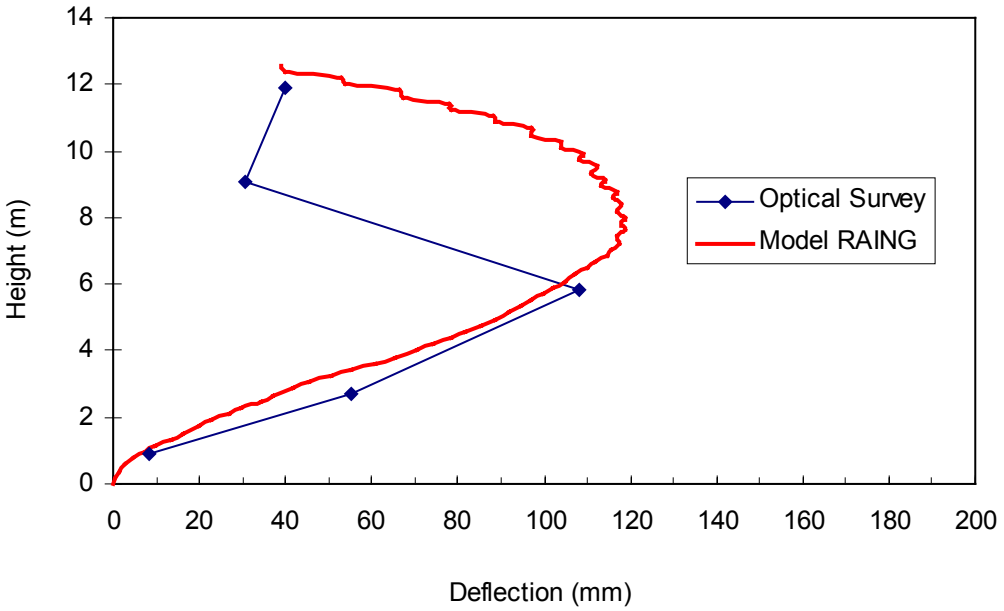

(b)

Figure 9.3.1 Face deflection of Rainier Avenue wall: (a) end of construction, and (b) after surcharge.

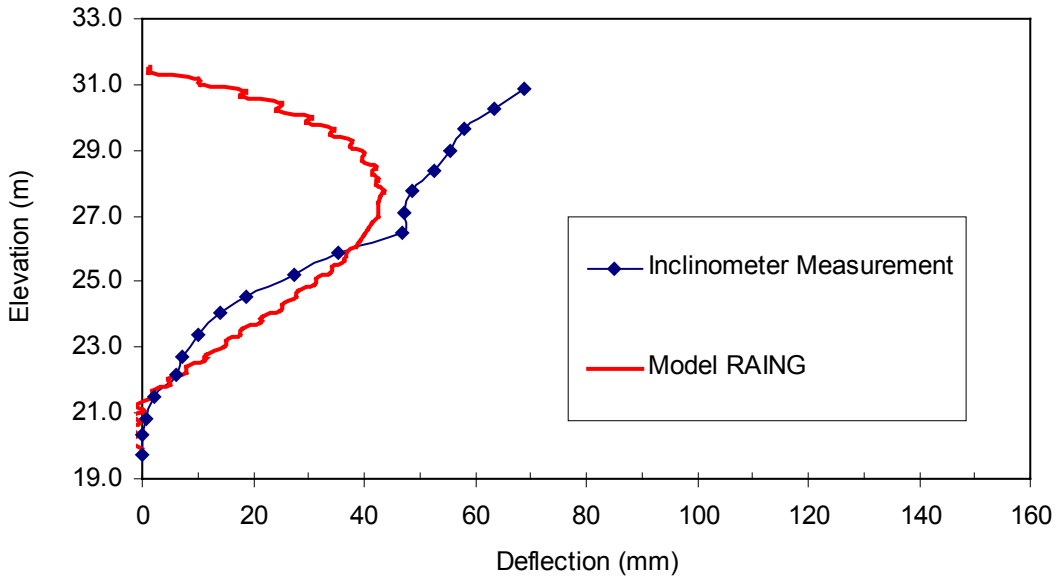

(a)

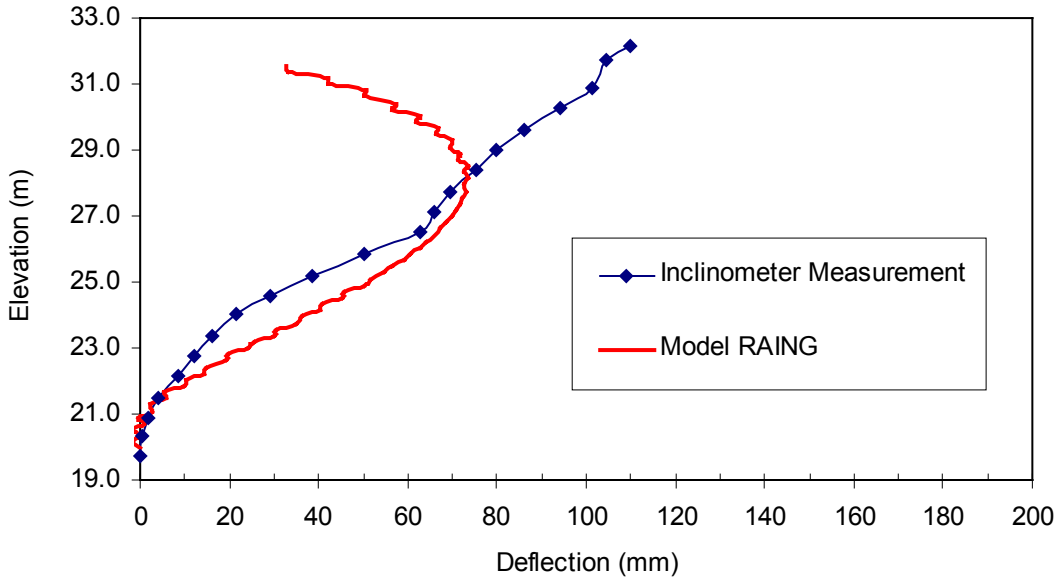

(b)

Figure 9.3.2 Wall deformation of Rainier Avenue wall at 2.75m behind the wall face: (a) end of construction, and (b) after surcharge.

Modeling results shown in Figure 9.3.2 had different predictions from the inclinometer measurements above the location where the maximum face deflection occurred. Reasons why the inclinometer measurements showed a maximum wall deflection at top of the wall are not clear at present.

9.3.2 Algonquin Concrete Panel Faced Walls

Model ALGPC2 was able to predict both the shape and maximum deflection of the geogrid wall within reasonable agreement (Figure 9.3.3). As shown in Figure 9.3.3, Model ALGPC2 under-predicts the maximum face deflection of the geogrid wall by only about 5 mm. The results of Models ALGPC1 and ALGPC3 also showed reasonable agreement with the behavior of the steel reinforced walls (Wall 1 and Wall 3) (Figures 9.3.4 and 9.3.5). Because of the high stiffness of the reinforcement of Walls 1 and 3, the magnitudes of face deflections and the reinforcement strains are very small. Thus the potential error in the measurements due to the accuracy of the optical survey could be very close to the magnitude of the measurements themselves. As shown in Figures 9.3.4 and 9.3.5, Models ALGPC1 and ALGPC3 predicted very small survey face deflections, and the difference between predicted and measured maximum deflection is only about 5 mm.

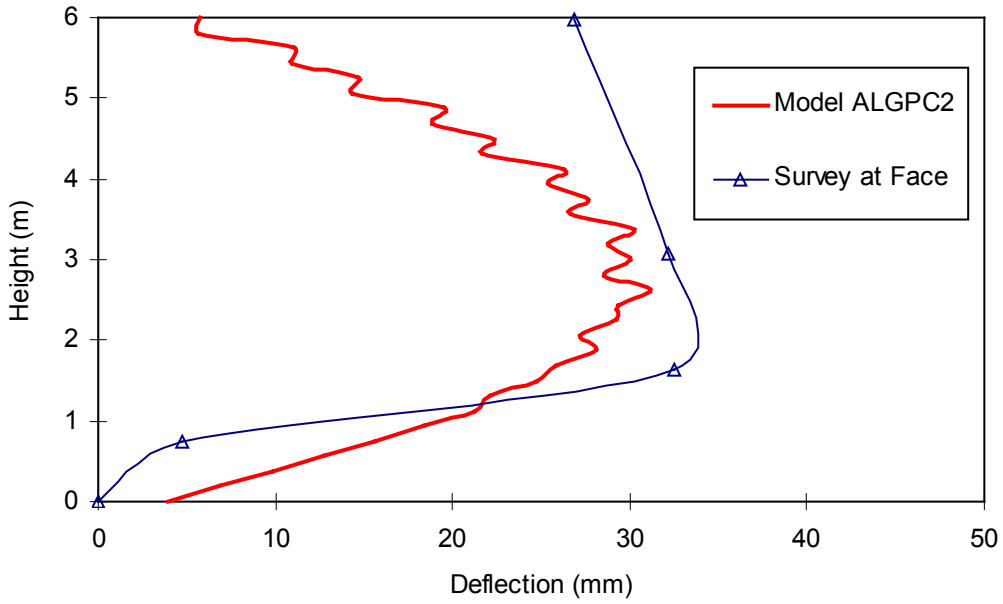

Figure 9.3.3 Predicted and measured wall face deflection of Algonquin concrete panel faced Wall 2 (geogrid wall).

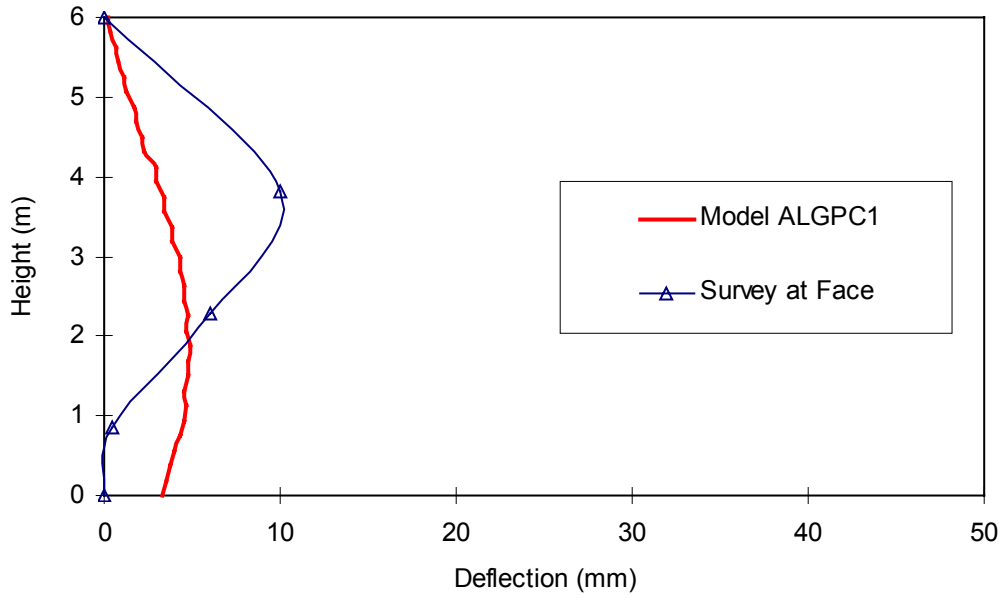

Figure 9.3.4 Predicted and measured wall face deflection of Algonquin concrete panel faced Wall 1 (steel strips wall).

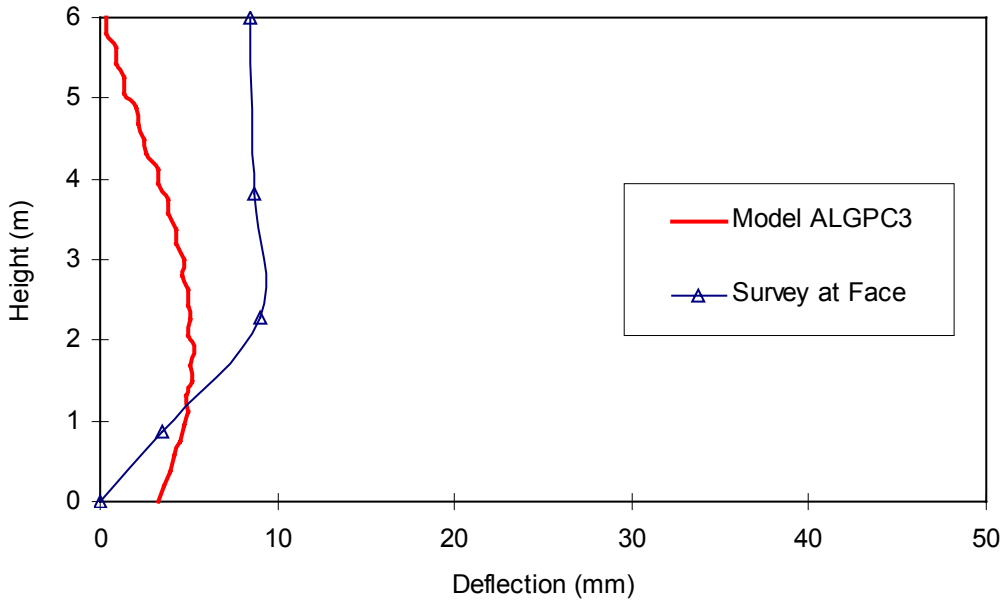

Figure 9.3.5 Predicted and measured wall face deflection of Algonquin concrete panel faced Wall 3 (steel bar mats wall).

9.3.3 Algonquin Modular Block Faced Wall

Model ALGMB1 was able to predict the instrumentation measurements within a reasonable range. Figure 9.3.6 shows the prediction of Model ALGMB1 compared to the measurements obtained from the inclinometer behind the wall face. Model ALGMB1 tends to over-estimate the wall deflection at the location where maximum face deflections were predicted by about 10 mm at the end of construction and by about 25 mm after surcharge was applied. Possible reason for this over-estimation is the input friction used for the interface between facing blocks was smaller than actual fiction occurred in between the blocks of this wall.

Figure 9.3.7 shows the modeling result comparing to the measurements of the inclinometer located 2.7 m behind the wall face. In Figure 9.3.7, “folds” or “jogs” were observed on the predicted soil deflection curves. This is because soil elements located next to reinforcement have a smaller deformation than the soil elements located in between the reinforcement layers. Especially at the lower half of the wall, jogs and folds in the modeling results become more obvious. As shown in Figure 9.3.7, the average results of Model ALGMB1 had a reasonable agreement with the inclinometer measurements at end of the construction in the bottom half of the wall. It tended, however, to over-estimate the wall deflection by about 25 mm after surcharge is applied.

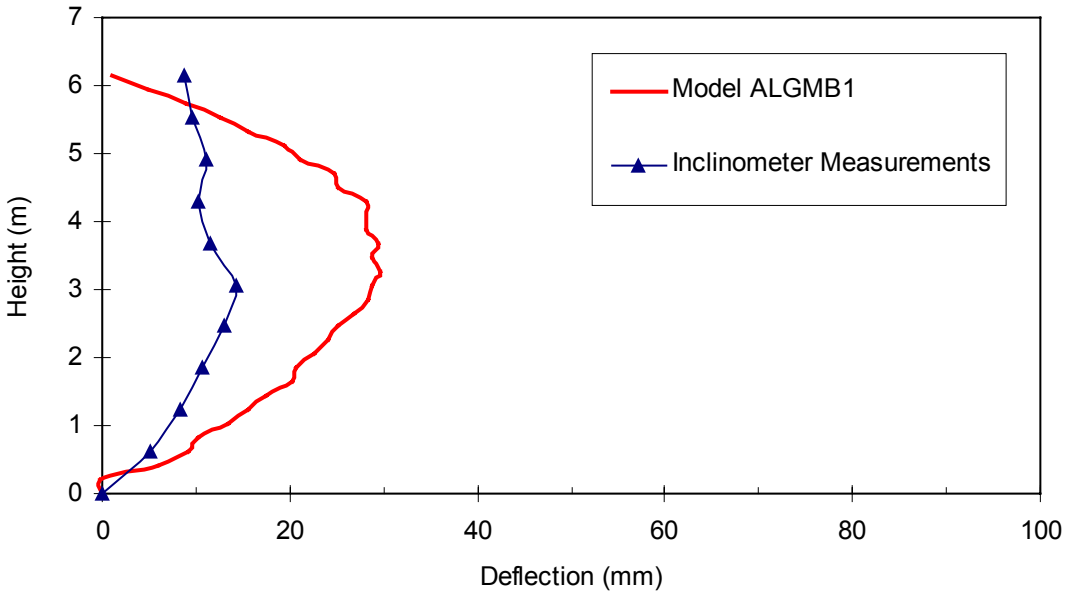

(a) End of construction

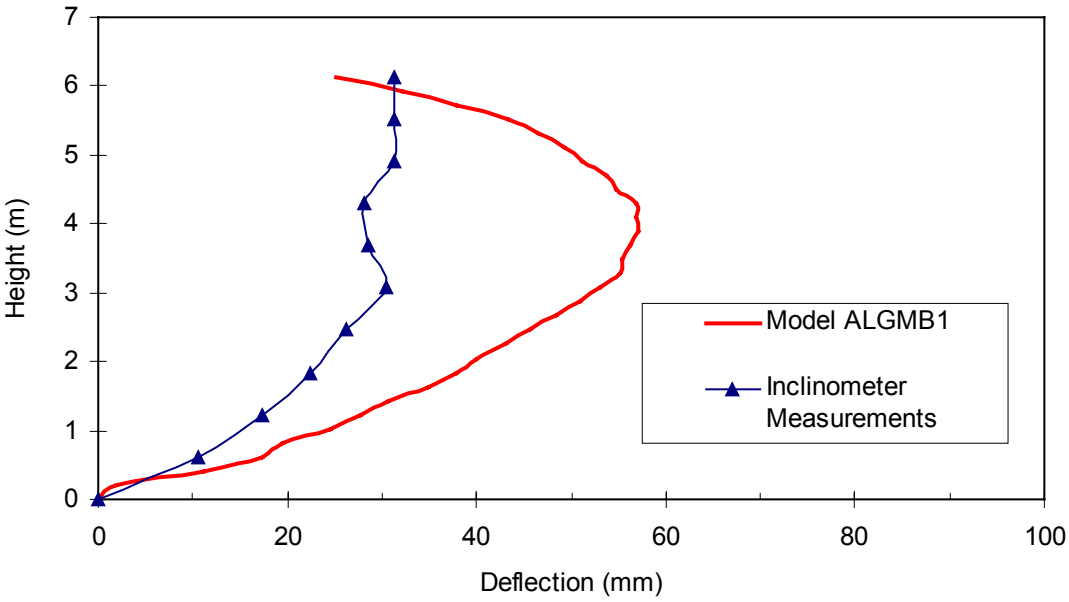

(b) After surcharge

Figure 9.3.6 Predicted and measured wall face deflection of Algonquin modular block faced wall.

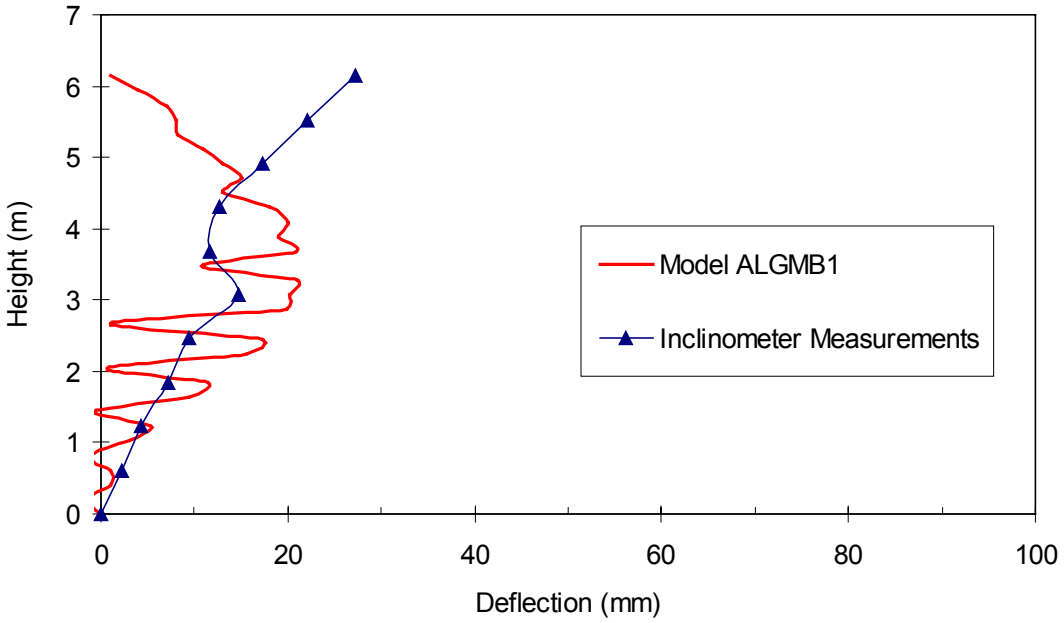

(a) End of construction

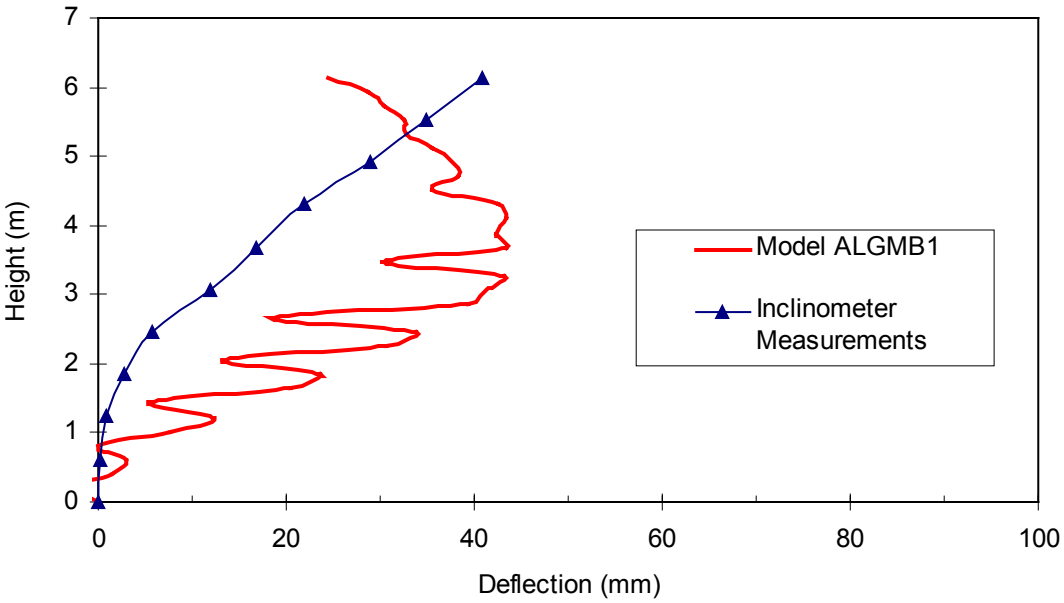

(b) After surcharge

Figure 9.3.7 Predicted and measured wall deflection (2.7m behind the wall face) of Algonquin modular block faced wall.

9.3.4 Algonquin Wrapped Face Wall

Figure 9.3.8 shows the wall deflection prediction of the Algonquin wrapped face wall obtained from Model ALGWF1. However, no field measurements were available for comparison (Christopher, 1993). In Figure 9.3.8, "folds" similar to the deflection prediction of Model ALGMB1 (Figure 9.3.7) were also obtained. Especially at the wall face, bulging in between the reinforcement layers was observed. The maximum wall deflection was found at 2.1 m above the ground, at the water level of the retaining water pond (Figure 9.2.6). Before the retaining water was removed, wall deflections below that location were found to be significantly smaller than the wall deflections above that location. This observation suggests that the retaining water pond really maintained the stability of the wall. After the retaining water pond was removed, the modeling result showed that the wall deflections increased about 20 mm to 30 mm in the lower half of the wall and 10 mm to 15 mm in the upper half of the wall (Figure 9.3.8)

9.3.5 Discussion and Conclusions

1. The developed models were able to reproduce the field measurements of deflections of various GRS walls within reasonable ranges. The material property determination procedures and modeling techniques developed in this research were found to be suitable for predicting the external performance of various GRS walls.

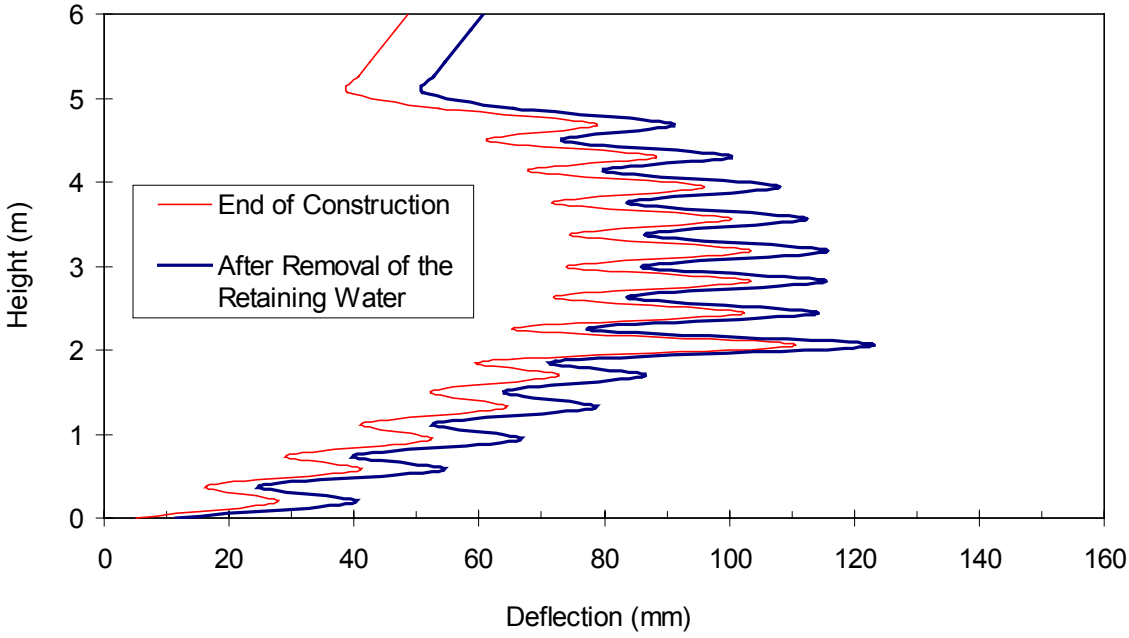

Figure 9.3.8 Predicted face deflection of Algonquin wrapped faced wall.

2. Different predictions were found between the modeling results and inclinometer measurements, especially above the locations of maximum wall deflections predicted by the numerical models (Figures 9.3.2, 9.3.6, and 9.3.7). The inclinometer measurements indicated a maximum wall deflection at the top of the wall, while the modeling results indicated a maximum deflection at about two-thirds height of the wall. A possible explanation is that the inclinometer tubing was not perfectly bonded with the backfill soil, i.e. soil might move around the tubing. To verify the difference between the inclinometer measurements and modeling prediction, the internal strain and stress information such as reinforcement strain distributions and reinforcement tension distributions obtained from both modeling results and instrumentation measurements were analyzed to determine the actual strain magnitudes that occurred in the upper one-third of these walls. Results of these internal strain and stress analyses are presented in the following sections.

3. For GRS walls with complicated facing systems such as modular block facing, accurate deflection predictions relied on not only correct input properties of soil and geosynthetic, but also on the correct input properties of the interface between blocks and reinforcements that were inserted in between the blocks. In Model ALGMB1, input properties of the interfaces between blocks were determined using the manufacturer's information because actual material properties were not reported in the references.

4. Modeling results also show that soil elements located next to reinforcement layers indicate smaller deformations than the soil elements located in between the reinforcements. Especially at the bottom half of the GRS walls or at the face of the wrapped face wall where no structural facing units are used to confine the bulges, this interlayer reinforcing phenomenon becomes more obvious (Figures 9.3.7 and 9.3.8).

9.4 Modeling Results II—Reinforcement Strain Distribution

9.4.1 WSDOT Rainier Avenue Wall

Figure 9.4.1 shows the strain distribution of the instrumented geosynthetic reinforcement layers (Layers 4, 9, 17, and 26) of Model RAING compared with the strain gage and extensometer measurements at end of construction. Layers 4, 9, 17, and 26 were the instrumented layers of the four different reinforcement materials used in the wall (Figure 9.2.2). Figure 9.4.2 is similar to Figure 9.4.1 but shows the reinforcement strain distribution after surcharge was applied.

As shown in Figures 9.4.1 and 9.4.2, the results of Model RAING show excellent agreement with instrumentation measurements of Layer 4, for both maximum strain magnitudes and locations at end of construction and after surcharge.

Reinforcement strain distribution and magnitudes of Layer 9 were also successfully reproduced by Model RAING. At the end of construction, Model RAING was able to verify the maximum strain locations and the reinforcement strain magnitudes of layer 9 (Figure 9.4.1). After surcharge, Model RAING tended to over-predict the reinforcement strains by only 0.3% to 0.7% overall, yet it had very close prediction of the location of the maximum reinforcement strain (Figure 9.4.1).

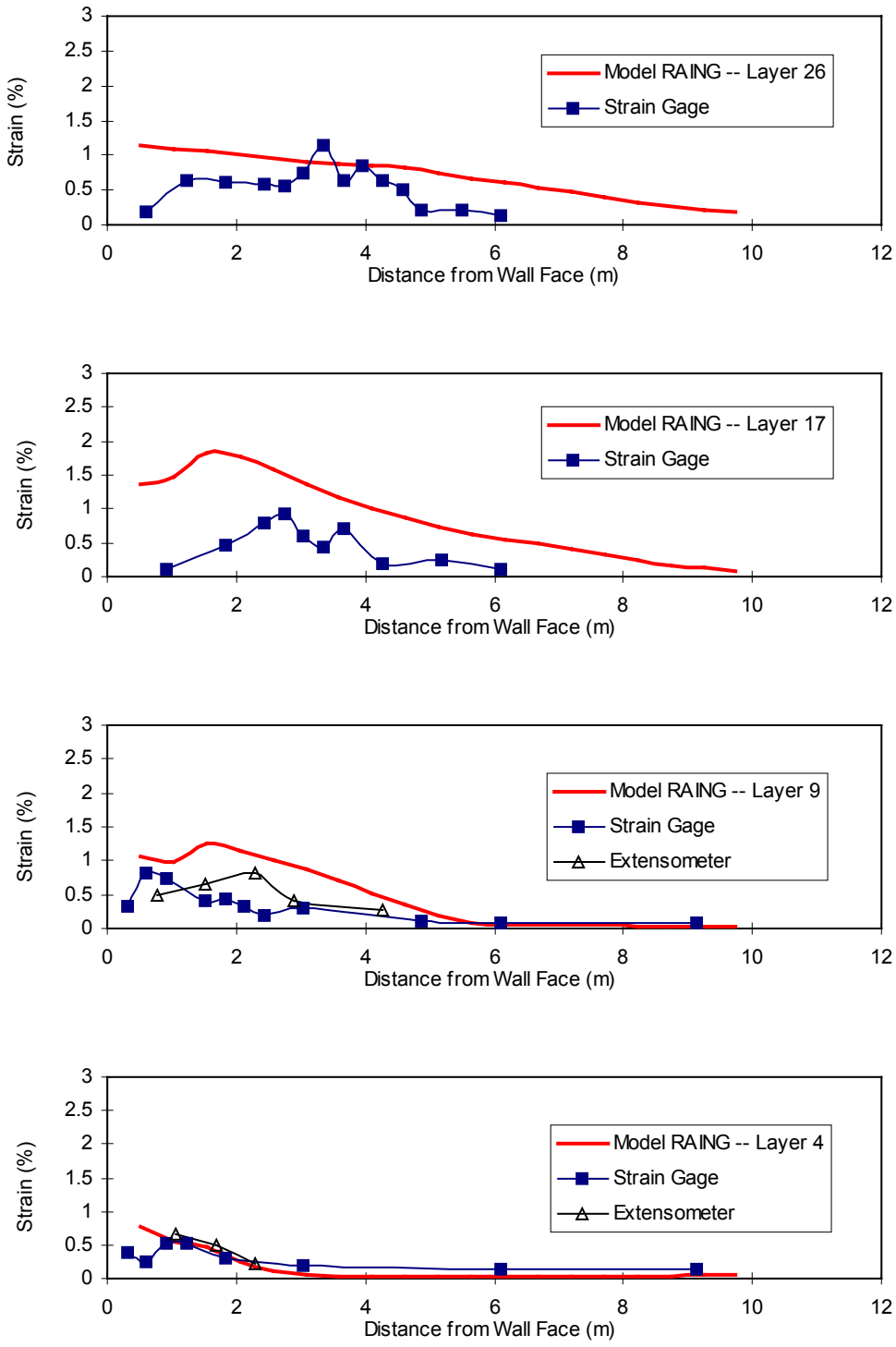

Figure 9.4.1 Predicted and measured reinforcement strain distributions of Rainier Avenue wall, end of wall construction.

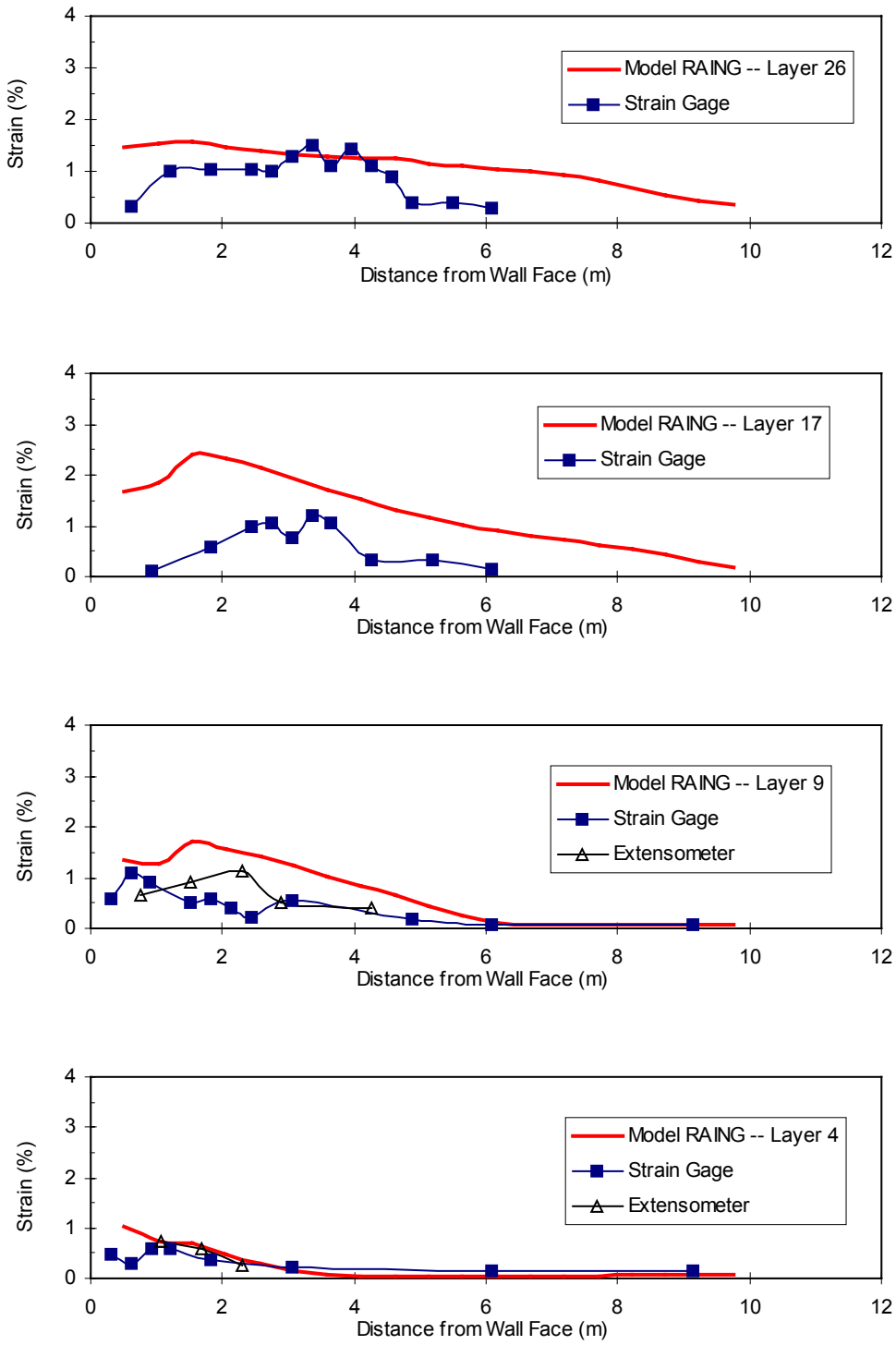

Figure 9.4.2 Predicted and measured reinforcement strain distributions of Rainier Avenue wall, after surcharge.

Model RAING tended to over-estimate the reinforcement strains at higher elevations of the Rainier Avenue wall, and it predicted maximum strain locations different from those observed by instrumentation measurements. However, the differences between the prediction and instrumentation measurements are less than 1.5% of maximum strain magnitudes and within 0.5 m to 1.0 m of the location of the maximum strain. For Layer 17, results of Model RAING showed a single peak strain at 1.75 m behind the wall face with magnitudes of 1.8% at end of construction and 2.5% after surcharge (Figures 9.4.1 and 9.4.2). The measured peak strains were located at 3m behind the wall face and had magnitudes of 1.0% at end of construction and 1.2% after surcharge (Figures 9.4.1 and 9.4.2). Generally speaking, reinforcement strain distributions predicted by Model RAING covered the measured distribution reasonably well.

For Layer 26, as shown in Figures 9.4.1 and 9.4.2, Model RAING gave very good predictions of magnitudes of the maximum reinforcement strains. However, different from the instrumentation measurements which indicated a peak strain at 3.8 m behind the wall face, Model RAING predicted the maximum reinforcement strain at the wall face for both end-of-construction and after-surcharge stages. Possible reasons for the difference is that, in Model RAING, the reinforcement elements were attached to the material element nodes to avoid the violation of strain compatibility during iterations. Reinforcement elements of Layer 26 at the wall face presented a maximum strain at wall face because reinforcement strains inside the backfill were relatively small at this

elevation. The reinforcement strain caused by the bulges at wall face in between the horizontal reinforcement layers turns out to be the maximum reinforcement strain because the reinforcement elements were hard tied onto the material elements nodes.

9.4.2 Algonquin Concrete Panel Faced Walls

Results of Model ALGPC2 showed a good agreement to the measured reinforcement strain distributions (Figure 9.4.3). For the lower half of the wall, Model ALGPC2 tended to over-predict the reinforcement strains at layer 1 by only 0.3%, but it showed an excellent agreement with the measurements at layers 2 and 3 (Figure 9.4.3). Results of Model ALGPC2 tended to under-predict the reinforcement strains at upper half of the wall; however, the difference was less than 0.3% (Figure 9.4.3).

For steel reinforced walls, Model ALGPC1 and ALGPC3 also showed reasonable predictions to the measured reinforcement strain distributions of Walls 1 and 3 of Algonquin FHWA test walls (Figures 9.4.4 and 9.4.5). Because of the high stiffness of the reinforcement of Walls 1 and 3, the magnitudes of the reinforcement strains are very small. Models ALGPC1 and ALGPC3 predicted very small reinforcement strains, and the difference between predicted and measured maximum strain is less than 0.03% except where the strain gage measurements appear to have been defective.

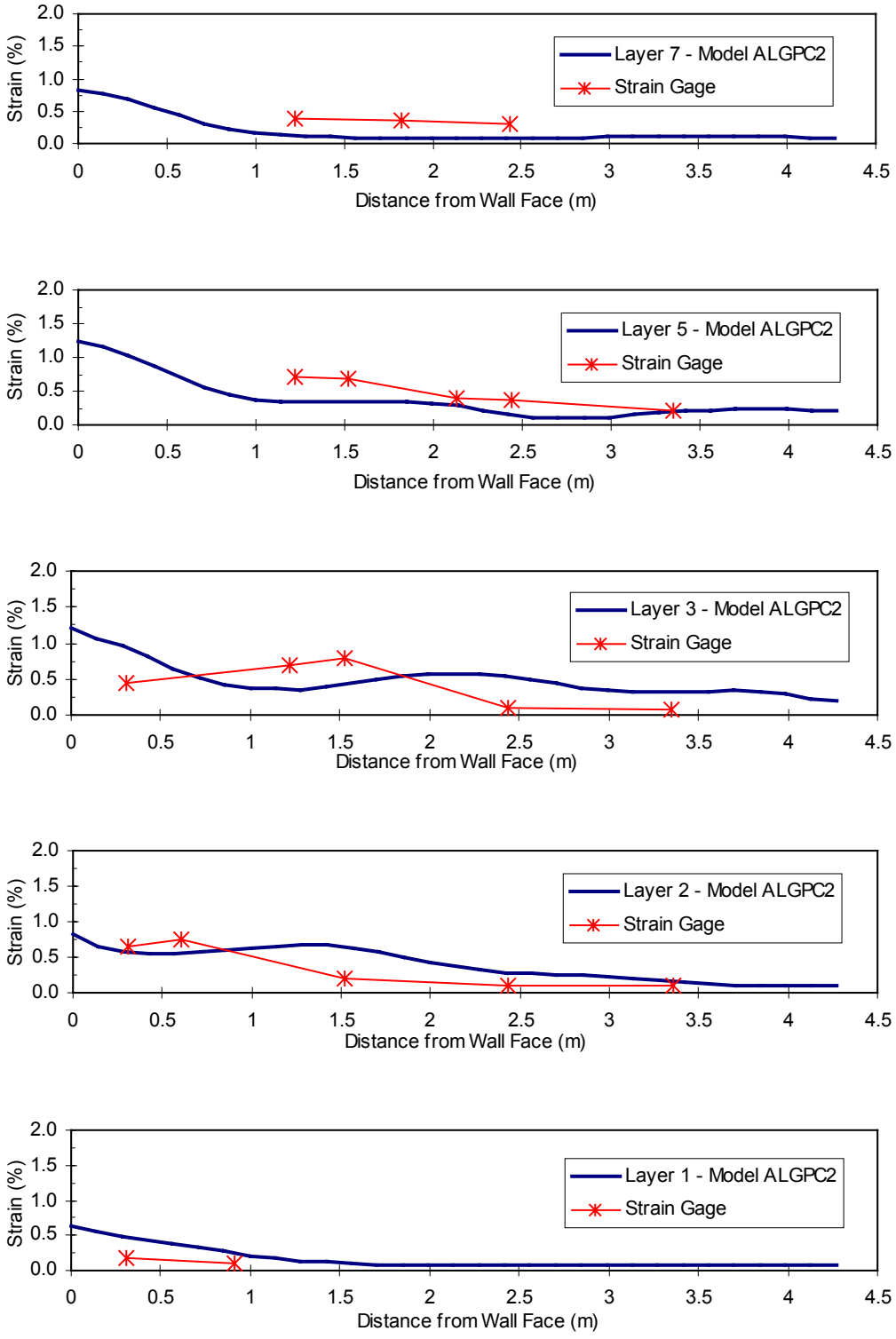

Figure 9.4.3 Predicted and measured reinforcement strain distributions of Algonquin concrete panel faced wall, Wall 2 (geogrid reinforced).

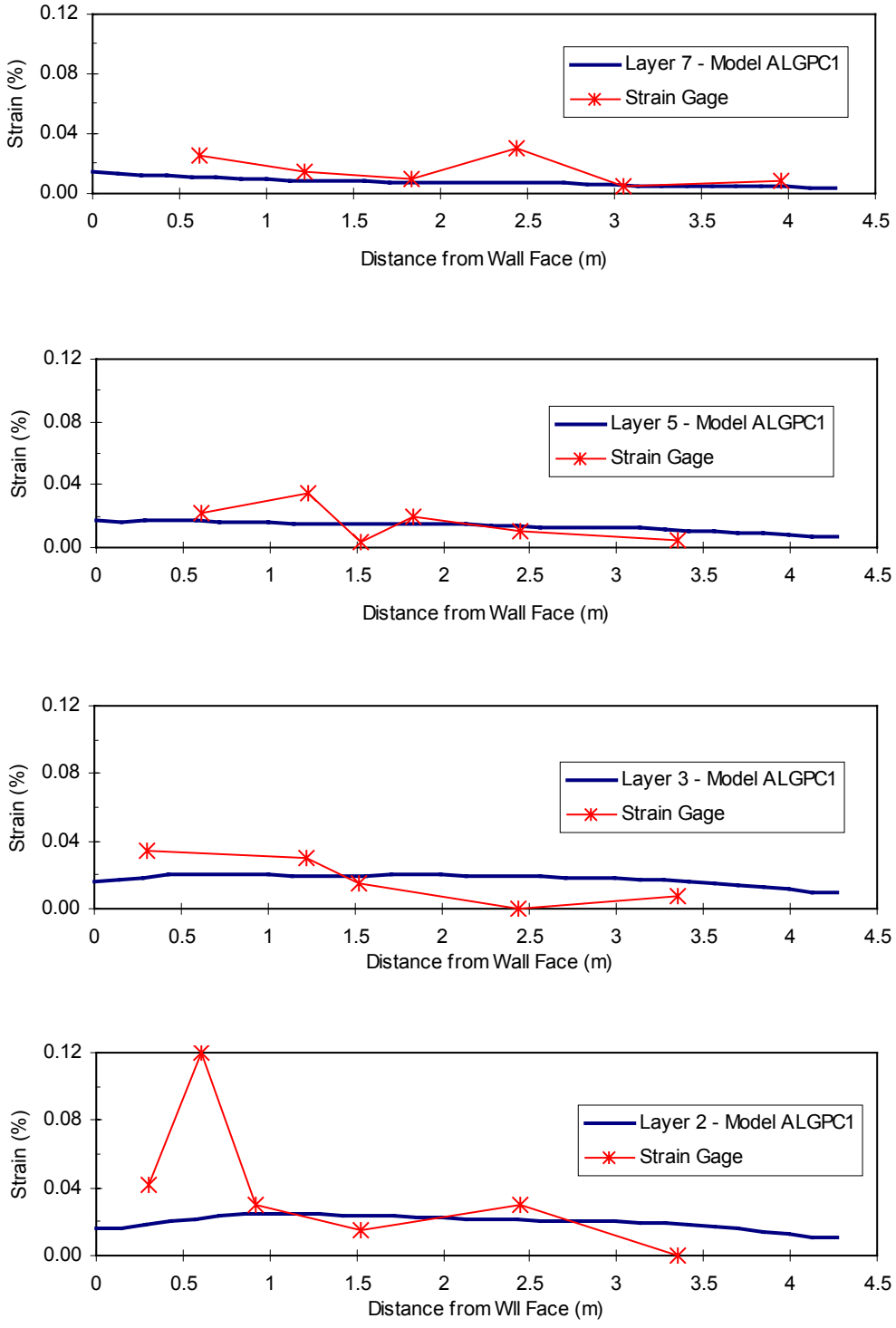

Figure 9.4.4 Predicted and measured reinforcement strain distributions of Algonquin concrete panel faced wall, Wall 1 (steel reinforced).

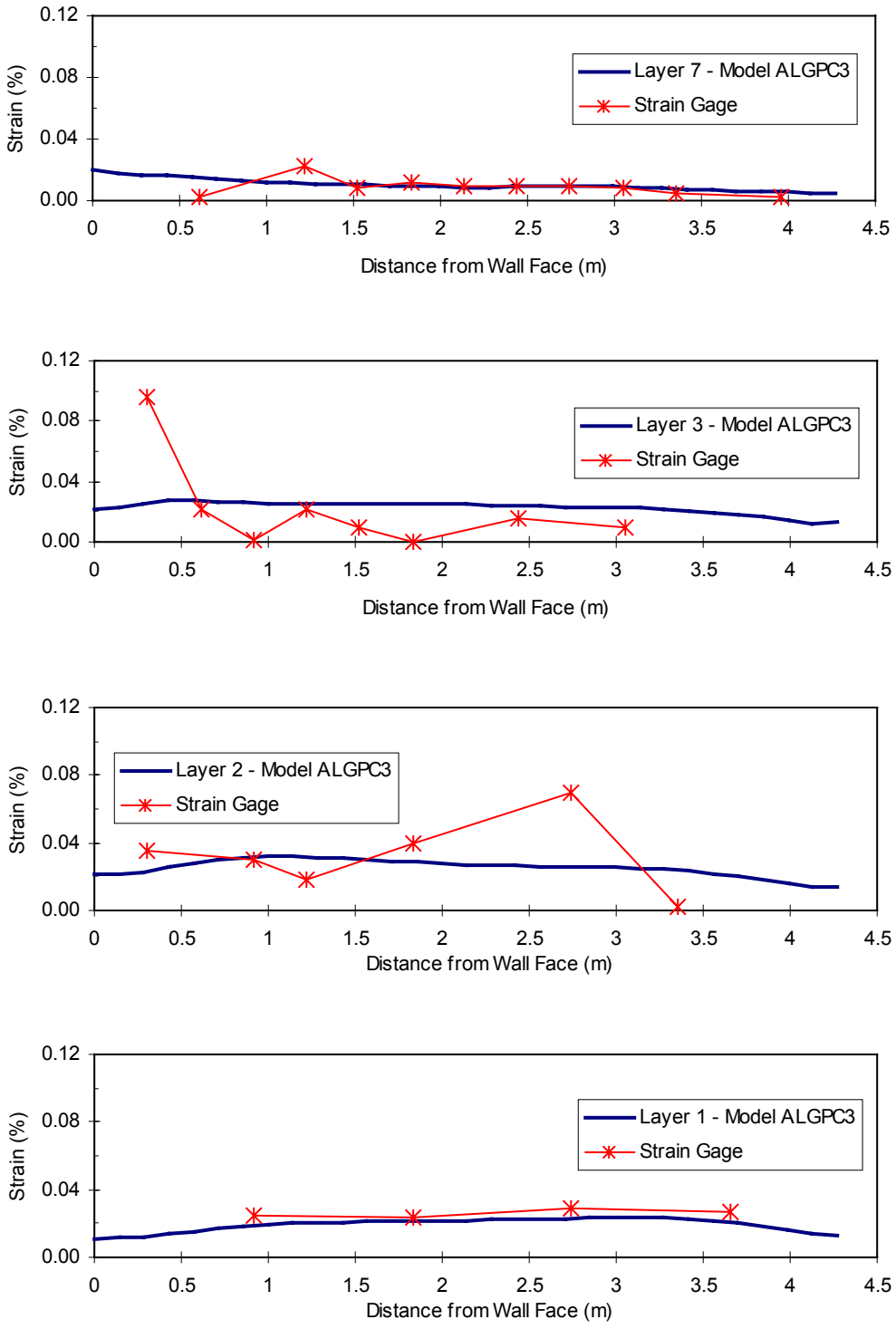

Figure 9.4.5 Predicted and measured reinforcement strain distributions of Algonquin concrete panel faced wall, Wall 3 (steel reinforced).

9.4.3 Algonquin Modular Block Faced Wall

Model ALGMB1 was able to predict the reinforcement strains of the Algonquin modular block faced wall quite well for stages both at end of construction and after surcharge. Figures 9.4.6 and 9.4.7 show the modeling results compared to the strain gage measurements. Results of Model ALGMB1 showed a very good agreement to the measurements at end of construction in both distributions and magnitudes (Figure 9.4.6). Even after surcharge was applied, it only tended to over-predict the maximum reinforcement strains by average 0.5% (Figure 9.4.7).

As shown in Figures 9.4.3, 9.4.6 and 9.4.7, both predicted and measured reinforcement strains in the upper reinforcement layers were smaller than those of the reinforcement layers at locations where the maximum wall deflections occurred (around two-thirds of the wall height). This observation suggests that the deflection predictions of the numerical models and optical face surveys might be more reasonable than the inclinometer measurements, i.e. only small deformations probably occurred at the top of the GRS walls.

9.4.4 Algonquin Wrapped Face Wall

Figures 9.4.8 and 9.4.9 show the modeling results of Model ALGWF1 compared to the strain gage measurements at end of construction and after removal of the retaining water pond. As shown in Figures 9.4.8 and 9.4.9, Model ALGWF1 was able to predict both distributions and magnitudes of the reinforcement strains within a reasonable

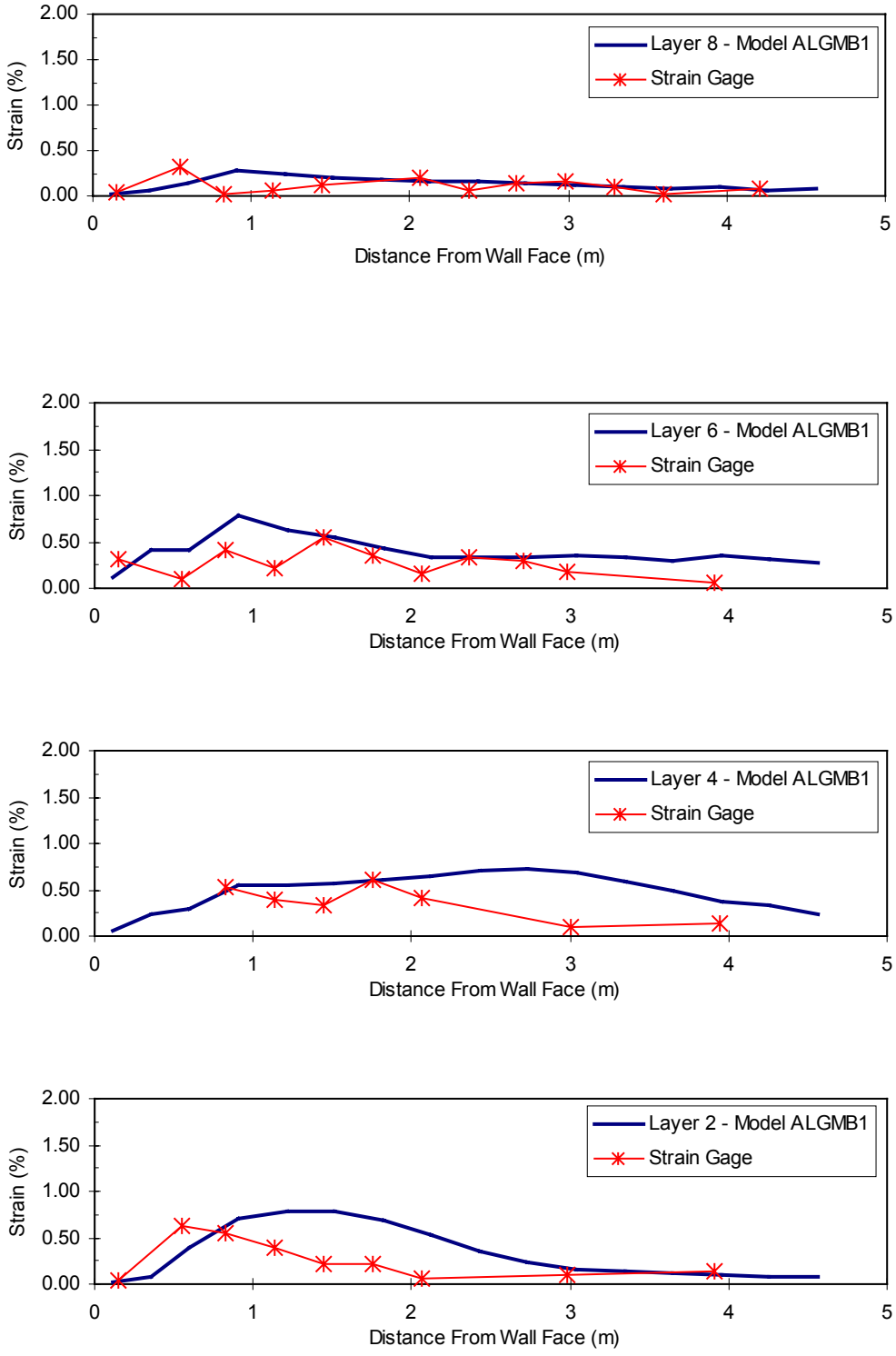

Figure 9.4.6 Predicted and measured reinforcement strain distributions of Algonquin modular block faced wall, end of construction.

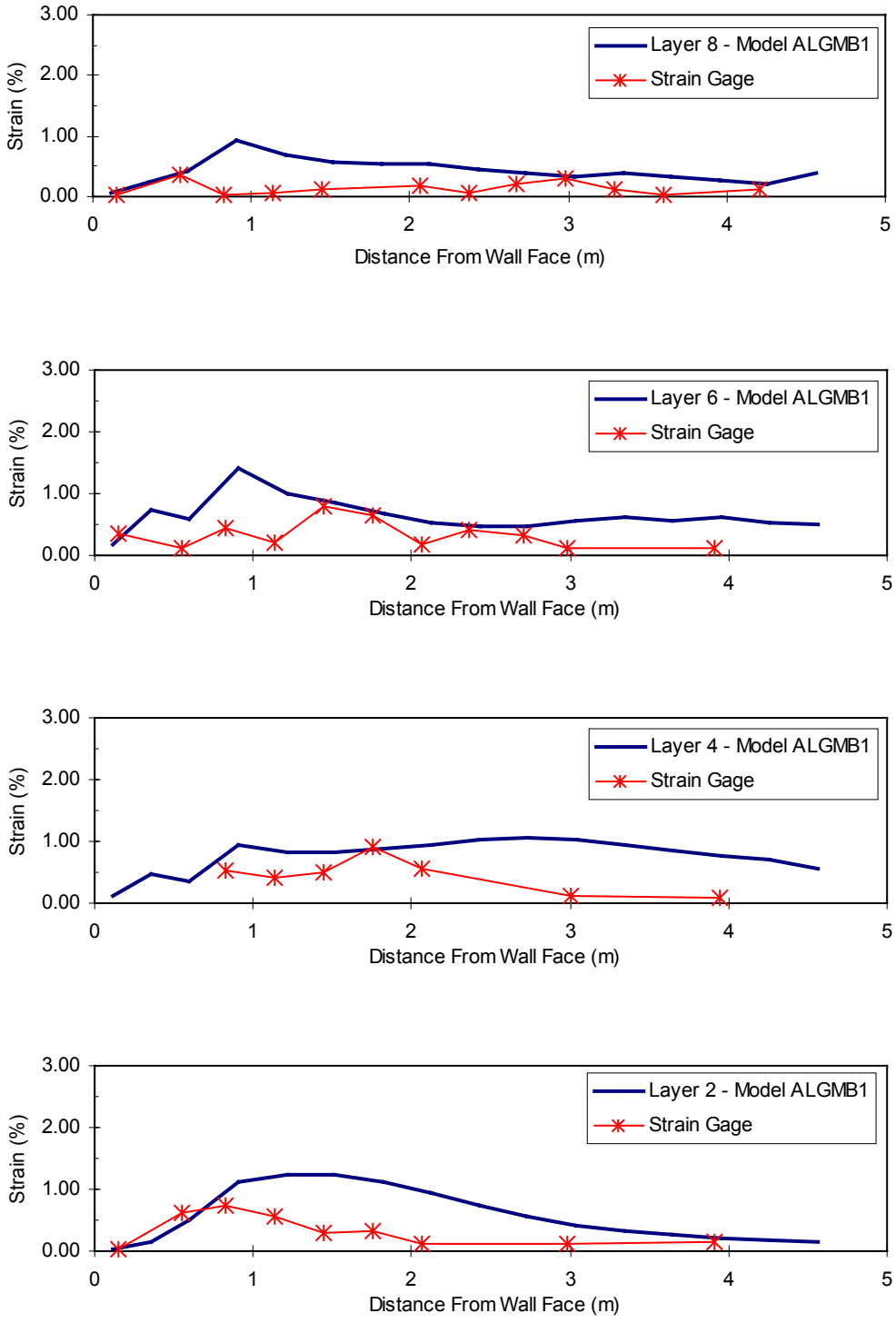

Figure 9.4.7 Predicted and measured reinforcement strain distributions of Algonquin modular block faced wall, after surcharge.

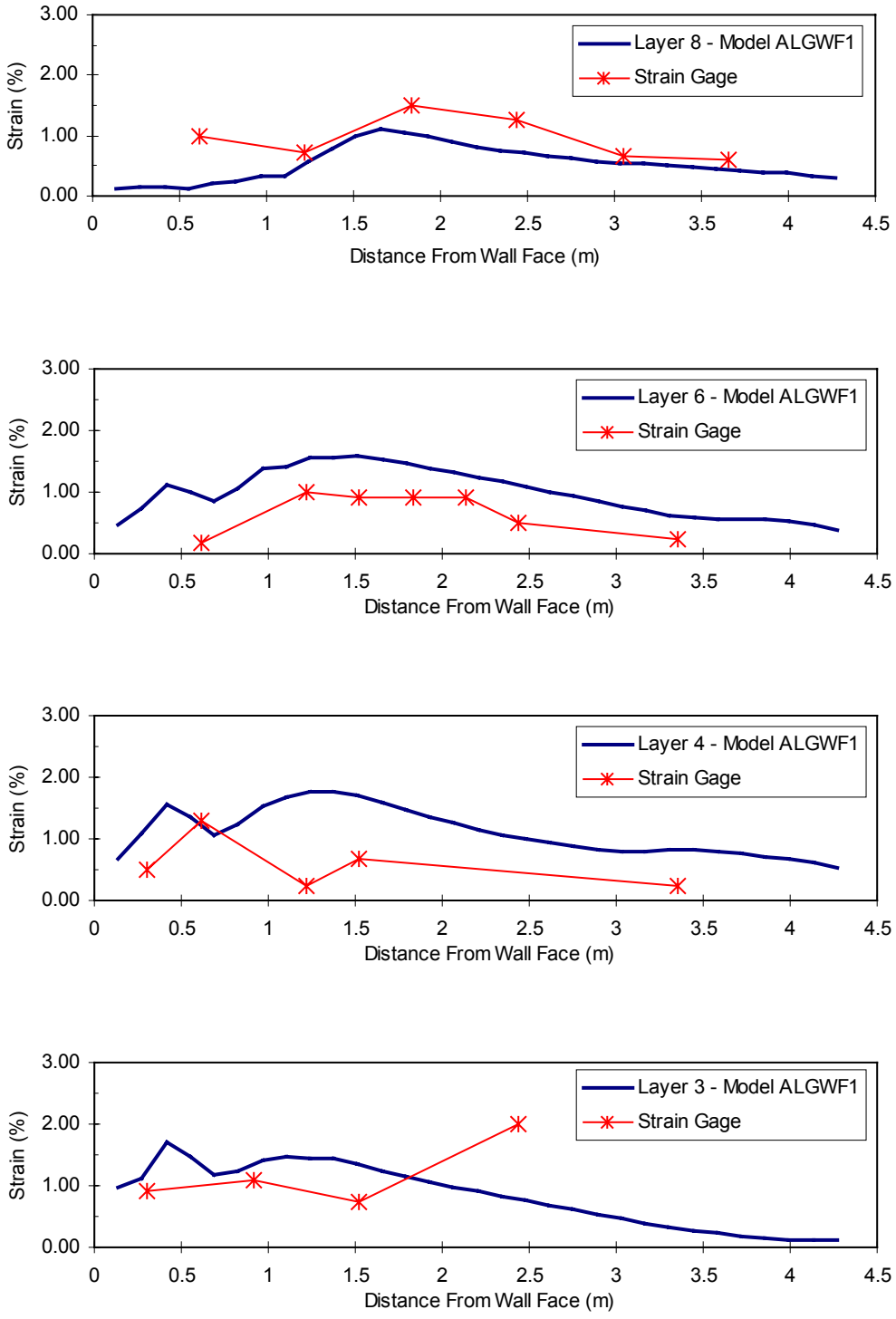

Figure 9.4.8 Predicted and measured reinforcement strain distributions of Algonquin wrapped face wall, end of construction.

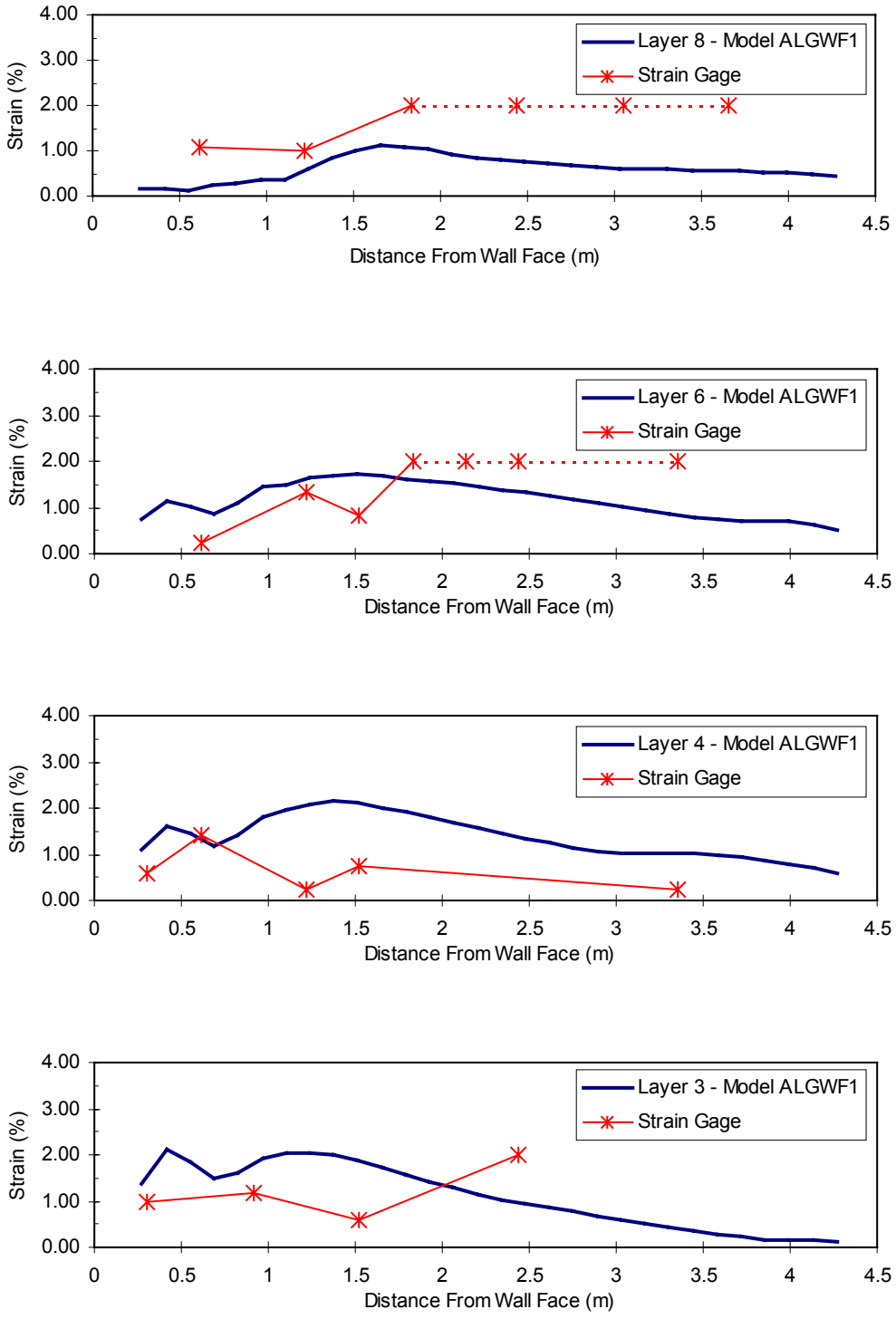

Figure 9.4.9 Predicted and measured reinforcement strain distributions of Algonquin wrapped face wall, after removing the retaining water.

range at end of construction as well as after removing the retaining water face support. At end of construction, Model ALGWF1 only under-predicted the reinforcement strain by 0.5% to 0.8% at the topmost layer (Layer 8). It tended to over-predict the reinforcement strain by 0.2% to 1.0% at Layers 3, 4, and 6 (Figure 9.4.8). Similar results were also found after removing the retaining water. Model ALGWF1 tended to over-predict the reinforcement strains at lower layers (Layers 3 and 4) by an average of 1.2%, and under-predict the reinforcement strains at Layer 8 (Figure 9.4.9). A possible reason for the differences between the predicted and measured reinforcement strains is that the input properties of the nonwoven reinforcement and gabion basket were determined based on the manufacturer's information of similar materials. The actual material properties were not reported in the documentation (Christopher, 1993).

9.4.5 Discussion and Conclusions

1. The developed models were able to reproduce reasonably well in most cases the reinforcement strain distributions of various GRS walls. The material property determination procedures and modeling techniques developed in this research were found to be also suitable for predicting the internal strain levels of various GRS walls.

2. Accurate material properties were also found to be the key to reproducing the internal performance data of GRS walls. Results of Model RAING and ALGPC2 showed better predictions of reinforcement strains than the results of Model

ALGMB1 and ALGWF1 because information about material properties of the Rainier Avenue wall and Algonquin concrete panel faced wall was more complete.

3. Results of Model ALGMB1 and ALGWF1verified that numerical models developed using modeling techniques described in Chapter 8 were able to provide reasonable working strain information of GRS walls, even when insufficient material information was available and material properties had to be determined based on information from similar materials.

4. Results of Model ALGWF1 also showed that procedures based on the UCD test result reported by Boyle (1995) to determine the in-soil stiffness from in-isolation tests of nonwoven geosynthetics were appropriate. The input stiffness of the nonwoven geosynthetic reinforcement was determined by multiplying the 2% strain in-isolation stiffness by five.

9.5 Modeling Results III—Reinforcement Tension Distributions

Distributions of reinforcement tensions of each layer obtained from the developed numerical models were found to be different from the distribution assumed in present design procedures. For example, the tie-back wedge method assumes that the reinforcement tension is highest at the bottom of the wall and decreases with wall height to the smallest values at top of the wall. Modeling results shown in this section indicated that the reinforcement tensions increased from top of the wall as the depth increased, and reached their maximum value at elevations between 0.5H to 0.2H, where H is the height of the wall. After reaching their maximum values, the reinforcement tensions started to decrease and had very small values at the bottom of the walls. In this section, reinforcement tension predictions of the developed numerical models are presented and compared to the tie-back wedge method (Equation 9.5.1).

$$T_{reinf} = K_a \cdot \gamma \cdot z \cdot S_v \qquad \text{(Eq. 9.5.1)}$$

where T_{reinf} = calculated reinforcement tension

K_a = active lateral earth pressure coefficient

γ = unit weight of soil

z = depth from top of the wall

S_v = vertical spacing of the reinforcement layers

9.5.1 WSDOT Rainier Avenue Wall

Figure 9.5.1 shows the distributions of average reinforcement tensions (T_{ave}) that were reduced from results of Model RAING versus the normalized height. The average

reinforcement tensions (T_{ave}) were determined by multiplying the average predicted reinforcement strains with the in-soil low strain rate reinforcement stiffness to represent the overall reinforcement tensions. Modeling results shown in Figure 9.5.1 indicate that the values of T_{ave} increased as the height of the wall decreased at the upper half of the wall, and they decreased with height of wall at lower half of the wall. The highest value of T_{ave} appeared at the height equal to 0.25H. Reinforcement tensions calculated using Equation 9.5.1 were also plotted in Figure 9.5.1 for comparison. As shown in Figure 9.5.1, the reinforcement tensions calculated by the tie-back wedge method appear to be much higher than the predicted reinforcement tensions especially at the lower half of the wall. This observation verifies that the tie-back method tends to over-design the reinforcement tensions at lower part of the wall. Possible reasons for this are that the conventional method uses the lateral earth pressure distribution without modifications for soil-reinforcement interactions and toe restraint provided by the soil foundation in front of the wall.

9.5.2 Algonquin Concrete Panel Faced Walls

The distribution of reinforcement tension in Model ALGPC2 was also found to be different than that was assumed in the tie-back method. Figure 9.5.2 shows the predicted reinforcement tension distribution compared to reinforcement tensions calculated using Equation 9.5.1. As shown in Figure 9.5.2, the predicted reinforcement tensions are smaller than the calculated reinforcement tensions, especially at the bottom of the wall. Model ALGPC2 indicates that the actual maximum reinforcement

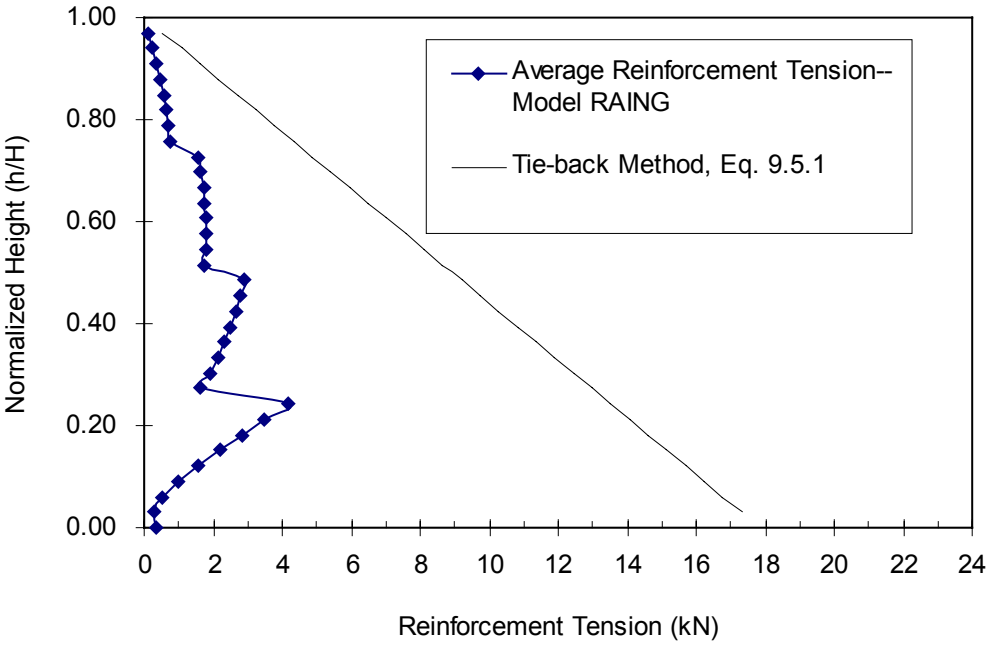

(a) End of construction

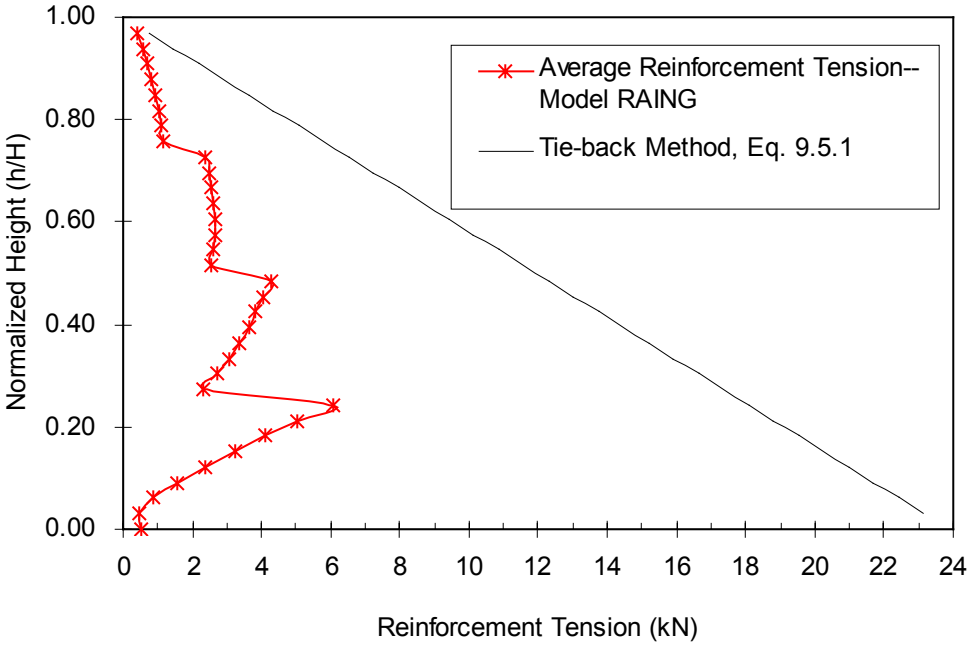

(b) After surcharge

Figure 9.5.1 Distributions of reinforcement tensions of Rainier Avenue wall.

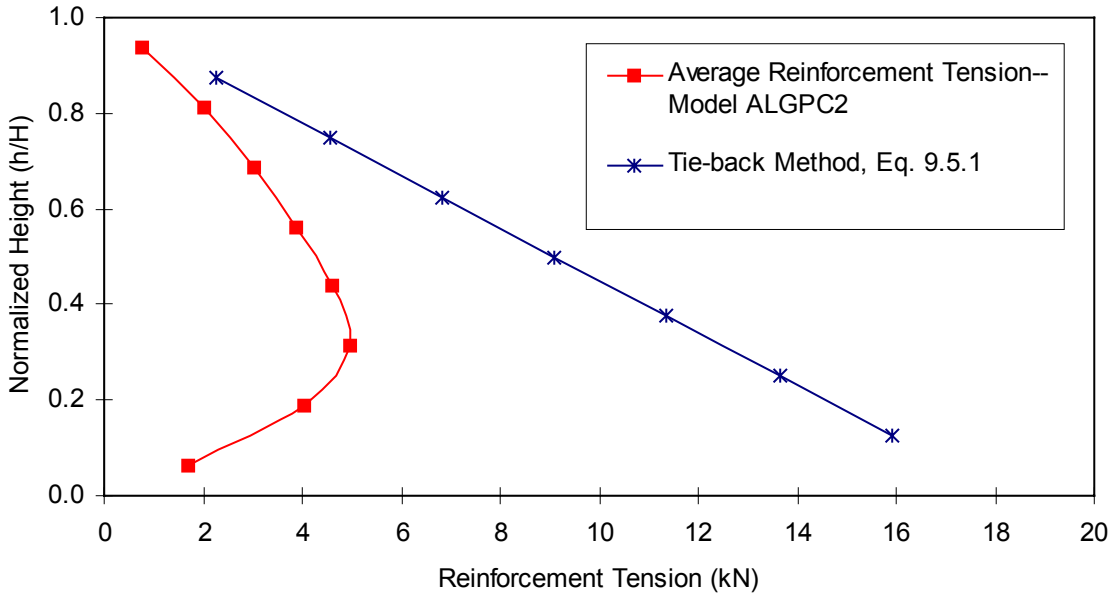

Figure 9.5.2 Distribution of reinforcement tensions of Algonquin concrete panel faced geogrid wall.

tension occurred at a height of about 0.3H instead of at the bottom of the wall, as predicted by the tie-back method.

Modeling results of ALGPC1 and ALGPC3 showed that reinforcement tension distributions of the steel reinforced walls had shapes similar to that of the geogrid wall, but they had higher reinforcement tension values than those of geosynthetic reinforcement (Figure 9.5.3). As shown in Figure 9.5.3, the tie-back method was able to predict the tensions of steel reinforcements quite well, especially in the upper half of the wall.

9.5.3 Algonquin Modular Block Faced Wall

Similar to the modeling results of the case histories presented in previous sections, reinforcement tensions predicted by Model ALGMB1 were found to be smaller than those calculated using the Equation 9.5.1 (the tie-back method) (Figure 9.5.4). The maximum reinforcement tension of the Algonquin modular block faced wall occurred at about 0.5H at end of construction and at about 0.4H after surcharge (Figure 9.5.4).

9.5.4 Algonquin Wrapped Face Wall

Figure 9.5.5 shows that, even in a designed-to-fail GRS wall such as the Algonquin wrapped face wall, the actual reinforcement tensions were still smaller than the reinforcement tension calculated using the tie-back method. Results of Model ALGWF1 also indicated that the maximum reinforcement tensions occurred at around 0.3H (Figure 9.5.5).

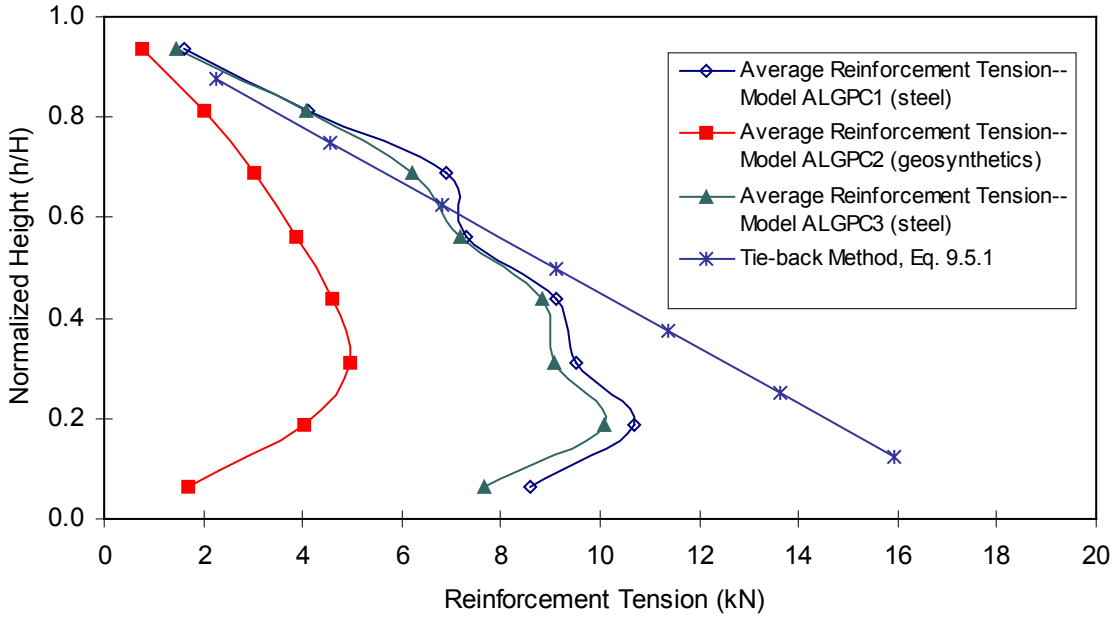

Figure 9.5.3 Distributions of reinforcement tensions of Algonquin concrete panel faced walls.

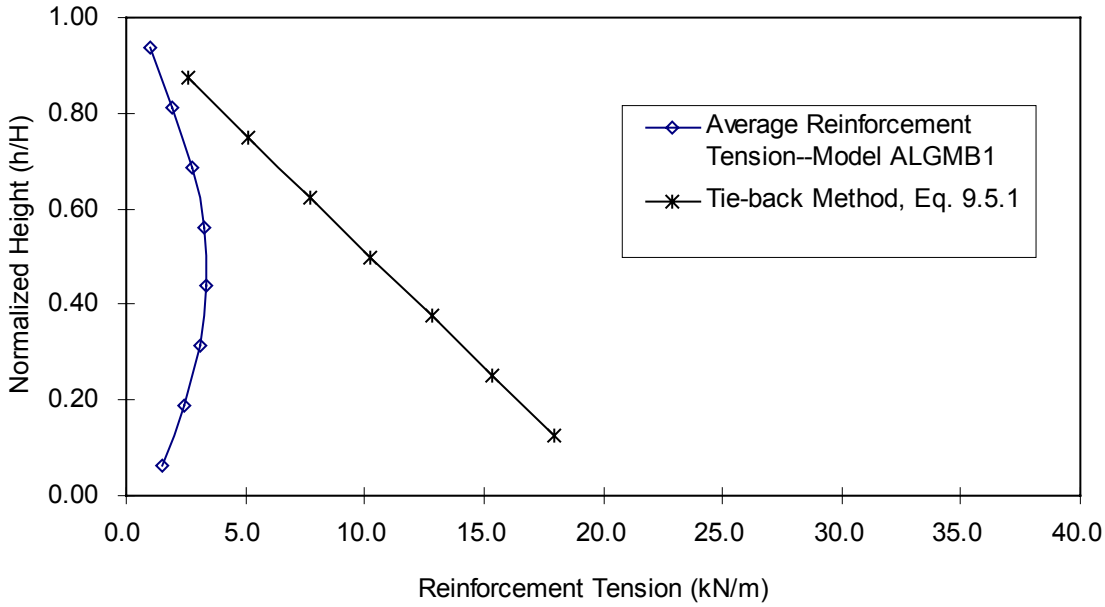

(a) End of construction

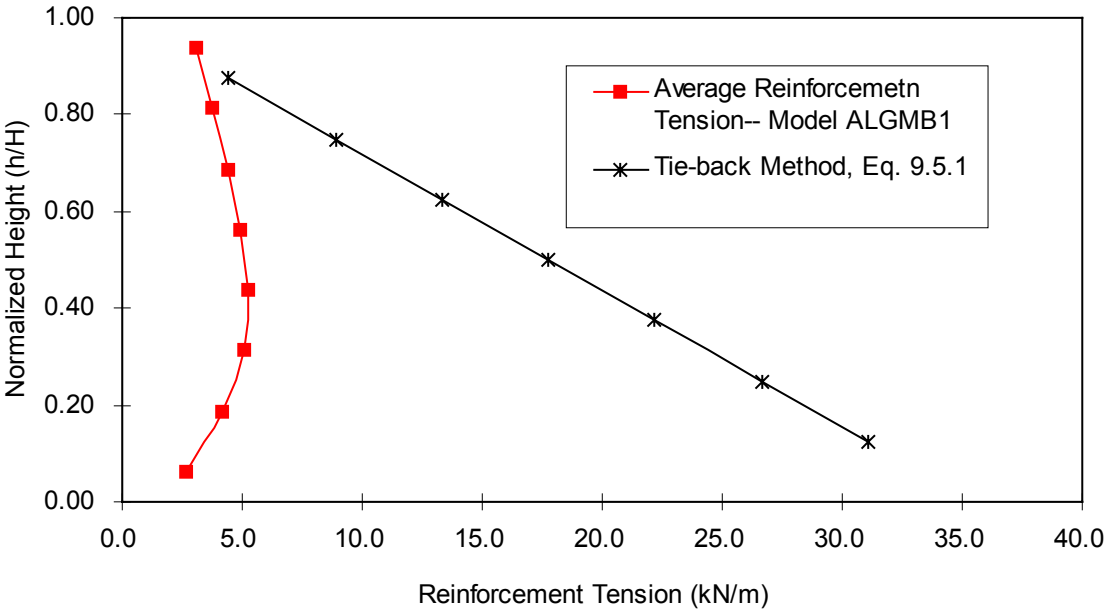

(b) After surcharge

Figure 9.5.4 Distributions of reinforcement tensions of Algonquin modular block faced wall.

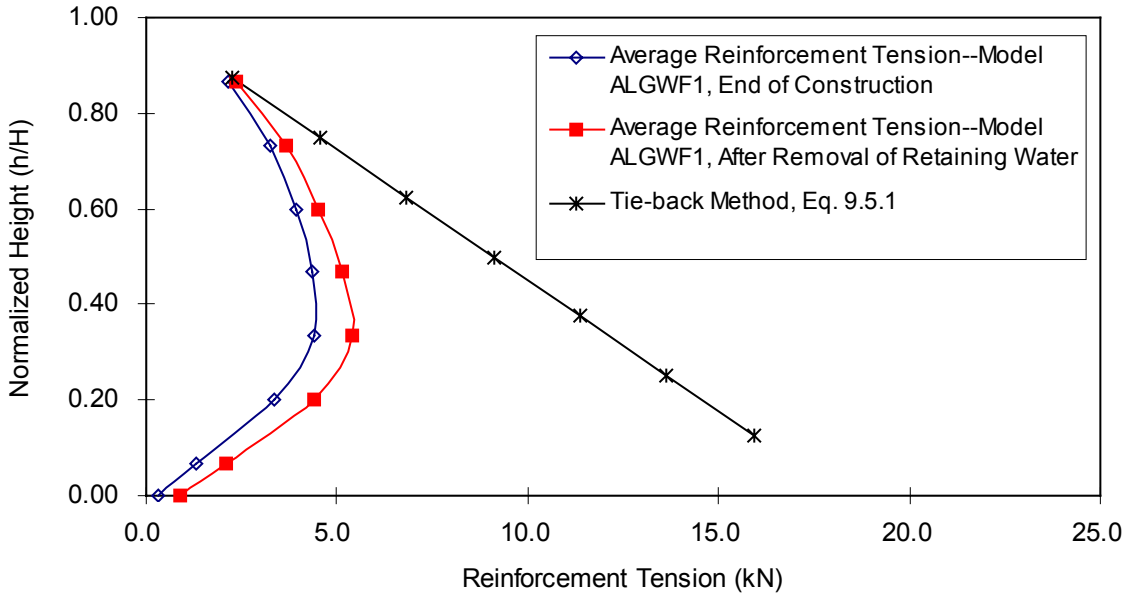

Figure 9.5.5 Distributions of reinforcement tensions of Algonquin wrapped face wall.

9.5.5 Discussion and Conclusions

1. Reinforcement tensions calculated using Equation 9.5.1 (the tie-back wedge method) appeared to be much higher, especially at the lower half of the walls, than those predicted by the numerical models that were able to reproduce both external and internal performance of GRS walls. This observation verifies that the conventional design method tends to over-design the reinforcement tensions in the lower part of the wall. Possible reasons are that the conventional method uses the lateral earth pressure distribution without modifications for soil-reinforcement interactions and toe restraint.

2. Modeling results also showed that actual locations of maximum reinforcement tensions of GRS walls occurred at heights between 0.2H to 0.5H instead of at bottom of the walls, as predicted by the tie-back method.

9.6 Summary and Conclusions

1. Numerical models that were developed using material property determination procedures described in Chapter 7 and modeling techniques described in Chapter 8 were able to reproduce both external and internal performance of GRS walls within reasonable ranges.

2. Accurate material properties are concluded as the key to a successful performance modeling of GRS walls. Results of Models RAING and ALGPC showed better predictions of wall deflection and reinforcement strain distributions than the results of Models ALGMB1 and ALGWF1 because information of material properties of the Rainier Avenue wall and Algonquin concrete panel faced wall were more complete.

3. For GRS walls with complicated facing systems such as modular block facing, accurate deflection predictions rely on not only correct input properties of soil and geosynthetic, but also on the correct input properties of the interfaces between blocks and reinforcement inserted between the blocks. In Model ALGMB1, input properties of the interfaces between blocks were determined using the manufacturer's information because actual material properties were not reported in the references. Input properties of reinforcements inserted between blocks can be determined using connection test data, if available.

4. Modeling results also indicate that soil elements located adjacent to reinforcement

layers have smaller deformations than soil elements located between the reinforcements. Especially at the lower half of the GRS walls or at the face of a wrapped face wall where no structural facing units are used to confine the bulges, this reinforcing phenomenon becomes more obvious (Figures 9.3.7 and 9.3.8).

5. Differences were found between the modeling results and inclinometer measurements, especially above the locations of maximum wall deflections predicted by the numerical models (Figures 9.3.2, 9.3.6, and 9.3.7). The inclinometer measurements indicated a maximum wall deflection at the top of the wall, while the modeling results indicated a maximum deflection at about two-thirds height of the wall. Both predicted and measured results of reinforcement strain distributions verified that the deflection predictions of the numerical models and optical face survey are more reasonable than the inclinometer measurements, i.e. only small deformation occurred at top of the GRS walls. As shown in Figures 9.4.3, 9.4.6 and 9.4.7, both predicted and measured reinforcement strains in the upper reinforcement layers were smaller than those of the reinforcement layers at locations where the maximum wall deflections occurred (about two-thirds of the wall heights).

6. Results of Models ALGMB1 and ALGWF1verified that numerical models developed using modeling techniques described in Chapter 8 were able to provide reasonable working strain information of GRS walls when insufficient material properties were provided and input material properties were determined from

information on similar materials.

7. Results of Model ALGWF1 also showed that procedures used to determine the in-soil stiffness from in-isolation test data for nonwoven geosynthetics were appropriate. The input stiffness of the nonwoven geosynthetic reinforcement was determined by multiplying the 2% strain in-isolation stiffness by five. This modification was based on the UCD test result reported by Boyle (1995).

8. Reinforcement tensions calculated using Equation 9.5.1 (the tie-back wedge method) appeared to be much higher, especially at the lower half of the wall, than those predicted by the numerical models that were able to reproduce both external and internal performance of GRS walls. This observation verifies that the conventional design method tends to over-design the reinforcement tensions, especially in the lower part of the wall. Possible reasons are that the conventional method uses a lateral earth pressure distribution without modifications for soil-reinforcement interactions and toe restraint.

9. Modeling results also showed that actual locations of maximum reinforcement tensions of GRS walls occurred at heights between 0.2H to 0.5H instead of at bottom of the walls, as predicted by the tie-back method.

Chapter 10

Prediction of Performance of Full Scale GRS Test Walls

As a collaborative part of this research, a program to build and test large scale GRS walls in the laboratory was conducted at the Royal Military College of Canada (RMCC). The test walls were designed to systematically change design factors such as reinforcement stiffness and spacing. FLAC models of these test walls were developed in an attempt to make performance predictions before the walls were constructed (so called "Class A" predictions). The purposes of this exercise were to:

1. Further examine and improve the developed modeling techniques,

2. Investigate the effects of reinforcement stiffness and reinforcement spacing on wall performance under high surcharges, and

3. Examine the feasibility of using the developed modeling techniques to perform parametric analyses of design factors such as reinforcement stiffness and spacing.

In this chapter, a brief description of the RMCC test program as well as the results of the Class A predictions are presented. Differences between real walls and the experimental walls tested in laboratory are also discussed.

10.1 Full Scale GRS Test Walls

The detailed testing program, including material properties, test facility and instrumentation, and the test results were reported by Burgess (1999). All three RMCC test walls had the same height (3.6m) and width (3.4m). They were all built on a concrete laboratory floor. Backfill material was a clean sand with a friction angle equal to 42 deg and no cohesion. Detailed triaxial and plane strain test results of the RMC sand were presented in Chapter 7. The reinforcement was a high-density polypropylene geogrid product (Tensar BX1100). The geogrid reinforcement was oriented with its machine direction (weak direction) in the plane strain direction of the test facility to ensure that large wall deflection developed during tests (Burgess, 1999). Reinforcement stiffness of this geogrid in the machine direction was 110 kN/m at 2% strain after low strain rate reduction described in Chapter 7. The embedded length of the reinforcement was 2.5 m.

Commercially available Pisa II blocks manufactured by Unilock Ltd in Georgetown, Ontario were used as the facing system unit of this study. The blocks were approximately 300 mm in depth, 150 mm high, 200 mm wide, and had a mass of 20 kg per unit (Burgess, 1999). The interlock between blocks relied on a concrete key on the top that matched a slot in the bottom of each block, as well as the friction between the contact surfaces of the blocks. All test walls were fully instrumented, and performance data were collected during construction and surcharging. Figure 10.1.1 shows the typical cross section of the test walls with instrumentation layout.

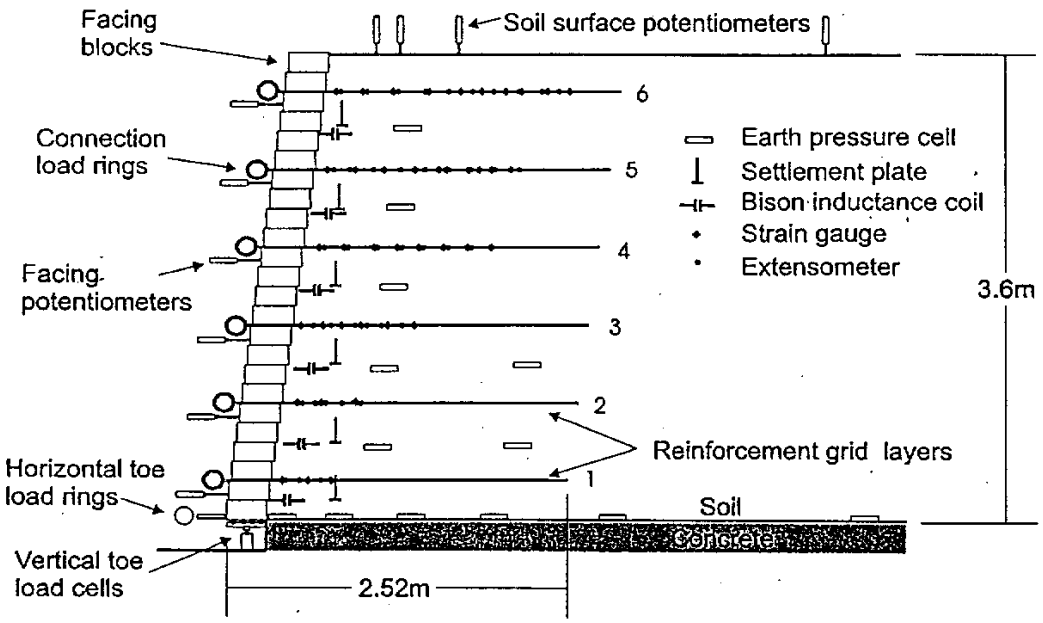

Figure 10.1.1 Typical cross section of the RMCC test walls with instrumentation layout (after Burgess, 1999).

Table 10.1.1 Summary of RMC test walls.

Wall Number	Ultimate Strength of Reinforcement T_{ult} (kN/m)	Back-Calculated Factor of Safety*	Reinforcement Spacing, S_v (m)	Maximum Surcharge Applied, P_s (kPa)
1	12	2.9	0.6	115
2	6**	1.5	0.6	85
3	12	2.0	0.9	95

* Factors of safety is calculated without taking surcharges into consideration.

** The same geogrid used in Wall 1. Reinforcement stiffness and strength were assumed to be reduced 50% by removing every second longitudinal member of the grid.

Surcharge was applied on the top of the walls using confined airbags. This method allowed incremental surcharge control and a relatively high surcharge to be applied. Table 10.1.1 lists the factor of safety, ultimate strength of the reinforcement, and maximum surcharge applied to the walls.

10.2 Modeling Result

Three FLAC models were developed to model the performance of test Walls 1, 2, and 3. Model RMC1 was first developed to reproduce the performance of Wall 1. The trial model of RMC1 failed to predict the performance of Wall 1 because precise information of the rather complicated boundary conditions, such as the toe restraint, and the plane strain soil properties were not available at the time of initial prediction. Model RMC1 was later modified to include improved laboratory boundary conditions, plane strain soil test results and the low confining pressure dilation angle of the RMC sand. Although successful prediction was obtained from this improved Model RMC1, this was not a true Class A prediction because the improved modeling of Wall 1 was done after the construction and surcharging of Wall 1 were complete.

Models RMC2 and RMC3 were developed based on the improved Model RMC1 and used to perform Class A predictions of test Walls 2 and 3. Both models were able to predict the performance of test Walls 2 and 3 without any additional modifications. Because these predictions were made before the instrumentation results become available, they were true Class A predictions.

In the following sections, modeling results of Models RMC1, RMC2, and RMC3 are presented and compared with the face deflection measurements and strain gage measurements of the reinforcement of test Walls 1, 2, and 3.

10.2.1 Wall 1

Figure 10.2.1 shows the predicted and measured wall face deflections at end of construction. Although Model RMC1 underestimated the face deformation at end of construction, the maximum difference between the prediction and measurement was only about 6 mm. The most likely reason for this underestimation is that the numerical model did not include any additional movements due to the construction procedures such as backfill compaction. Figure 10.2.2 shows the additional wall deflections after three surcharge stages (50 kPa, 70 kPa, and 115 kPa) were applied. Results of Model RMC1 showed a very good agreement to the measurements of wall face deflections. Model RMC1 was able to predict the maximum face deflections at all different surcharge stages (only three are shown in Figure 10.2.2 for clarity) and only slightly overpredicted the deflections at top of the wall. Numerical model tended to overestimate the wall face deflection at top of the wall after surcharge was applied. This result could be improved somewhat by decreasing the contact area of the surcharge pressure. Full contact between airbag and backfill soil was assumed in the numerical models. During the tests of Walls 1 and 2, a decrease of the surcharge contact area (area between the airbag and backfill soil) behind the wall face due

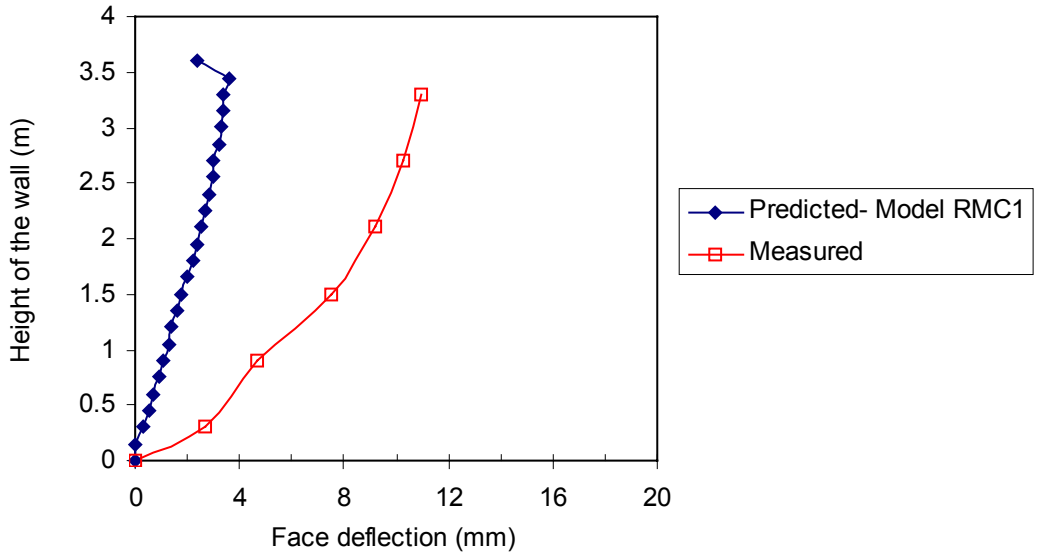

Figure 10.2.1 Predicted and measured wall face deflection of Wall 1, at the end of construction.

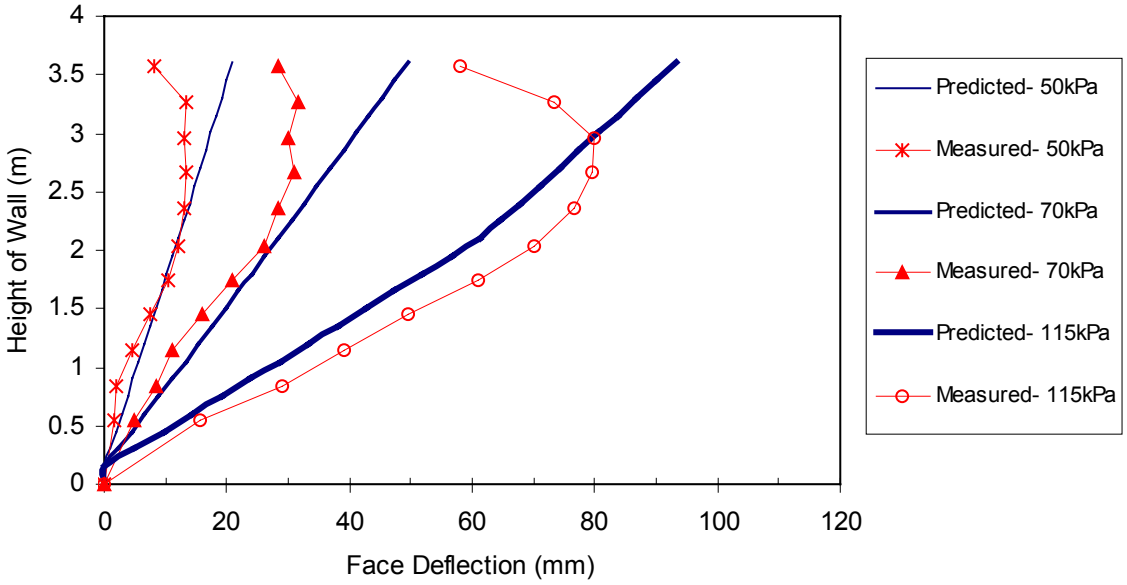

Figure 10.2.2 Additional wall face deflection of Wall 1 after surcharges of 50, 70, and 115 kPa, respectively.

to the inflation of the airbag was observed by Burgess (1999). However, the actual surcharge contact area was not reported by him, so no exact decrease in surcharge contact area could be modeled. This is probably the reason why the prediction had a different shape than the measurements and also differed than the modeling results of case histories shown in Chapter 9.

Figures 10.2.3 to 10.2.6 show the predicted and measured reinforcement strains at end of construction and for three typical surcharge stages. As shown in Figure 10.2.3b, results of Model RMC1 shows a good agreement to the strain gage measurements of reinforcement layers located at upper half of the test wall (Layers 4 to 6). Although Model RMC1 tended to underestimate the reinforcement strains in lower half of the wall, the maximum differences between the predictions and the measurements were less than 0.6%. Figure 10.2.4 shows that, after the 50 kPa surcharge was applied, Model RMC1 gave very good predictions of reinforcement strains in the upper portion of the wall (Layer 4 to 6), and still underestimated the reinforcement strains in the lower portion of the wall by about 1%. Similar observations were also found in the results of the 70 kPa surcharge stage (Figure 10.2.5). However, as the surcharge increased, differences between the prediction and measurements also increased. As shown in Figure 10.2.6, result of RMC1 tended to overpredict the reinforcement strain in the lower half of the wall by 2 to 3%; yet there still was reasonable agreement to the strain gage measurements in the upper half of the wall at the last surcharge stage (115 kPa).

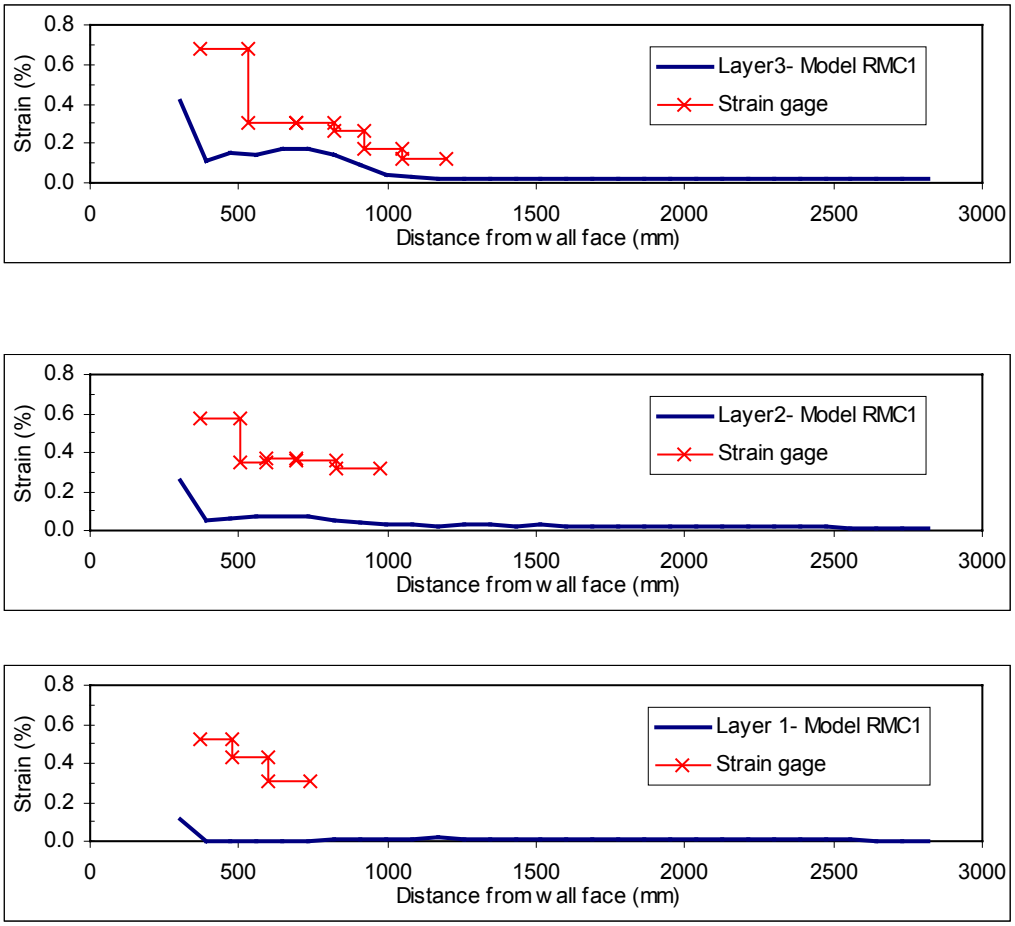

Figure 10.2.3a Predicted and measured reinforcement strains of Wall 1 at end of construction—layers 1 to 3.

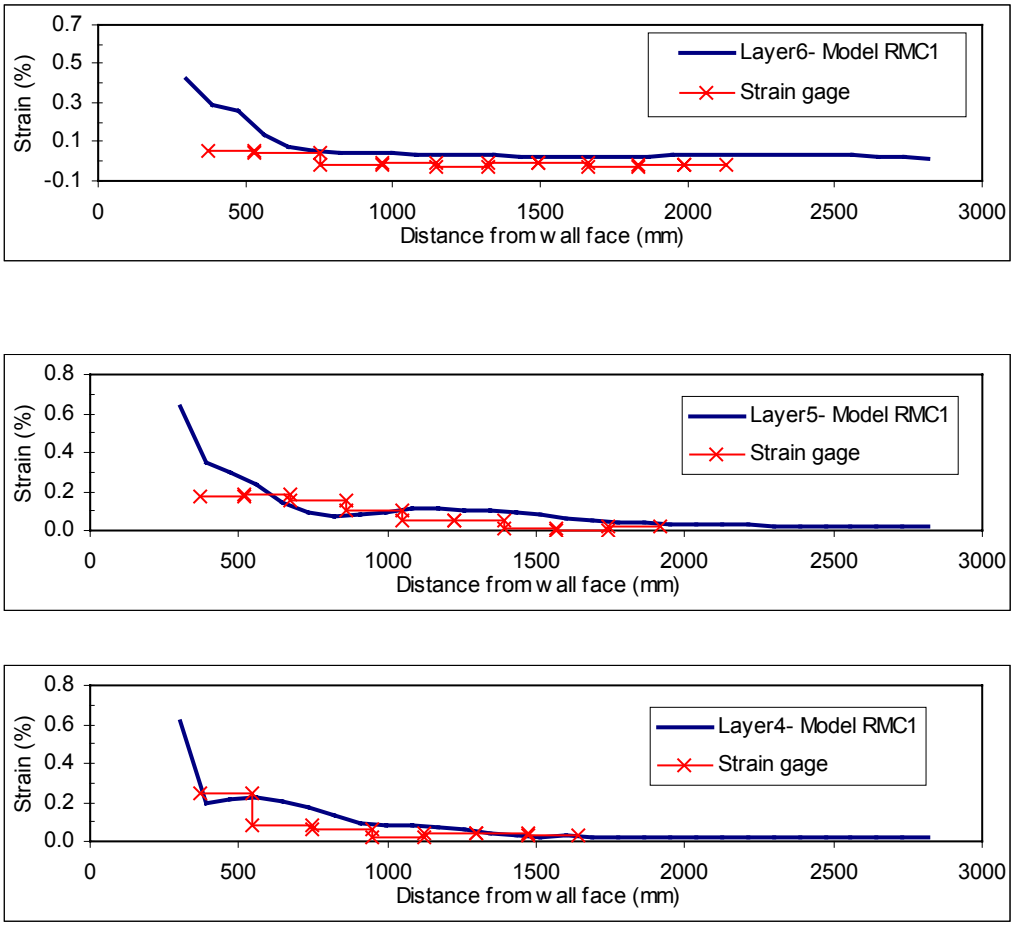

Figure 10.2.3b Predicted and measured reinforcement strains of Wall 1 at end of construction—layers 4 to 6.

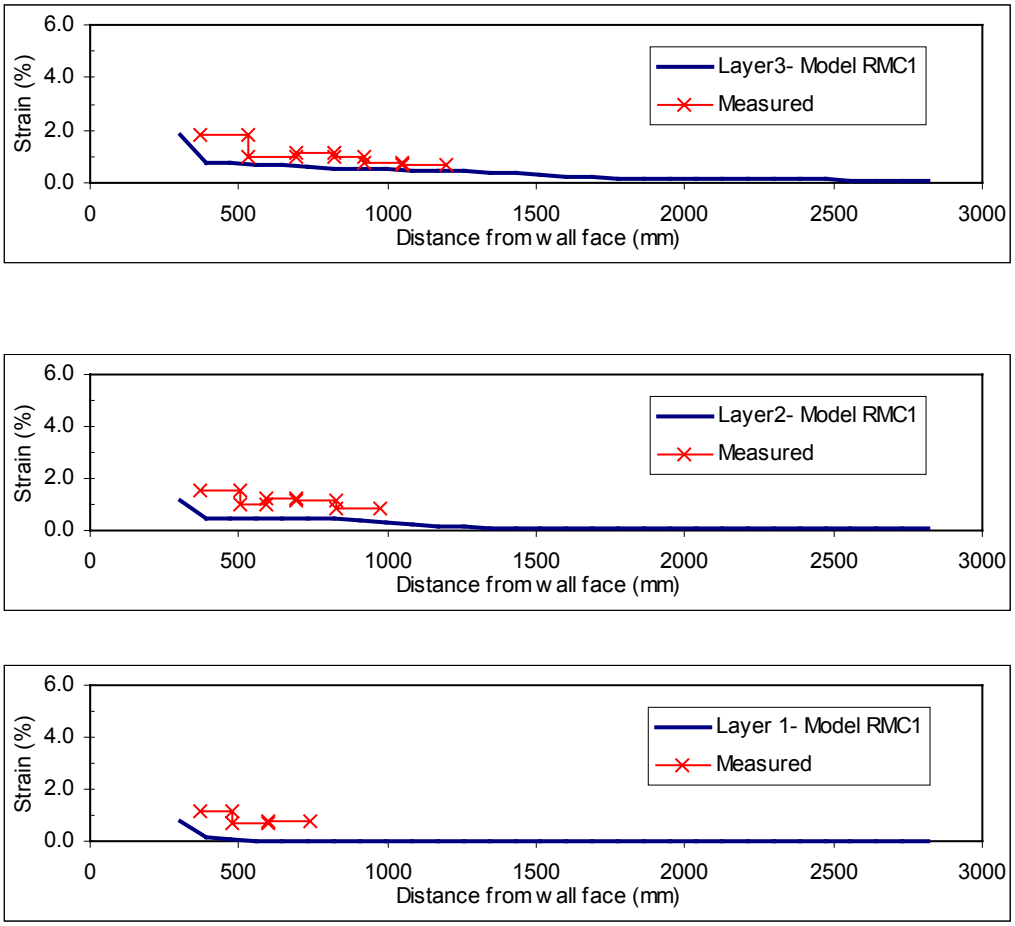

Figure 10.2.4a Predicted and measured reinforcement strains of Wall 1 after 50kPa surcharge—layers 1 to 3.

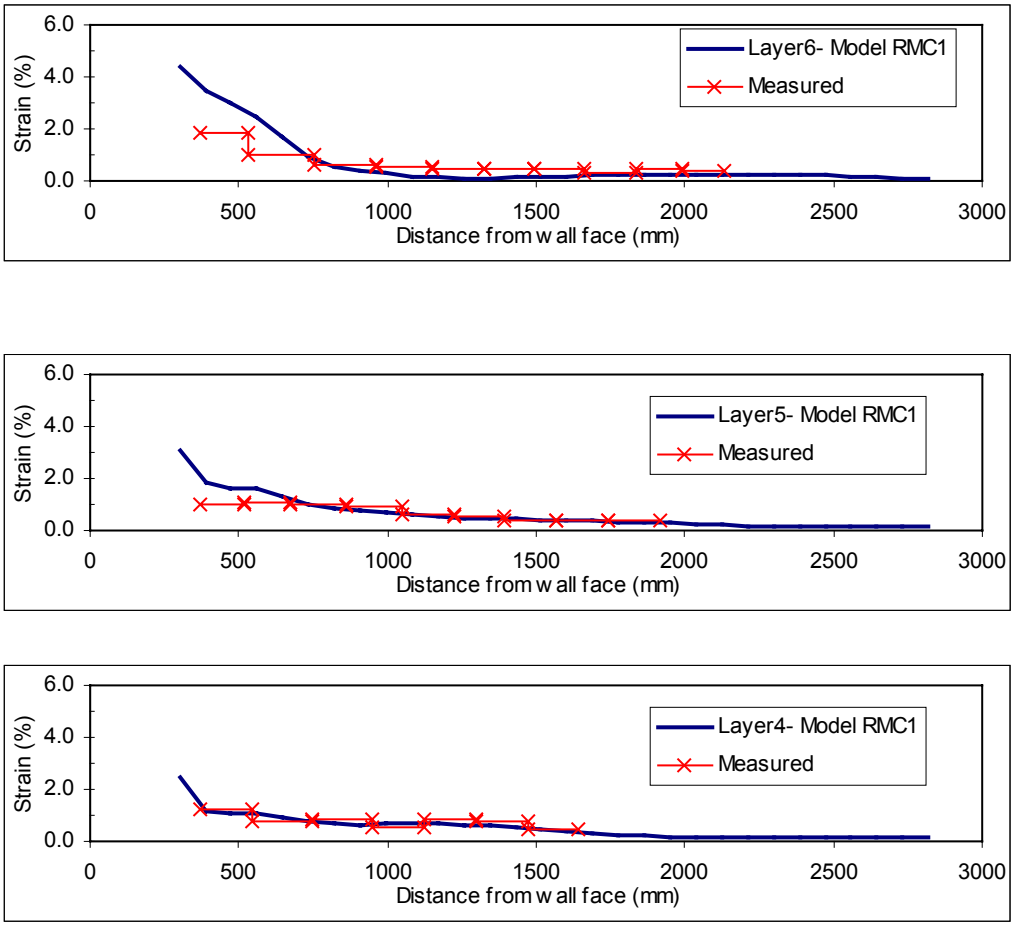

Figure 10.2.4b Predicted and measured reinforcement strains of Wall 1 after 50kPa surcharge—layers 4 to 6.

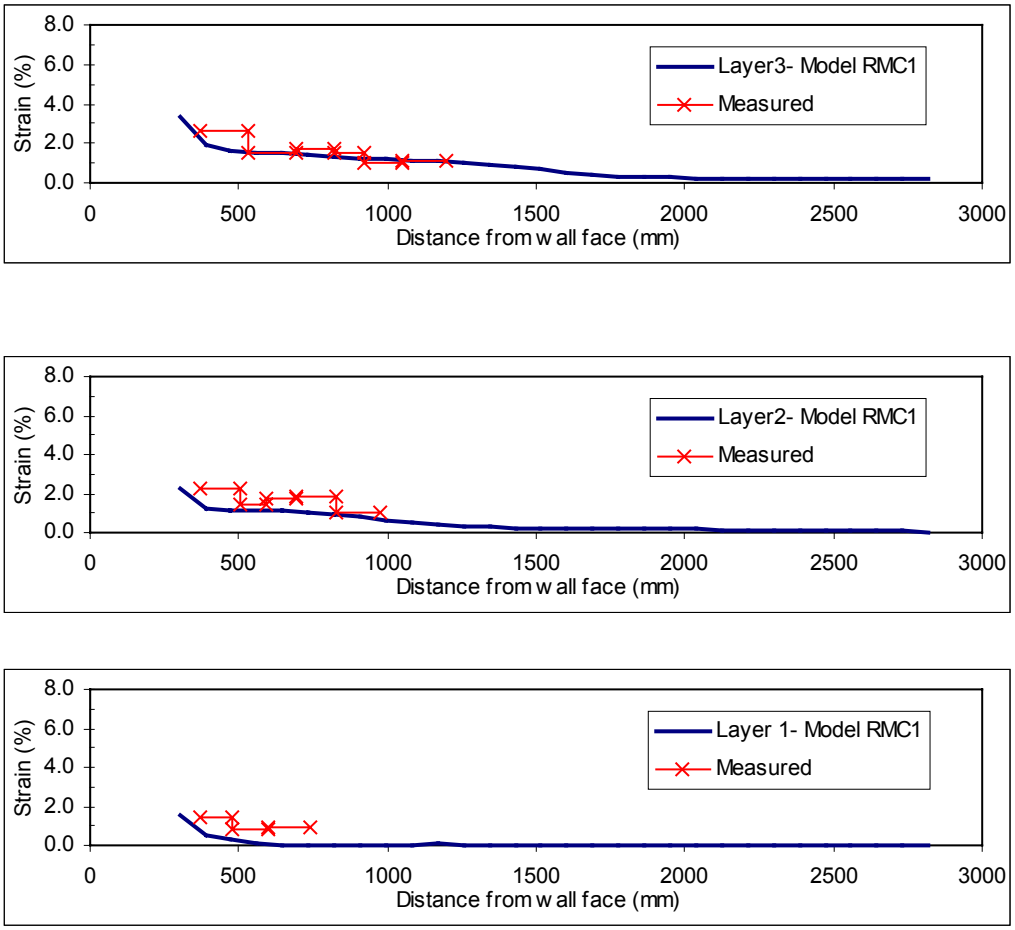

Figure 10.2.5a Predicted and measured reinforcement strains of Wall 1 after 70kPa surcharge—layers 1 to 3.

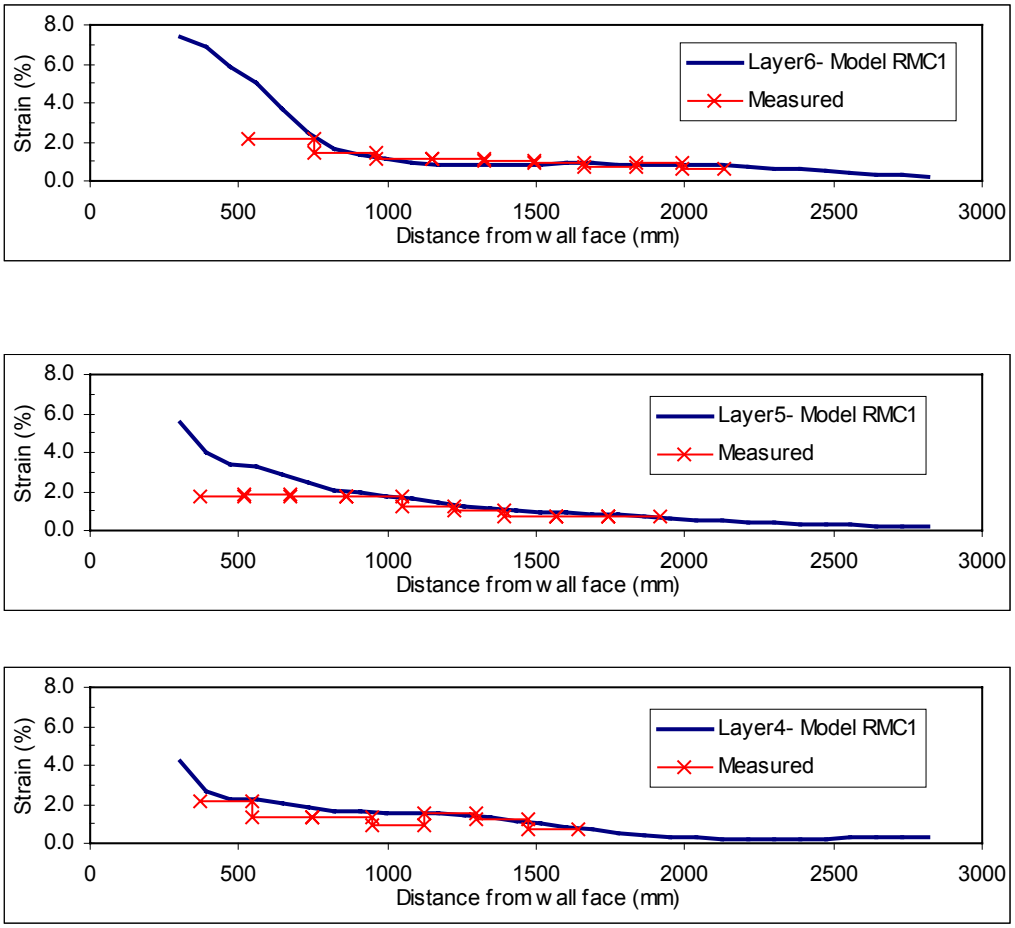

Figure 10.2.5b Predicted and measured reinforcement strains of Wall 1 after 70kPa surcharge—layers 4 to 6.

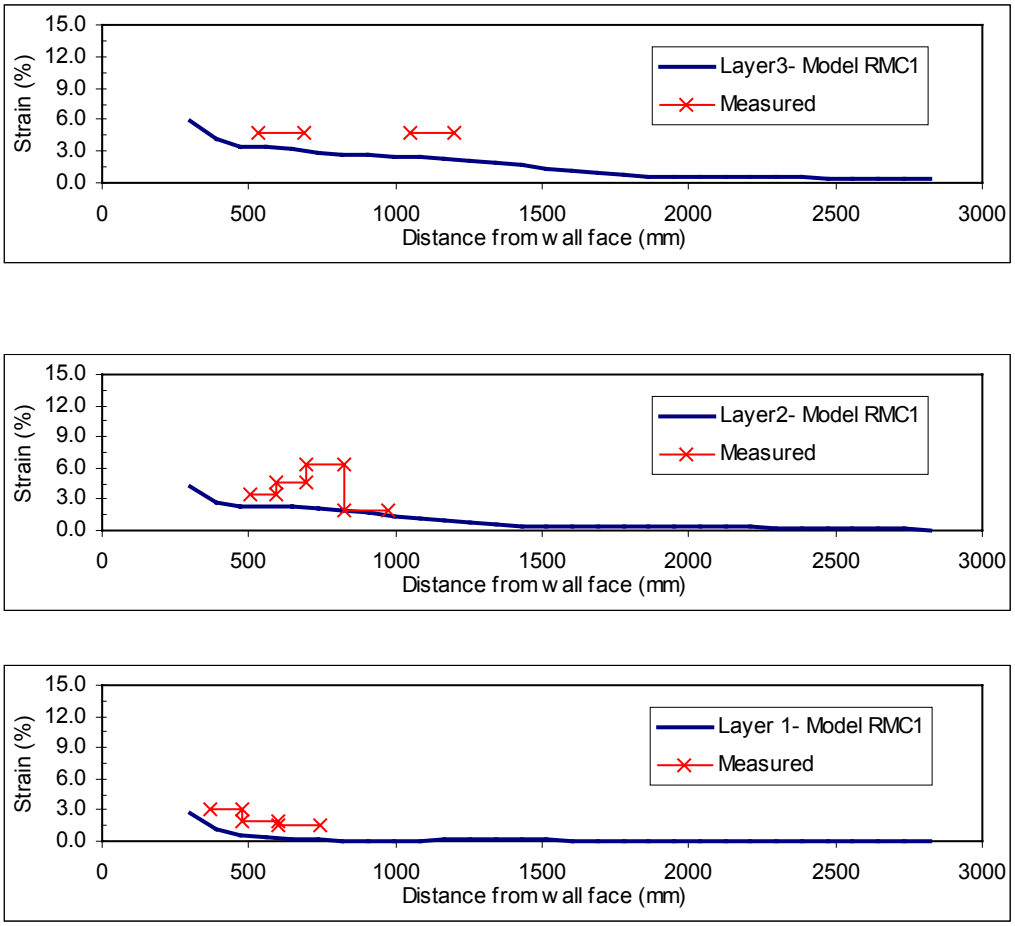

Figure 10.2.6a Predicted and measured reinforcement strains of Wall 1 after 115kPa surcharge—layers 1 to 3.

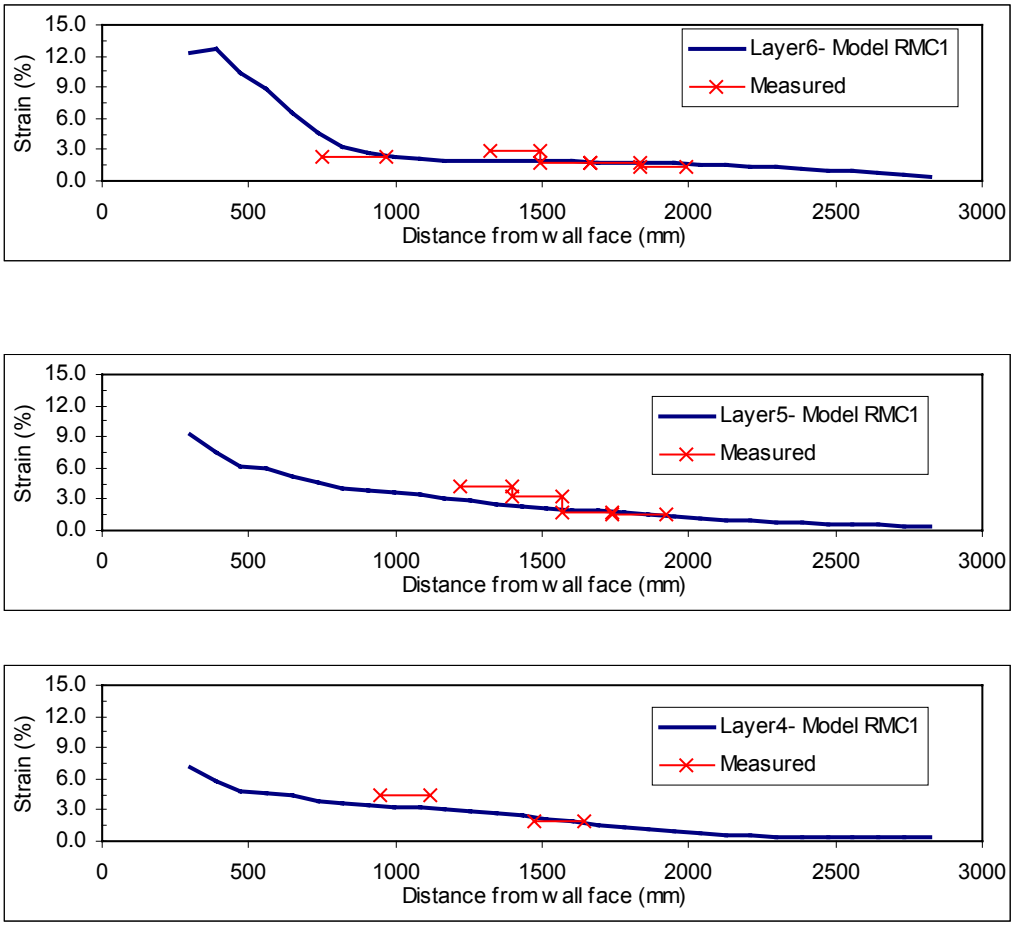

Figure 10.2.6b Predicted and measured reinforcement strains of Wall 1 after 115kPa surcharge—layers 4 to 6.

10.2.2 Wall 2

Test Wall 2 had the same geometry design and backfill soil as Wall 1; the only difference between Walls 1 and 2 was the reinforcement stiffness. The reinforcement stiffness and strength of Wall 2 was decreased by 50% from that of Wall 1 by eliminating every second longitudinal member of the same geogrid used in Wall 1. The improved Model RMC1 was modified into Model RMC2 by decreasing the modulus and yielding strength of the reinforcement to 50% of the value used in Model RMC1. Different from the analysis performed on Wall 1, true Class A predictions were performed on test Walls 2 and 3. Performance predictions of these two test walls were made before the instrumentation became available, and the modeling results were compared to the instrumentation measurements without any modification. For Walls 2 and 3, surcharge stages of 30, 40, and 50 kPa were used as the typical surcharge stages for comparing the predicted and measured wall performance. The reason for choosing these three surcharge stages is that the input reinforcement stiffnesses of these test walls were determined at 2% strain, and results of Models RMC2 and RMC3 indicated that test Walls 2 and 3 developed average strains around 2% at these surcharge stages.

Model RMC2 was able to predict the performance of Wall 2 within a reasonable range. Figure 10.2.7 shows the wall face deflections at end of construction. As with Wall 1 Model RMC2 tended to underpredict the maximum deflection, but the difference was less than 10 mm. After surcharges were applied, Model RMC2 tended

to overpredicted the measurements by 30 to 40 mm at the locations of maximum deflections (Figure 10.2.8).

Possible reasons for this overestimation are that the longitudinal member removing process was assumed to reduce the stiffness of the geogrid by 50%. However, the actual stiffness of this modified geogrid was not determined (Burgess, 1999), either in-isolation or when confined by soil. (Performance predictions of Model RMC2 could be improved by arbitrarily increasing the reinforcement modulus from 50% to 70% of the original modulus of this geogrid.)

For the internal strain levels of Wall 2, the results of Model RMC2 showed a very good agreement with the strain gage measurements (Figures 10.2.9 to 10.2.12). As shown in Figure 10.2.9, Model RMC2 was able to predict the reinforcement strain distribution of Wall 2 within a reasonable range. Similar to the modeling results of Model RMC1, Model RMC2 underpredicted the reinforcement strain by less then 0.6% in the lower half of the wall, but had a very good agreement to the measurements in the upper half of the wall. Figures 10.2.10 and 10.2.11 show the modeling results compared to the strain gage measurements at two typical surcharge stages of 30 and 40kPa. Model RMC2 gave very good predictions of reinforcement strains in the lower half of the wall but tended to overpredict them by 1 to 1.5% in the upper half of the wall. However, modeling results of the surcharge stage of 50kPa had a very good agreement to the measurements throughout the full wall height (Figure 10.2.12).

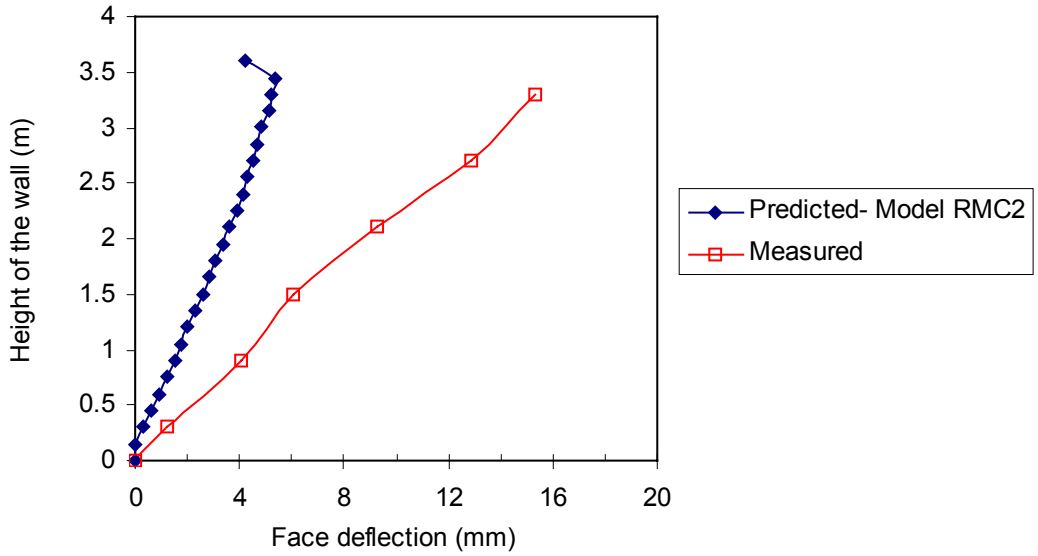

Figure 10.2.7 Predicted and measured wall face deflection of Wall 2, at the end of construction.

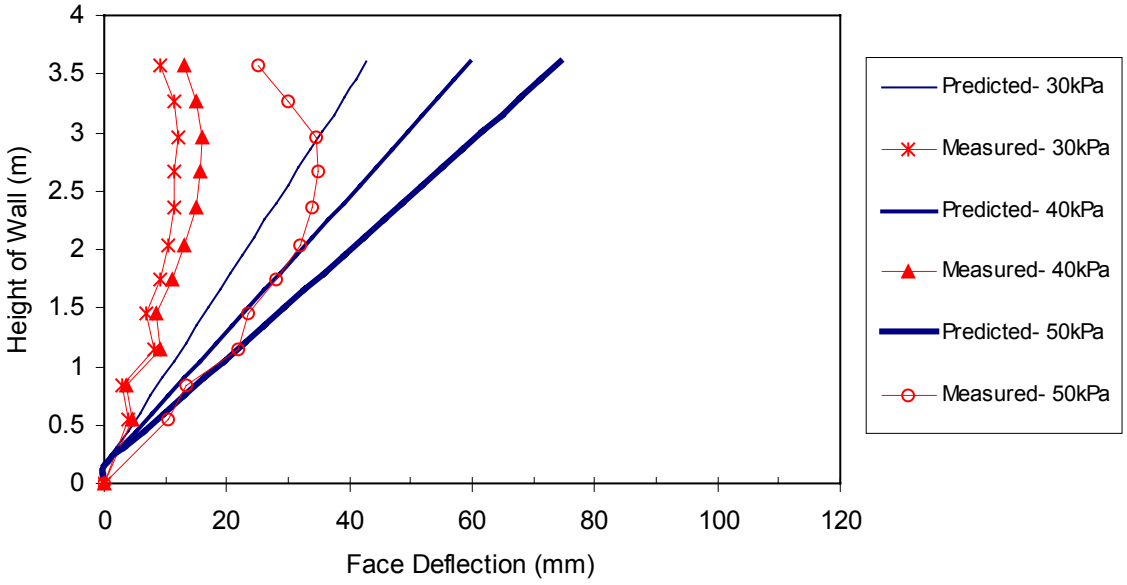

Figure 10.2.8 Additional wall face deflection of Wall 2 after surcharges of 30, 40, and 50kPa, respectively.

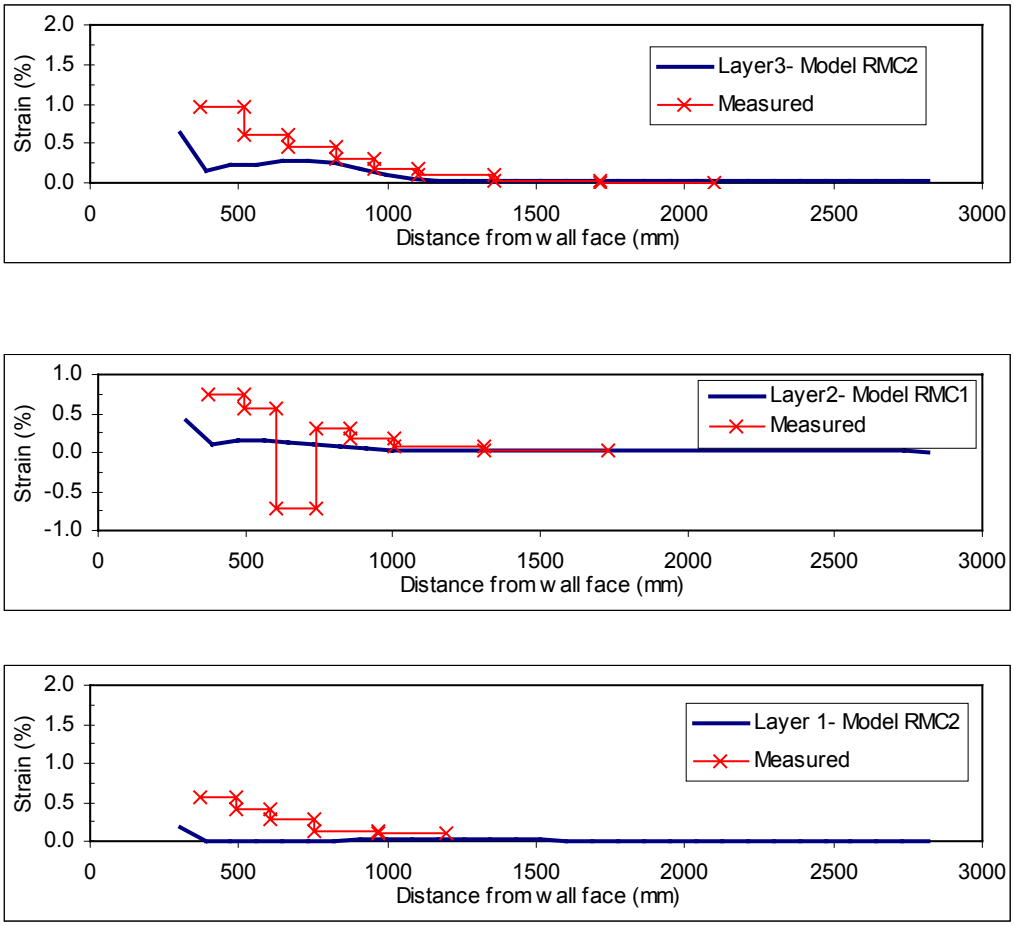

Figure 10.2.9a Predicted and measured reinforcement strains of Wall 2 at end of construction—layers 1 to 3.

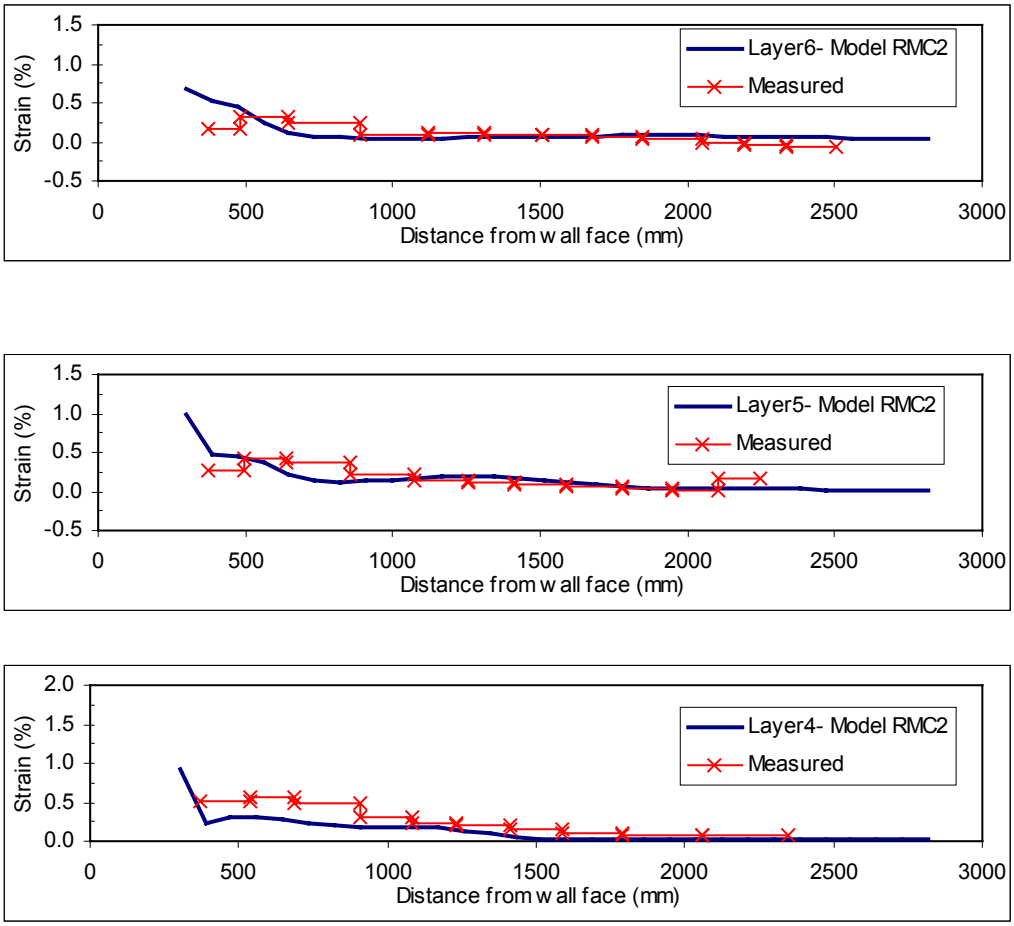

Figure 10.2.9b Predicted and measured reinforcement strains of Wall 2 at end of construction—layers 4 to 6.

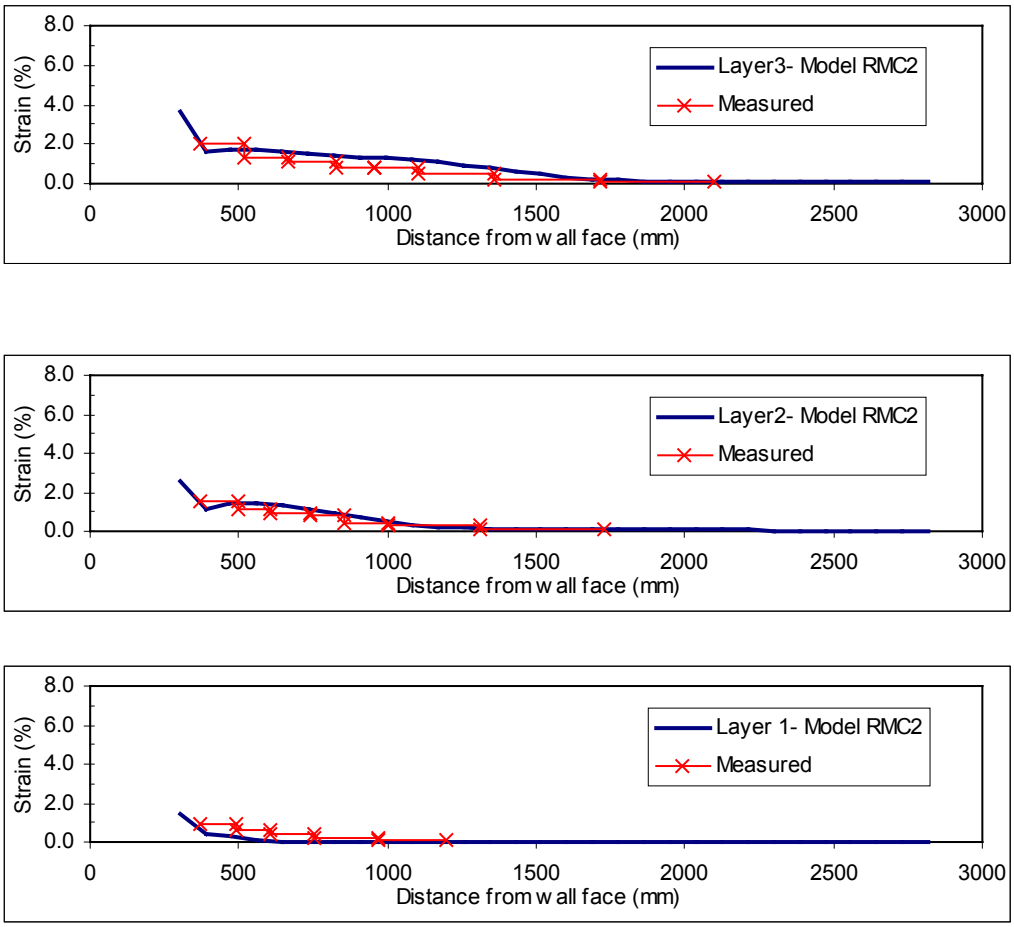

Figure 10.2.10a Predicted and measured reinforcement strains of Wall 2 after 30kPa surcharge—layers 1 to 3.

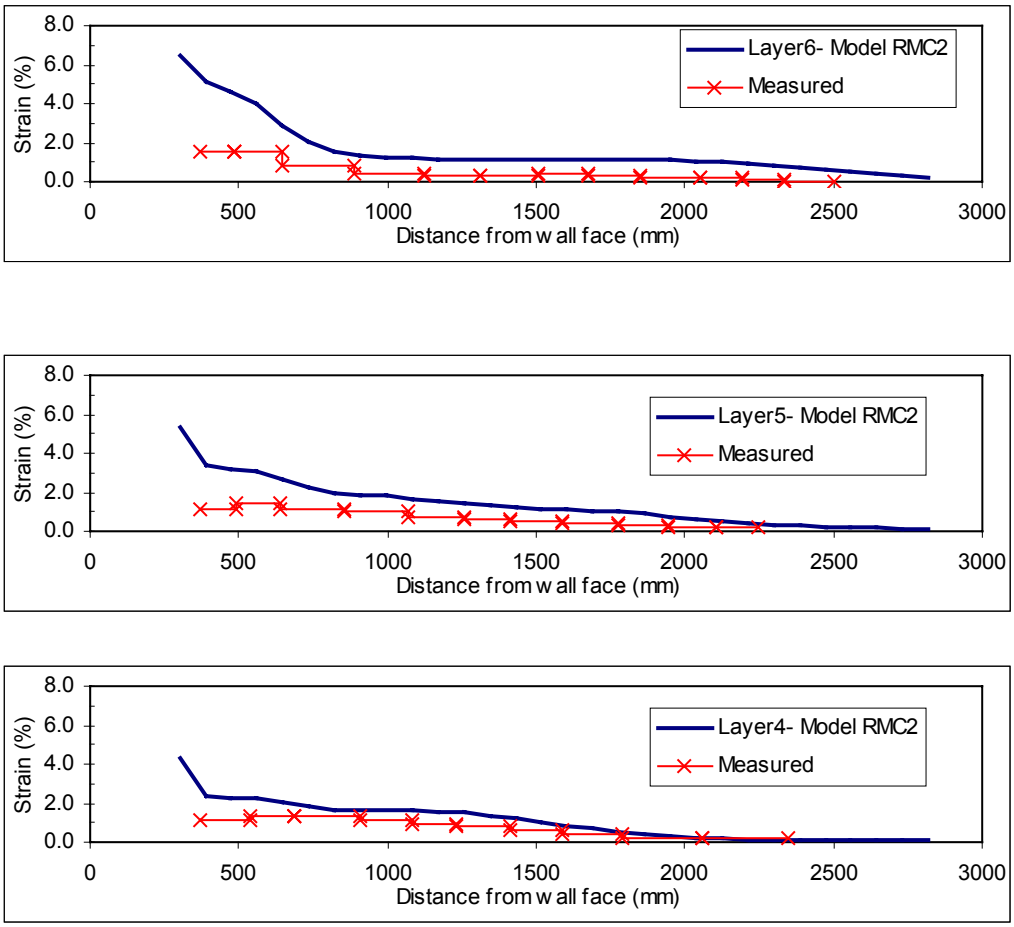

Figure 10.2.10b Predicted and measured reinforcement strains of Wall 2 after 30kPa surcharge—layers 4 to 6.

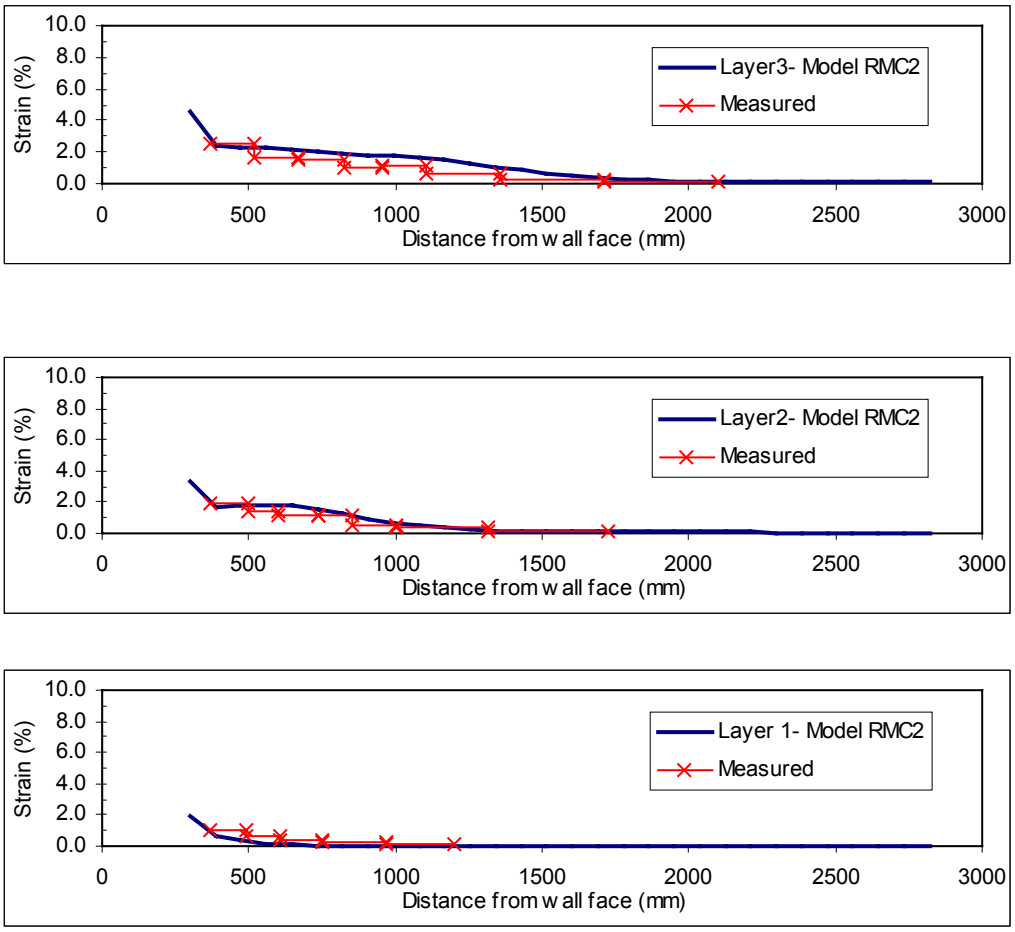

Figure 10.2.11a Predicted and measured reinforcement strains of Wall 2 after 40kPa surcharge—layers 1 to 3.

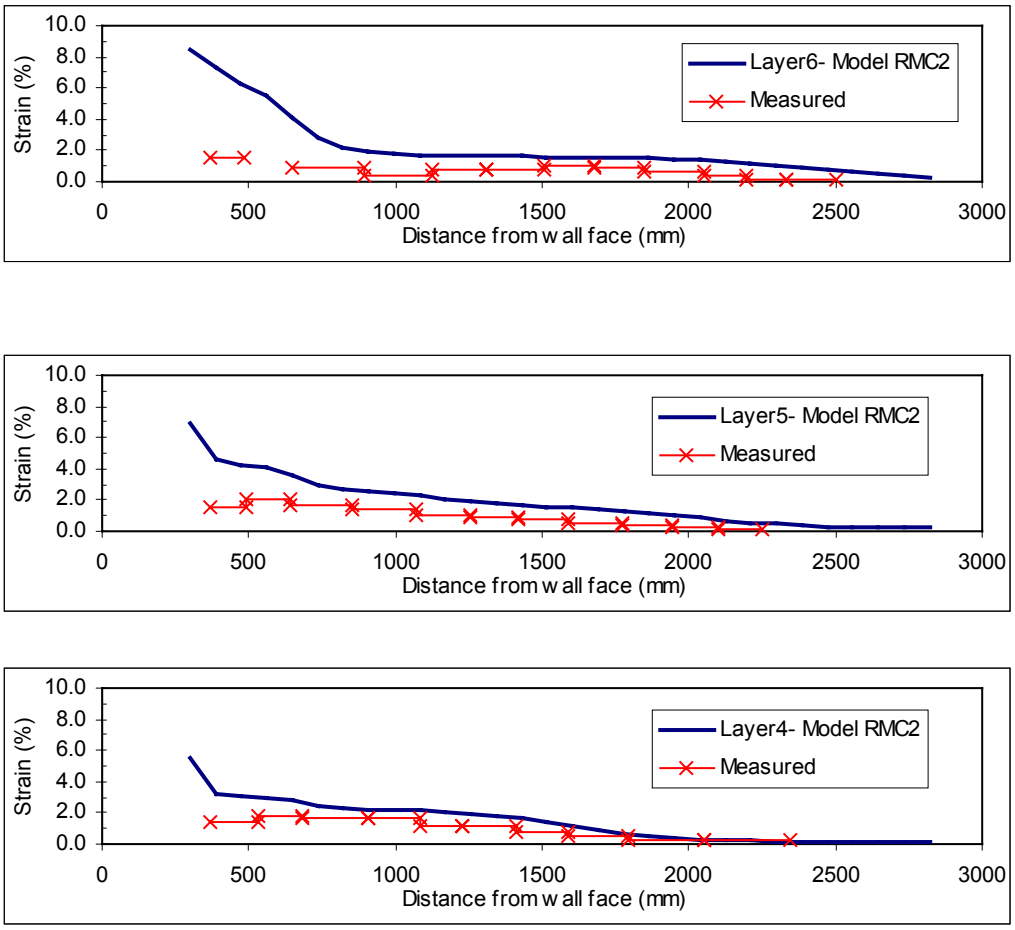

Figure 10.2.11b Predicted and measured reinforcement strains of Wall 2 after 40kPa surcharge—layers 4 to 6.

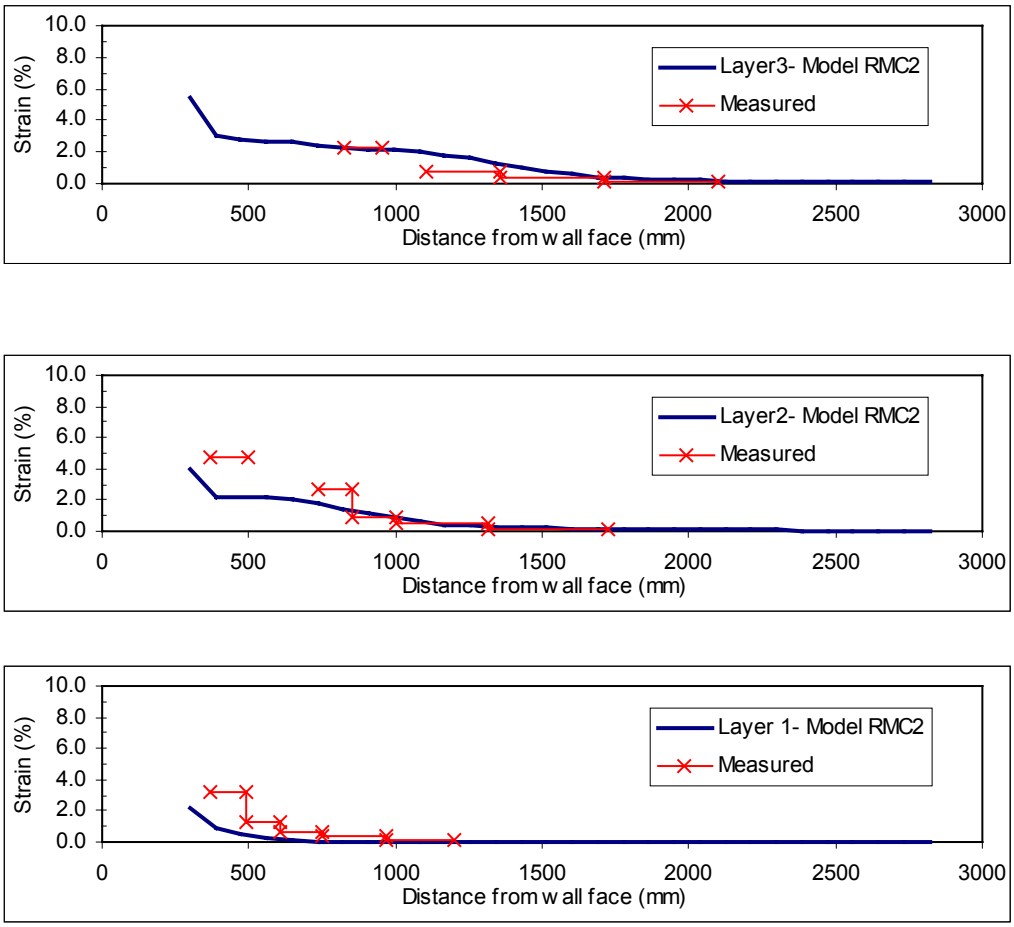

Figure 10.2.12a Predicted and measured reinforcement strains of Wall 2 after 50kPa surcharge—layers 1 to 3.

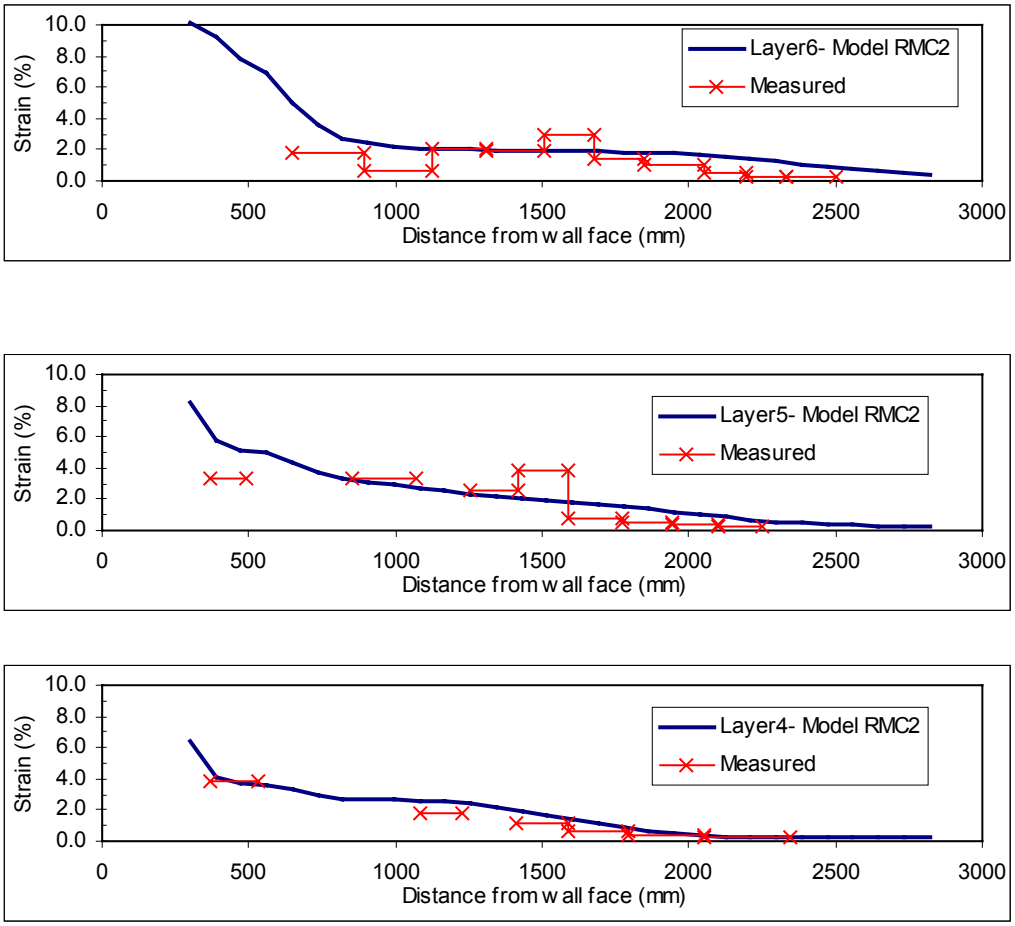

Figure 10.2.12b Predicted and measured reinforcement strains of Wall 2 after 50kPa surcharge—layers 4 to 6.

10.2.3 Wall 3

Test Wall 3 was designed using the same backfill and reinforcement materials as Wall 1. However, in Wall 3, the reinforcement spacing was increased to 0.9 m, or 50% more than the reinforcement spacing used in Walls 1 and 2 (Table 10.1.1). Model RMC3 was developed by increasing the reinforcement spacing of Model RMC1. Performance prediction of Wall 3 was made using Model RMC3 before the instrumentation measurements became available, another true Class A prediction. However, unfortunately, wall deflection and reinforcement strain data was not fully reduced when this disseration was in preparation. Modeling results were only compared to the raw data of the wall face deflection survey at the end of construction and raw strain gage measurements.

However, results of Model RMC3 indicated that a successful Class A prediction was achieved. Figure 10.2.13 shows the predicted and measured wall face deflections at end of construction. Model RMC3 underpredicted the maximum face deflection by only 6 mm. Reduced face deflection measurements after surcharges were not available at the time when this dissertation was in preparation.

Figures 10.2.14 to 10.2.17 show that Model RMC3 made reasonable predictions of the reinforcement strains. At the end of construction stage, Model RMC3 underpredicted the reinforcement strains by 0.2 to 0.6% in the lower half of the wall and by less than 0.3% in the upper half of the wall (Figure 10.2.14). For three typical

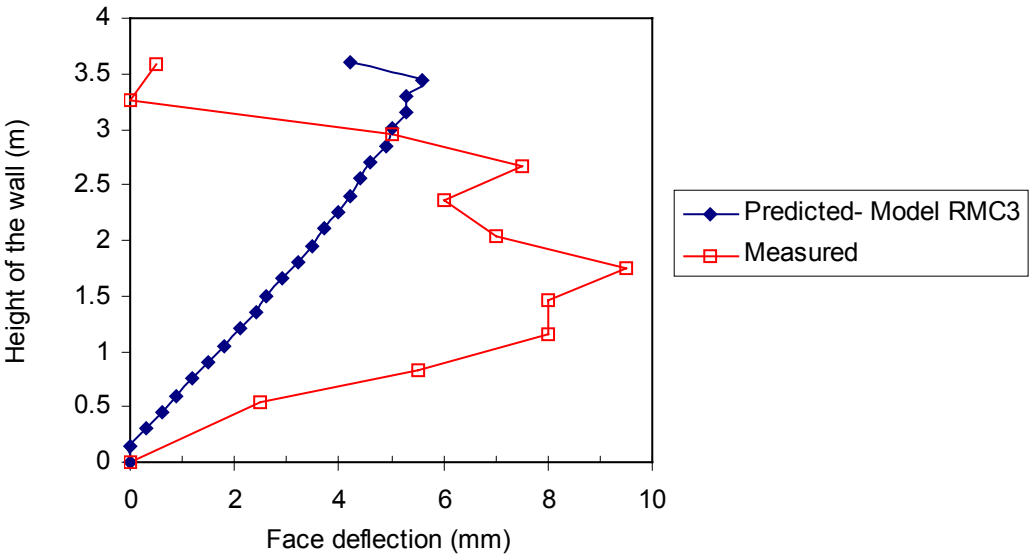

Figure 10.2.13 Predicted and measured wall face deflection of Wall 3, at the end of construction.

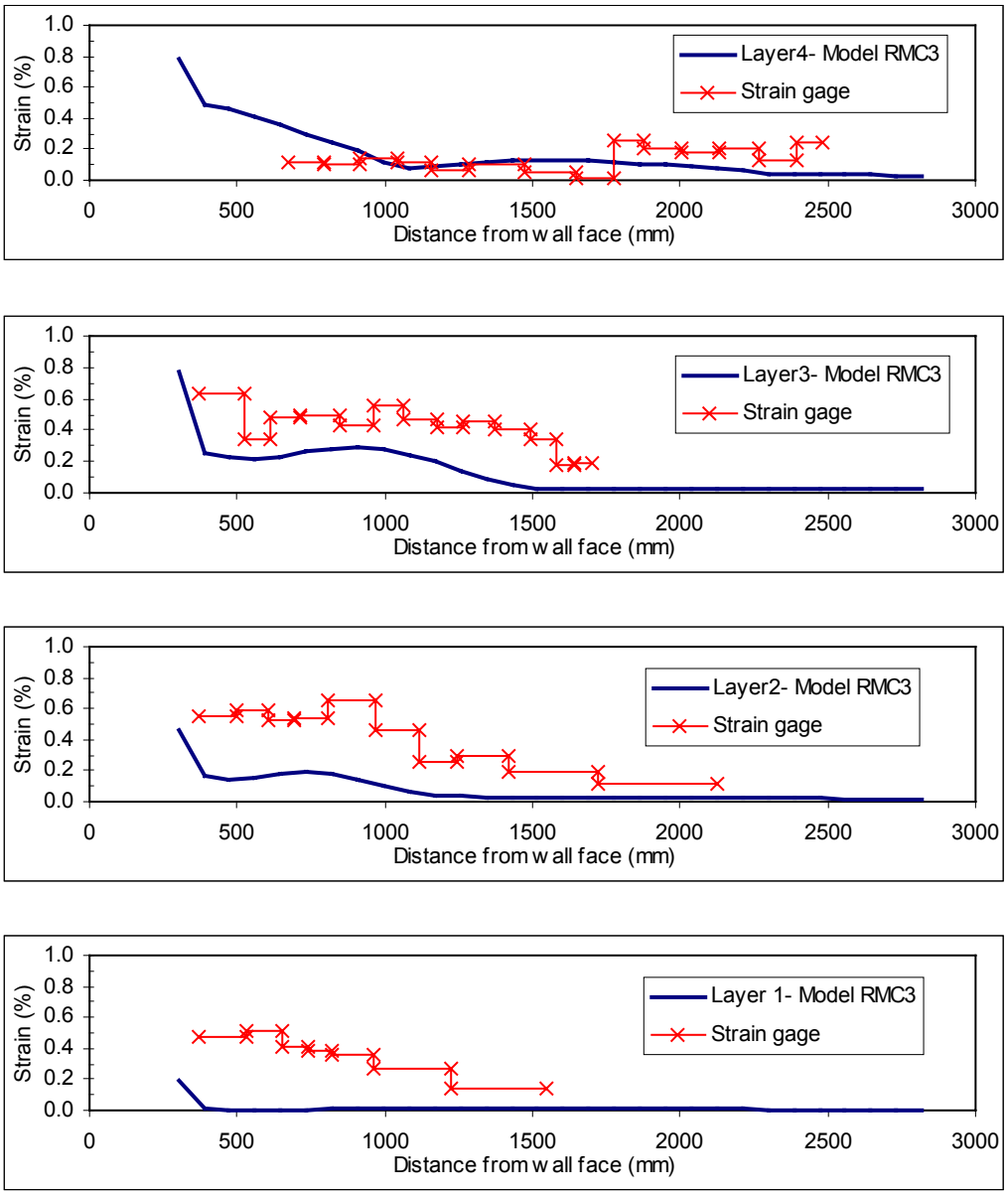

Figure 10.2.14 Predicted and measured reinforcement strains of Wall 3 at end of construction.

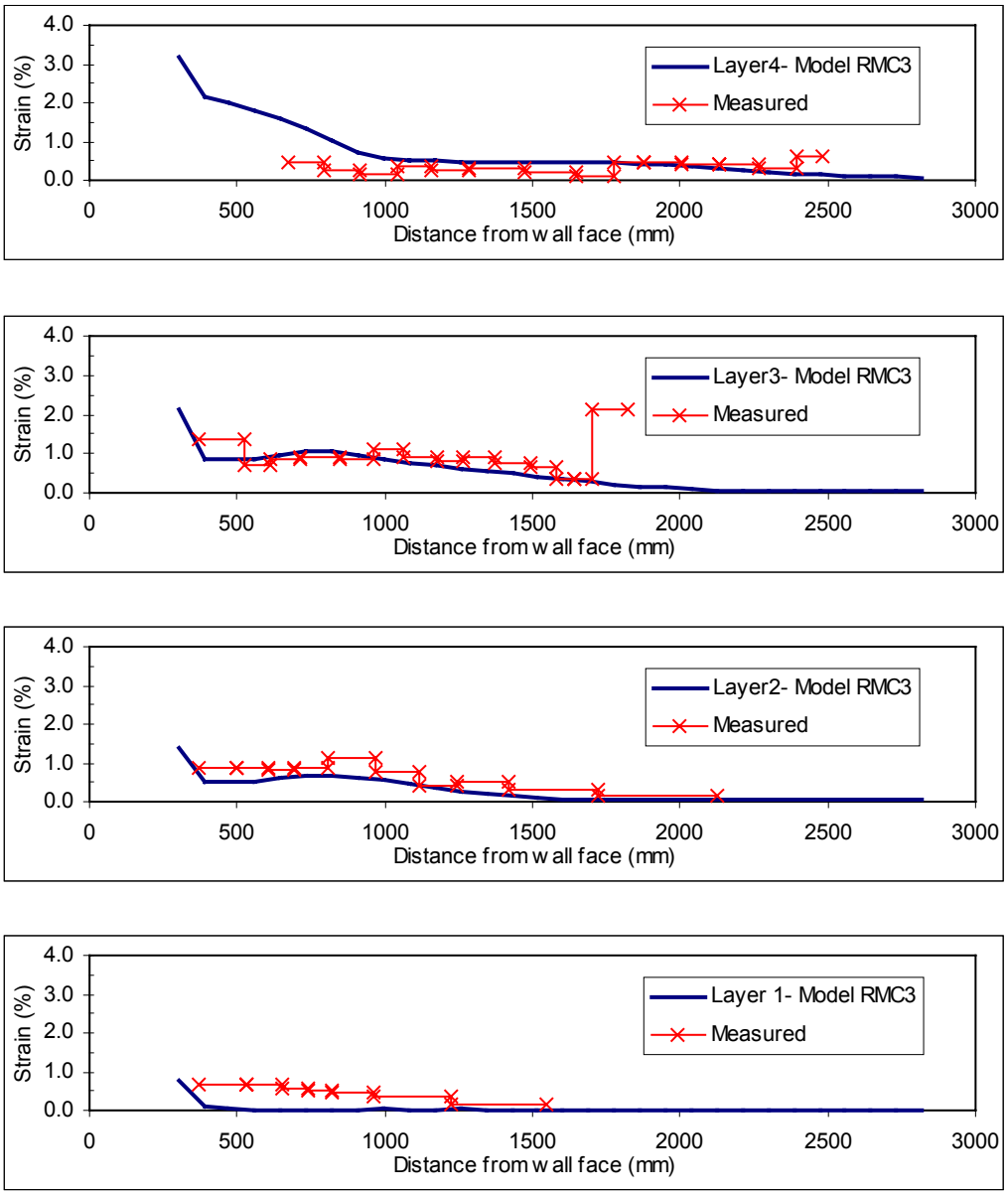

Figure 10.2.15 Predicted and measured reinforcement strains of Wall 3 after 30kPa surcharge.

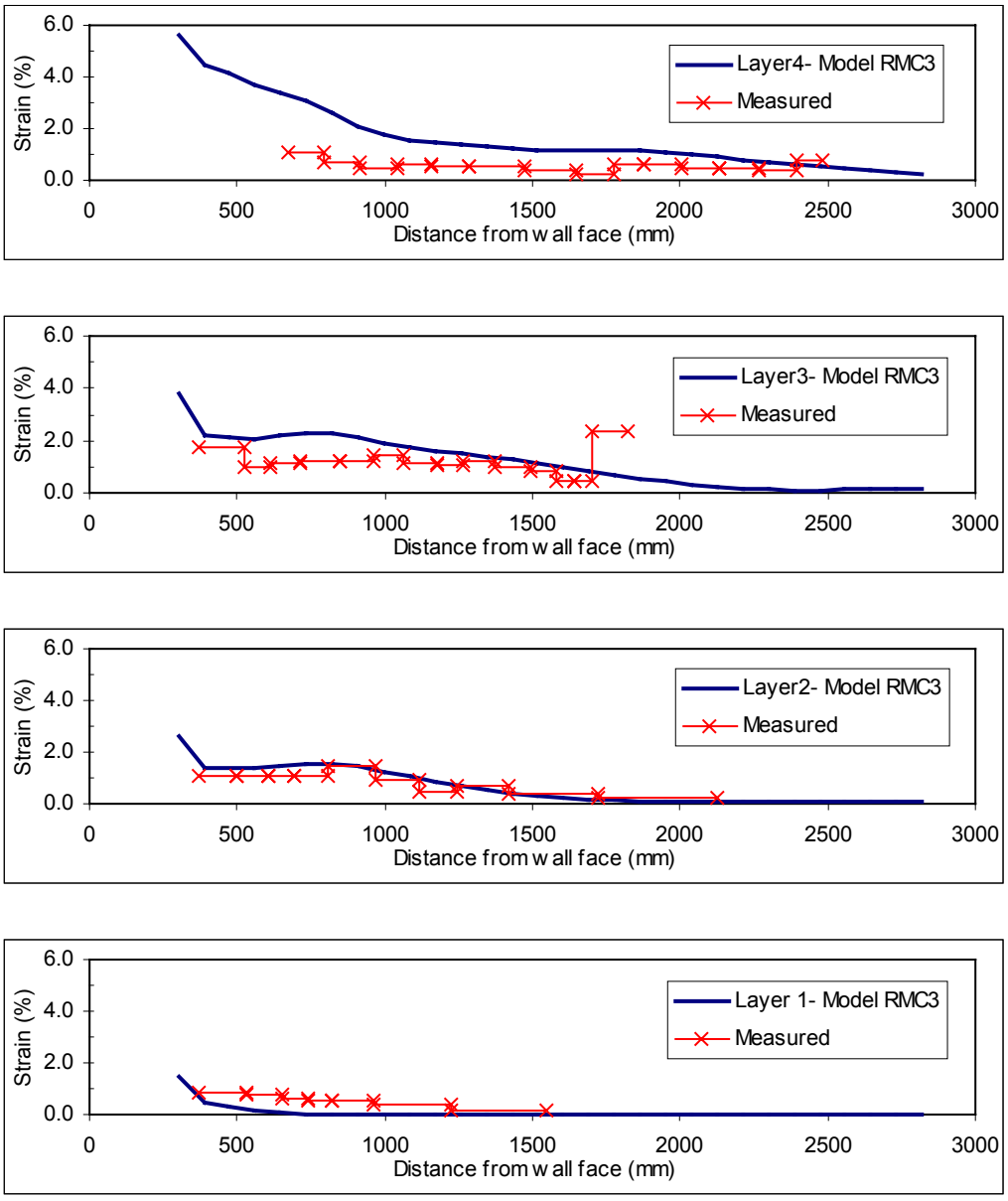

Figure 10.2.16 Predicted and measured reinforcement strains of Wall 3 after 40kPa surcharge.

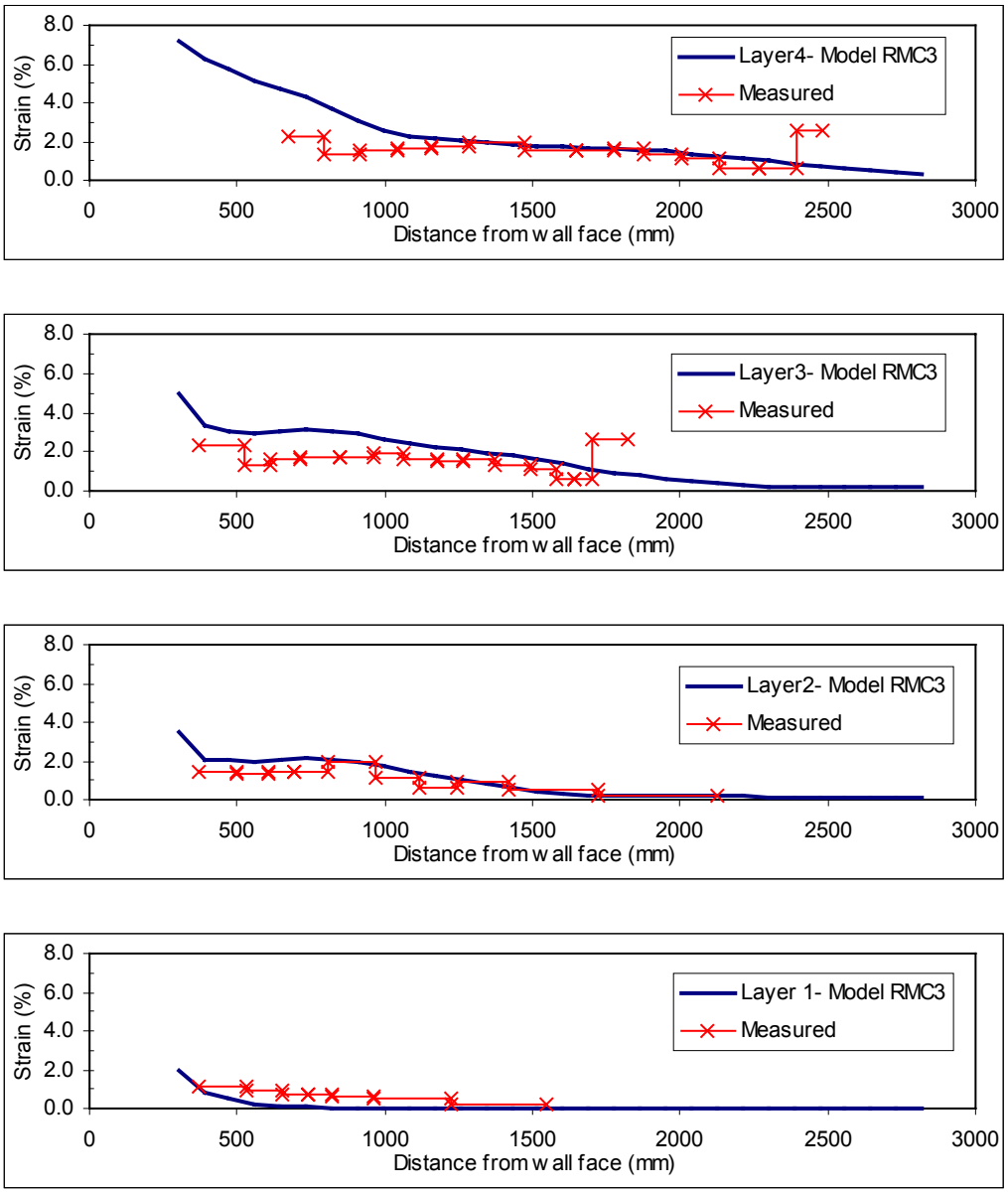

Figure 10.2.17 Predicted and measured reinforcement strains of Wall 3 after 50kPa surcharge.

surcharge stages (30 kPa, 40 kPa, and 50 kPa), Model RMC3 was able to predict the reinforcement strain distributions of Wall 3 quite well (Figures 10.2.15 to 10.2.17). It tended to underpredict the reinforcement strains only at Layer 1 by 0.5 to 1% for the 30kPa surcharge stage, and had very good strain predictions for the other three reinforcement layers (Figure 10.2.15). For the 40 kPa and 50 kPa surcharge stages, Model RMC3 was able to predict quite well the reinforcement strains of all layers (Figures 10.2.16 and 10.2.17).

10.3 Difference Between Test Walls and Real Walls

The RMCC test walls were built in the laboratory in order to have better control of the materials, instrumentation, and construction. However, when utilizing information obtained from the test wall to extrapolate to the behavior of real walls, as well as to calibrate numerical models, following differences between test walls and real walls have to be considered:

1. The toes of the test walls were restrained by hydraulic jacks in order to measure the reaction forces at the toe under the modular blocks (Figure 10.2.1). The hydraulic jacks were then released after last surcharge stage was reached. This type of toe restraint was very different from those of real walls. It was also very difficult to be accurately simulated in FLAC.

2. Surcharge of the test wall was applied using airbags. This is different from the surcharge applied by real soil in that the contact area at the edge between the airbag and the backfill decreased as the airbag inflated.

3. The RMCC test walls were built on a very stiff concrete foundation surrounded by three reinforced concrete reaction walls. Movements of the backfill soil were confined at the bottom of the wall. Therefore, the deformation and stress distributions at the bottom of the test walls, especially at the area around the toe of the wall, are very different from those of real walls built on soil foundations.

Comparison of the performance of the in-laboratory test wall (Wall 1) and the test wall built in the field (Algonquin modular block wall) are presented and discussed in the following section.

10.4 Discussions and Conclusions

1. Numerical models tended to underpredict the wall face deflection at end of the construction by only about 6 to 10mm. The most likely reason for this underestimation is that the additional movement due to the construction procedures such as soil compaction was not considered in the FLAC models.

2. Numerical models tended to overestimate the wall face deflection at top of the wall after surcharge was applied. This result could be improved somewhat by

decreasing the contact area of the surcharge pressure. Full contact between airbag and backfill soil was assumed in the numerical models. During the tests of Walls 1 and 2, a decrease of the surcharge contact area (area between the airbag and backfill soil) behind the wall face due to the inflation of the airbag was observed by Burgess (1999). However, the actual surcharge contact area was not reported by him, so no exact decrease in surcharge contact area could be modeled.

3. Overall, the FLAC models tended to underpredict the reinforcement strains in the lower half of the test walls. A possible reason of this underestimation is that the FLAC models did not model the toe restraint of the test wall very well.

4. By comparing the results of RMC1, RMC2, and RMC3, improved predictions of Wall 1 and Wall 3 were made. Test wall Wall 2 was constructed using the same geogrids as that of Walls 1 and 3 but with every second longitudinal member of the grid removed. This process was assumed to reduce the stiffness of the geogrid by 50%. However, the actual stiffness reduction of this modified geogrid was not measured, and no possible modification in stiffness when the geogrid was confined by soil was considered. Performance predictions of Model RMC2 could be improved by increasing the reinforcement modulus from 50% to 70% of the original modulus of this geogrid.

5. Both numerical models and post-construction observations of the test walls indicated that large differential settlements occurred between the facing blocks and the backfill soil. However, the strain gage measurements did not show any strain peaks near the blocks.

6. The stiff concrete foundation of the test walls did affect both the face deflection profile and the reinforcement tension distribution, as shown in the normalized plots of Figures 10.4.1 and 10.4.2. Figures 10.4.1 and 10.4.2 show the results of RMCC Wall 1 compared to the FHWA Algonquin modular block faced wall that was described in Chapter 9. Figure 10.4.1 indicates that the maximum face deflection of the wall with a stiff concrete foundation is located at top of the wall, while that of the wall with a soil foundation is located near the middle of the wall. Figure 10.4.2 also indicates that a stiff foundation has a similar effect on the reinforcement tension distributions. The maximum reinforcement tension of the test wall with a stiff concrete foundation occurred at a height of 0.8H, but the maximum reinforcement tension of the test wall with a soil foundation occurred at a height of 0.5H.

It should be emphasized that performance predictions presented in this chapter are Class A prediction results, i.e. these modeling results were made before the construction of these test walls. Refinement is always possible after prediction. For example, face deflection predictions after surcharge can be further improved by

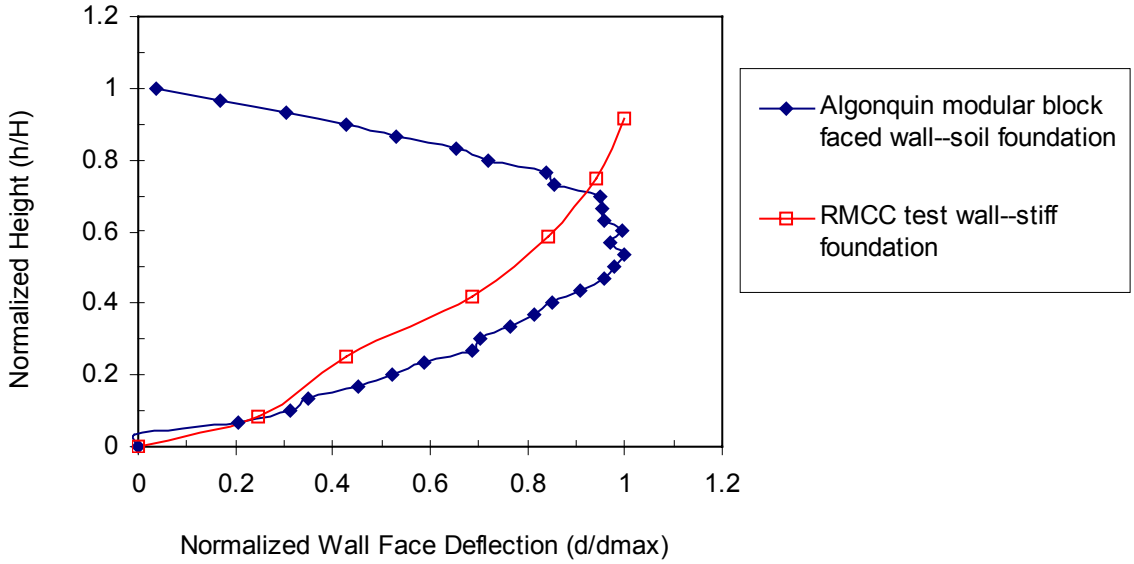

Figure 10.4.1 Normalized face deflections for GRS test walls with different foundations.

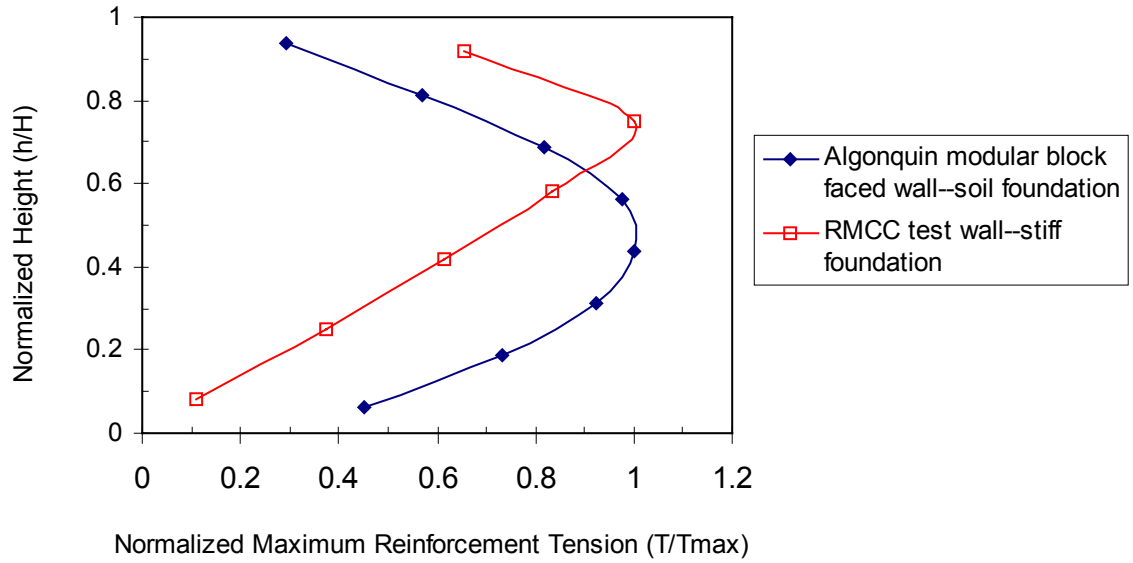

Figure 10.4.2 Normalized maximum reinforcement tension distributions for GRS test walls with different foundations.

decreasing the contact area of the surcharge. Moreover, performance simulation of test Wall 2 can be improved by increasing the reinforcement modulus from 50% to 70% of the original modulus of the geogrid used in test Walls 1 and 3.

Chapter 11
Analytical Models of Lateral Reinforced Earth Pressure and Composite Modulus of Geosynthetic Reinforced Soil

Two important design factors in present GRS wall design procedures are the distribution of lateral earth pressure and the reinforcement stiffness. These two factors are determined based on properties of the individual construction materials of the GRS wall. Present designs requires an assumption of the lateral earth pressure distribution, and the in-isolation stiffness of geosynthetic reinforcement is usually used. Available evidence from full-scale and model GRS walls indicates that present design procedures tend to significantly overestimate the internal lateral stress distribution within the structure (Bell et al., 1983; Allen et al., 1992; Rowe and Ho, 1993; Christopher, 1993). Modeling results presented in Chapter 9 of this thesis also suggest that the soil-only coefficients of lateral earth pressure and in-isolation stiffness of geosynthetics are not appropriate for characterizing the working stress or strain distribution inside GRS walls.

In order to analyze the composite GRS behavior, two new terms, the coefficient of lateral reinforced earth pressure, K_{comp}, and composite modulus of geosynthetic reinforced soil, E_{comp}, are introduced in this research. In this chapter, the analytical models, derivations, and applications of both K_{comp} and E_{comp} are presented. Information on the working stress and strain obtained from the results of parametric

study that are presented in Chapter 12 are characterized using these two GRS composite terms.

11.1 Lateral Reinforced Earth Pressure

An important internal design consideration of GRS retaining structures is the lateral earth pressure distribution behind the face of the wall. However, none of the lateral earth pressure distributions used in present GRS wall design procedures have clearly taken the reinforcing effects contributed by reinforcement into account. An alternate approach to obtain the distribution of lateral reinforced earth pressure behind the wall face was developed in this research (Lee, 1999). This alternate approach combines the conventional lateral earth theory (Rankine earth pressure theory) and reinforcement tension using free body diagrams.

11.1.1 Analytical Model of Lateral Reinforced Earth Pressure

Figure 11.1.1 shows the lateral earth pressure distribution behind the face of a conventional unreinforced retaining wall. In Figure 11.1.1, F_{soil} represents the total earth force supported by the facing blocks. H and H_s are height of the wall and location of the F_{soil}, respectively. Equation 11.1.1 is the general mathematical expression of the lateral earth pressure distribution for this case.

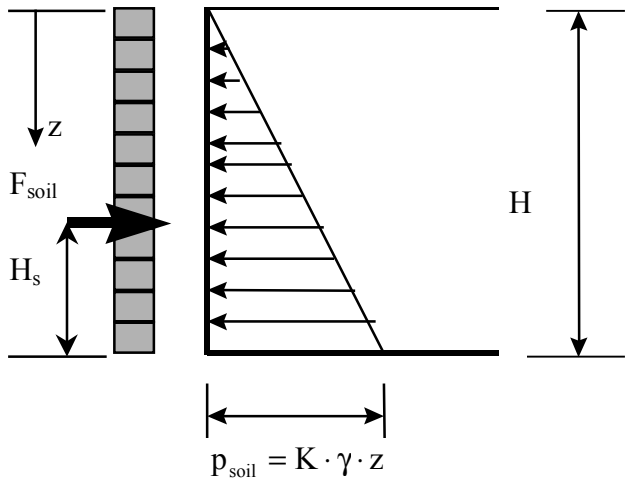

Figure 11.1.1 Lateral earth pressure distribution of an unreinforced retaining wall.

$$p_{soil} = K \cdot \gamma \cdot z \qquad \text{(Eq. 11.1.1)}$$

where K = lateral earth pressure coefficient,

γ = unit weight of soil, and

z = depth from top of the wall.

When planar reinforcements such as geosynthetics are inserted into the wall backfill, the lateral earth pressure distribution is changed because of the presence of the reinforcement tensions, as shown schematically in Figure 11.1.2. In Figure 11.1.2, F_{total} represents the total force of the GRS retaining structure supported by the facing system, and H_1 is the location of F_{total}. t_n is the reinforcement tension per unit width at reinforcement layer n.

The lateral GRS composite distribution can be determined by superposing the lateral earth pressure and the reinforcement tensions behind the wall face (Figure 11.1.3). In order to characterize the lateral earth pressure distribution of the GRS composite, a new lateral pressure coefficient, K_{comp}, is defined as the composite lateral earth pressure coefficient of the geosynthetic reinforced soil.

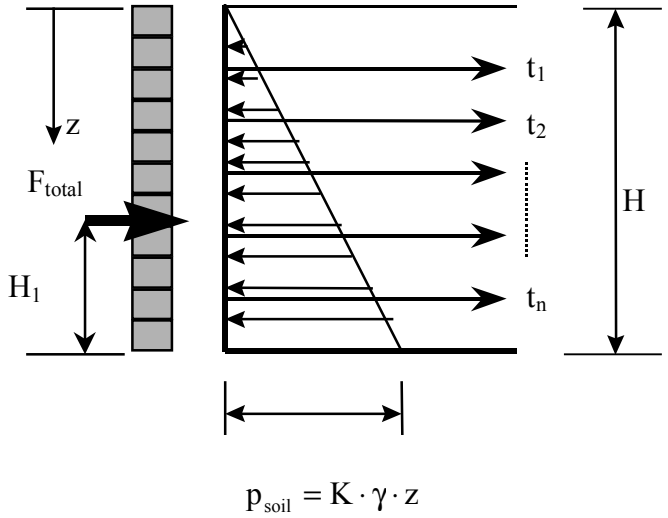

Figure 11.1.2. Lateral earth pressure distribution in a geosynthetic reinforced retaining wall.

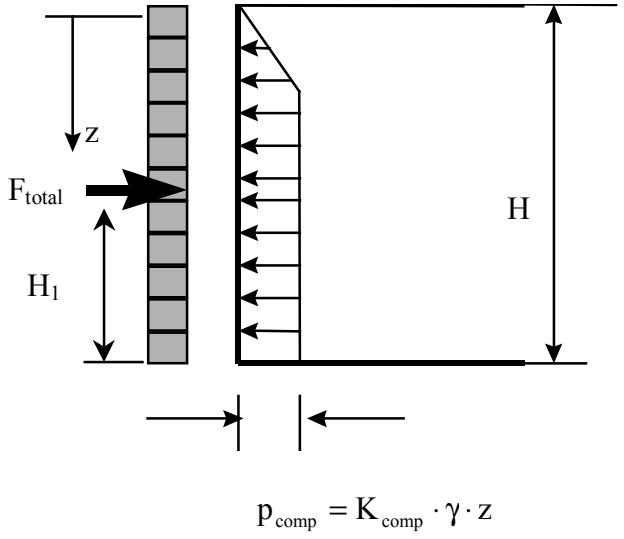

Figure 11.1.3 Lateral composite pressure distribution of a reinforced retaining wall.

The mathematical expression of K_{comp} at any depth from the top of the backfill can be derived by comparing Figures 11.1.2 and 11.1.3 (Equation 11.1.2).

$$F_{total}(z) = F_{soil}(z) - \sum_{i=1}^{n} t_i \qquad \text{(Eq. 11.1.2)}$$

where $F_{total}(z)$ = total force supported by the facing at depth z,

$F_{soil}(z)$ = Total earth force supported by the facing at depth z, and

$\sum_{i=1}^{n} t_i$ = Total tensile forces of reinforcement at depth z.

By introducing the integral forms of the F_{total} and F_{soil}, Equation 11.1.2 can be re-written as Equation 11.1.3.

$$F_{total}(z) = \int_0^z p_{comp}(z)dA = \int_0^z p_{soil}(z)dA - \sum_{i=1}^{n} t_i \qquad \text{(Eq. 11.1.3)}$$

By assuming that the retaining wall has width equal to unity (dA = dz) and performing the integration with definitions of the lateral earth pressure distributions as shown in Figures 11.1.1, 11.1.2, and 11.1.3, Equation 11.1.3 can be reduced to Equation 11.1.4.

$$F_{total}(z) = K_{comp} \cdot \gamma \cdot \frac{z^2}{2} = K_{soil} \cdot \gamma \cdot \frac{z^2}{2} - \sum_{i=1}^{n} t_i \qquad \text{(Eq. 11.1.4)}$$

The mathematical expression of the composite lateral earth pressure coefficient at any depth can then be obtained by rearranging Equation 11.1.4 (Equation 11.1.5).

$$K_{comp}(z) = K_{soil} - \frac{2 \cdot \sum_{i=1}^{n} t_i}{\gamma \cdot z^2} \qquad \text{(Eq. 11.1.5)}$$

Reinforcement tensions needed to stabilize the backfill soil at depth z can also be obtained by rearranging Equation 11.1.4 (Equation 11.1.6).

$$\sum_{1}^{n} t_i(z) = \frac{\gamma \cdot z^2}{2} \cdot (K_{soil} - K_{comp}) \qquad \text{(Eq. 11.1.6)}$$

11.1.2 Value of K_{comp}

Direct measurements of the lateral earth pressures behind the face of the GRS retaining walls are not available today because accurate field measurements of earth pressures are virtually impossible to obtain. It is also difficult to determine K_{comp} using Equation 11.1.5 because the state of the backfill soil (K_{soil}), whether active, at rest, or passive, is hard to determine. However, reliable prediction of the GRS composite lateral earth pressures can be obtained from well-developed numerical models that are capable of reproducing the internal strain measurements within a GRS wall using Equation 11.1.7, provided that the in-soil modulus of the reinforcement is known. In Equation 11.1.7, modeling results of horizontal stresses of soil elements behind the

wall faces were used as the horizontal geosynthetic reinforced earth pressure, σ_h, in the equation.

$$K_{comp}(z) = \frac{\sigma_h}{\gamma \cdot z} \qquad \text{(Eq. 11.1.7)}$$

where σ_h = horizontal geosynthetic reinforced earth pressure obtained from numerical models.

Modeling results of the WSDOT Rainier Avenue wall, the FHWA Algonquin concrete panel geogrid wall, and the FHWA Algonquin modular block faced wall were reduced to obtain typical values of K_{comp} for different types of GRS walls. Figures 11.1.4 to 11.1.6 show the values of K_{comp} that were obtained from modeling results, as well as the active lateral earth pressure coefficient, K_a, and the lateral earth pressure coefficient at rest, K_o. Values of K_{comp} shown in Figures 11.1.4 to 11.1.6 were determined using Equation 11.1.7. Table 11.1.1 summarizes the typical values of coefficient of lateral reinforced earth pressure, K_{comp}, K_a, and K_o.

11.1.3 Discussion and Conclusions

1. Equation 11.1.5 shows that the GRS composite lateral earth pressure distribution is a function of the height of the wall, unit weight and the lateral earth pressure coefficient of the backfill soil, and the distribution of the reinforcement tension.

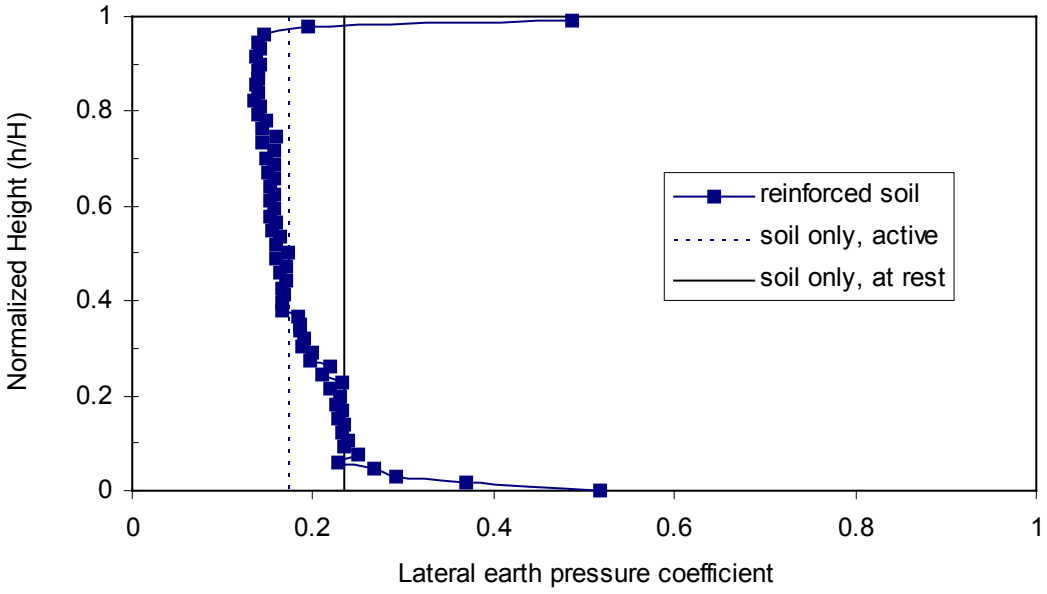

Figure 11.1.4 Lateral earth pressure coefficient of Rainier Avenue wall.

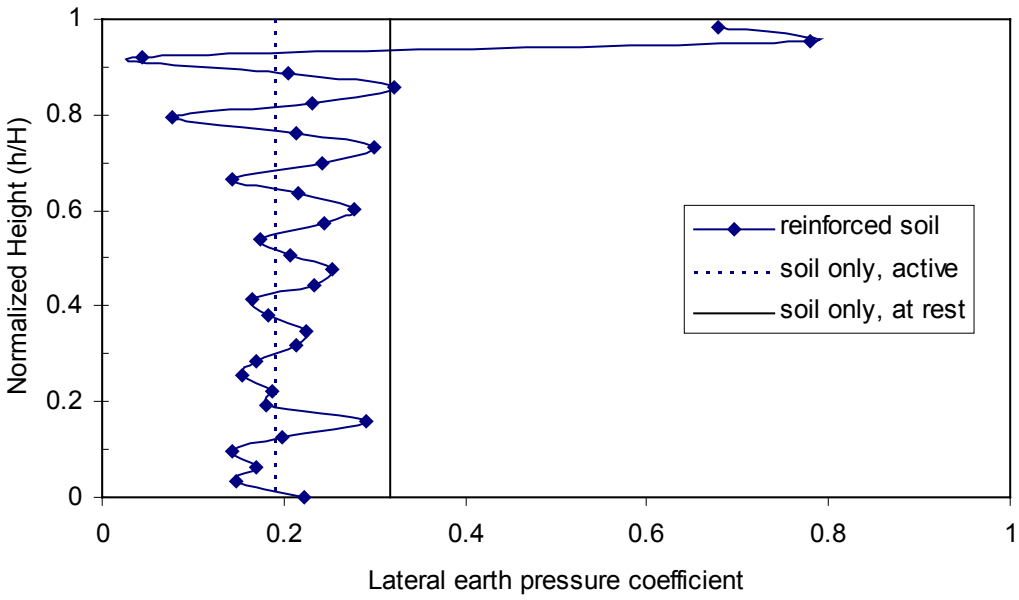

Figure 11.1.5 Lateral earth pressure coefficient of Algonquin concrete panel geogrid wall.

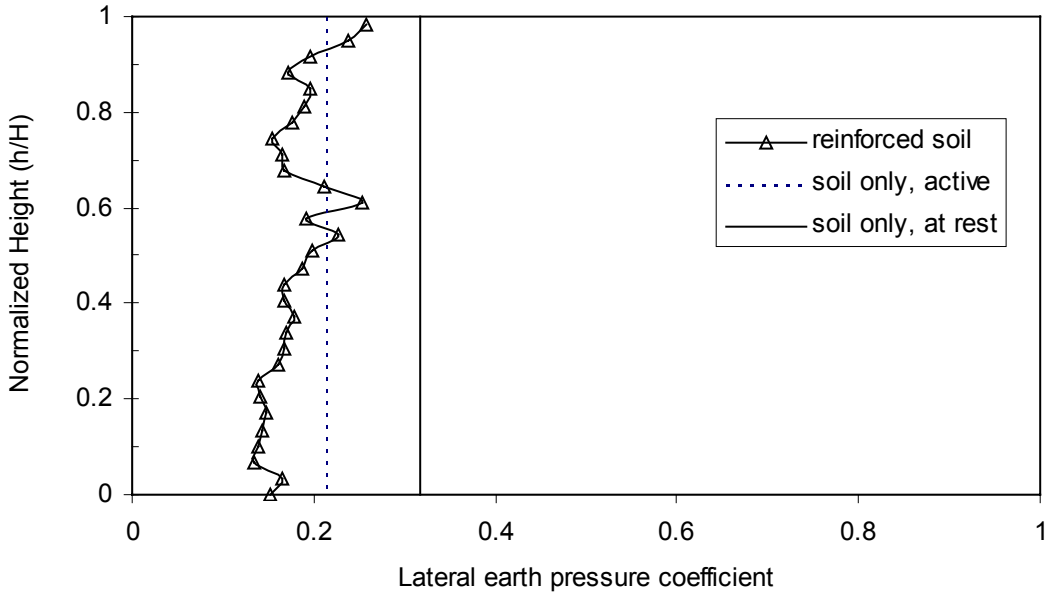

Figure 11.1.6 Lateral earth pressure coefficient of Algonquin modular block faced wall.

Table 11.1.1 Lateral earth pressure coefficients of GRS walls.

Wall Names	K_{comp}[1]	K_a[2]	K_0[3]
Rainier Avenue wall	0.178	0.172	0.234
Algonquin concrete panel geogrid wall	0.20	0.19	0.318
Algonquin modular block faced wall	0.174	0.214	0.318

[1] Average of values shown in Figures 11.1.4 to 11.1.6.
[2] calculated using Coulomb's equation.
[3] 1 - sinϕ.

2. Equation 11.1.5 also indicates that the lateral geosynthetic reinforced earth pressures behind the wall face can be less than the active lateral earth pressures when the backfill reaches its active state and the reinforcement starts to provide tensile forces that reinforce the backfill. Result shown in Figure 11.1.6 and most of the heights of Figures 11.1.4 and 11.1.5 confirms this observation.

11.2 GRS Composite Modulus, E_{comp}

Another term that was developed in this research is the GRS composite modulus E_{comp}. E_{comp} was developed based on the theory of composite materials. It was used to characterize the modeling results of the parametric study described in Chapter 12. Horizontal face deflections of GRS walls of different designs were found to have a very good correlation with E_{comp}. In the following sections, derivation of E_{comp} is presented. Applications of E_{comp} are presented in both Chapters 12 and 14.

Figure 11.2.1 shows a typical cross section of a GRS wall and a GRS element cut from it. Following assumptions were made in order to simplify the derivations:

1. Deformation of the GRS element is uniform, i.e., there is no interlayer movement between soil and reinforcement.
2. Width of GRS element equals unity.
3. Stress-strain behavior of the soil and reinforcement follows Hooke's Law ($\sigma = E \cdot \varepsilon$).

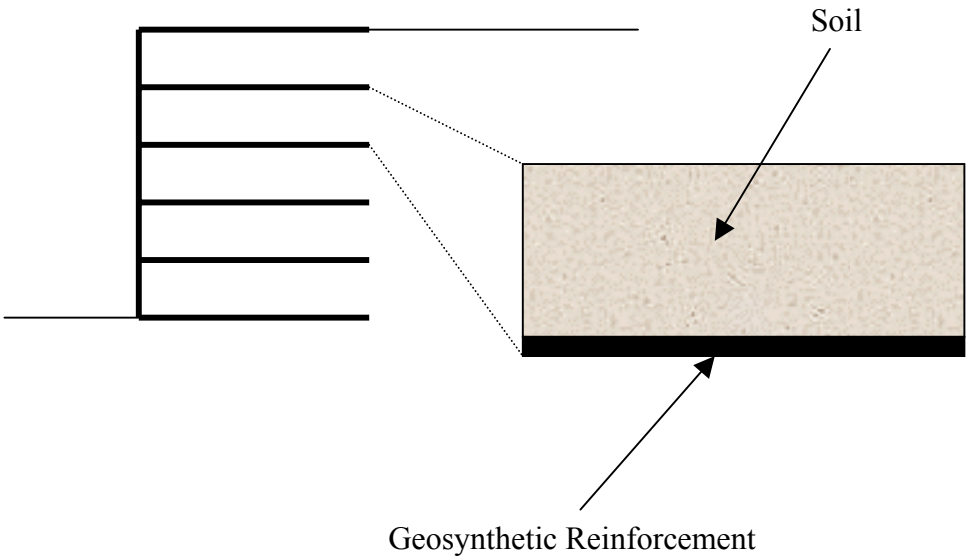

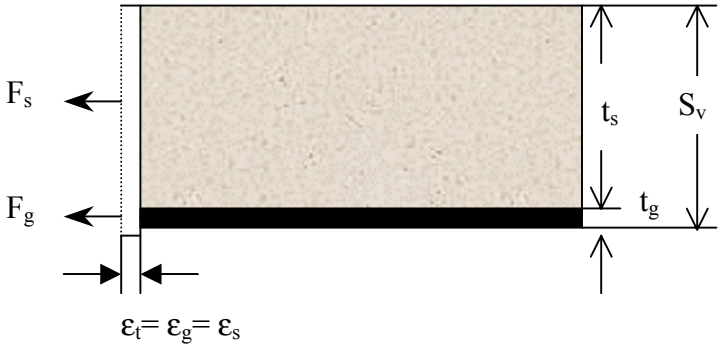

Figure 11.2.1 GRS element inside a GRS wall.

11.2.1 Derivation of E_{comp}

As shown in Figure 11.2.1, the total horizontal force acting on the GRS element can be expressed as Equation 11.2.1.

$$F_t = F_g + F_s \qquad \text{(Eq. 11.2.1)}$$

where F_t = total force of GRS composite,
F_g = reinforcement force, and
F_s = soil force.

Equation 11.2.1 can also be expressed in term of stresses and areas (Equation 11.2.2).

$$\sigma_t \cdot A_t = \sigma_g \cdot A_g + \sigma_s \cdot A_s \qquad \text{(Eq. 11.2.2)}$$

where σ_t= total stress in the GRS composite,
A_t= total cross section area of GRS composite,
σ_g= reinforcement stress,
A_g= cross section area of reinforcement,
σ_s= soil stress, and
A_s= cross section area of soil.

Equation 11.2.2 can be further simplified by introducing the assumption that the width of the wall is equal to unity (Equation 11.2.3).

$$\sigma_t \cdot S_v = \sigma_g \cdot t_g + \sigma_s \cdot t_s \qquad \text{(Eq. 11.2.3)}$$

where S_v = height of the GRS composite (reinforcement spacing),

t_g = thickness of reinforcement, and

t_s = thickness of soil.

Equation 11.2.3 can be rewritten as Equation 11.2.4 using the stress-strain relationship described by Hooke's Law ($\sigma_i = E_i \cdot \varepsilon_i$).

$$E_{comp} \cdot \varepsilon_t \cdot S_v = E_g \cdot \varepsilon_g \cdot t_g + E_s \cdot \varepsilon_s \cdot t_s \qquad \text{(Eq. 11.2.4)}$$

where E_{comp}= modulus of GRS composite,

ε_t= total strain of GRS composite,

E_g= modulus of reinforcement,

ε_g= strain of reinforcement,

E_s= modulus of soil, and

ε_s= strain of soil.

Strains ε_t, ε_g, and ε_s in Equation 11.2.4 can be cancelled out because uniform deformation was assumed (Equation 11.2.5).

$$E_{comp} \cdot S_v = E_g \cdot t_g + E_s \cdot t_s \qquad \text{(Eq. 11.2.5)}$$

Rearranging Equation 11.2.5 and with the relation between t_g, t_s, and S_v as shown in Figure 11.2.1, E_{comp} can be obtained as Equation 11.2.6:

$$E_{comp} = E_g \cdot \frac{t_g}{S_v} + E_s \cdot \frac{(S_v - t_g)}{S_v} \qquad \text{(Eq. 11.2.6)}$$

where $S_v - t_g \approx S_v$, and

$E_g = \frac{J}{t_g}$, where J is the stiffness of the reinforcement.

Formulation of E_{comp} then becomes:

$$E_{comp} \approx \frac{J}{t_g} \cdot \frac{t_g}{S_v} + E_s \cdot \frac{S_v}{S_v} = \frac{J}{S_v} + E_s \qquad \text{(Eq. 11.2.7)}$$

11.2.2 Discussion and Conclusions

1. Equation 11.2.7 is the expression for horizontal modulus of the GRS composite. Derivation of vertical composite modulus of GRS element is different. Moduli calculated using Equation 11.2.7 are only appropriate for characterizing the horizontal working stress or strain information of GRS walls.

2. The in-soil and low strain rate adjustments discussed in Chapter 7 of this thesis have to be applied to the in-isolation reinforcement stiffness before it is used in Equation 11.2.7.

3. Plane strain soil modulus is suggested for use in Equation 11.2.7 when analyzing GRS retaining structures. E_s, the soil modulus, can be obtained from strength test data or estimated using a confining pressure dependent hyperbolic soil modulus model. Details of estimating plane strain soil modulus are described in Chapter 7 of this thesis as well.

Chapter 12
Parametric Study of the Internal Design Factors of GRS Walls

12.1 Introduction

After the successful performance predictions of case histories and large-scale test walls, extensive parametric studies were performed to investigate the influence of internal design factors such as layer spacing, soil strength properties, reinforcement stiffness, and facing types. The results of the parametric analyses were recorded and analyzed in terms of GRS wall performance factors such as internal stress-strain levels and wall face deflections. The purposes of the parametric study were to:

1. Investigate the sensitivity of the modeling results to the input material properties,
2. Examine the influence of the internal design factors on the performance of GRS retaining structures, and
3. Make attempts to improve the internal design of GRS walls based on the working stress information obtained from the parametric study.

Two types of parametric analyses were performed in this research. In the first type, numerical models of the WSDOT Rainier Avenue wall (Model 5008P) and the FHWA Algonquin concrete panel test walls (Models AlgW1, AlgW2, and AlgW3) were used as the fundamental models of the parametric study. Internal design factors such as soil friction angle and reinforcement stiffness were systematically varied in the models. These analyses were performed by varying only one design factor in each group while

the other factors were fixed. The second type of parametric study was performed using a large number of GRS wall models with different internal stability design factors. Design factors such as wall height, layer spacing, soil strength properties, and reinforcement properties were systematically introduced into GRS wall models to observe the interaction effects of these design factors. In this chapter, results of the parametric study are presented and discussed.

12.2 Preliminary Parametric Study I -- Rainier Avenue Wall

The first parametric study was performed on Model 5008P to examine its sensitivity to the input material properties. Maximum face deflections of the model walls were examined by systematically varying the input material properties such as the reinforcement stiffness, the soil friction angle, and the soil cohesion. Table 12.2.1 lists the values of the material properties that were input into Model 5008P. Only one design factor (input material property) was changed in each group while the other factors were fixed.

The results of this parametric analysis have already been presented by Holtz and Lee (1997). Figures 12.2.1 to 12.2.3 show the results of this preliminary study. The maximum deflections increased when the tensile modulus of geosynthetics decreased (Figure 12.2.1). The same tendency was also observed in Figure 12.2.2; the maximum deflection increased when the soil friction angle decreased. Although the maximum deflections decreased slightly when the soil cohesion was decreased from 8 kPa to 6 kPa, they increased as the soil cohesion decreased further (Figure12.2.3).

Table 12.2.1 Input material properties used in parametric study.

Input material properties	Values
Reinforcement stiffness	12.5%, 25%, 50%, and 75% of the original reinforcement stiffnesses (Table 9.2.1)
Soil friction angle	30, 35, 40, 45, 50, and 55 degrees
Soil cohesion	0, 2, 4, 6, and 8kPa

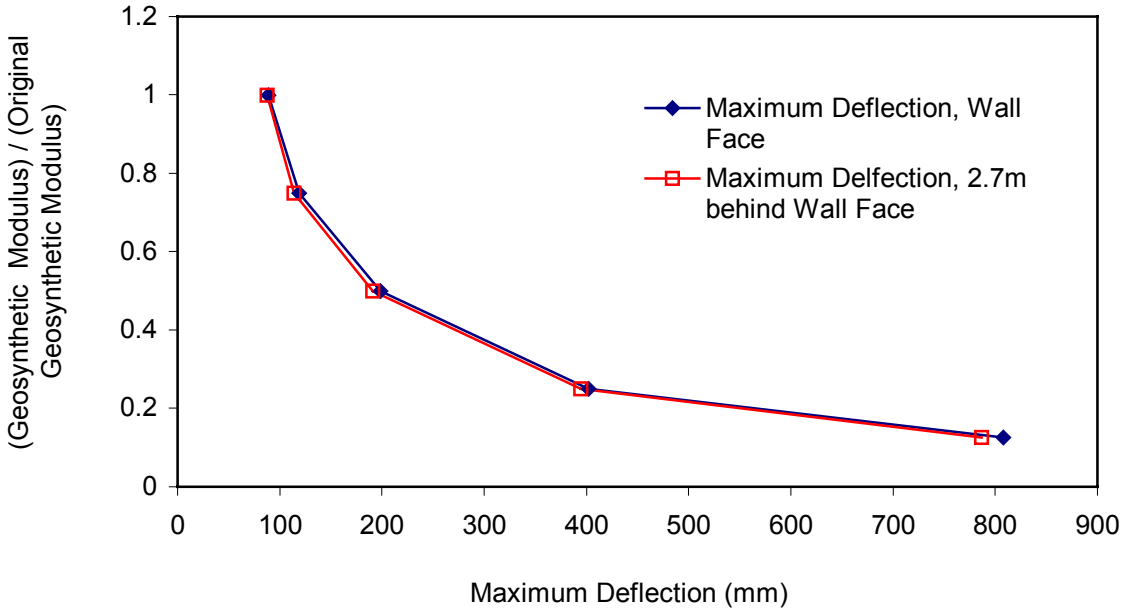

Figure 12.2.1 Maximum deflection vs. geosynthetic modulus.

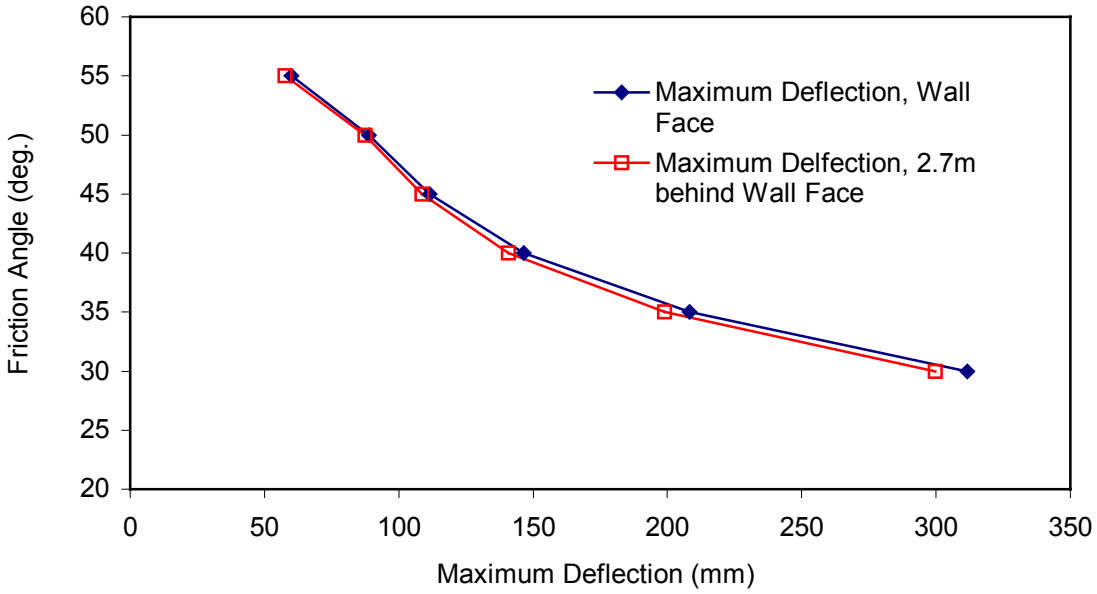

Figure 12.2.2 Maximum deflection vs. soil friction angle.

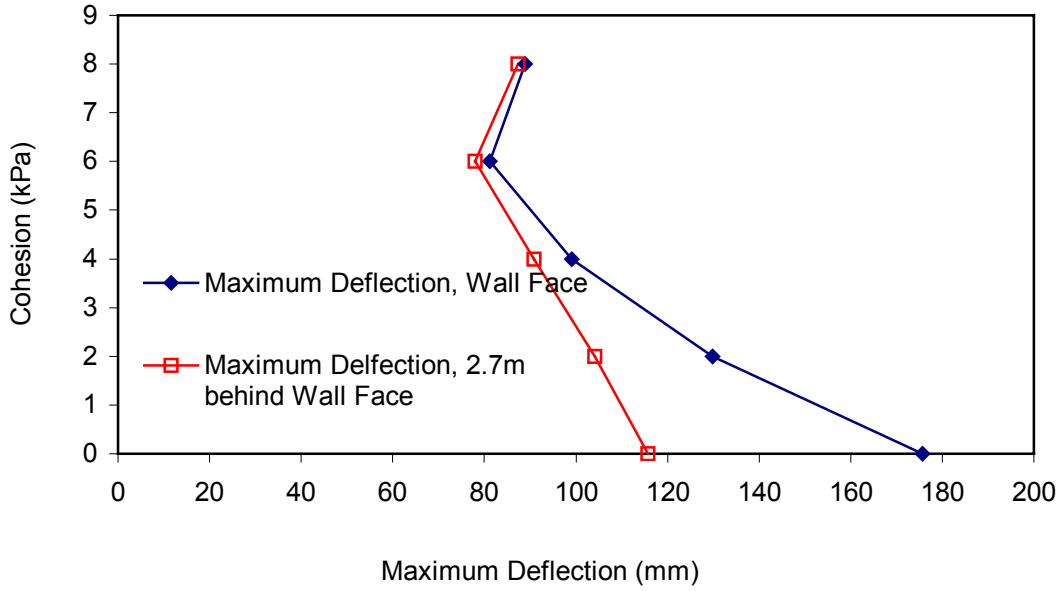

Figure 12.2.3 Maximum deflection vs. soil cohesion

The overall deflections of the wall model increased as the strength properties of materials decreased.

12.3 Preliminary Parametric Study II – Algonquin Concrete Panel Walls

A parametric study was also performed on models of FHWA Algonquin concrete panel faced wall (Lee, Holtz, and Allen, 1999). In this study, reinforcement stiffness was chosen as the controlling factor because the analysis results could be correlated to the measurements of three test walls (Table 9.3.1). A set of FLAC models was created based on Model Alg-W2. They had the same geometry, reinforcement layout, input soil properties, and input concrete panel properties as that model. Different stiffnesses and therefore the properties of the built-in interface of the reinforcement (cable elements) were systematically introduced into these FLAC models, as given in Table 12.3.1; a total of six FLAC models were developed for this parametric study. Both wall performance and working stress-strain distribution were monitored and analyzed.

Modeling results of maximum face deflections were plotted versus the reinforcement modulus in Figure 12.3.1. The results indicated that increasing reinforcement stiffness significantly decreases maximum face deflections. This tendency was further verified by the results shown in Figure 12.3.2, in which accumulative inclinometer deflections at 1.8 m behind the wall face decreased as the reinforcement stiffness increased. Also as shown in Figure 12.3.2, walls reinforced

Table 12.3.1 Summary of the models of the parametric study.

Model name	Reinforcement modulus, (kN/m)	Notes
Alg-W1	54690	Reinforcement modulus was equal to the modulus of steel strips (Algonquin Wall 1).
Alg-W3	37860	Reinforcement modulus was equal to modulus of bar mats (Algonquin Wall 3).
Alg-W2-200%	2040	Reinforcement modulus was 200% of the geogrid modulus in Wall 2.
Alg-W2	1020[a]	Reinforcement modulus was equal to the modulus of the geogrid used in Algonquin Wall 2.
Alg-W2-50%	510	Reinforcement modulus was 50% of the geogrid modulus in Wall 2.
Alg-W2-25%	255	Reinforcement modulus was 25% of the geogrid modulus in Wall 2.

[a] Including 50% reduction because of strain rate effects

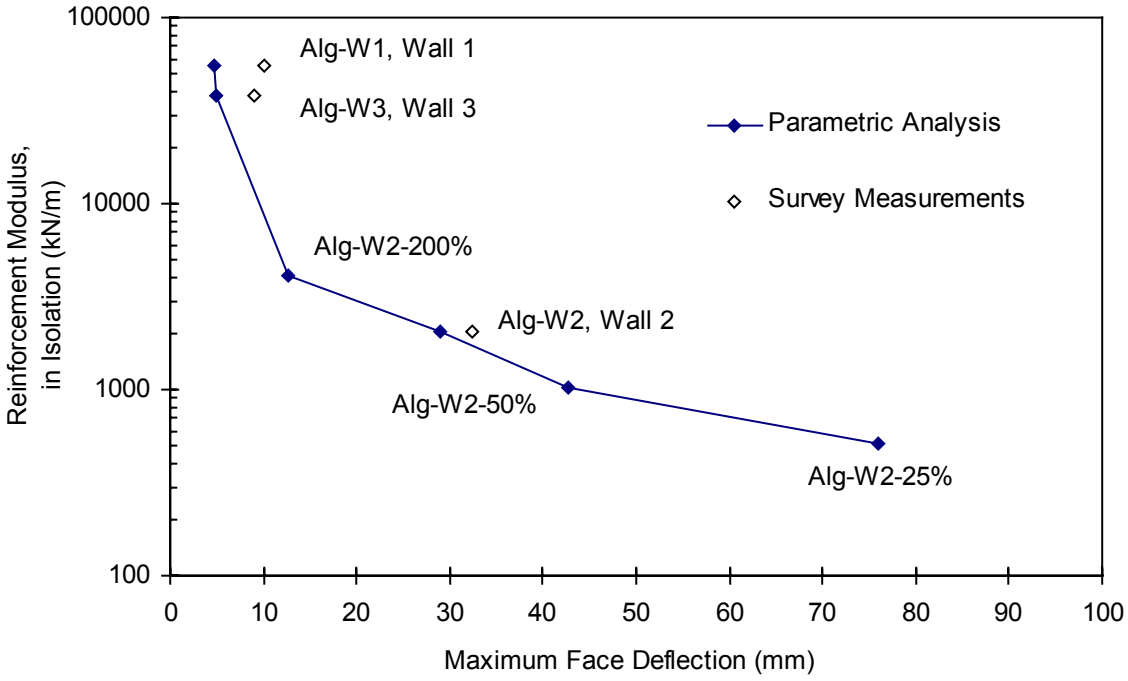

Figure 12.3.1 Maximum face deflection vs. reinforcement modulus.

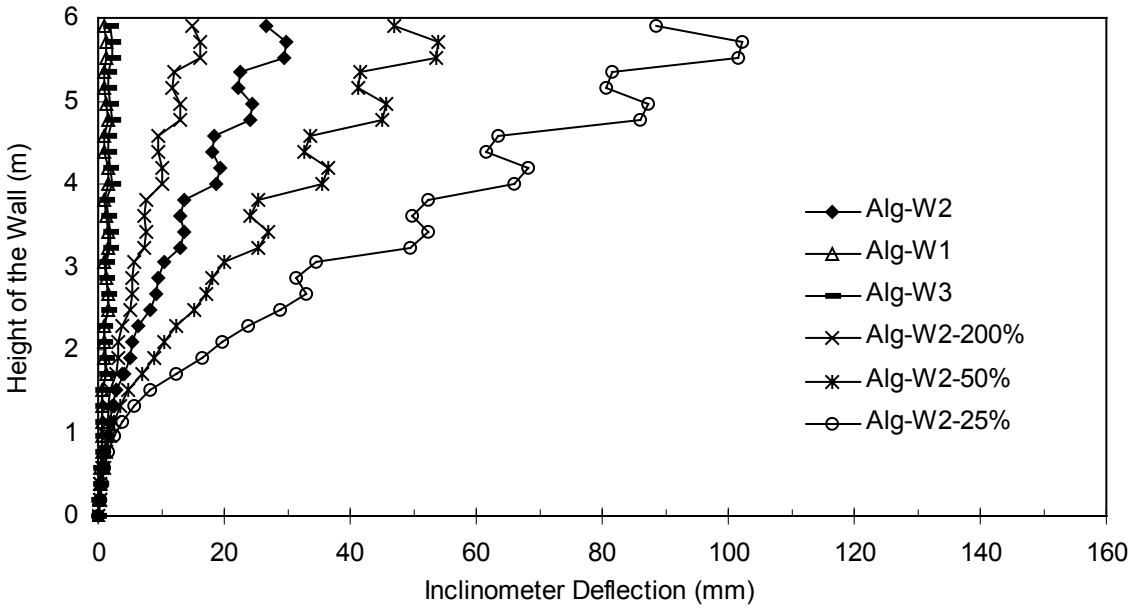

Figure 12.3.2 Modeling results showing accumulated inclinometer deflections, at 1.8m behind wall face.

with very high stiffness reinforcement such as steel strips and bar mats (Walls 1 and 3) had almost the same deflections. This shows that there was a point of diminishing returns at which increasing reinforcement stiffness did not reduce the overall wall face deflection.

Figure 12.3.3 summarizes the reinforcement strain distribution obtained for all the reinforcement stiffnesses analyzed. Both peak strain and overall strain in the reinforcement increased as the reinforcement stiffness decreased. All the peak strains occurred at the wall facing except at layer 1 of Model Alg-W2-25% (case with low reinforcement stiffness). Results of Model Alg-W2-25% showed that the peak strain of layer 1 was located at about 0.17 m from wall face. Moreover, decreasing the reinforcement stiffness tended to cause the higher strain zones of the reinforcement to extend further back from the wall face into the backfill (Figure 12.3.3).

Figure 12.3.4 shows the maximum reinforcement tensions as a function of reinforcement stiffness. It shows that reinforcement with relatively high stiffness such as steel reinforcement developed larger reinforcement loads than did low stiffness reinforcement such as geosynthetics. As shown in Figures 12.3.3 and 12.3.4, as the reinforcement stiffness decreased sufficiently to result in peak reinforcement strains of 3 to 4% or more, the load in the reinforcement did not continue to decrease; instead, it began to increase as reinforcement stiffness decreased. Interestingly, based on triaxial

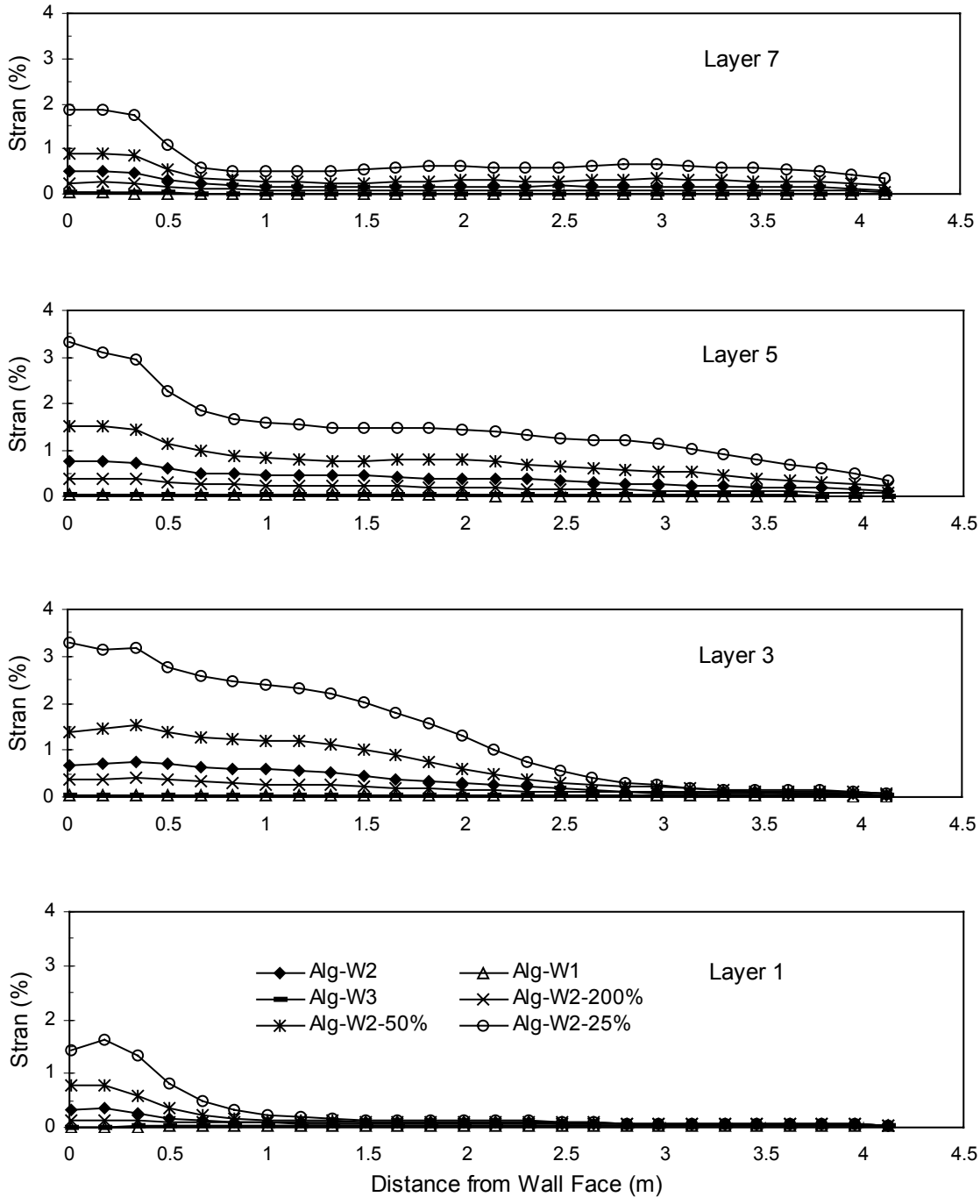

Figure 12.3.3 Reinforcement strain distribution.

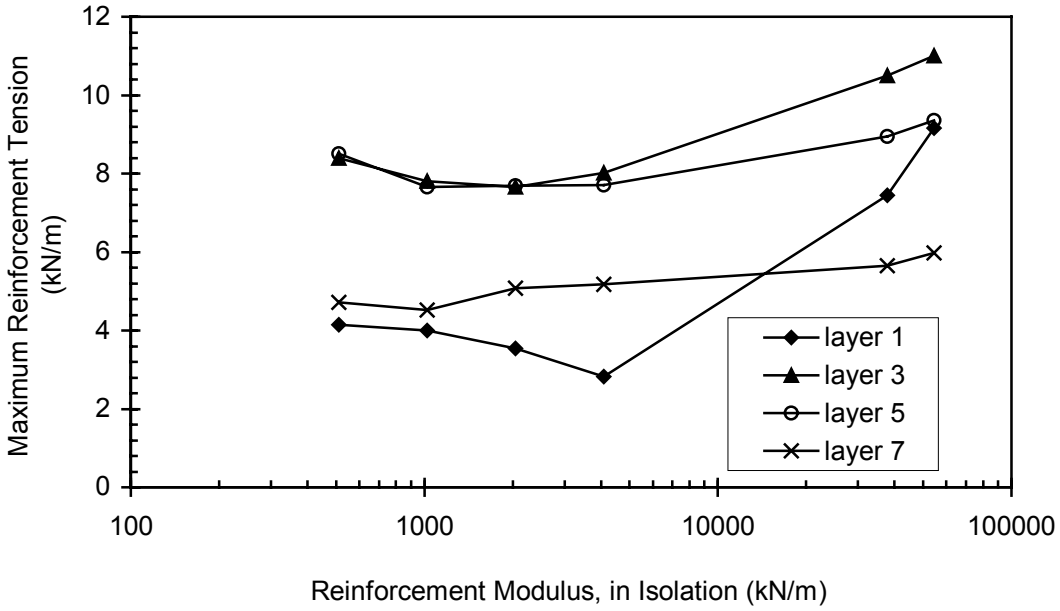

Figure 12.3.4 Maximum reinforcement tension vs. reinforcement stiffness.

tests conducted on this wall backfill (Christopher, 1993), the shear strain corresponding to the peak shear strength for the soil was on the order of 2 to 4% strain. Figure 12.3.4 also shows that the maximum reinforcement load occurs in the middle of the wall (layers 3 and 5) for all the reinforcement stiffnesses analyzed.

12.4 Analyses Matrix of the Major Parametric Study

In order to further investigate the influence of the internal design factors on the performance of GRS walls, an extensive parametric analysis program was performed. Internal design factors including soil strength properties, reinforcement stiffness, reinforcement layer spacing, facing system, and toe restraint were systematically varied in three fundamental wrapped faced GRS wall models. These models were modified from numerical models developed for the 3.6m high RMCC test walls, the 6.1m high Algonquin FHWA test walls, and the 12.6m high Rainier Avenue wall.

A total of 256 models were analyzed by systematically introducing combinations of the controlling factors described above into the three fundamental models. Of these, 72 models failed to reach the final construction stage because internal instability occurred; thus a total of 184 GRS wall models were fully analyzed in this parametric study. Table 12.4.1 lists the nine groups of models that were analyzed; each group was categorized by their heights and facing systems. In each group, backfill soil properties, reinforcement properties, vertical spacing of reinforcement, and toe restraint were systematically changed in order to examine the combined influence of these design

Table 12.4.1 Model groups of parametric analysis.

Group	Wall Height, H (m)	Vertical Spacing, S_v (m)	Facing System
A	12.6	0.38	Wrapped face
B	6.1	0.76	Wrapped face
C	3.6	0.6	Wrapped face
D	6.1	0.38	Wrapped face
E	6.1	0.76	Wrapped face with secondary reinforcement
F	6.1	0.76	Modular block face
G	6.1	0.76	Concrete panel face
H	6.1	0.38	Modular block face
I	6.1	0.38	Concrete panel face

factors on GRS wall performance. The general boundary conditions, design factors, and ranges of the design factors are described in the following sections.

12.4.1 General Boundary Conditions and Design Factors

Following are the general boundary conditions and design factors of the models analyzed in this parametric study:

1. Vertical face—all models had a vertical face because walls with vertical faces had larger deflections than walls with battered faces.

2. No foundation failure—all model walls were built on a foundation that had good soil properties; thus bearing capacity failure of the foundation was not a concern of this analysis.

3. Extended boundary conditions—for all models, the backfill was extended backward a distance equal to the embeded reinforcement length from the end of the reinforcement. The foundation soil in front of the wall was also extended a distance equal to the embedded reinforcement length from the toe of the wall. The depth of foundation soil was equal to the height of the wall.

4. Uniform reinforcement stiffness and spacing—all layers of reinforcement inside each model wall had the same stiffness and vertical spacing.

5. Ratio of reinforcement length to wall height—all model walls had a reinforcement length to wall height ratio equal to 0.8.

12.4.2 Controlled Factor I—Backfill Soil Properties

Seven types of granular soils were chosen as the backfill materials for the parametric analysis. Table 12.4.2 lists the unit weight, friction angle, dilation angle, lateral earth pressure coefficients, and the parameters of the hyperbolic soil modulus model described in Chapter 7 (Duncan et al., 1980). These soil properties were set up to represent good quality backfill (Soil Type VII) to poor quality backfill (Soil Type I) materials.

12.4.3 Controlled Factor II—Reinforcement Stiffness and Spacing

Reinforcement stiffness (J) in the parametric analysis ranged from 55 kN/m to 60,000 kN/m and represented the reinforcement stiffness of very weak geosynthetics to steel reinforcement. Three vertical spacings (S_v), 0.38m (1.25ft), 0.76m (2.5ft), and 1.14m (3.75ft), were used in the parametric analysis models. The correlated global stiffness (J_g), defined as the reinforcement stiffness divided by the vertical spacing (Christopher et al., 1990, Christopher, 1993), ranged from 92 kN/m^2 to 157,895 kN/m^2.

Table 12.4.2 Soil properties used in parametric analysis models.

Soil Type	Unit Weight (kN/m^3)	Friction Angle (deg)	Dilation Angle (deg)	Lateral Earth Pressure Coefficient at rest[a], K_0	Hyperbolic Soil Modulus Model Parameters
I	16.68	25	10	0.58	K =800, R_f =0.73, and n =0.5
II	17.66	30	10	0.5	K =1000, R_f =0.73, and n =0.5
III	18.64	35	10	0.43	K =1200, R_f =0.73, and n =0.5
IV	19.62	40	15	0.36	K =1400, R_f =0.73, and n =0.5
V	20.60	45	15	0.29	K =1600, R_f =0.73, and n =0.5
VI	21.58	50	15	0.23	K =1800, R_f =0.73, and n =0.5
VII	22.56	55	20	0.18	K =2100, R_f =0.73, and n =0.5

[a] Calculated using equation $K_0 = 1\text{-}\sin\phi$.

12.4.4 Controlled Factor III—Toe Restraint

Four types of toe restraint were used in the parametric models. They are the free toe (no restraint), toe embedment of 5% of the wall height, toe embedment of 10% of the wall height, and fixed toe (no displacement allowed).

12.4.5 Controlled Factor IV—Facing Systems

As indicated in Table 12.4.1, four common facing systems of GRS walls were used in the design of the parametric models. They were wrapped face (Groups A, B, C, and D), wrapped face with secondary reinforcements (Group E), modular block face (Group F and H), and concrete panel face (Group G and I). Secondary reinforcement refers to the short horizontal layers of reinforcement that are inserted in between the primary reinforcement layers near wall face. The size of the modular block was 190mm in height and 600mm in depth (including the drainage stone column). The depth of the concrete panel was 140mm. Because FLAC is a two dimensional analysis program, the width of the structural facing systems was equal to the one unit length of the models; in this analysis, the length unit of all models was one meter.

12.5 Analysis Result I—Face Deflection

Because the wall face bulged out in between the reinforcement layers, especially in models with large reinforcement spacings (Group B and C), only the face deflections at reinforcement layers were recorded and analyzed. Face deflections of the bulges were difficult to characterize because plastic failure was found in many soil elements located in between the reinforcement layers.

In this section, the analysis results are shown as normalized wall height (h/H, where h is the height at which the deflection was measured and H is the full height of the wall) versus the face deflections at reinforcement layers (Figures 12.5.1 to 12.5.7). The influences of soil and geosynthetic reinforcement properties on the distributions and magnitudes of the face deflections are discussed separately first (Figures 12.5.1 to 12.5.7). A composite material approach is then presented in an effort to summarize the maximum face deflections with considerations of both soil and reinforcement properties (Figure 12.5.8). The following observations and conclusions and discussions about wall face deflections were obtained from the modeling results:

1. Face deflections of GRS walls were found to be affected by the quality of the backfill. Figures 12.5.1 to 12.5.4 show typical wall deflection results of Groups A, B, C, and D GRS walls, but with different types of backfill soils. As shown in the figures, the overall deflections increased as the soil strength decreased.

2. Face deflections of GRS walls were also found to be affected by the reinforcement stiffness. Figures 12.5.5 to 12.5.7 show the typical wall deflection results of Group A, B, C, and D walls that were built using reinforcements with different global reinforcement stiffnesses. As shown in the figures, the overall deflections increased as the global stiffness decreased.

3. By comparing Figures 12.5.1, 12.5.4, 12.5.5, and 12.5.6, 12.6 m walls had larger wall face deflections than 6.1 m walls, even with the same vertical spacing and reinforcement length to wall height ratio.

4. Walls with smaller vertical spacing deformed less than walls that had the same height but larger spacings (Figures 12.5.2, 12.5.4, and 12.5.6).

5. Deflection profiles shown in these figures indicate that maximum deflection of walls with small spacings occurred at the middle of the wall (0.5H, where H is height of the wall), and maximum deflection of walls with large spacings occurred at a height about 0.6H.

6. Deflection profiles shown in Figures 12.5.2, 12.5.3, 12.5.6, and 12.5.7 also indicated that larger deflections occurred at upper half of large spacing walls that had local failures at wall face. Evidence of tilting of walls with large reinforcement spacings was observed.

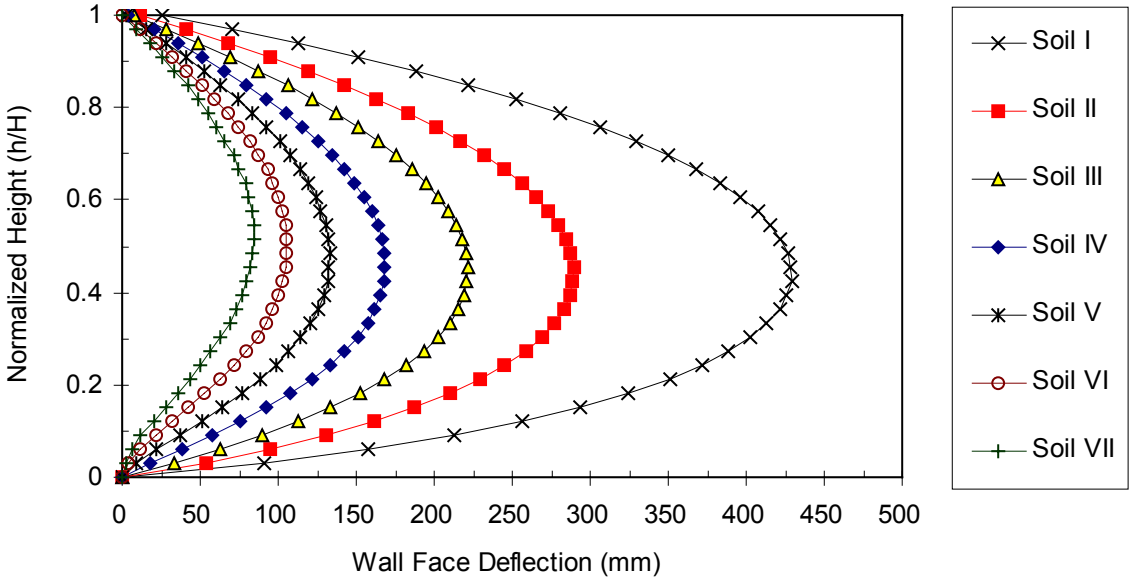

Figure 12.5.1 Face deflection profiles of Group A models (wrapped face, H=12.6m, S_v=0.38m, J_g=1316kN/m^2) with soil properties varied.

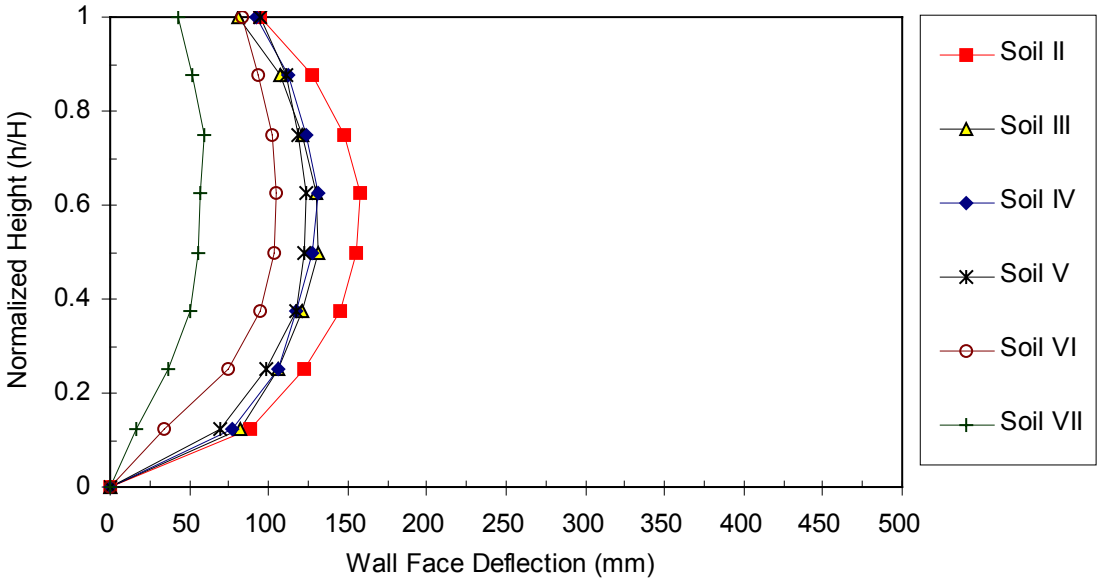

Figure 12.5.2 Face deflection profiles of Group B models (wrapped face, H=6.1m, S_v=0.76m, J_g=1312kN/m^2) with soil properties varied.

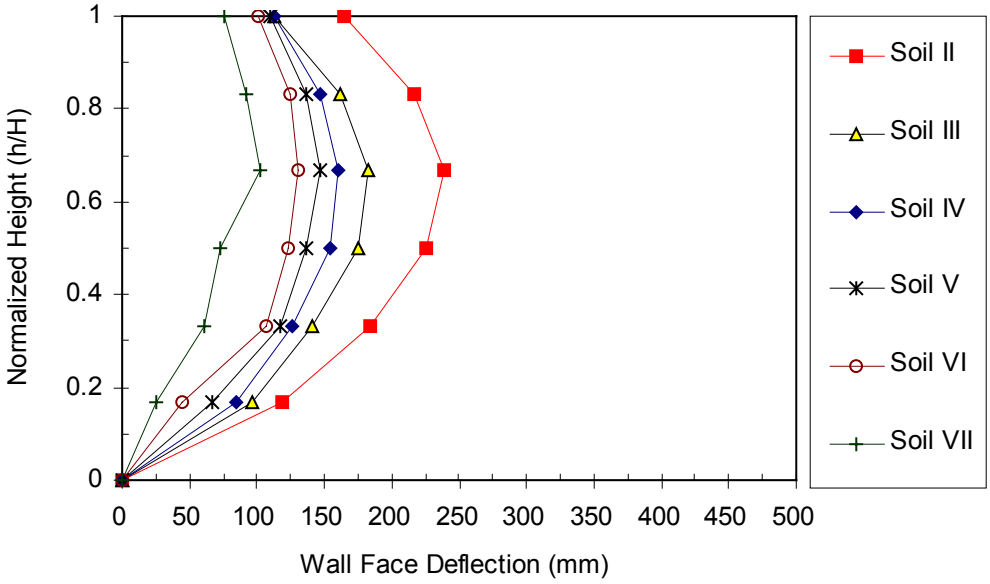

Figure 12.5.3 Face deflection profiles of Group C models (wrapped face, H=3.6m, S_v=0.6m, J_g=183kN/m^2) with soil properties varied.

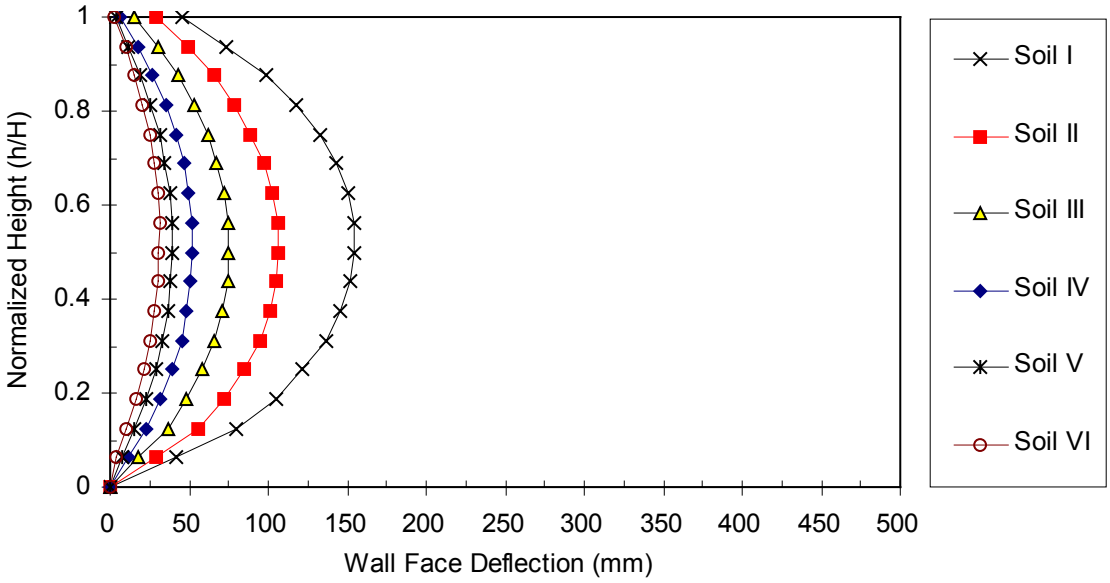

Figure 12.5.4 Face deflection profiles of Group D models (wrapped face, H=6.1m, S_v=0.38m, J_g=1316kN/m^2) with soil properties varied.

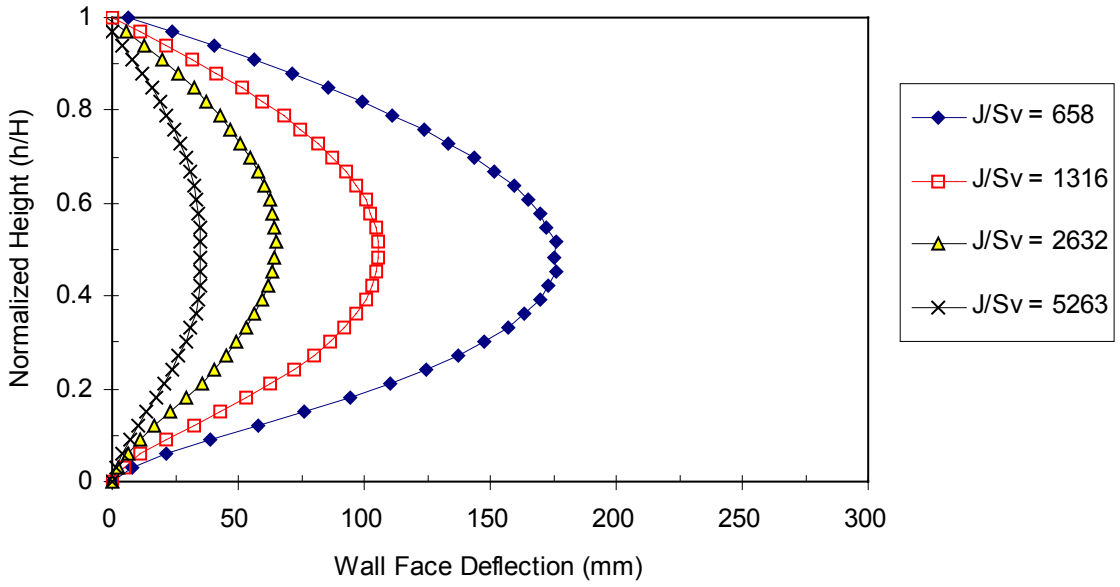

Figure 12.5.5 Face deflection profiles of Group A models (wrapped face, H=12.6m, S_v=0.38m, Type VI soil) with reinforcement stiffness varied.

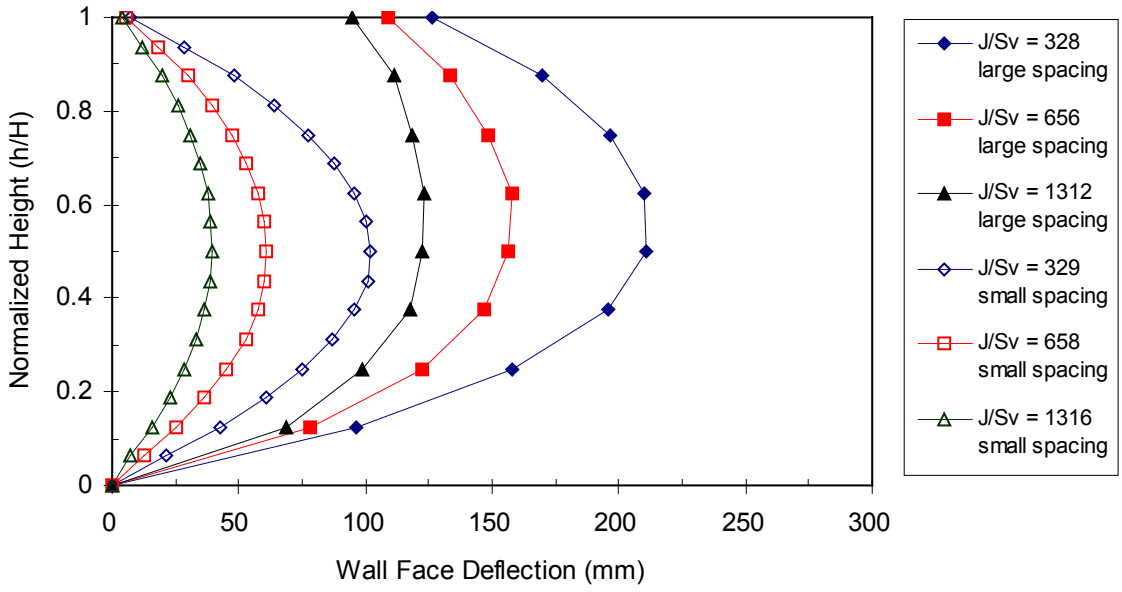

Figure 12.5.6 Face deflection profiles of Group B and D models (wrapped face, H=6.1m, S_v=0.38m and 0.76m, Type V soil) with reinforcement stiffness varied.

7. Modeling results shown in Figure 12.5.6 indicated that, even when designed with similar global stiffness, large spacing walls still possessed larger deflections than the small spacing walls.

In order to summarize the maximum deflections of all model walls with considerations of both soil and reinforcement properties, the composite GRS modulus (E_{comp}) defined and formulated in Chapter 11 was used (Equation 11.2.7). Figure 12.5.8 shows the normalized maximum wall deflection, maximum deflection (d_{max}) divided by the wall height (H), versus the initial composite GRS modulus ($E_{comp,\ ini}$). $E_{comp,\ ini}$ was used because most of the face deflections were observed to occur during construction. To determine the $E_{comp,\ ini}$, E_{soil} in Equation 11.2.7 was calculated using the hyperbolic soil modulus model (Equation 7.1.3) by giving confining pressure equal to $0.5K_o\gamma S_v$ (the confining pressure at middle of each "fresh-placed" lift). The normalized maximum face deflections showed very good correlation to the $E_{comp,\ ini}$ for both large spacing and small spacing walls (Figure 12.5.8). Results shown in Figure 12.5.8 indicated that the normalized maximum deflections increased as the $E_{comp,\ ini}$ decreased.

$$E_{comp} = \frac{J}{S_v} + E_s \qquad \text{(Eq. 11.2.7)}$$

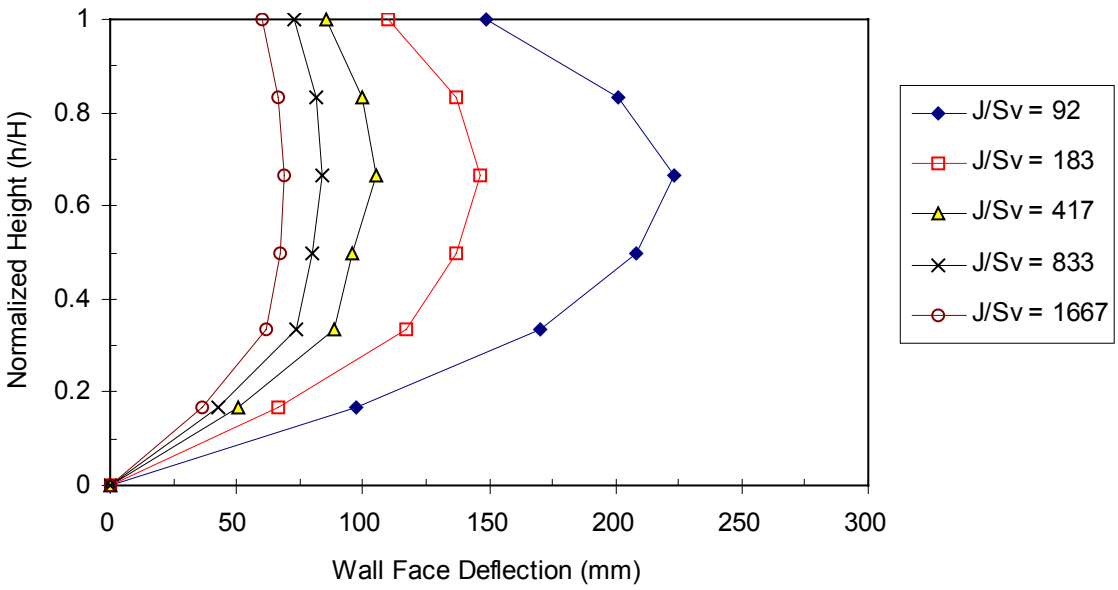

Figure 12.5.7 Face deflection profiles of Group C models (wrapped face, H=3.6m, S_v=0.6m, Type V soil) with reinforcement stiffness varied.

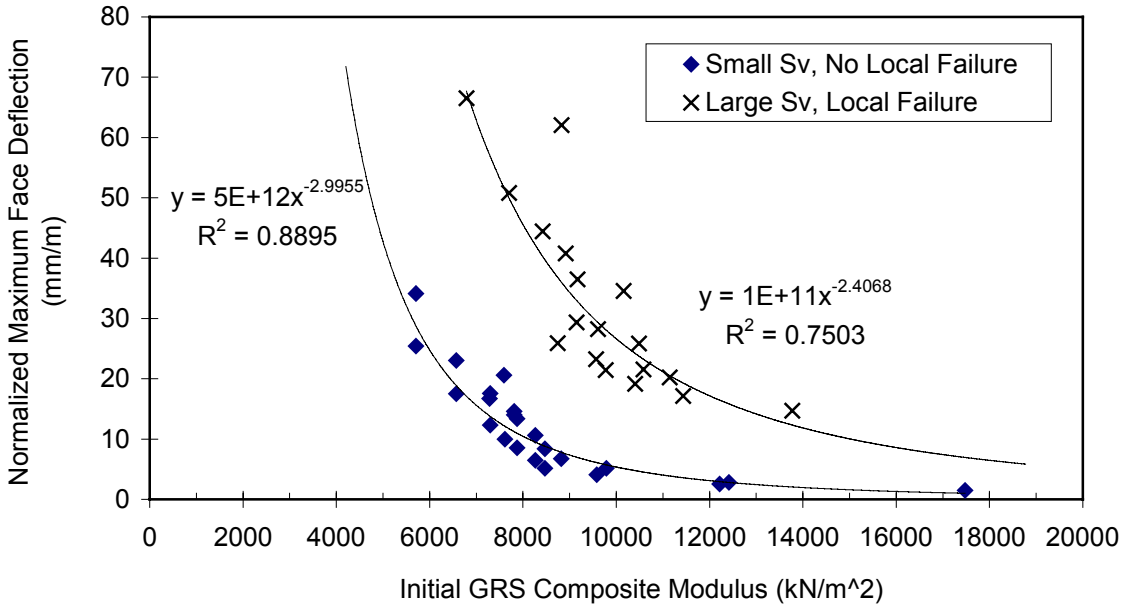

Figure 12.5.8 Initial GRS composite modulus versus the normalized maximum face deflection.

Also shown in Figure 12.5.8, for the small spacing walls, the maximum deflections increased rapidly even with a small decrease in $E_{comp, ini}$ when the $E_{comp, ini}$ had values smaller than 8,000 kN/m^2. For the large spacing walls, the normalized maximum deflection increased rapidly with a small deduction of $E_{comp, ini}$ as soon as the $E_{comp, ini}$ was smaller than 10,000 kN/m^2.

12.6 Analysis Result II—Reinforcement Tension

12.6.1 Characterization of Reinforcement Tensions

Figure 12.6.1 shows the typical results of reinforcement tension distributions along a reinforcement layer. As shown in Figure 12.6.1, T_{peak} was defined as the maximum reinforcement tension along the reinforcement layer, and T_{ave} was defined as the average reinforcement tension of each layer. Because the reinforcement elements inside numerical models used in this parametric study were attached to the material element nodes, as described in Section 8.5.6, these numerical models tended to overpredict T_{peak} at the face of the wrapped face wall or the connections of the structural faced wall. Figure 12.6.2 shows typical distributions of both T_{peak} and T_{ave}. The maximum value of T_{peak} of all layers inside a GRS wall was defined as T_{peak_max}, and the maximum value of T_{ave} of All layers was defined as T_{ave_max}.

As shown in Figure 12.6.2, distributions of T_{peak} and locations of $T_{peak, max}$ are more difficult to characterize than T_{ave}. In this study, in order to analyze the influences of both soil and reinforcement properties on the overall reinforcement tension

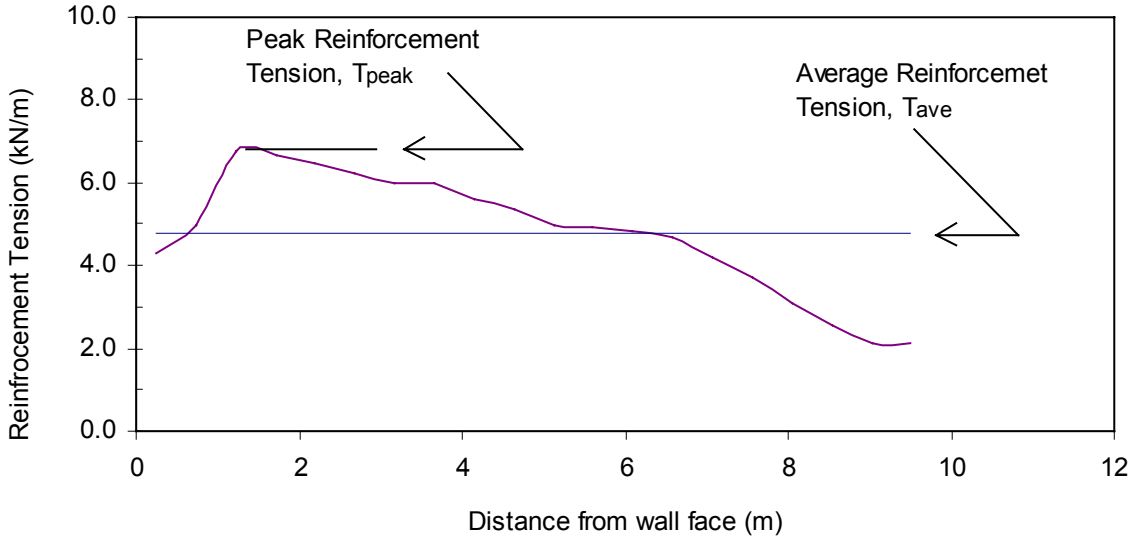

Figure 12.6.1 Typical reinforcement tension distribution along a reinforcement layer.

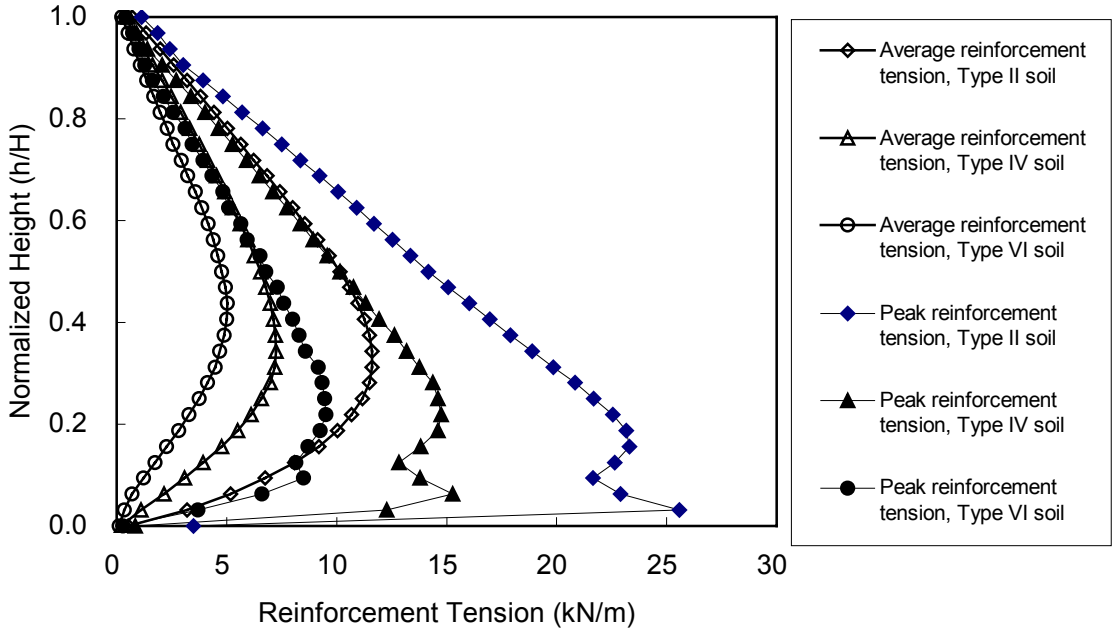

Figure 12.6.2 Typical average and peak reinforcement tension distributions of GRS walls with different backfills.

distributions, analysis results were presented using T_{ave}. As shown in Figures 12.6.3 to 12.6.11, distributions of T_{ave} of Groups A, B, C, and D models with different soil properties or reinforcement properties were plotted versus the normalized height. Relations between T_{peak_max} and T_{ave_max} of different GRS walls are discussed in Chapter 14.

12.6.2 Analysis Results

The influences of the soil and reinforcement properties on the magnitudes and distributions of T_{ave}, as well as on the locations of the T_{ave_max}, can be summarized as follows:

1. T_{ave} was found to be affected by the quality of the backfill soils. Figures 12.6.3 to 12.6.6 show the T_{ave} distributions of Group A, B, C, D walls with different types of backfill soils. As shown in the figures, the overall reinforcement tensions increased as the soil strength decreased.

2. T_{ave} was also found to be affected by the reinforcement stiffness. Figures 12.6.7 to 12.6.10 show the T_{ave} distributions of Group A, B, C, and D walls that were designed with different global reinforcement stiffnesses. Results shown in these figures indicate that the overall reinforcement tensions increased as the reinforcement stiffness increased.

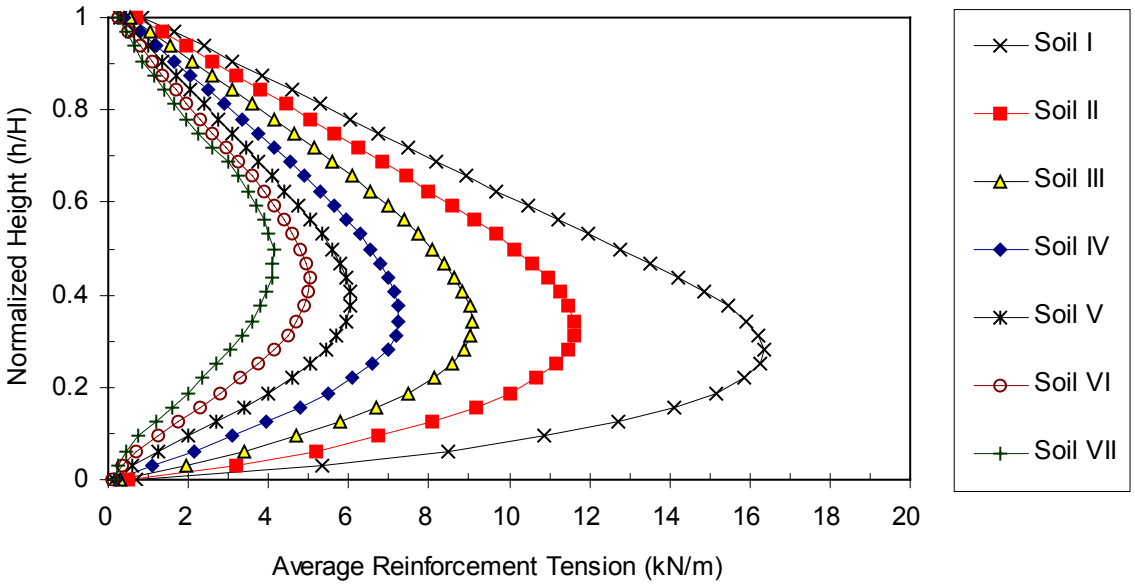

Figure 12.6.3 Reinforcement tension distributions of Group A models (wrapped face, H=12.6m, S_v=0.38m, J_g=1316kN/m^2) with soil properties varied.

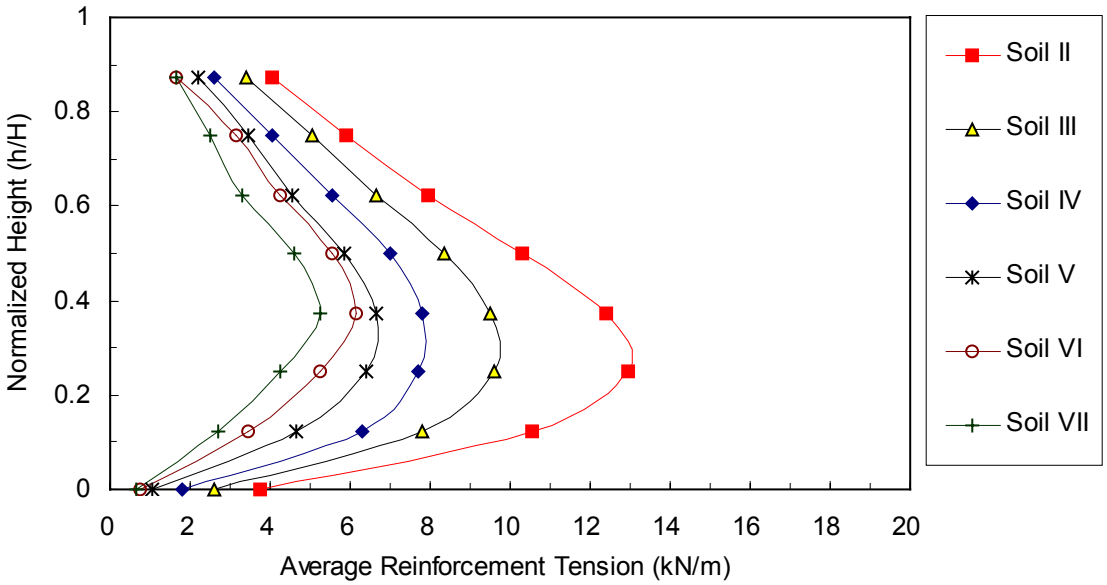

Figure 12.6.4 Reinforcement tension distributions of Group B models (wrapped face, H=6.1m, S_v=0.76m, J_g=1312kN/m^2) with soil properties varied.

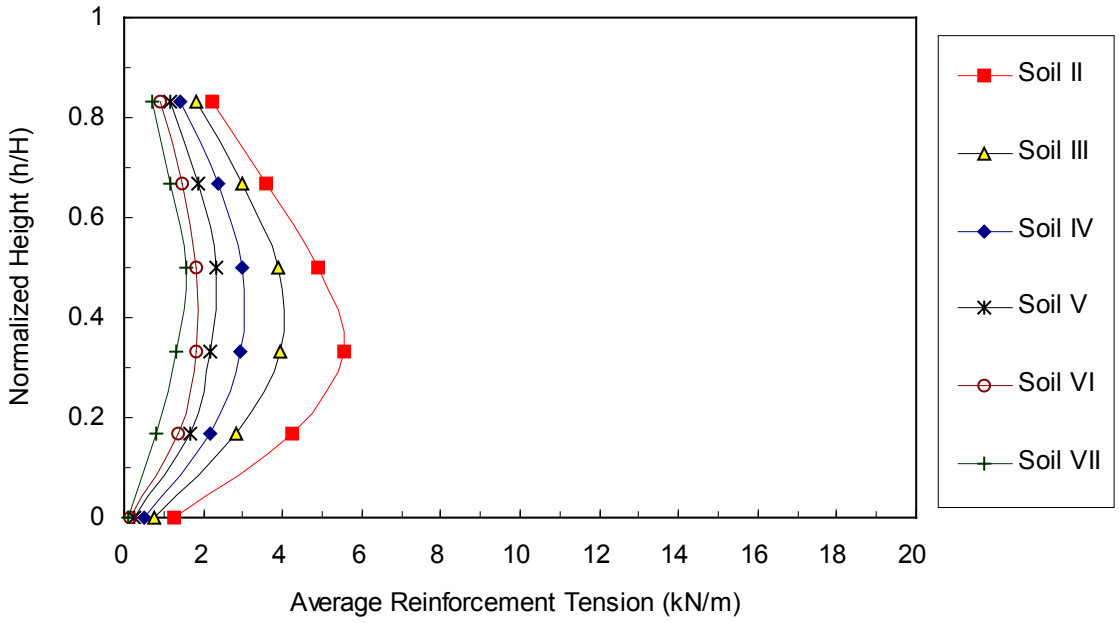

Figure 12.6.5 Reinforcement tension distributions of Group C models (wrapped face, H=3.6m, S_v=0.6m, J_g=183kN/m^2) with soil properties varied.

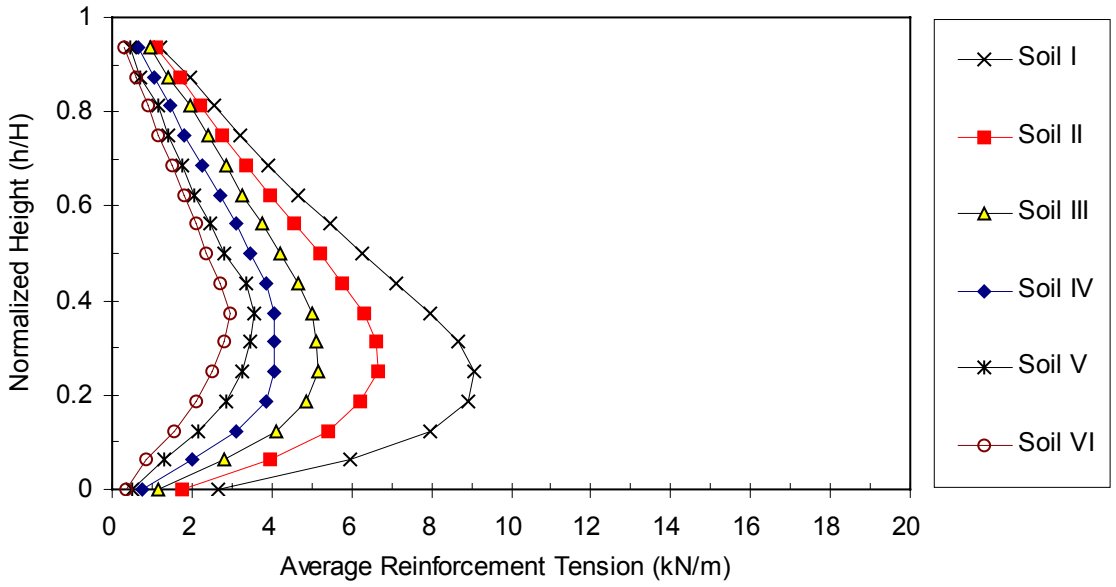

Figure 12.6.6 Reinforcement tension distributions of Group D models (wrapped face, H=6.1m, S_v=0.38m, J_g=1316kN/m^2) with soil properties varied.

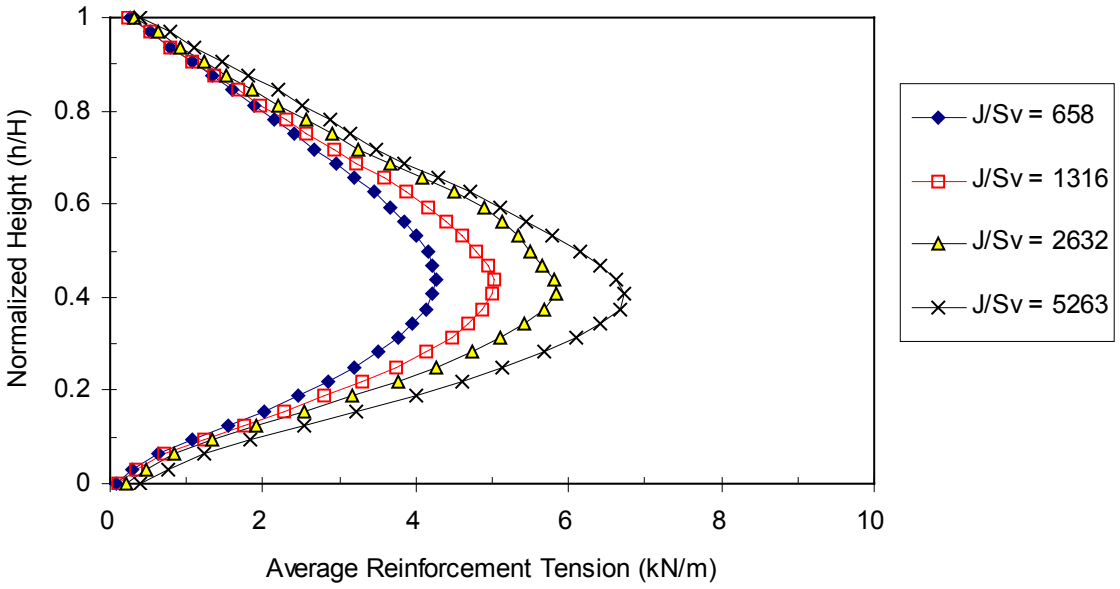

Figure 12.6.7 Reinforcement tension distributions of Group A models (wrapped face, H=12.6m, S_v=0.38m, Type VI soil) with reinforcement stiffness varied.

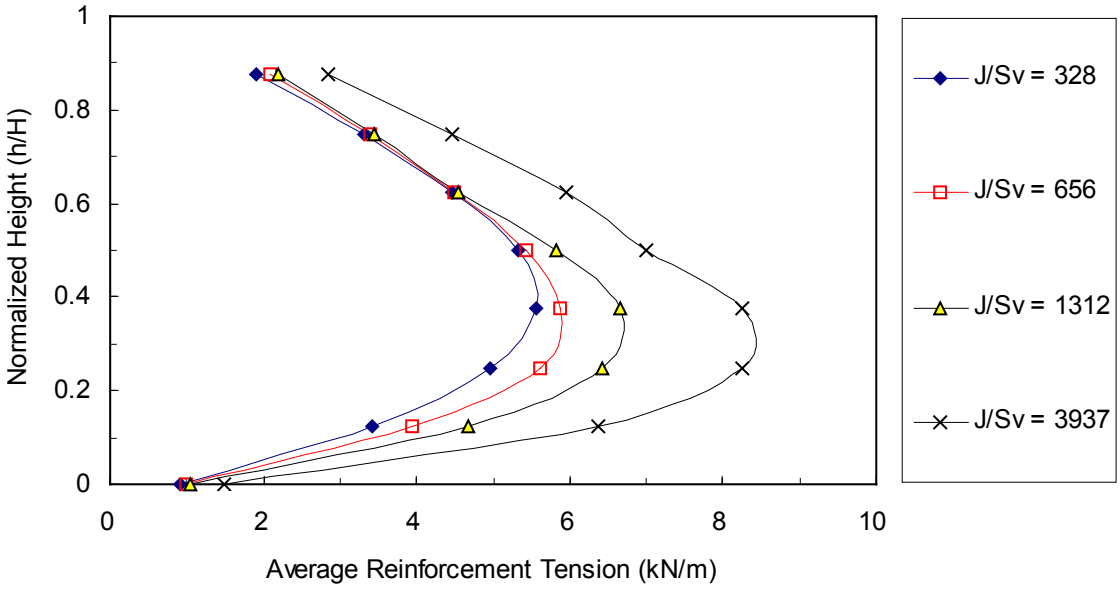

Figure 12.6.8 Reinforcement tension distributions of Group B models (wrapped face, H=6.1m, S_v= 0.76m, Type V soil) with reinforcement stiffness varied.

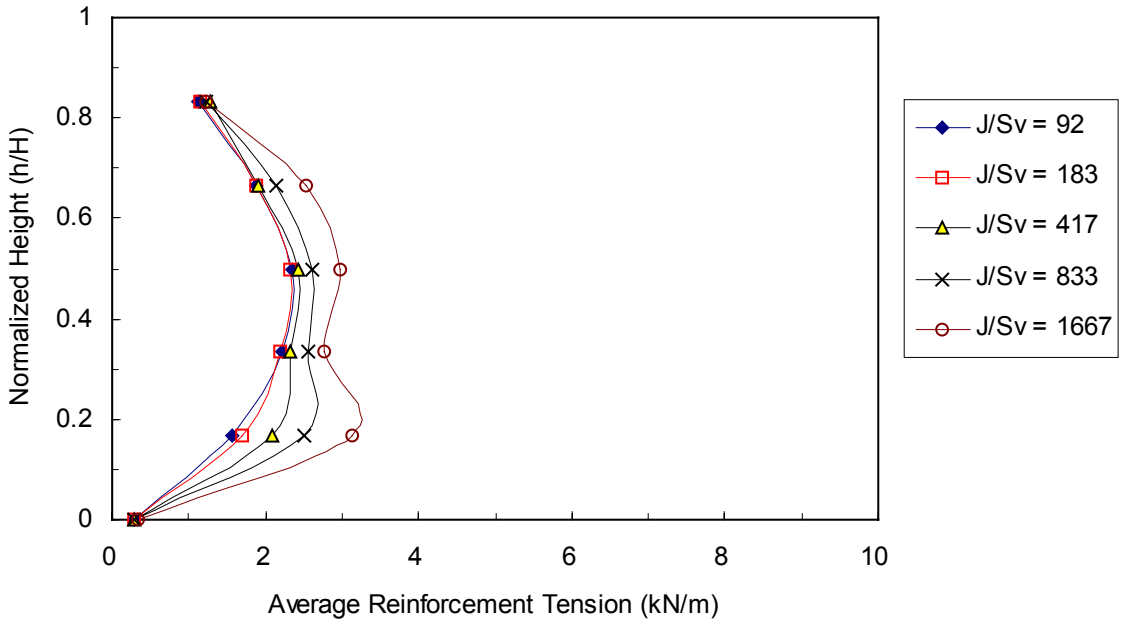

Figure 12.6.9 Reinforcement tension distributions of Group C models (wrapped face, H=3.6m, S_v=0.6m, Type V soil) with reinforcement stiffness varied.

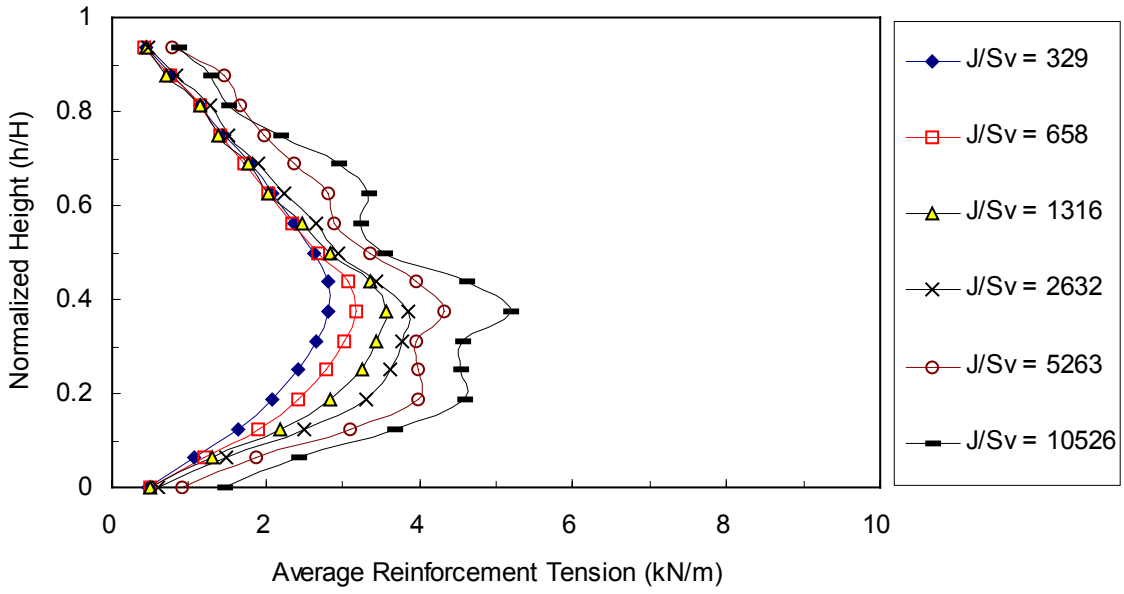

Figure 12.6.10 Reinforcements tension distributions of Group D models (wrapped face, H=6.1m, S_v=0.38m, Type V soil) with reinforcement stiffness varied.

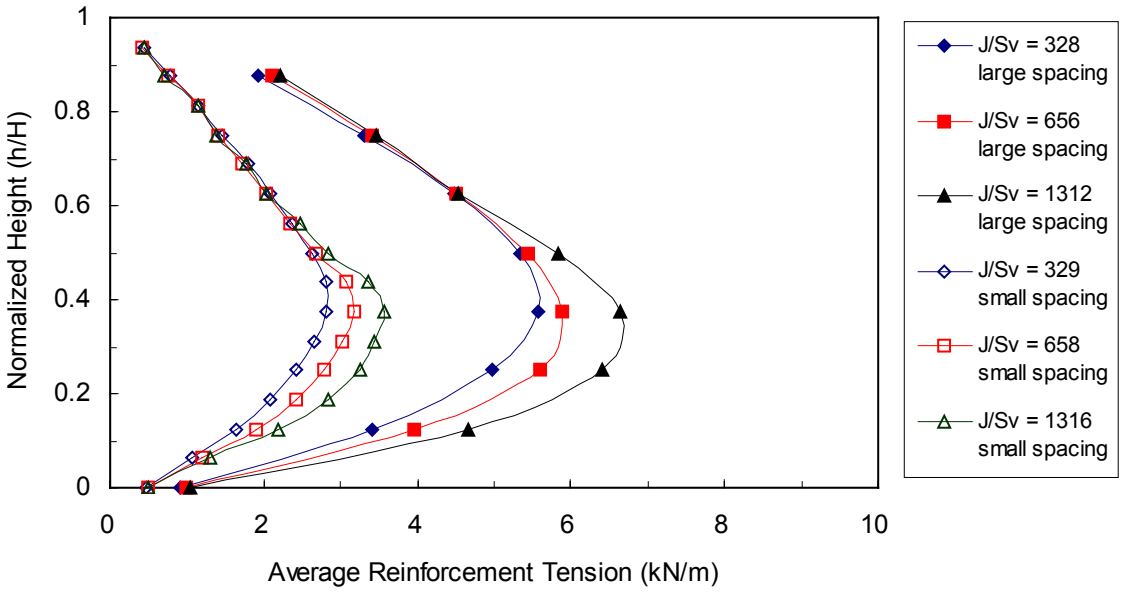

Figure 12.6.11 Reinforcements tension distributions of walls with different spacings (Group B and D).

3. Modeling results shown in Figures 12.6.3, 12.6.6, 12.6.7 and 12.6.10 indicate that the T_{ave} distributions of Group A and D (small spacing, wrapped face walls) had a triangular shape. As shown in the figures, T_{ave} first increased as the height of the wall increased. It reached its maximum values at the middle to one-third of the height of the walls, and then started to decrease as the height increased.

4. Locations of the maximum average reinforcement tensions (T_{ave_max}) were found to be affected by the quality of the backfill soils rather than the reinforcement stiffnesses. As shown in Figures 12.6.3 to 12.6.6, locations of T_{ave_max} varied from 0.5H (Type VII soil) to 0.3H (Type I soil). No noticeable changes of T_{ave_max} locations were found for walls that were designed using the same backfill soil but with different reinforcement stiffnesses (Figures 12.6.7 to 12.6.10).

5. Results in Figures 12.6.7, 12.6.8, and 12.6.10 show that the reinforcement tensions in the upper half of the walls did not increase very much as the global reinforcement stiffnesses increased from 329 to 2632 kN/m^2. However, reinforcement tensions in the lower half of the wall as well as T_{ave_max} did increase as the global reinforcement stiffnesses increased.

6. The large spacing walls (Group B) possessed higher reinforcement tensions than small spacing walls (Group D), even though the walls were designed with similar global reinforcement stiffnesses (Figure 12.6.11).

12.7 Analysis Result III—Effects of Toe Restraint

The major purpose of designing GRS walls with toe restraint is to increase the sliding resistance. However, the influence of the toe restraint on the performance of GRS walls was not carefully examined before. In this study, different degrees of toe restraints were added on the three fundamental models to investigate the influence of the toe restraints on performance of GRS walls. Moreover, quality of the backfill of these models was also varied to further examine the correlation between the degree of the influence of toe restraints and the backfill qualities. Results of these toe-restraint models were presented in the similar formats as the modeling results presented in previous sections, i.e. normalized height versus face deflection profiles or average reinforcement tension distributions.

Both face deflections and reinforcement tension distributions of GRS walls were found to be affected by different degrees of toe restraint. Figures 12.7.1 to 12.7.3 show the typical face deflection results of the walls that were designed with different types of toe restraints compared to the walls without any toe restraint. Figures 12.7.4 to 12.7.6 show the influence of different toe restraints (no restraint, 0.05H embedment, 0.1H embedment, and fixed toe) on the reinforcement tension distributions.

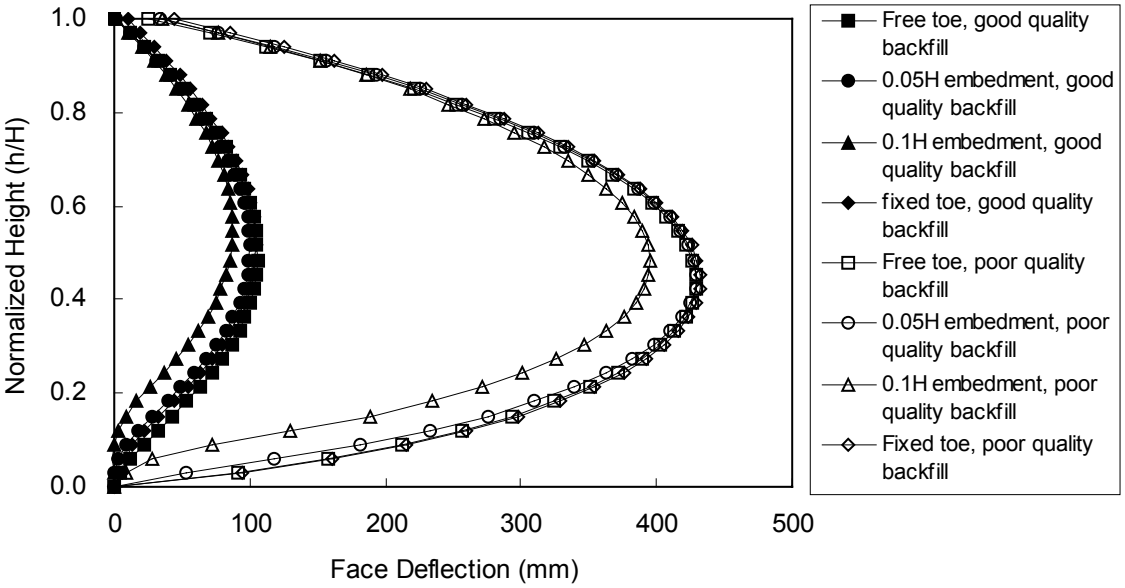

Figure 12.7.1 Face deflections of GRS walls with different toe restraints (wrapped face, H=12.6m, S_v=0.38m, Type VI and II soil).

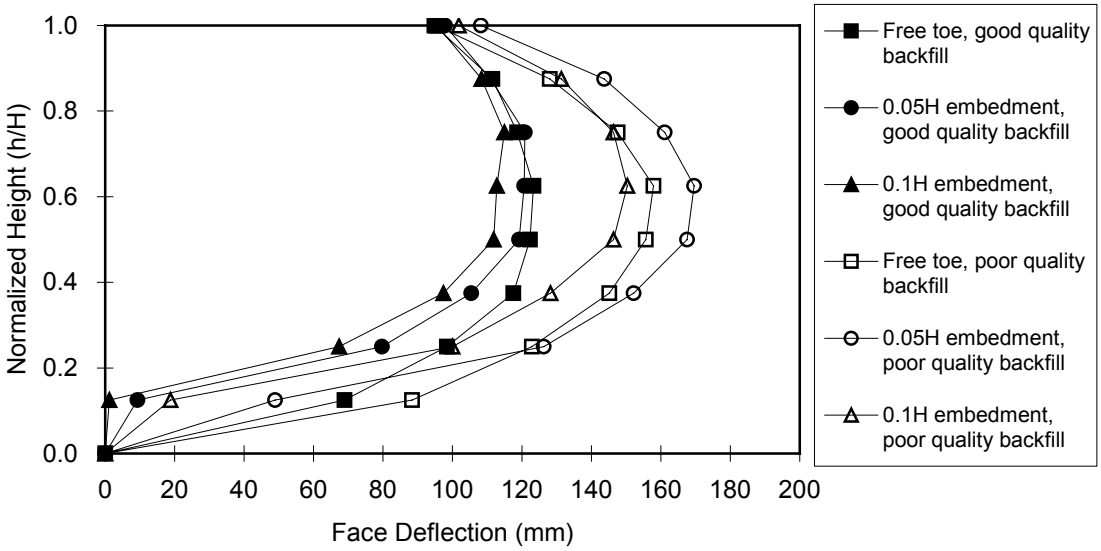

Figure 12.7.2 Face deflections of GRS walls with different toe restraints (wrapped face, H=6.1m, S_v=0.76m, Type V and II soil).

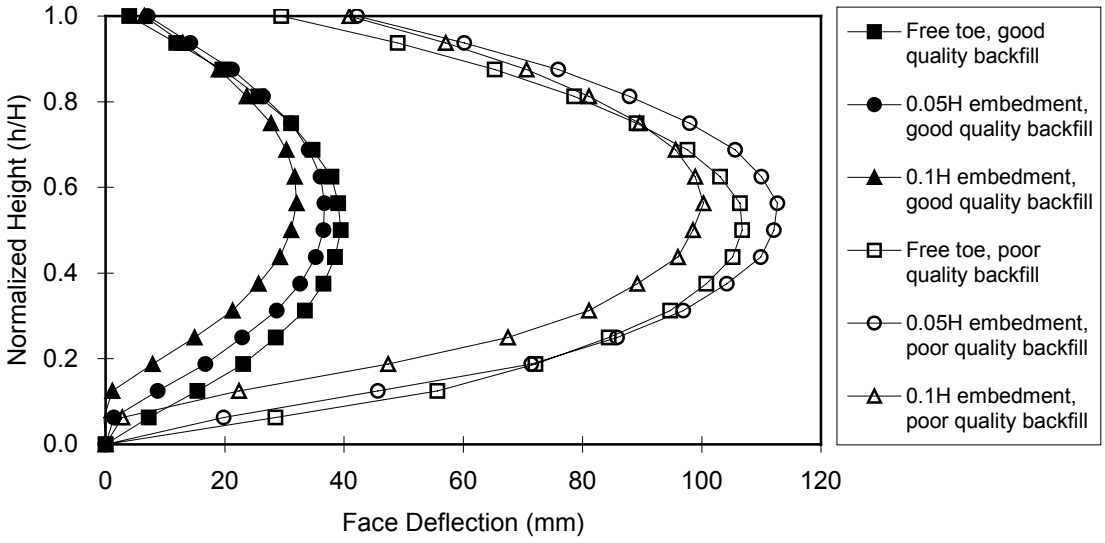

Figure 12.7.3 Face deflections of GRS walls with different toe restraints (wrapped face, H=6.1m, S_v=0.38m, Type V and II soil).

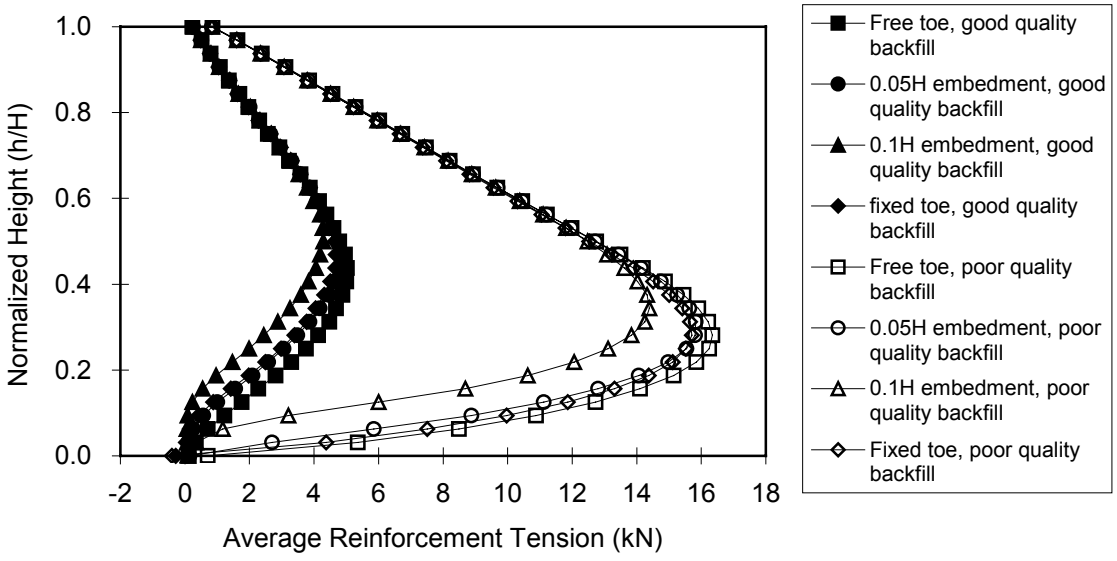

Figure 12.7.4 Reinforcement tension distributions of GRS walls with different toe restraints (wrapped face, H=12.6m, S_v=0.38m, Type VI and II soil).

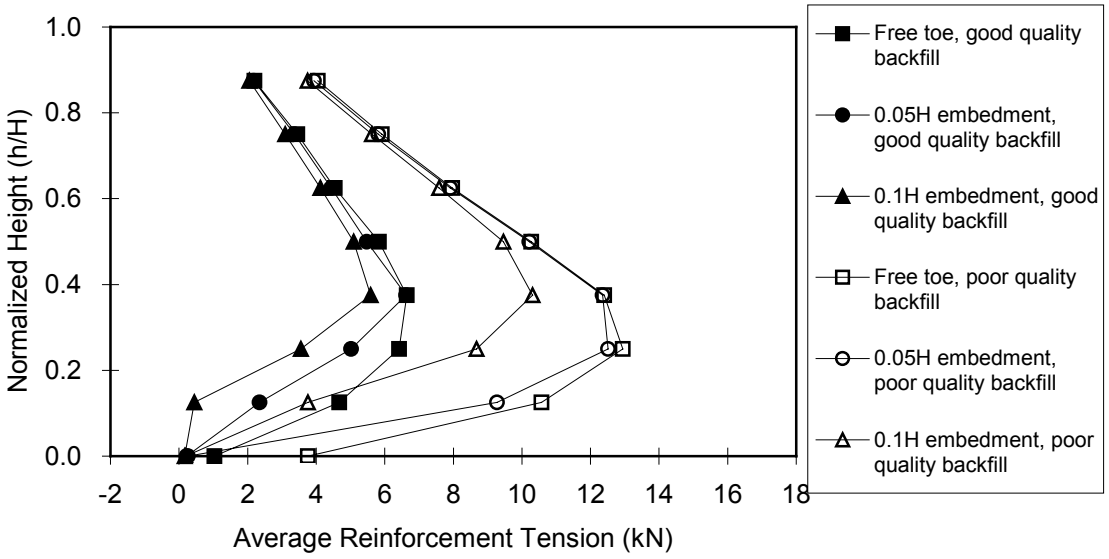

Figure 12.7.5 Reinforcement tension distributions of GRS walls with different toe restraints (wrapped face, H=6.1m, S_v=0.76m, Type V and II soil).

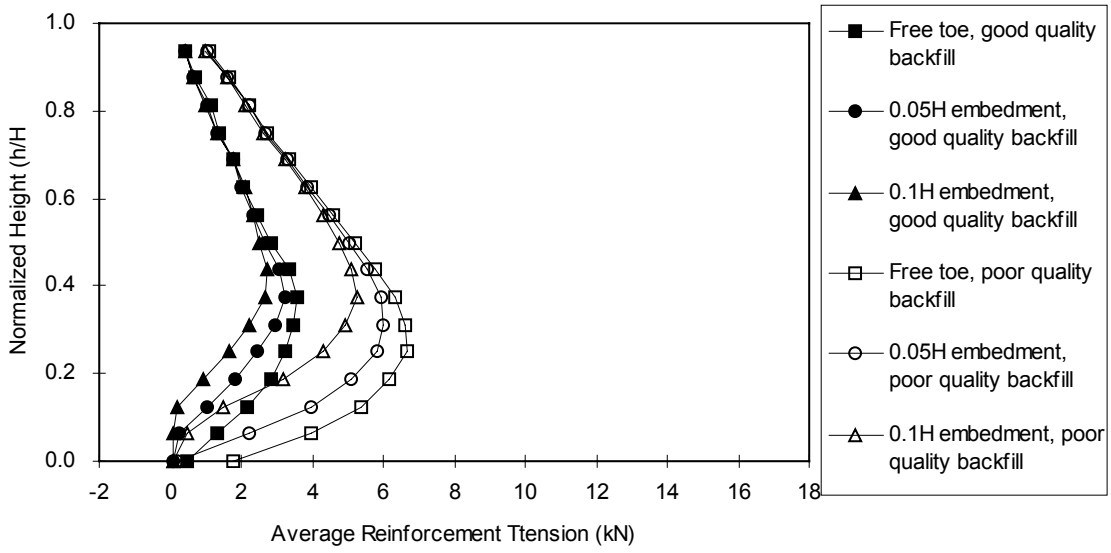

Figure 12.7.6 Reinforcement tension distributions of GRS walls with different toe restraints (wrapped face, H=6.1m, S_v=0.38m, Type V and II soil).

A discussion of these modeling results follows:

1. Among three toe restraints (0.05H embedment, 0.1H embedment, and fixed toe), 0.1H embedment was found to be the most effective to reduce the face deflection and reinforcement tensions.

2. For 12.6m high small spacing walls (Group A), fixed toe or embedded toe to 0.05H seemed to have small effect on both face deflections and reinforcement tension distributions (Figures 12.7.1 and 12.7.4). However, embedding the toe to 0.1H reduced the face deflections and reinforcement tensions, especially in the lower half of the walls (Figures 12.7.1 and 12.7.4).

3. For 6.1m high GRS walls with large spacings (Group B), face deflections actually increased when the toe was embedded to 0.05H, especially for walls with poor quality backfill such as the Type II soil (ϕ = 30 deg); however, the face deflections were able to be reduced by embedding the toe to 0.1H (Figure 12.7.2). Both 0.1H and 0.05H embedment had less effect on the reinforcement tensions in the upper half of the wall, but they both reduced the reinforcement tensions in the lower half of the wall (Figure 12.7.5)

4. For 6.1m GRS walls with small spacings (Group D), the face deflections only increased when the toe of the wall was embedded to 0.05H and poor quality

backfill (Type I soil) was used (Figure 12.7.3). When the wall was built with good quality backfill (Type V soil), embedding the toe to 0.05H could still reduce the face deflections (Figure 12.7.3). Both 0.1H and 0.05H embedment had less effect on the reinforcement tensions at upper half of the wall, but they were able to reduce the reinforcement tensions at lower half of the wall (Figure 12.7.6).

12.8 Analysis Result IV—Effects of Different Facing Systems

Three common wall facing systems, a wrapped face with secondary reinforcement, a modular block face, and a concrete panel face, were added to 6.1m high wrapped face models, including Group B (S_v = 0.76m) and Group D (S_v = 0.38m) models. Effects of these facing systems on the wall face deflections as well as reinforcement tension distributions were analyzed and compared to those of the wrapped face walls. Results of models with different facing systems were presented in the similar formats as the results of wrapped face walls presented in Sections 12.5 and 12.6—normalized height versus face deflection profiles and average reinforcement tension distributions.

The following points summarize the results of these analyses:

1. As shown in Figure 12.8.1, maximum wall deflections of the wrapped face walls can be reduced by using all three facing systems, especially for the large spacing walls.

2. Wrapped face walls designed with secondary reinforcements were found to have results similar to those walls with structural facing systems when the E_{comp} of their backfills was higher than about 10,500 kN/m^2 (Figure 12.8.1). Secondary reinforcement provided less improvement to the face deflection for walls that had E_{comp} lower than about 10,500 kN/m^2 (Figure 12.8.1).

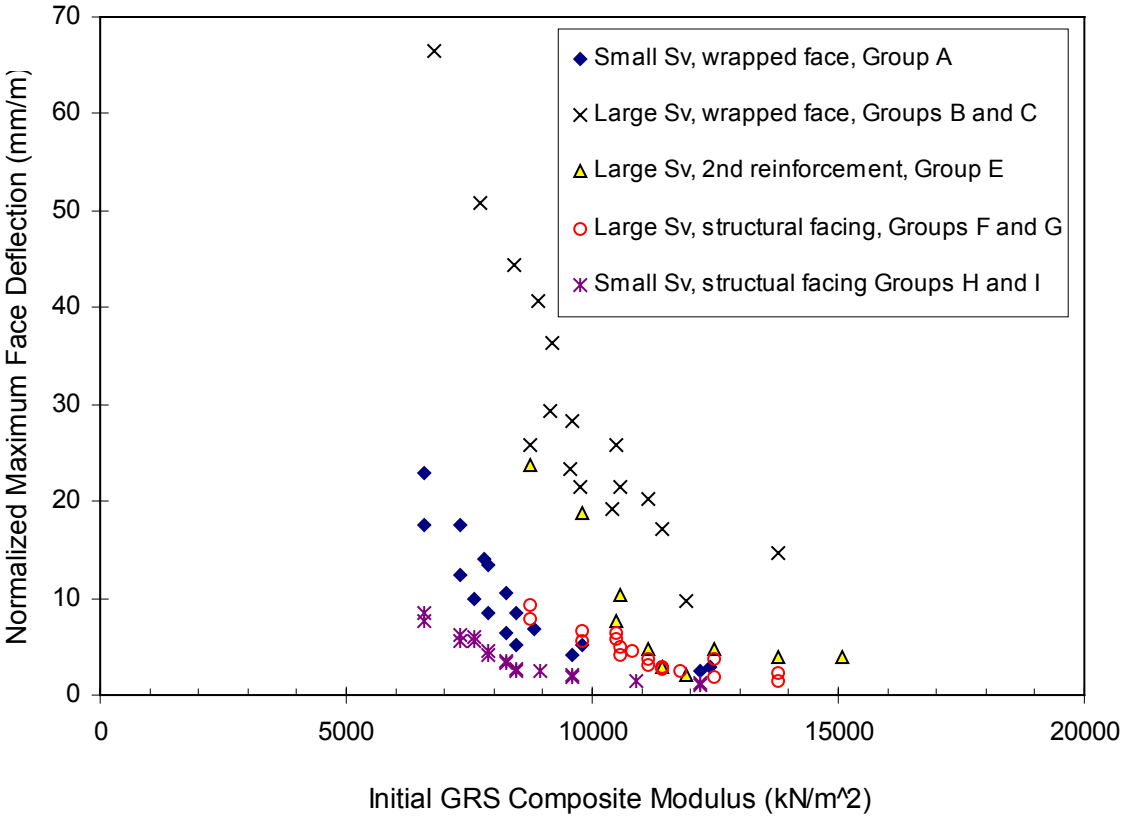

Figure 12.8.1 Maximum face deflections of walls with different facing systems.

3. By using the structural facing systems such as modular blocks and concrete panels, the face deflections of walls with large spacing were similar to small spacing wrapped face walls (Figure 12.8.1). For small spacing walls, the maximum face deflections were also reduced with the aid of the structural facing systems; however, the improvement was not as great as for the large spacing walls (Figure 12.8.1).

4. As shown in Figures 12.8.2 and 12.8.3, for most cases analyzed, the reinforcement tensions inside the wrapped face GRS walls were able to be reduced using the secondary reinforcement. However, for walls with weak backfill (Type II soil), secondary reinforcement not only increased the reinforcement tension but also raised the elevation of the maximum reinforcement tension (Figure 12.8.2).

5. Results of Figures 12.8.4, 12.8.5, 12.8.6, and 12.8.7 indicated that the modular block face was able to decrease the reinforcement tensions of both large and small spacing wrapped face walls. Especially for walls with weak backfill such as Type II soil, great improvements were found for both large and small spacing walls (Figures 12.8.4 and 12.8.6).

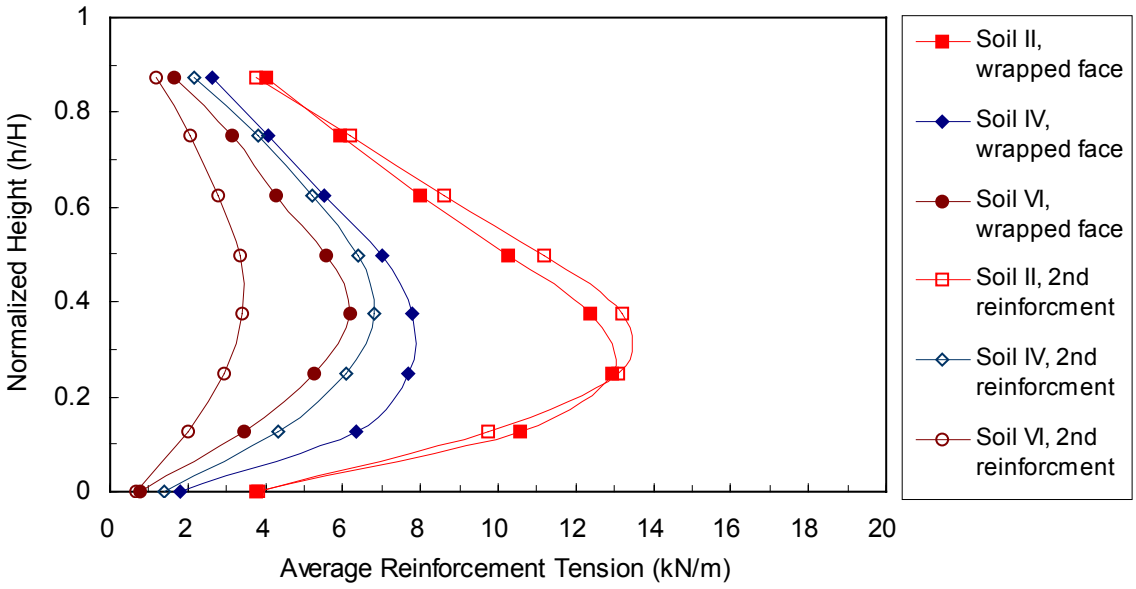

Figure 12.8.2 Reinforcement tension distributions of walls with secondary reinforcement, Group E models (J/S_v = 1316 kN/m^2, soil properties varied).

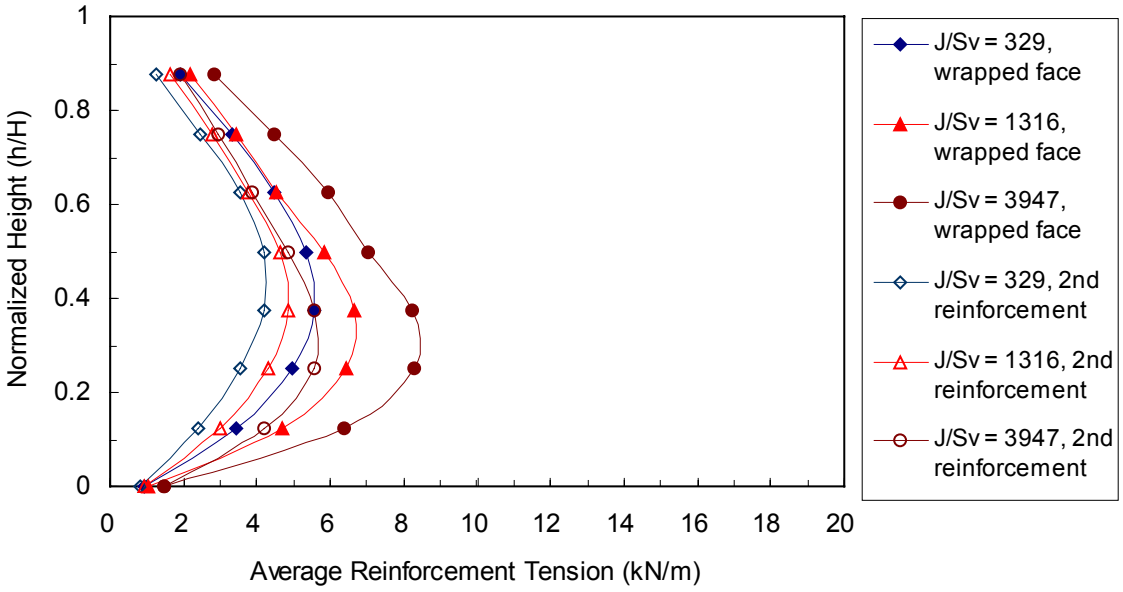

Figure 12.8.3 Reinforcement tension distributions of walls with secondary reinforcement, Group E Models (Type V soil, J/S_v varied).

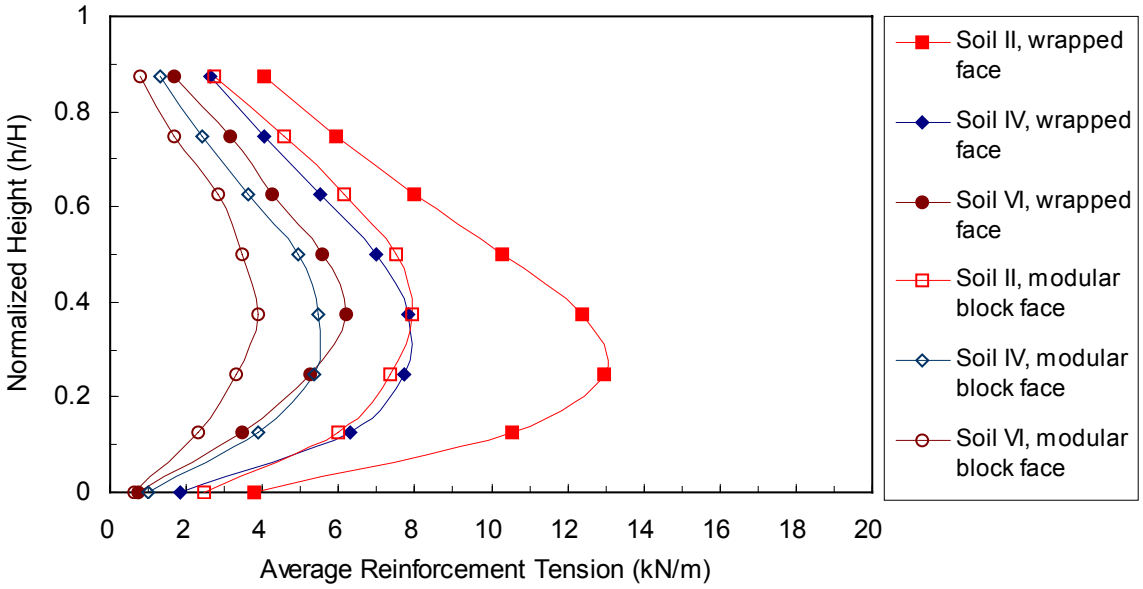

Figure 12.8.4 Reinforcement tension distributions of walls with modular block face, Group F models (S_v = 0.76m, J/S_v = 1316 kN/m^2, soil properties varied).

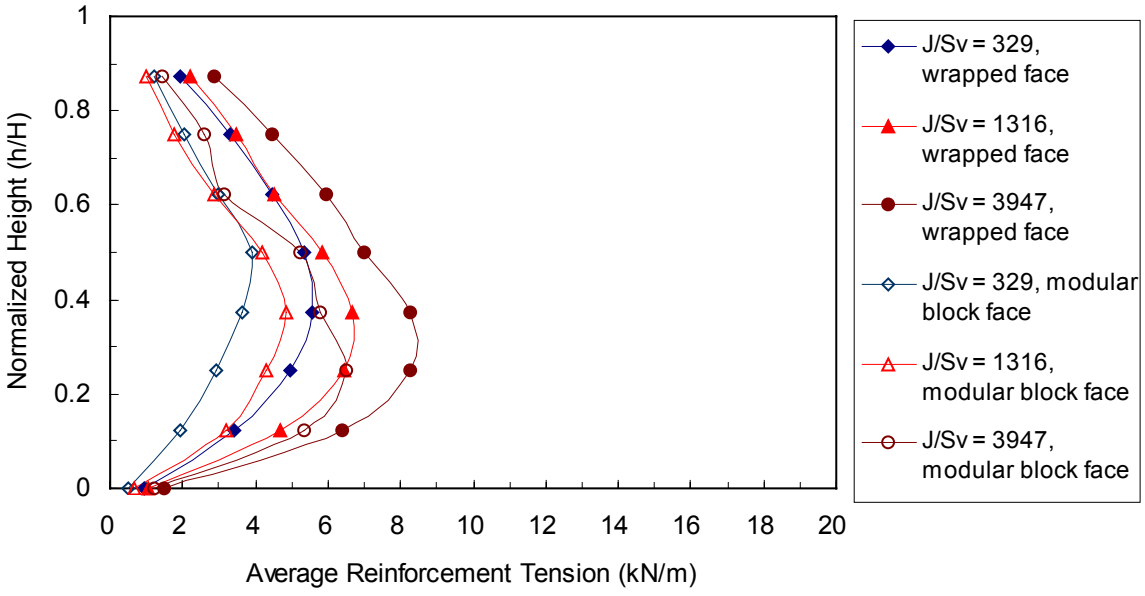

Figure 12.8.5 Reinforcement tension distributions of walls with modular block face, Group F models (S_v = 0.76m, Type V soil, J/S_v varied).

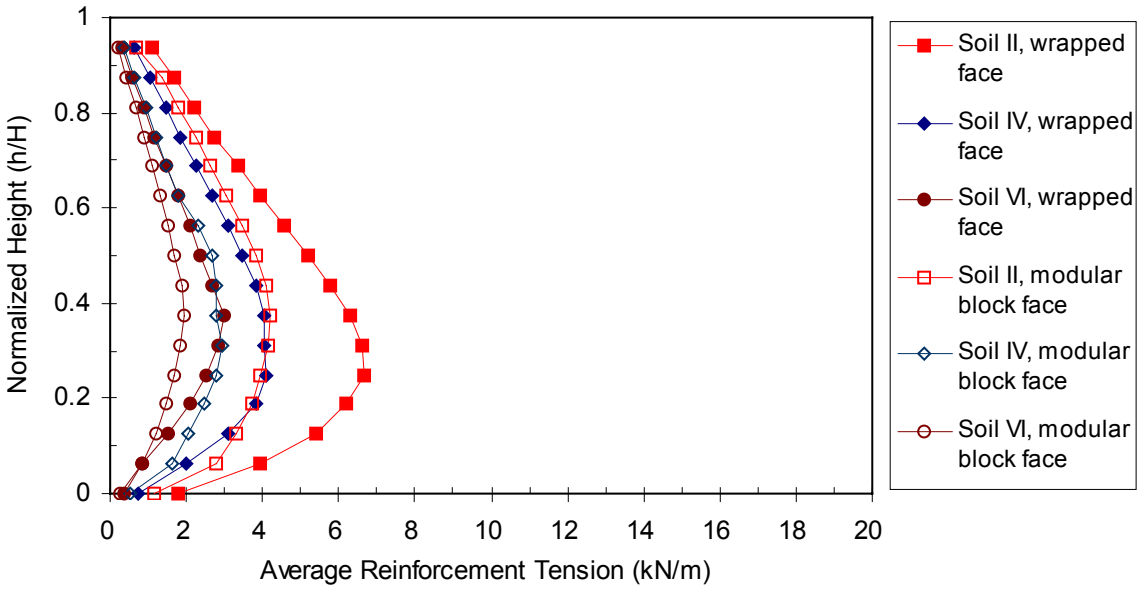

Figure 12.8.6 Reinforcement tension distributions of walls with modular block face, Group H models (S_v = 0.38m, J/S_v = 1316 kN/m^2, soil properties varied).

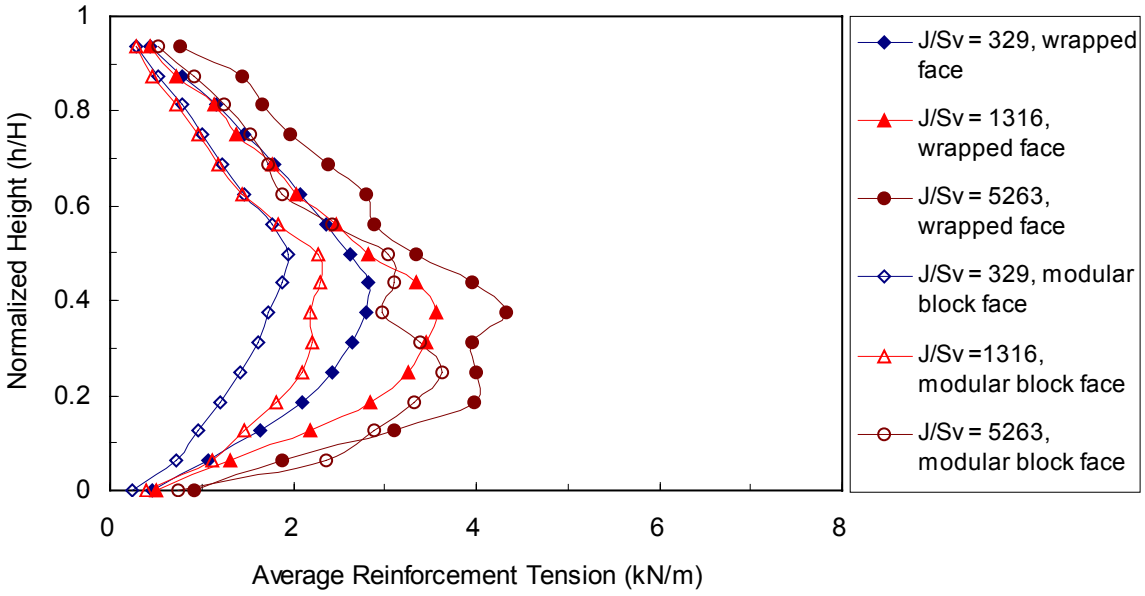

Figure 12.8.7 Reinforcement tension distributions of walls with modular block face, Group H models (S_v = 0.38m, Type V soil, J/S_v varied).

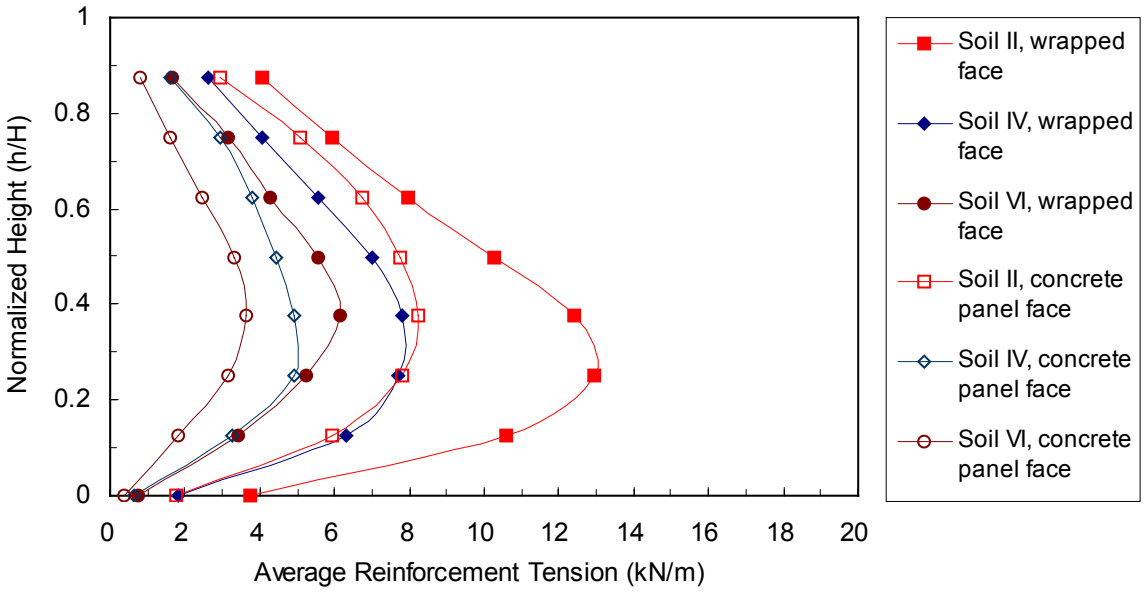

Figure 12.8.8 Reinforcement tension distributions of walls with concrete panel face, Group G models (S_v = 0.76m, J/S_v = 1316 kN/m^2, soil properties varied).

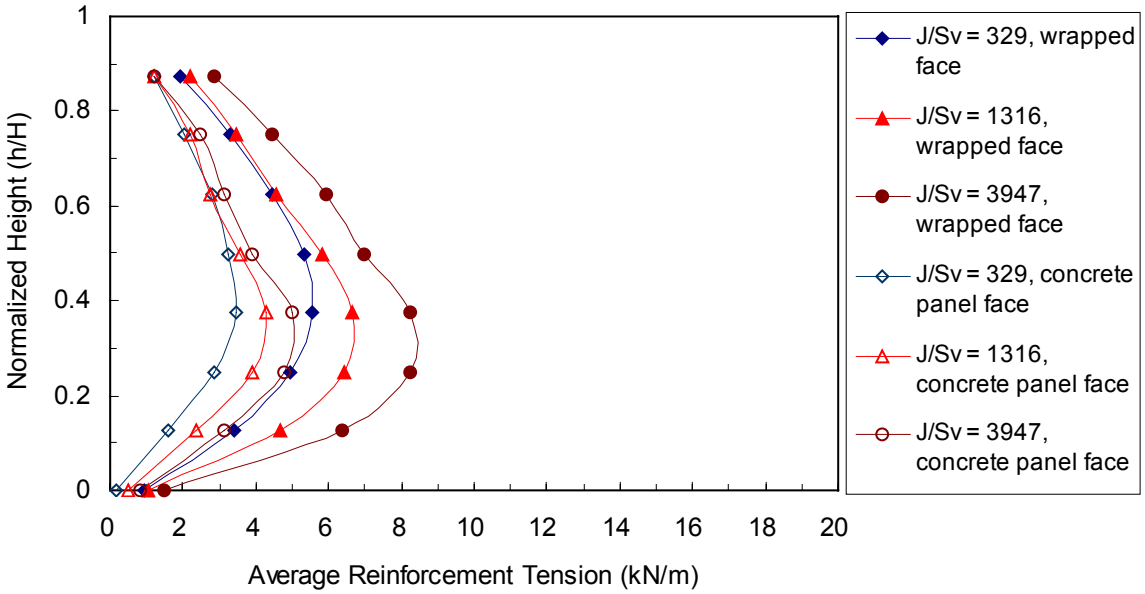

Figure 12.8.9 Reinforcement tension distributions of walls with concrete panel face, Group G models (S_v = 0.76m, Type V soil, J/S_v varied).

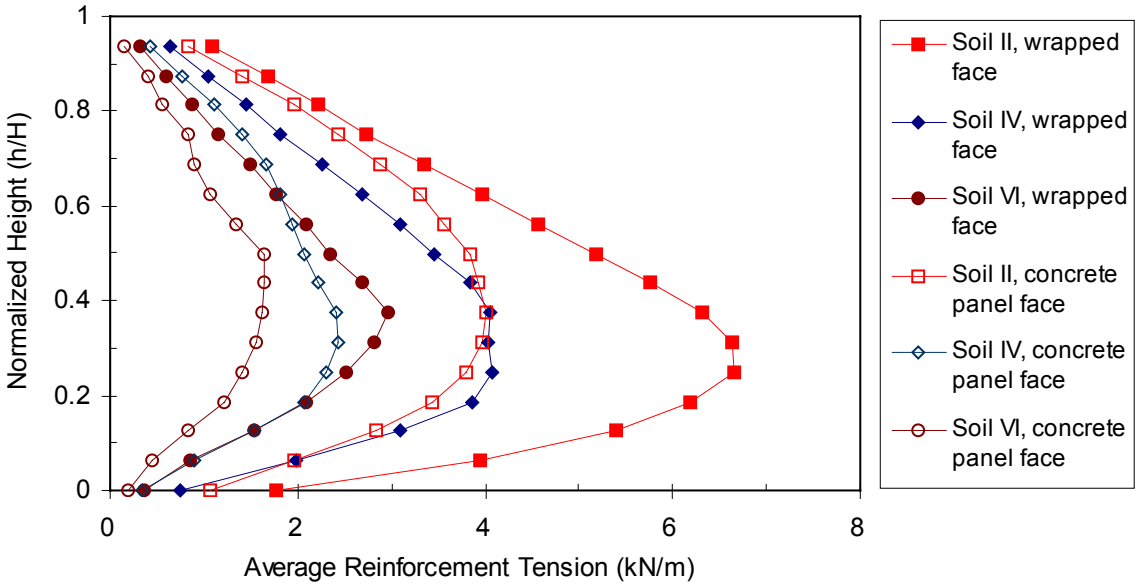

Figure 12.8.10 Reinforcement tension distributions of walls with concrete panel face, Group I models (S_v = 0.38m, J/S_v = 1316 kN/m^2, soil properties varied).

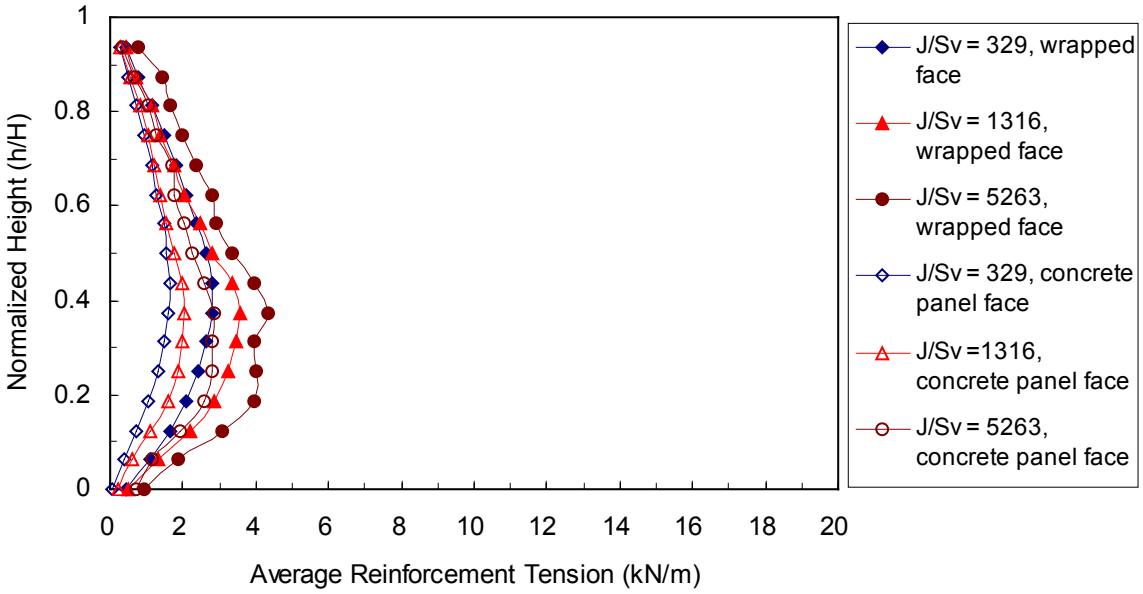

Figure 12.8.11 Reinforcement tension distributions of walls with concrete panel face, Group I models (S_v = 0.38m, Type V soil, J/S_v varied)

6. Performance of the concrete panel faced walls was found to be very similar to that of modular block faced walls. Figures 12.8.8, 12.8.9, 12.8.10, and 12.8.11 indicated that the concrete panel face was able to decrease the reinforcement tensions of both large and small spacing wrapped face walls. Improvements were also found for walls with weak backfill (Figures 12.8.4 and 12.8.6).

12.9 Summary and Conclusions

1. Local failures were observed near the faces of GRS walls with larger vertical reinforcement spacings. For wrapped face GRS walls that were designed with the same global stiffnesses but different vertical reinforcement spacings, the large spacing walls exhibited much higher face deflections than the small spacing ones (Figure 12.5.5).

2. Face deformation of GRS walls was found to be affected by both the strength properties of the backfill and the global reinforcement stiffness. Parametric analysis results shown in Section 12.5 indicated that face deflections of GRS walls increased as the soil strength properties decreased. Face deflections decreased as the global reinforcement stiffness increased. A good correlation was found between the GRS composite modulus (E_{comp}) and normalized maximum face deflection (d_{max}/H) (Figures 12.5.8 and 12.8.1).

3. Reinforcement tensions in GRS walls were also found to be affected by both the strength properties of the backfill and the global reinforcement stiffness. Parametric

analysis results shown in Section 12.6 indicated that overall reinforcement tensions in the GRS walls increased as the soil strength properties decreased. Overall reinforcement tensions also increased as the global reinforcement stiffness increased. However, the reinforcement tensions started to increase when the walls were designed using very weak reinforcement because of the large strains exhibited (Figure 12.3.4).

4. Toe restraint was able to reduce the maximum face deflections and reinforcement tensions (Figures 12.7.1 to 12.7.6). Among three toe restraints (0.05H embedment, 0.1H embedment, and fixed toe), 0.1H embedment was found to be the most effective toe condition to improve the performance of GRS walls, especially for walls designed with poor quality backfill.

5. For large spacing walls, secondary reinforcement was found to be only effective for improving performance of walls with good quality backfill. Both face deflections and reinforcement tensions of GRS walls with good quality backfill could be decreased using secondary reinforcement (Figures 12.8.1, 12.8.2 and 12.8.3).

6. Structural facing systems such as modular blocks and concrete panels were able to improve the stability and reduce the deformation of GRS walls, especially walls with large spacings. Using structural facing systems could reduce maximum face deflections (Figure 12.8.1) as well as reinforcement tensions (Figures 12.8.4 to 12.8.11) of both large and small spacing wrapped face walls.

7. In contrast to the tie-back wedge method that predicts a maximum reinforcement tension at the bottom of the wall, results of the parametric analyses indicated that locations of the maximum overall (average) reinforcement tensions occurred between 0.25H (poor quality backfill) to 0.5H (good quality backfill).

Chapter 13
Anisotropic Model for Geosynthetic Reinforced Soil Composite Properties

Instead of analyzing the geosynthetic reinforcement and soil separately, an effort was made in this research to develop numerical analyses based on composite material concepts. In the composite approach, the GRS element was considered to be a reinforced composite material. Theory of anisotropic material under plane strain loading conditions described in Chapter 4 was used to analyze the different stress-strain behavior in the different principal directions of the GRS composite. The author has published preliminary results of this research (Holtz and Lee, 1997; Lee and Holtz, 1998).

13.1 Behavior of Geosynthetic Reinforced Soil Element

For a GRS element shown in Figure 13.1.1, different reinforcing mechanisms have been found in different principal directions (Hausmann, 1990; Boyle, 1995). In the horizontal directions, soil is reinforced by the tensile forces developed along the geosynthetic and then transmitted into the soil. In the vertical direction, soil is also reinforced because additional resistance to the gravity force is provided by the horizontally placed reinforcement. In Figure 13.1.1, the vertical direction is defined as direction 1 and the horizontal directions are defined as directions 2 and 3. The geosynthetic reinforcement is placed on a plane perpendicular to direction 1 but also parallel to directions 2 and 3. Therefore, the different reinforcing mechanisms of a

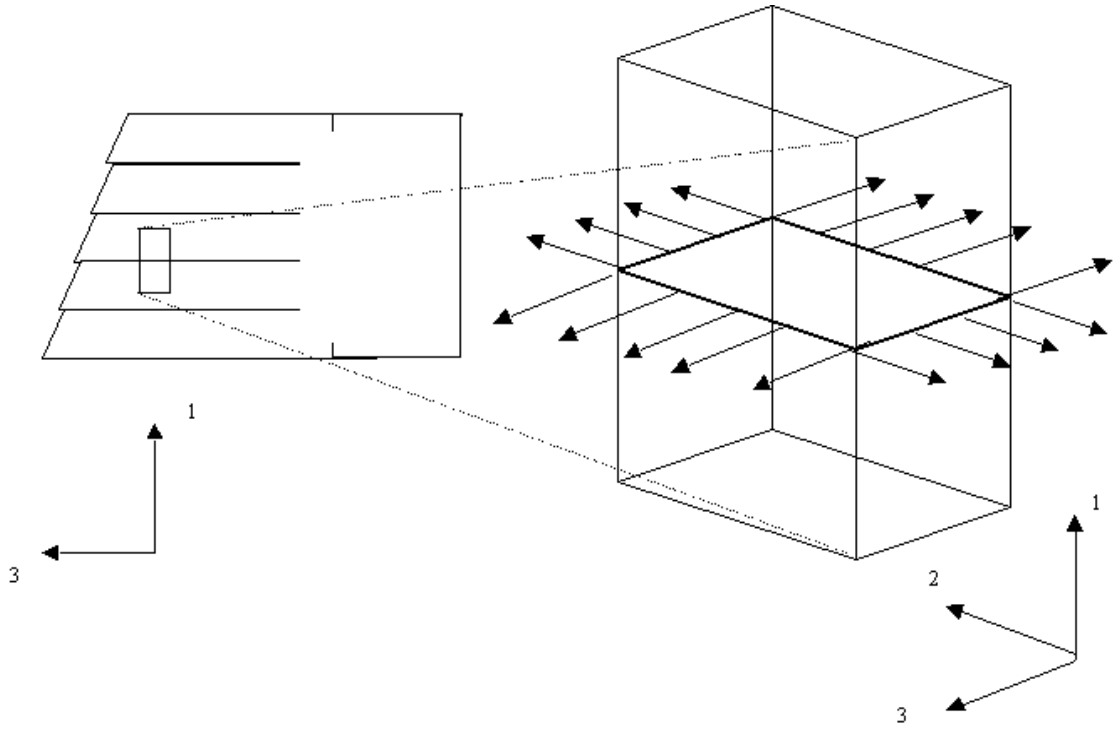

Figure13.1.1 Geosynthetic reinforced soil element.

GRS element in the different principal directions can be described using orthotropic anisotropic elasticity (Eq. 4.1.2). $\mathbf{E}_1$, $\mathbf{E}_2$, $\mathbf{E}_3$, $\boldsymbol{\nu}_{32}$, $\boldsymbol{\nu}_{23}$, $\boldsymbol{\nu}_{13}$, $\boldsymbol{\nu}_{12}$, $\boldsymbol{\nu}_{21}$, and $\boldsymbol{\nu}_{31}$ in Eq. 4.1.2 are then defined as the composite elastic moduli and Poisson's ratios of the GRS element.

$$\begin{bmatrix} \boldsymbol{\varepsilon}_{11} \\ \boldsymbol{\varepsilon}_{22} \\ \boldsymbol{\varepsilon}_{33} \end{bmatrix} = \begin{bmatrix} \frac{1}{\mathbf{E}_1} & \frac{-\boldsymbol{\nu}_{21}}{\mathbf{E}_2} & \frac{-\boldsymbol{\nu}_{31}}{\mathbf{E}_3} \\ \frac{-\boldsymbol{\nu}_{21}}{\mathbf{E}_1} & \frac{1}{\mathbf{E}_2} & \frac{-\boldsymbol{\nu}_{32}}{\mathbf{E}_3} \\ \frac{-\boldsymbol{\nu}_{31}}{\mathbf{E}_1} & \frac{-\boldsymbol{\nu}_{23}}{\mathbf{E}_2} & \frac{1}{\mathbf{E}_3} \end{bmatrix} \cdot \begin{bmatrix} \boldsymbol{\sigma}_{11} \\ \boldsymbol{\sigma}_{22} \\ \boldsymbol{\sigma}_{33} \end{bmatrix} \qquad \text{(Eq. 4.1.2)}$$

Equations 4.1.2 can be further simplified by assuming that the geosynthetic has same in-soil stress-strain strength properties in both the machine and cross machine directions. Based on this assumption, the same stress-strain behavior is assigned to directions 2 and 3, i.e., $\mathbf{E}_1 = \mathbf{E}_v$, $\mathbf{E}_2 = \mathbf{E}_3 = \mathbf{E}_h$, $\boldsymbol{\nu}_{32} = \boldsymbol{\nu}_{23} = \boldsymbol{\nu}_{hh}$, $\boldsymbol{\nu}_{31} = \boldsymbol{\nu}_{21} = \boldsymbol{\nu}_{hv}$, and $\boldsymbol{\nu}_{13} = \boldsymbol{\nu}_{12} = \boldsymbol{\nu}_{vh}$ (Eq. 4.1.3).

$$\begin{bmatrix} \boldsymbol{\varepsilon}_{11} \\ \boldsymbol{\varepsilon}_{22} \\ \boldsymbol{\varepsilon}_{33} \end{bmatrix} = \begin{bmatrix} \frac{1}{\mathbf{E}_v} & \frac{-\boldsymbol{\nu}_{hv}}{\mathbf{E}_h} & \frac{-\boldsymbol{\nu}_{hv}}{\mathbf{E}_h} \\ \frac{-\boldsymbol{\nu}_{vh}}{\mathbf{E}_v} & \frac{1}{\mathbf{E}_h} & \frac{-\boldsymbol{\nu}_{hh}}{\mathbf{E}_h} \\ \frac{-\boldsymbol{\nu}_{vh}}{\mathbf{E}_v} & \frac{-\boldsymbol{\nu}_{hh}}{\mathbf{E}_h} & \frac{1}{\mathbf{E}_h} \end{bmatrix} \cdot \begin{bmatrix} \boldsymbol{\sigma}_{11} \\ \boldsymbol{\sigma}_{22} \\ \boldsymbol{\sigma}_{33} \end{bmatrix} \qquad \text{(Eq. 4.1.3)}$$

Moreover, for GRS elements inside a retaining structure, the plane strain loading conditions are appropriate. In Figure 13.1.1, plane strain conditions indicate that there is no strain in direction 2 (i.e. $\varepsilon_{22} = \gamma_{12} = \gamma_{23} = 0$ in Eq. 4.1.3). Equations 4.1.4 and 4.1.5 can then be used to describe the transversely isotropic elastic behavior of a GRS element under plane strain loading conditions. Composite moduli of the GRS element can be solved using this model with adequate material testing data, e.g., from the plane strain test results.

$$\varepsilon_{22} = 0 = -\nu_{vh}\frac{\sigma_{11}}{E_v} + \frac{\sigma_{22}}{E_h} - \nu_{hh}\frac{\sigma_{33}}{E_h} \qquad \text{(Eq. 4.1.4)}$$

$$\begin{bmatrix}\varepsilon_{11}\\ \varepsilon_{33}\end{bmatrix} = \begin{bmatrix}\left(\frac{1}{E_v} - \frac{\nu_{hv}^{\,2}}{E_h}\right) & \left(\frac{-\nu_{hv} - \nu_{hv}\nu_{hh}}{E_h}\right)\\ \left(\frac{-\nu_{hv} - \nu_{hv}\nu_{hh}}{E_h}\right) & \left(\frac{1}{E_h} - \frac{\nu_{hh}^{\,2}}{E_h}\right)\end{bmatrix} \cdot \begin{bmatrix}\sigma_{11}\\ \sigma_{33}\end{bmatrix} \qquad \text{(Eq. 4.1.5)}$$

13.2 Interpreting UCD Test Results Using the Tranversely Isotropic Elasticity Model

The UCD was designed to test a GRS element under plane strain loading conditions to simulate the GRS element inside GRS soil structures (Boyle, 1995). The UCD specimen is exactly a GRS element shown in Figure 13.1.1 with plane strain loading conditions. Therefore, the developed transversely isotropic elasticity model can be applied to interpret the UCD test results.

Equations 13.2.1 to 13.2.3 were rearranged from Equations 4.1.4 and 4.1.5.

$$\nu_{hv} = \frac{\sigma_{22} - \nu_{hh}\sigma_{33}}{\sigma_{11}} \qquad \text{(Eq. 13.2.1)}$$

$$E_h = \frac{1}{\varepsilon_{33}} \cdot \left[B\sigma_{11} + (1 - C)\sigma_{33}\right] \qquad \text{(Eq. 13.2.2)}$$

$$E_v = \frac{E_h \cdot \sigma_{11}}{\varepsilon_{11}E_h + A\sigma_{11} - B\sigma_{33}} \qquad \text{(Eq. 13.2.3)}$$

Where $A = \nu_{hv}^2$

$B = -\nu_{hv} - \nu_{hv}\nu_{hh}$

$C = \nu_{hh}^2$

Also $\nu_{vh} = \nu_{hv}\, E_v/E_h$.

The terms σ_{11}, σ_{22}, σ_{33}, ε_{11}, and ε_{33} in Equations 13.2.1 to 13.2.3 were obtained by reducing the UCD test data. However, there are still three unknowns (E_v, E_h, ν_{hh}, and ν_{hv}) remaining in Equations 13.2.1 to 13.2.3, so numerical analysis was performed to solve these equations. The steps of the numerical analysis were:

1. Formulate a spreadsheet using Equations 13.2.1 to 13.2.3,

2. Insert a reasonable range of values for Poisson's ratio ν_{hh} or ν_{hv} into the spreadsheet, and
3. Compute the composite moduli $\mathbf{E}_v$ and $\mathbf{E}_h$ using the spreadsheet.

13.3 Composite GRS Moduli

UCD test data were input into the developed transversely isotropic elasticity model to solve for the composite GRS moduli. There were twenty sets of UCD test data used as input into the transversely isotropic elasticity model to obtain the composite GRS moduli. Three of them were tests of unreinforced soil at different confining pressures to obtain the plane strain vertical and horizontal soil moduli. In the other tests, four different types of geosynthetics at different confining pressures were used. These geosynthetics were similar to the reinforcement material used in the WSDOT Rainier Avenue wall.

Table 13.3.1 shows the test numbers, effective soil confining pressures and geosynthetics information for UCD tests that were used to obtain the composite moduli. Table 13.3.2 shows the sampled stress and stain information that was reduced from the raw UCD test data. Table 13.3.3 lists names, material types, and 2% strain wide width tensile test moduli of geosynthetics used in the UCD tests. The stress and strain information was taken at conditions when the lateral strain equaled 1% and for the horizontal plane Poisson's ratio equal to 0.3. The transversely isotropic elasticity model was applied to soil-only UCD tests to obtain the plane strain vertical and

Table 13.3.1 General Information of UCD Tests

UCD Test No. (Boyle, 1995)	Effective Soil Confining Pressure (kPa)	Geosynthetic Information (Name, 2% Mwwt[1] (kN/m), material type)
115	12.4	Soil only
79	12.3	GTF 200, 103, polypropylene
77	10.4	GTF 375, 204, polypropylene
76	11.2	GTF 500, 357, polypropylene
98	10.6	GTF 1225T, 1126, polyester
112	24.6	Soil only
65	23.9	GTF 200, 103, polypropylene
67	23.3	GTF 200, 103, polypropylene
74	23.5	GTF 200, 103, polypropylene
81	23.1	GTF 200, 103, polypropylene
70	21.7	GTF 375, 204, polypropylene
73	22.0	GTF 375, 204, polypropylene
71	19.3	GTF 500, 357, polypropylene
99	22.5	GTF 1225T, 1126, polyester
100	25.0	GTF 1225T, 1126, polyester
111	21.3	GTF 1225T, 1126, polyester
54	47.6	Soil only
62	47.5	GTF 200, 103, polypropylene
55	43.6	GTF 375, 204, polypropylene
106	47.3	GTF 1225T, 1126, polyester

[1] Wide Width Tensile test modulus (ASTM D 4595).

Table 13.3.2 Sampled Stress-Strain Information from UCD tests

UCD Test No. (Boyle, 1995)	Vertical Strain (%)	Horizontal Strain (%)	Vertical Stress (kPa)	Lateral Stress[1] (kPa)	Effective GRS Composite Lateral Stress[2] (kPa)
115	0.63	0.52	88.6	80.2	12.4
79	0.92	1.04	248.5	241.8	20.7
77	1.28	1.00	312.9	303.9	26.4
76	1.42	1.00	376.4	368.3	32.0
98	1.26	1.00	498.5	489.4	61.5
112	0.49	1.00	217.8	197.9	24.6
65	1.09	1.00	345.9	326.1	32.9
67	1.12	1.00	344.0	327.7	28.3
74	1.17	1.01	351.9	330.8	30.2
81	1.13	1.01	319.9	299.7	28.4
70	1.19	1.00	396.1	376.7	37.9
73	1.45	1.01	413.5	392.7	37.1
71	1.49	1.00	531.6	512.4	47.1
99	1.36	1.00	593.8	574.3	76.1
100	1.36	1.00	522.5	503.0	64.6
111	1.78	1.00	765.0	745.6	90.7
54	0.83	1.01	306.8	263.4	47.6
62	1.21	1.00	423.9	379.9	54.5
55	0.98	1.00	514.2	470.8	55.8
106	1.45	1.00	835.6	791.1	98.7

[1] Lateral stress in the direction which there is no strain (plane strain controlled direction).

[2] Calculated using the equation $\sigma_{3comp} = \sigma_{ESCP} + \frac{T_{in-soil}}{A}$ (Boyle, 1995), where σ_{ESCP} is the effective soil confining pressure and A = effective lateral area of specimen.

Table 13.3.3 Geosynthetic material used in UCD tests (Boyle 1995)

Name	Material Type	2% M_{wwt}[1] (kN/m)
GTF 200	Polypropylene	103
GTF 375	Polypropylene	204
GTF 500	Polypropylene	357
GTF 1225	Polyester	1126

[1]2% M_{wwt} = secant moduli from wide width tensile test at 2 % strain.

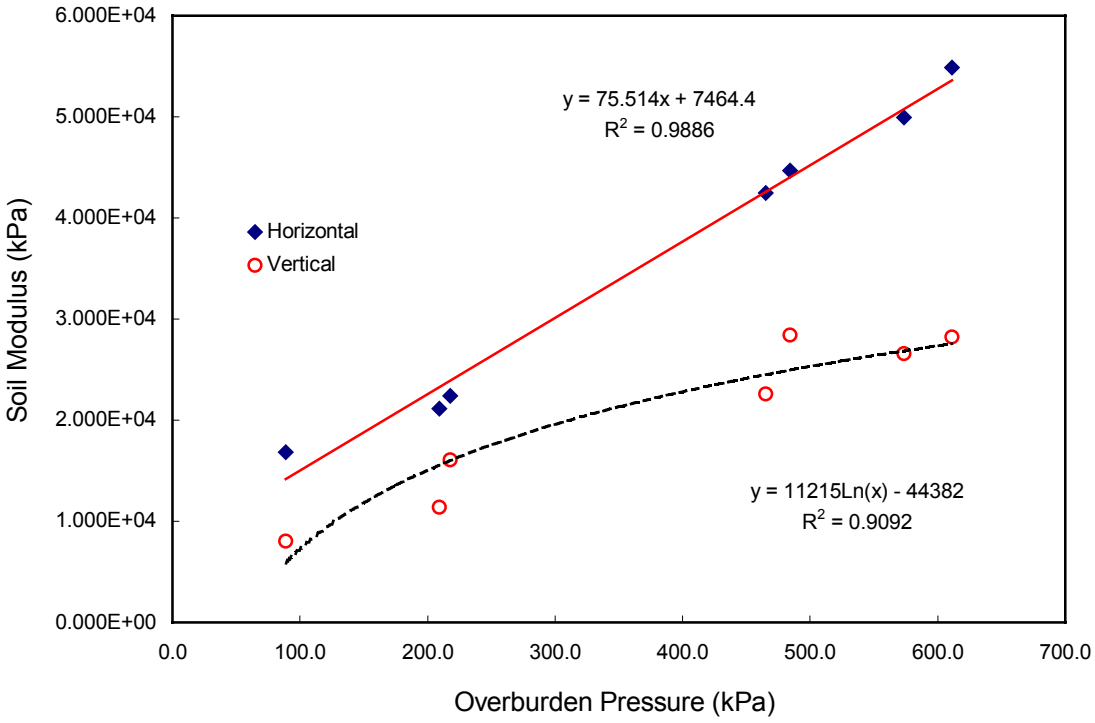

Figure 13.3.1 Plane strain soil moduli obtained from UCD tests.

horizontal soil moduli, in order to observe the reinforcing effect in both vertical and horizontal direction.

Figure 13.3.1 shows the plane strain soil moduli results. Larger moduli were found in the horizontal direction than in vertical direction because the UCD specimens were compacted to the desired density during specimen preparation. Both horizontal and vertical plane strain moduli increased as effective soil confining pressure increased. The horizontal plane strain moduli increased linearly as effective soil confining pressure increased; however, the vertical plane strain moduli increase was less at higher effective soil confining pressures.

Figure 13.3.2 shows the results of horizontal GRS composite moduli versus the effective soil confining pressure (ESCP), and Figure 13.3.3 shows the results of vertical GRS composite moduli versus the ESCP. ESCP is the confining pressure that is contributed by soil only; any confining pressure contributed by the tensile strength of geosynthetic reinforcement was not considered. In UCD test data, ESCP is the measured lateral soil pressure in direction 3, the direction that deformation was allowed. As shown in Figures 13.3.2 and 13.3.3, both vertical and horizontal composite moduli of GRS increased as the effective soil confining pressure increased for a single geosynthetic reinforcement. For different geosynthetic reinforcements, the tendency that composite moduli increased as the in-isolation tensile moduli of the geosynthetic reinforcement increased was also observed. In both the horizontal and

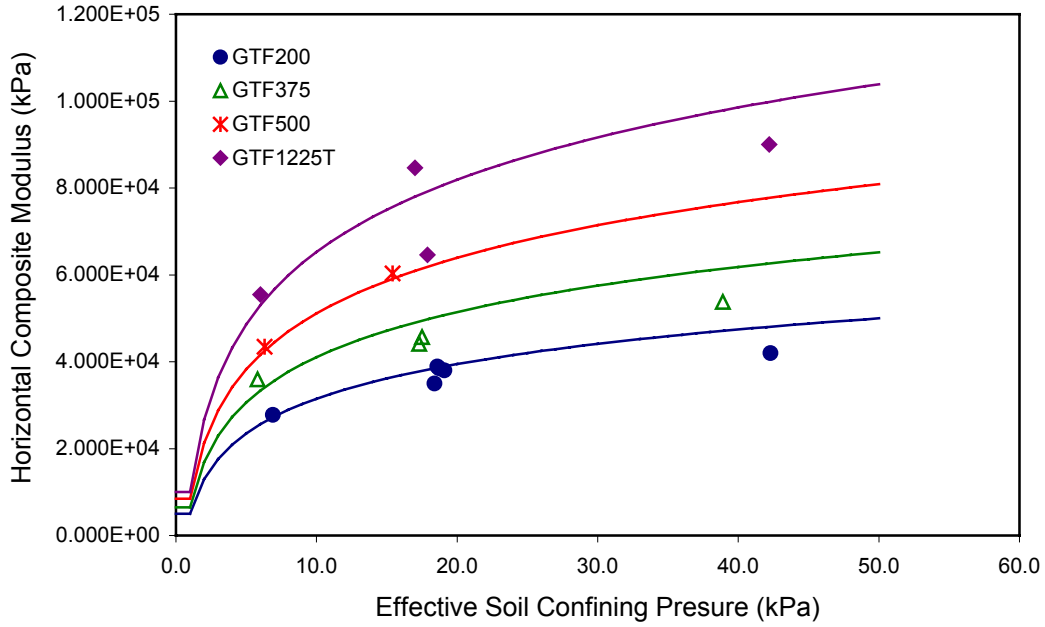

Figure 13.3.2 Horizontal composite moduli of GRS at 1% horizontal strain and with ν_{hh}=0.3.

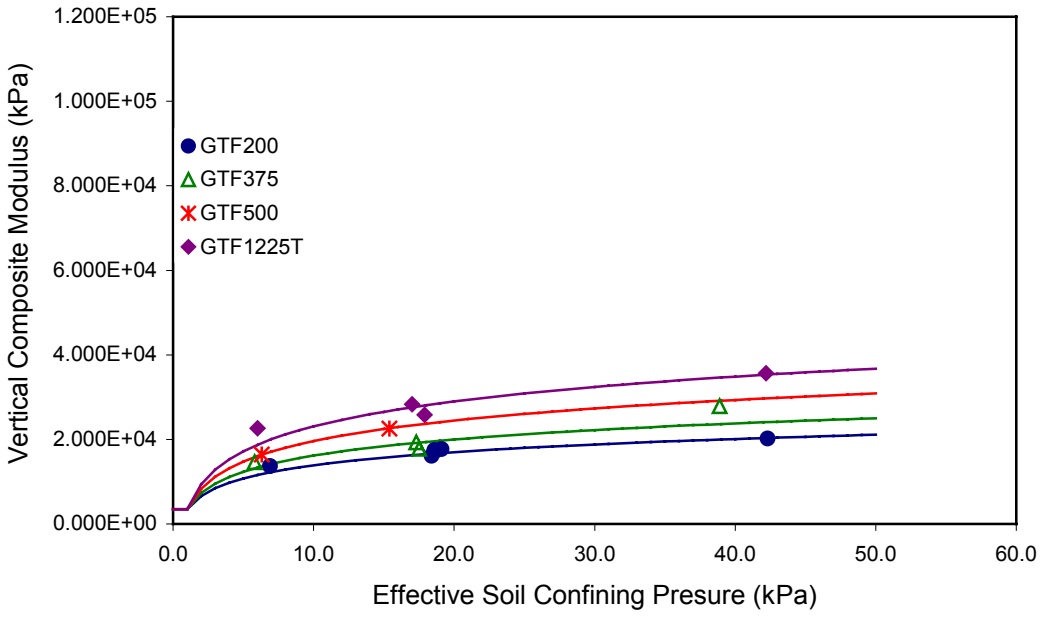

Figure 13.3.3 Vertical composite moduli of GRS at 1% horizontal strain and with ν_{hh}=0.3.

vertical directions, GRS composite moduli were found to be larger than the plane strain soil moduli. This strongly suggests that the geosynthetics contributed to the reinforcing function in the horizontal as well as in the vertical direction. Moreover, all the horizontal GRS composite moduli were found to be larger than all the vertical GRS composite moduli for GRS reinforced soil using certain geosynthetics under the ESCP range tested by Boyle (1995). This result confirmed that the horizontal direction is the major reinforcing direction. Empirical equations (Equations 13.3.1, 13.3.2, and Table 13.3.3) were also developed in an effort to characterize the moduli numerically (as the solid lines shown in Figures 13.3.2 and 13.3.3).

$$\mathbf{M_{HC} = A \cdot \log \sigma_{ESCP} + B} \qquad \text{(Eq. 13.3.1)}$$

$$\mathbf{M_{VC} = C \cdot \log \sigma_{ESCP} + D} \qquad \text{(Eq. 13.3.2)}$$

Where $\mathbf{M_{HC}}$ = horizontal GRS composite modulus, in kPa

$\mathbf{M_{VC}}$ = vertical GRS composite modulus, in kPa

A, B, C, D, are coefficients determined using UCD test data (Table 13.3.4).

Table 13.3.4 Coefficients **A, B, C,** and **D** for Equations 13.3.10 and 13.3.11, for 1% horizontal strain and Poisson's ratio of 0.3.

Geosynthetics	**A**	**B**	**C**	**D**
GTF 200	10500	4000	4500	2500
GTF 375	12500	6000	5000	3000
GTF 500	16500	8000	6000	3500
GTF 1225t	22500	9000	8000	3700

13.4 Numerical Models Using Composite GRS Properties

Two FLAC models (Models COMPA and COMPS) were created in order to verify the developed composite approach. GRS moduli obtained using the developed analytical model were input into Models COMPA and COMPS to simulate the performance of the WSDOT Rainier Avenue wall. Both Models COMPA and COMPS are the composite property models that consist of only anisotropic elastic material elements. Typical cross and instrumentation sections of Rainier Avenue wall were shown in Figures 9.2.1 and 9.2.2. Input properties of these anisotropic elastic material elements are the horizontal modulus, the vertical modulus, and Poisson's ratios in different principal directions. Model COMPA is the model that simulates the Rainier Avenue wall performance at the end of construction, and Model COMPS is the model that simulates the wall performance after applying the surcharge. The GRS composite strength properties obtained from transversely isotropic elasticity are used as the input properties for both models COMPA and COMPS.

Figures 13.4.1 and 13.4.2 show the results of the numerical analysis at 3m behind the wall. Inclinometer measurements at the same location as well as the result of Model 5008P (the discrete element model) were also plotted. Successful simulation results were obtained from both models COMPA and COMPS. The deflection results of both models COMPA and COMPS show good agreements with inclinometer measurements, both at the end of construction and after

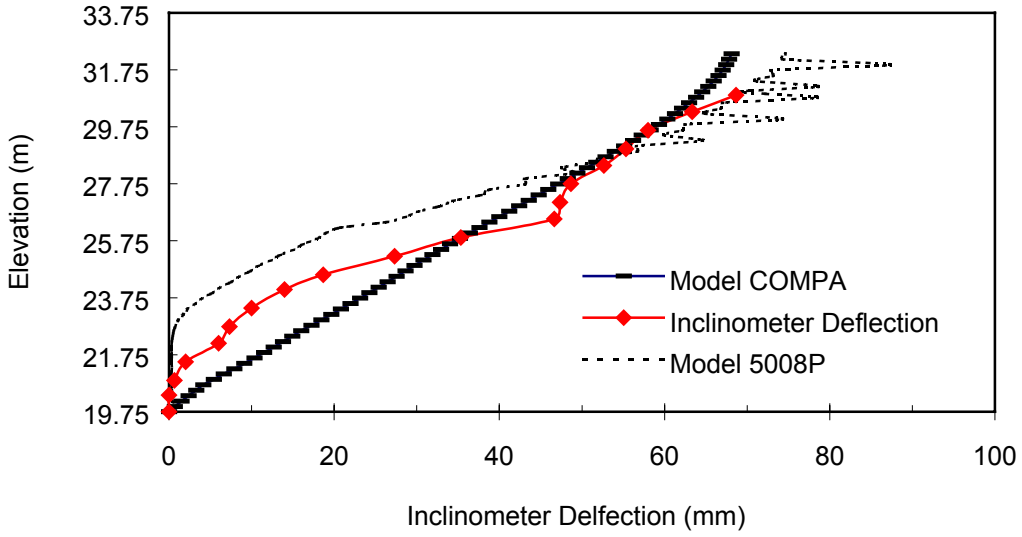

Figure 13.4.1 Results of deflections of Models COMPA and 5008P at 3m behind wall face.

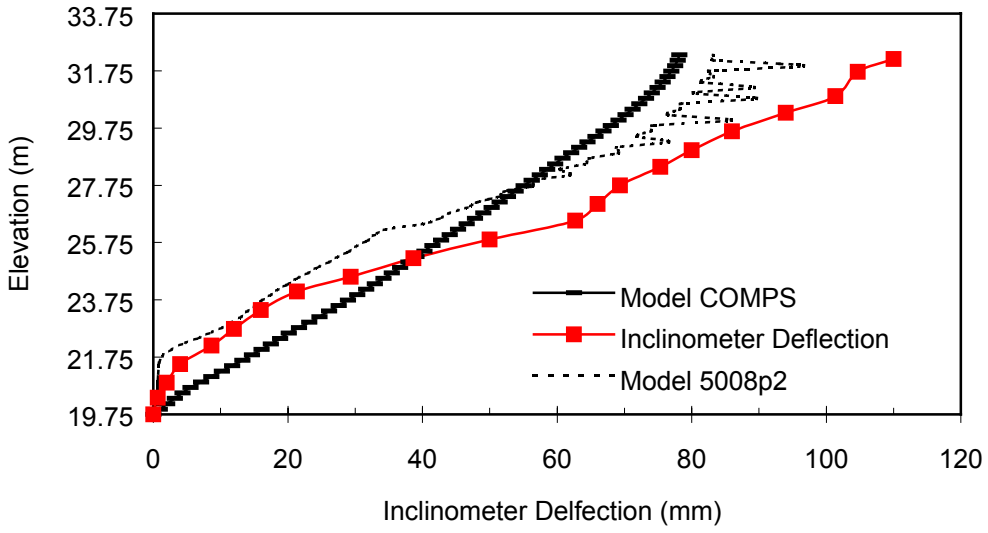

Figure 13.4.2 Results of deflections of Models COMPS and 5008P at 3m behind wall face.

Table 13.4.1 Measurements of strain gages and extensometers inside Rainier Avenue wall at locations 3m behind wall face (after Allen et al., 1992).

Elevations (m)	End of Construction		After Surcharge	
	SG (%)	ES (%)	SG (%)	ES (%)
21.27	0.25	--	0.31	--
23.17	0.4	0.45	0.6	0.6
26.21	0.9	--	1.2	--
29.63	0.8	--	1.4	--

SG: strain gage measurements.
ES: extensometer measurement.

surcharge was applied. As shown in Figure 13.4.1, model COMPA was able to predict the wall deflection at the upper half of the wall. It tended to overestimate the deflection at the lower half of the wall by an average of about 10mm. This result indicated that the wall had horizontal strains less than 1% below elevation 25.75m and close to 1% above this elevation because the input composite GRS moduli were sampled at 1% horizontal strain. This agreement of horizontal strains has been verified with strain measurements listed in Table 13.4.1.

Similar modeling results were also found in model COMPS. Figure 13.4.2 shows that Model COMPS tended to overestimate the deflection at the lower portion of the wall and underestimate the deflections at the upper portion of the wall. This result also verified the observation that the Rainier Avenue wall had horizontal strains less than 1% below elevation 25m and larger than 1% above this elevation (Figure 13.4.2). Measurements of strain gages and extensometers listed in Table 13.4.1 show that the Rainier Avenue wall had horizontal strains close to 1% at the end of construction and larger than 1% after surcharge at upper portion of the wall.

13.5 Conclusions

1. Feasibility of analyzing GRS composite properties using the developed transversely isotropic elasticity model has been demonstrated.

2. Different composite moduli of GRS elements were found in different principal directions using the transversely isotropic elasticity model; the assumption that different reinforcing mechanisms existing in different principal directions inside a GRS is further verified.

3. Because the input GRS composite properties were sampled at an average working strain of the Rainier Avenue wall (1%), numerical models COMPA and COMPS were able to predict quite well the field instrumentation measurements. To improve this approach so that it can be more universally applicable, the developed transversely isotropic elasticity model for GRS elements should be applied to additional UCD test results. The behavior of GRS composites sampled at different horizontal strains, for example, 0.5%, 1.5%, and 2%, should be analyzed. The stress-strain distribution of GRS retaining structures can then be further analyzed using composite property models with input of moduli sampled at these horizontal strains.

Chapter 14

Applications of Modeling Results: Performance Prediction and Design Recommendations for GRS Walls

In this chapter, methods of predicting GRS wall performance factors such as maximum face deflection and maximum reinforcement tension, as well as design recommendations for GRS walls are presented. The performance prediction methods were developed based on the results of the parametric study presented in Chapter 12. They were developed in an effort to provide preliminary working stress information for the initial designs of GRS walls. General conditions of using these methods to predict GRS wall performance are as same as the boundary conditions and design factors described in Section 12.4.1. These performance prediction methods include (1) a maximum face deflection prediction method (Section 14.1), (2) a maximum reinforcement tension prediction method (Section 14.2), and (3) a new method for predicting reinforcement tension distributions (Section 14.3). In the example problems that used the developed method to predict the GRS wall performance, verification was provided by the instrumentation measurements of the Algonquin concrete panel faced geogrid wall (Wall 2). Limitations of the prediction method are discussed in Section 14.4. Finally, design recommendations for GRS walls are presented in Section 14.5. These recommendations are based on the results of the case history modeling (Chapters 9 and 10) and the parametric study (Chapter 12).

14.1 Maximum Face Deflection

Figure 14.1.1 presents a simplified method to predict the maximum face deflection of GRS walls. Design curves shown in Figure 14.1.1 are the trend lines of the parametric study results shown in Figure 12.8.1. In Figure 14.1.1, GRS walls were categorized into three groups: (I) large spacing with a wrapped face, (II) large spacing with a structural facing or small spacing with a wrapped face, and (III) small spacing with a structural facing. These three curves were the trend lines of the modeling results of GRS walls that were designed with Type II (ϕ = 30 deg) to Type VII (ϕ = 55 deg) soils (Table 12.4.2) and global reinforcement stiffnesses between 500 to 5500 kN/m^2. They can be used to predict the face deflection if the material properties are given, or to estimate required reinforcement stiffness if the soil properties and tolerable deformation are given. Examples 14.1.1 and 14.1.2 show the sample calculations for utilizing Figure 14.1.1.

14.2 Reinforcement Tension

Maximum reinforcement tensions can be estimated using the analytical model presented in Chapter 11. Equation 11.1.6 is the expression for the accumulated reinforcement tension at a given depth from top of the wall. The reinforcement tension of an individual reinforcement layer (Equation 14.2.2) can be obtained by subtracting Equation 14.2.1 (the accumulated reinforcement tension of layer n-1) from Equation 11.1.6.

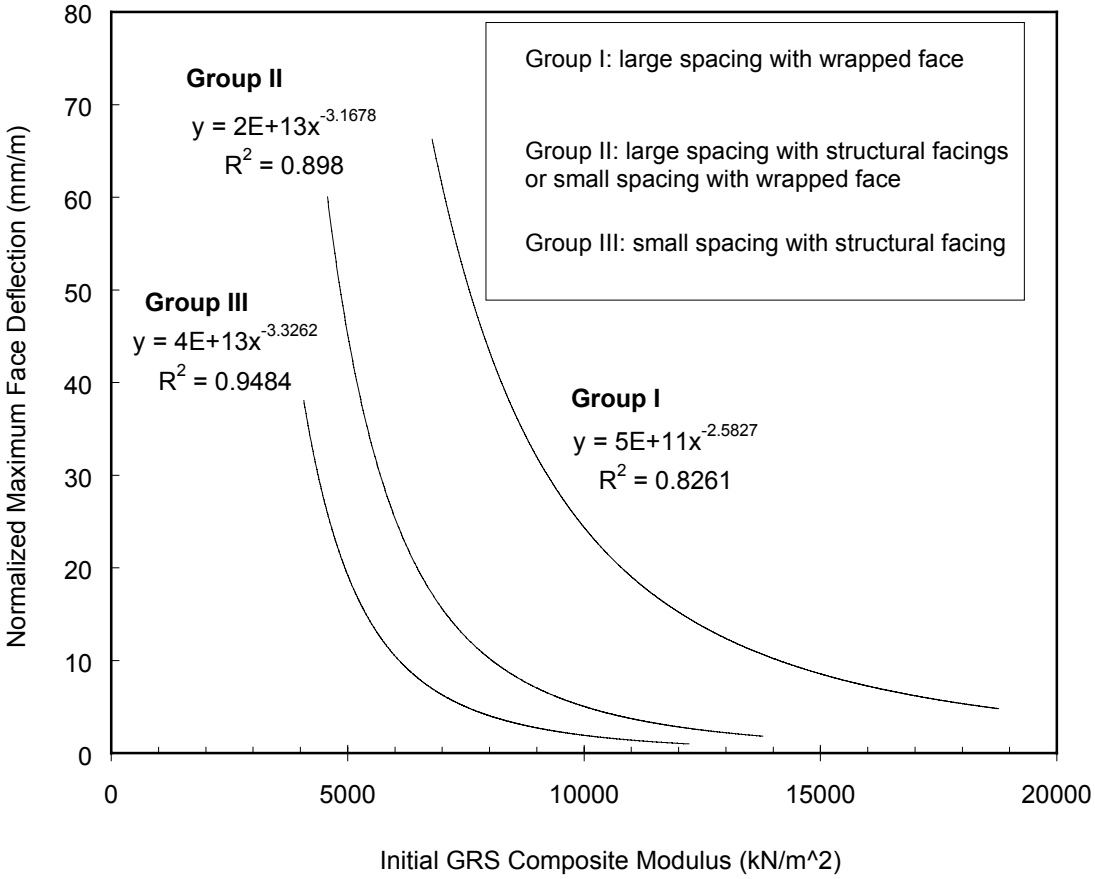

Figure 14.1.1 Maximum face deflection versus GRS composite modulus.

Example 14.1.1 Maximum face deflection prediction.

****

Given: 1. Wall height (H) = 6m, reinforcement spacing (S_v) = 0.8m, vertical face.

2. Backfill soil properties: $\gamma = 20.6$ kN/m^3, $\phi = 45$ deg, angular sand.

3. Reinforcement stiffness (J): 1000 kN/m (after in-soil and low strain rate modifications).

Solve:

Calculating the initial GRS composite modulus using Equation 11.2.7,

$$E_{comp} = \frac{J}{S_v} + E_s \qquad \text{(Eq. 11.2.7)}$$

where $\frac{J}{S_v} = \frac{1000}{0.8} = 1250 \cdot \frac{kN}{m^2}$, and calculating E_s using Equation 7.1.3 with R_f = 0.7, n = 0.5, K = 1600 (Table 12.4.2), and $\sigma_3 = K_0 \cdot \gamma \cdot \frac{S_v}{2} = 2.42$ kPa, where K_0 = 1-sinϕ.

$$E_s = \left[1 - \frac{R_f (1-\sin\phi)(\sigma_1 - \sigma_3)}{2c \cdot \cos\phi + 2\sigma_3 \cdot \sin\phi}\right]^2 \cdot K \cdot P_{atm} \cdot \left(\frac{\sigma_3}{P_{atm}}\right)^n = 10{,}088 \text{ kN/m}^2$$

$E_{comp} = 1250 + 10088 = 11{,}338$ kN/m^2

$S_v = 0.8\text{m} \rightarrow$ large spacing

Wall Types	D_{max}/H (mm/m)	d_{max} (mm)	Measured Face Deflection (mm)[a]
Wrapped face, Group I curve	17	102	--
Structural facing, Group II curve	5	30	32

[a] Measured maximum face deflection of Algonquin concrete panel face wall (J = 1020 kN/m, S_v = 0.76m, similar soil properties as given above)

****

Example 14.1.2 Calculating required reinforcement stiffness.

****

Given: 1. Wall height (H) = 10m, reinforcement spacing (S_v) = 0.4m, vertical face.

2. Backfill soil properties: $\gamma = 20.6$ kN/m^3, $\phi = 45$ deg, angular sand.

3. Tolerable maximum face deflections: 75 and 100mm for wrapped face walls, 25 and 50 mm for structural facing walls.

Solve:

$E_s = 7133$ kN/m^2 (as calculated in Example 14.1.1)

D_{max} (mm)	d_{max}/H (mm/m)	E_{comp} (kN/m^2)	$J/S_v = E_{comp} - E_s$ (kN/m^2)	J (kN/m^2)
75	7.5	9000	1867	747
100	10	8000	867	347
25	2.5	9000	1867	747
50	5	7500	367	147

****

$$\sum_{1}^{n} t_i(z) = \frac{\gamma \cdot z_n^{\,2}}{2} \cdot (K_{soil} - K_{comp}) \qquad \text{(Eq. 11.1.6)}$$

$$\sum_{1}^{n-1} t_i(z) = \frac{\gamma \cdot z_{n-1}^{\,2}}{2} \cdot (K_{soil} - K_{comp}) \qquad \text{(Eq. 14.2.1)}$$

$$t_n = \sum_{1}^{n} t_i - \sum_{1}^{n-1} t_i = \frac{\gamma}{2} \cdot (K_{soil} - K_{comp}) \cdot (z_n^2 - z_{n-1}^2) \qquad \text{(Eq. 14.2.2)}$$

Equation 14.2.2 can be rearranged as Equation 14.2.3, where z_n - z_{n-1} = S_v, the reinforcement spacing, and $\frac{(z_n + z_{n-1})}{2} \approx z_n$. Reinforcement tension at a given layer can then be expressed in terms of S_v and z_n (Equation 14.2.4).

$$t_n = \frac{\gamma}{2} \cdot (K_{soil} - K_{comp}) \cdot (z_n - z_{n-1}) \cdot (z_n + z_{n-1}) \qquad \text{(Eq. 14.2.3)}$$

$$t_n \approx (K_{soil} - K_{comp}) \cdot \gamma \cdot S_v \cdot z_n \qquad \text{(Eq. 14.2.4)}$$

The maximum reinforcement tension can be expressed using Equation 14.2.5:

$$T_{max} = (K_{soil} - K_{comp}) \cdot \gamma \cdot z_{t\,max} \cdot S_v$$

$$= \frac{(K_{soil} - K_{comp}) \cdot z_{t\,max}}{H} \cdot \gamma \cdot H \cdot S_v \qquad \text{(Eq. 14.2.5)}$$

where z_{tmax} = depth of T_{max} from top of the wall, and

H = height of wall.

As discussed in Chapter 11, soil properties as well as the arrangement and properties of the reinforcement controlled values of K_{comp}. Modeling results presented in Section 12.6 also indicated that the locations of the maximum reinforcement tensions were also affected by the soil properties. In order to analyze the modeling results using Equation 14.2.5, two indices, a soil index and a geosynthetic index, were defined to represent the term $\frac{(K_{soil} - K_{comp}) \cdot z_{t\,max}}{H}$. Equation 14.2.5 can be rewritten as Equation 14.2.6 by introducing these two indices into it.

$$T_{max} = \Phi_s \cdot \Phi_g \cdot \gamma \cdot H \cdot S_v \qquad \text{(Eq. 14.2.6)}$$

where Φ_s = soil index, and

Φ_g = geosynthetic index.

Numerical and statistical analyses were performed on the average reinforcement tension (T_{ave}) results obtained from all groups models of the parametric study in Chapter 12. The relationship between the soil index and soil properties as well as the relationship between geosynthetic index and geosynthetic properties was determined for GRS walls with different facing systems. Figure 14.2.1 shows the relation between the soil index and soil friction angles, and as shown in the figure, very good correlation was found. Figure 14.2.2 shows the relation between the geosynthetic

index and the global reinforcement stiffnesses that were corrected with considerations of in-soil and low strain rate effects. As shown in the figure, very good correlation was also found in this case for all models; however the geosynthetic indexes were not affected very much by the facing systems (Figure 14.2.2).

Magnitudes of the maximum average reinforcement tensions (T_{ave_max}) can be estimated using Equation 14.2.6. The soil and geosynthetic indices in Equation 14.2.6 can be determined using Figures 14.2.1 and 14.2.2. Design curves shown in Figures 14.2.3 and 14.2.4 are the trend lines of the modeling results shown in Figures 14.2.1 and 14.2.2. Table 14.2.1 shows the average ratios (a_T) of the maximum average reinforcement tension to the maximum peak reinforcement tension (T_{peak_max} / T_{ave_max}) of all models analyzed in this study. The maximum peak reinforcement tensions (T_{peak}) obtained from the numerical models tended to over-predict the actual peak reinforcement tensions in the GRS walls because the reinforcement elements were attached to the material element nodes. Details of this over-estimation were described in Section 8.5.6. From field measurements of case histories analyzed in this research, T_{peak} obtained from the numerical models with reinforcement elements attached to the nodes tended to over-predict the actual peak reinforcement tension by about 20%.

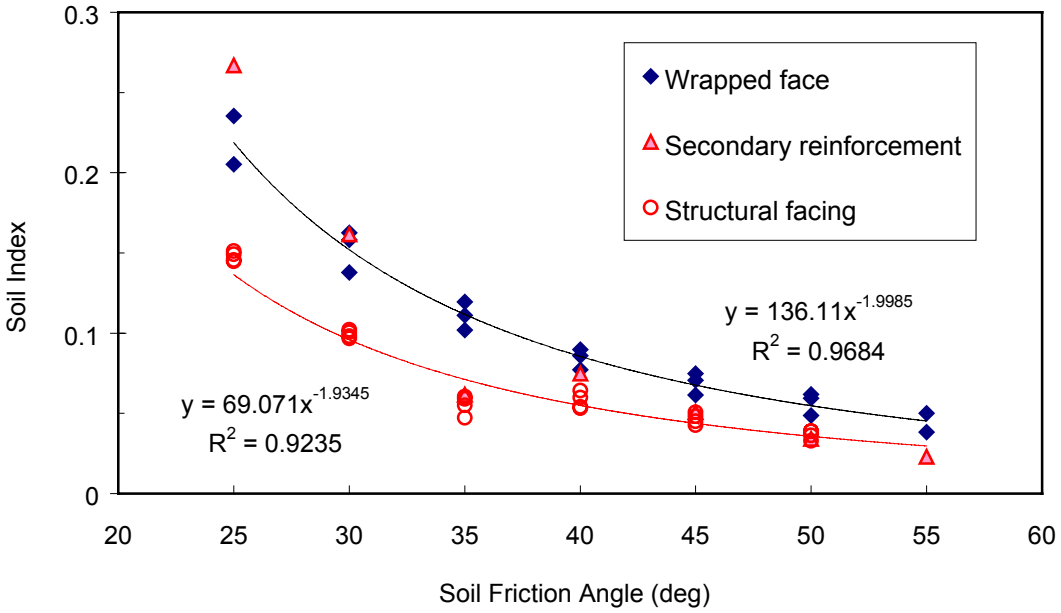

Figure 14.2.1 Soil index of walls with different facing systems.

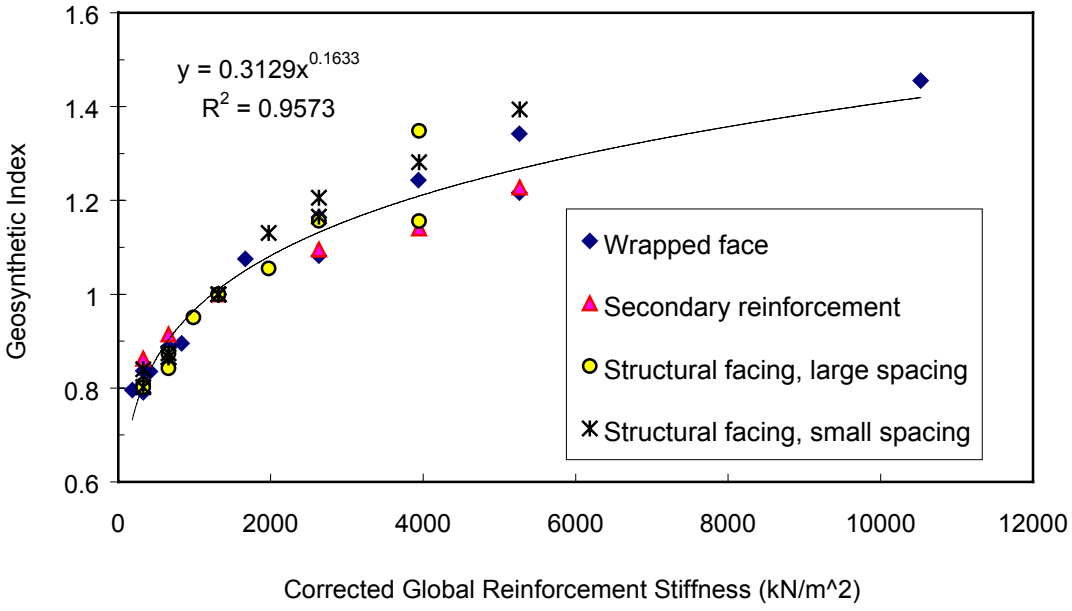

Figure 14.2.2 Geosynthetic index of walls with different facing systems.

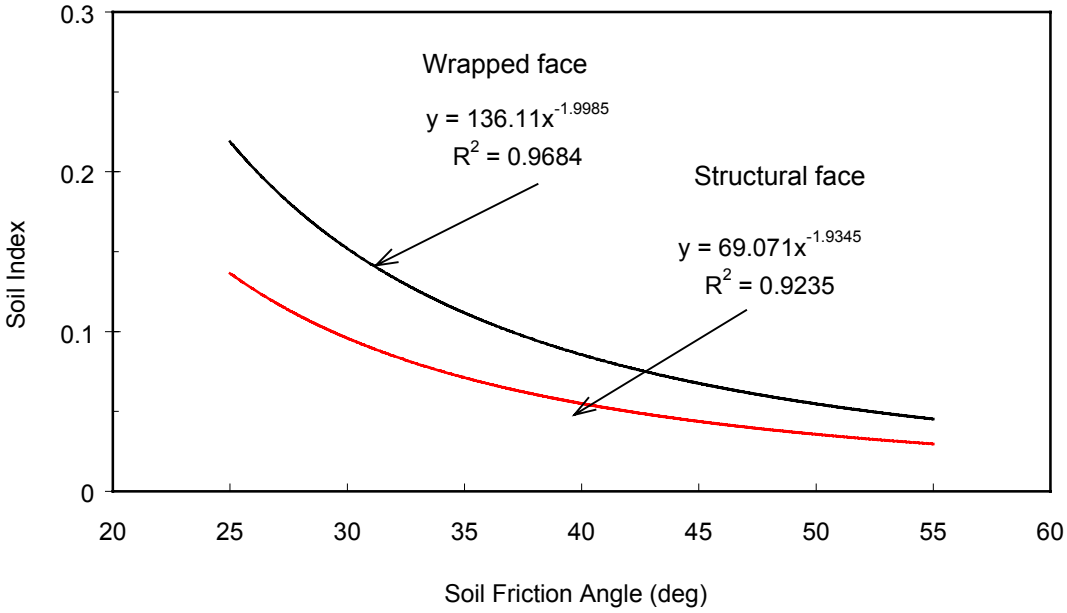

Figure 14.2.3 Design curves of soil index.

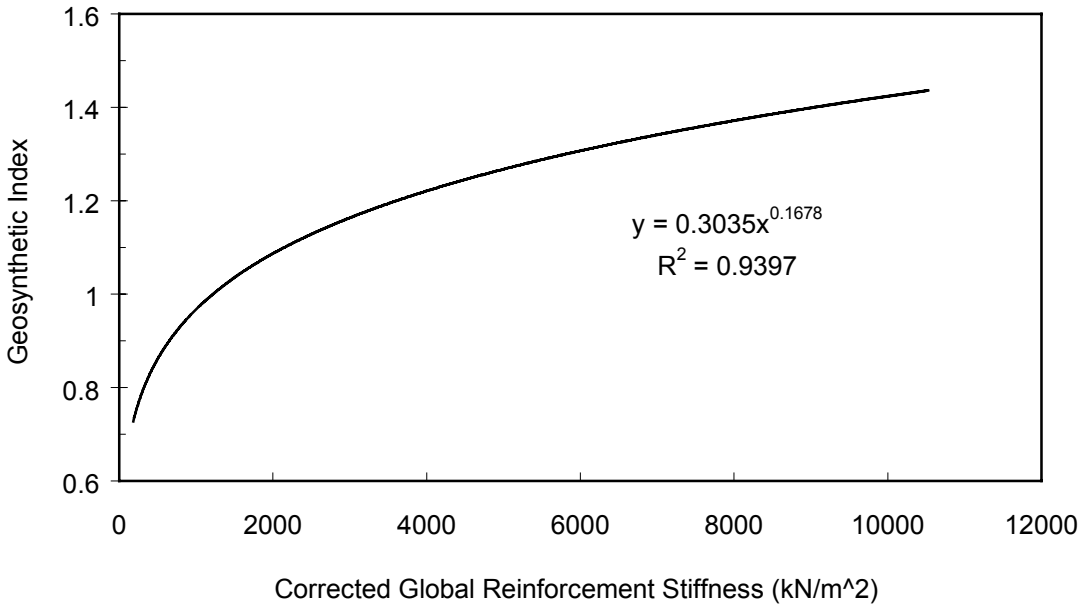

Figure 14.2.4 Design curve of geosynthetic index.

Maximum peak reinforcement tensions can be estimated using a_T and Equation 14.2.6 (Equation 14.2.7).

$$T_{peak\_max} = a_T \cdot T_{ave\_max} = a_T \cdot \Phi_s \cdot \Phi_g \cdot \gamma \cdot H \cdot S_v \qquad \text{(Eq. 14.2.7)}$$

where a_T = ratio of (T_{peak_max} / T_{ave_max}) (Table 14.2.1),

Φ_s = soil index, and

Φ_g = geosynthetic index.

Example 14.2.1 shows the sample calculation for determining the maximum reinforcement tensions using Equations 14.2.6 and 14.2.7 and design curves shown in Figures 14.2.3 and 14.2.4. In Example 14.2.1, maximum reinforcement strain of the given GRS wall is determined as 0.86%. The maximum reinforcement strain measured in Algonquin concrete panel Wall 2 (geogrid wall), which had similar material properties and geometry design as given in the example, was 0.8%.

Table 14.2.1 Values of a_T for different GRS walls.

Wall Types	a_T
Wrapped face, large spacing (S_v = 0.76m)	1.8
Wrapped face, small spacing (S_v = 0.38m)	1.5
Wrapped face, with secondary reinforcement, large spacing	1.7
Modular block face, large spacing	1.7
Modular block face, small spacing	1.5
Concrete panel face, large spacing	2.2
Concrete panel face, small spacing	1.8

Example 14.2.1 Maximum reinforcement tensions prediction.

****

Given: 1. Wall height (H) = 6m, reinforcement spacing (S_v) = 0.75 m, vertical face.

2. Backfill soil properties: $\gamma = 20.6$ kN/m^3, $\phi = 43$ deg, angular sand.

3. Reinforcement stiffness (J): 1000 kN/m (after in-soil and low strain rate modifications).

Solve:

$\Phi_s = 0.09$ (wrapped face) and 0.05 (structural face) for $\phi = 43$ deg

$\Phi_g = 1.05$ for $\dfrac{J}{S_v} = \dfrac{1000}{0.75} = 1333 \cdot \dfrac{kN}{m^2}$

$$T_{ave\_max} = \Phi_s \cdot \Phi_g \cdot \gamma \cdot H \cdot S_v \quad \text{(Eq. 14.2.6)}$$

$$T_{peak\_max} = a_T \, T_{ave\_max} \quad \text{(Eq. 14.2.7)}$$

where $\gamma = 20.6$ kN/m^3, H = 6m, and $S_v = 0.75$m.

Wall Types	T_{ave_max}, (kN/m) (Eq.14.2.6)	T_{peak_max}, (kN/m) (Eq. 14.2.7)	Corrected T_{max} (kN/m)[a]	T_{max} (kN/m) (Tie-back wedge method)[b]
Wrapped Face	8.8	15.8	12.6	17.6
Modular Face	4.9	8.3	6.6	17.6
Concrete Face	4.9	10.8	8.6	17.6

[a] Apply 20% reduction on T_{peak_max} obtained using Equation 14.2.7 (Section 8.5.6).
[b] $T_{max} = K_a \gamma H S_v$, where K_a is the active lateral earth pressure coefficient, $K_a = 0.19$ for $\phi = 43$ deg.

Maximum reinforcement strains can be also obtained by dividing the T_{peak_max} by the reinforcement stiffness:

	Wrapped Face Wall	Modular Block Faced Wall	Concrete Panel Faced Wall
Maximum Reinforcement Strain (%)	1.26	0.66	0.86

****

14.3 Reinforcement Tension Distributions

Results of case histories, laboratory test walls, and parametric study indicated that the actual reinforcement tension distributions inside the GRS walls were very different from the reinforcement tension distributions calculated using the tie-back wedge method. Results of the parametric analysis indicated that locations of the maximum reinforcement tensions occurred between 0.25H (poor quality backfill) to 0.5H (good quality backfill). The tie-back wedge method predicts a maximum reinforcement tension at the bottom of the wall. Moreover, modeling results presented in Chapter 9 also showed that the actual reinforcement tensions inside the GRS walls were smaller than the maximum reinforcement tensions predicted using the tie-back wedge method.

Figure 14.3.1 shows a trapezoid reinforcement tension distribution for GRS walls. This distribution was developed in order to cover all the reinforcement tension distributions that were observed in the field measurements (Chapter 9) and parametric study (Chapter 12). As shown in Figure 14.3.1, reinforcement tension increases from 0.2 T_{max} at top of the wall to the maximum reinforcement tension (T_{max}) at height equal to 0.6H. The reinforcement tension remains at T_{max} between 0.6H to 0.2H, and it decreases from T_{max} to 0.2 T_{max} at bottom of the wall.

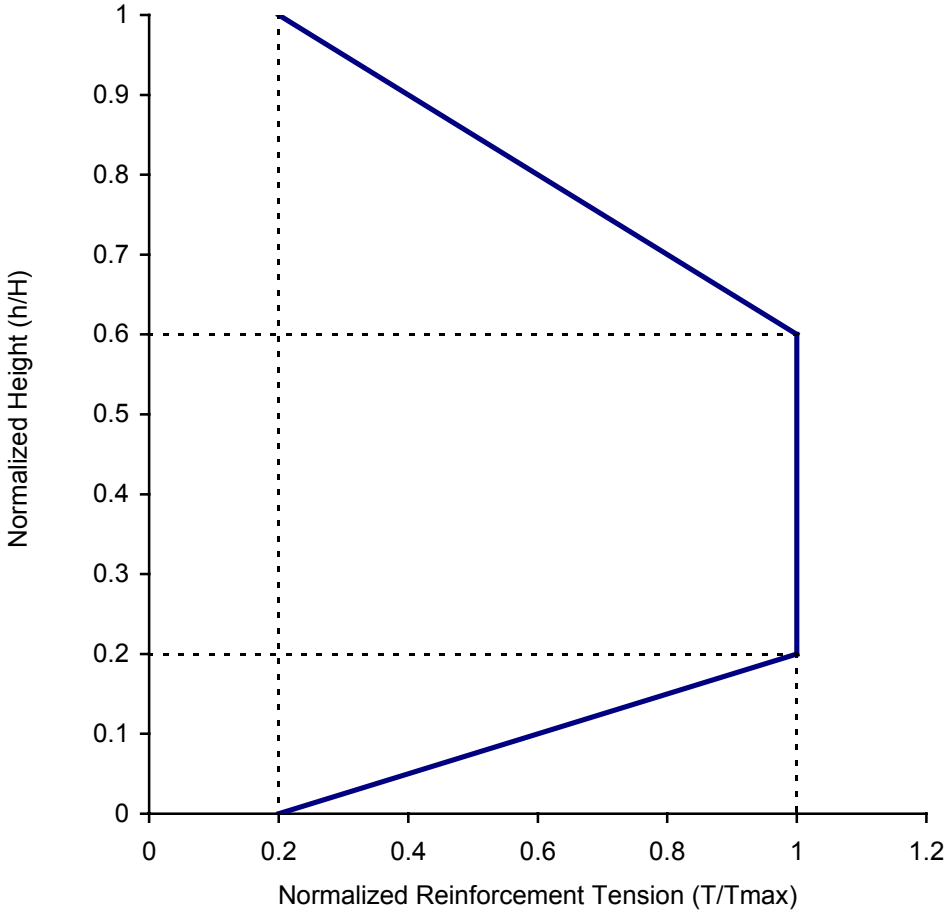

Figure 14.3.1 Reinforcement tension distribution of GRS walls.

T_{max} can be determined using Equations 14.2.6 and 12.4.7 and design curves shown in Figures 14.2.3 and 14.2.4 with modification to account for the over-prediction caused by attaching reinforcement elements to the material element nodes. Example 14.3.1 shows the procedures to determine the reinforcement tension distribution inside a GRS wall. Figure 14.3.2 shows the reinforcement tension distribution calculated in Example 14.3.1 compared to the tension distribution converted from the strain gage measurements (Algonquin concrete panel Wall 2). Excellent prediction was obtained by using the method presented in this chapter.

14.4 Limitations of the Performance Prediction Methods

Performance prediction methods presented in this chapter were developed based on the result of the extensive parametric study performed in this research (Chapter 12). Limitations of using these methods to predict performance of the GRS walls include the general boundary conditions, the ranges of the design factors, and geometry limits that are similar to those in the numerical models of the parametric study. Details of these limitations are described in the following sections.

14.4.1 Wall Geometry

Numerical GRS wall models analyzed in the parametric study have heights ranging from 12.6 m to 3.6 m., and all the models were designed with vertical faces. For GRS walls that are higher than 12.6 m, performance prediction made by the design curves presented in this chapter may not be reliable.

By comparing the analysis results of the parametric models and case histories presented in Chapter 9, both wall face deflections and reinforcement tensions of a battered face wall were found to be smaller than vertical face walls with the same backfill soil properties and reinforcement layout and properties. Therefore, design curves presented in this chapter tend to over-predict the performance of GRS walls with battered faces.

14.4.2 Boundary Conditions

For all models analyzed in the parametric study, the backfill was extended backward a distance equal to the embeded reinforcement length from the end of the reinforcement. The foundation soil in front of the wall was also extended a distance equal to the embedded reinforcement length from the toe of the wall. The depth of foundation soil was equal to the height of the wall. For GRS walls that have boundary conditions extending further than those described above, design curves presented in this chapter can be used to predict their performance. However, for GRS walls that have more complicated boundary conditions, such as GRS walls on a bedrock foundation or that have bedrock next to the reinforced zone, design curves presented in this chapter might not be appropriate.

These design curves were developed based on the results of numerical models that have no foundation failure and no embedment or constraint at the toe. Use of these

design curves is also limited to GRS wall cases without foundation soil failure and with free toe restraint.

14.4.3 Soil Properties

Design curves presented in this chapter were developed based on the results of the numerical models with backfill of Soil Type II to VII (Table 12.4.2). Therefore, these design curves are appropriate for predicting performance of GRS walls with backfill soil properties similar to Soil Type II to VII as listed in Table 12.4.2.

14.4.4 Reinforcement Properties and Arrangement

Design curves presented in this chapter were developed based on the results of the numerical models with reinforcement stiffness (global) ranging from 100 kN/m^2 to 5,000 kN/m^2. Moreover, the vertical spacing used in the parametric study ranged from 0.38 m to 0.76 m, and embedment length of the reinforcement was fixed to 80% of the wall height for all models. For GRS walls with reinforcement properties and arrangement other than those conditions described above, design curves presented in this chapter are not suitable for predicting their performance.

Example 14.3.1 Prediction of the reinforcement tension distribution.

****

Given: 1. Wall height (H) = 6m, reinforcement spacing (S_v) = 0.75m, vertical concrete panel face.

2. Backfill soil properties: $\gamma = 20.6$ kN/m^3, $\phi = 43$ deg, angular sand.

3. Reinforcement stiffness (J): 1000 kN/m (after in-soil and low strain rate modifications).

Solve:

$T_{max} = 8.6$ kN/m (Example 14.2.1)

Reinforcement Layer	h/H	Reinforcement Tension, (T_{max})	Reinforcement Tension, (kN/m)
1	0.000	0.20	1.7
2	0.063	0.45	3.9
3	0.188	0.95	8.2
4	0.313	1.00	8.6
5	0.438	1.00	8.6
6	0.563	1.00	8.6
7	0.688	0.82	7.1
8	0.813	0.57	4.9

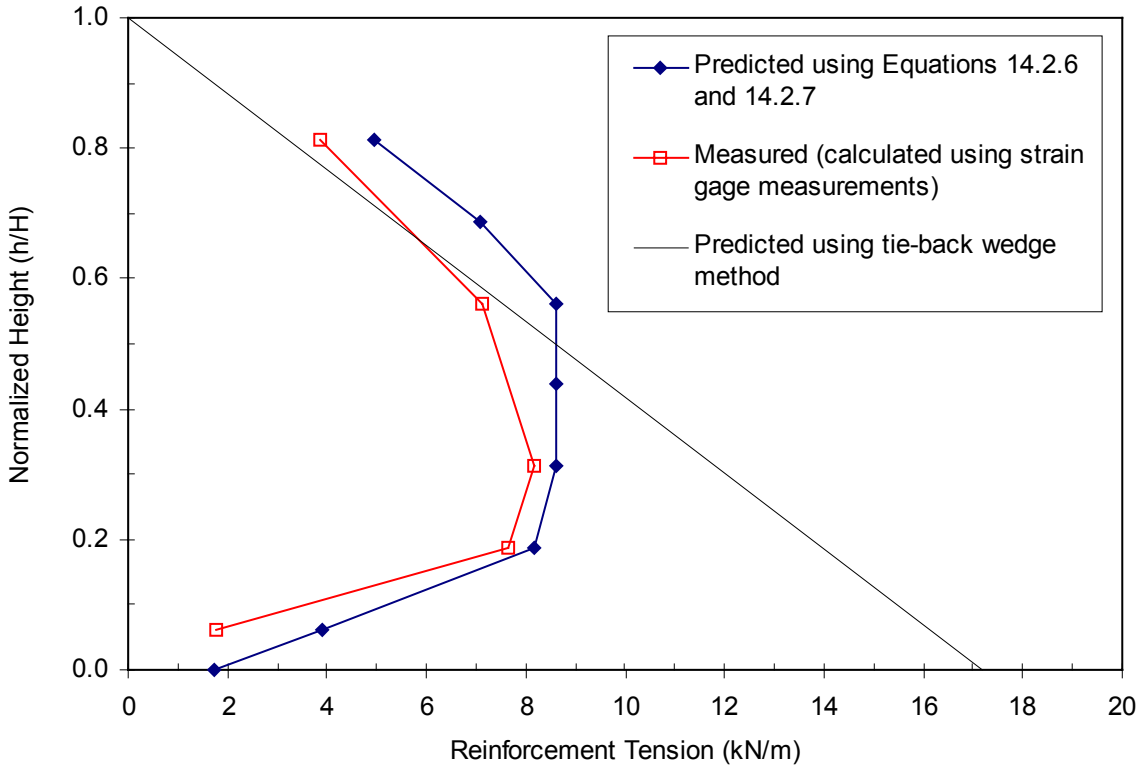

Figure 14.3.2 Predicted and measured reinforcement distribution of Algonquin concrete panel faced geogrid wall.

14.5 Design Recommendations for GRS Walls

1. Results of the parametric study indicate that the reinforcement lengths equal to 0.8H (H is the height of the wall) seems to be adequate. Even models designed with very poor quality backfill material (ϕ = 25 deg) or very weak reinforcement (J = 55 kN/m) showed no failures in the backfill behind the reinforced zone. Only localized failures were found at the face of wrapped walls with large spacing.

2. Reinforcement spacings larger than 0.6m are not recommended for use in the wrapped face wall design. Local failures were observed in the results of the wrapped face wall models with spacings larger than 0.6m. Face deflection profiles and reinforcement tension distributions of these large spacing wrapped face wall models shown in Chapter 12 also indicated that these local failures can cause internal instability such as outward rotation of the wall face.

3. Material properties such as plane strain soil properties and in-soil low strain rate reinforcement stiffnesses have to be carefully investigated when designing GRS retaining structures. Modeling results shown in Chapters 9 and 10 indicated that the performance of GRS walls can be accurately reproduced with correct material property information. To investigate the material properties inside the GRS retaining structures, property determination procedures presented in Chapter 7 can be used as a guideline.

4. If possible, good quality backfill (plane strain friction angle, ϕ_{ps}, larger than 35 deg) is recommended to use as the backfill material. Results of the parametric study indicated that GRS walls design with poor quality backfill would result in very large wall face deflections as well as large reinforcement tensions.

5. Reinforcement stiffness was found to have less effect on the wall deflection and reinforcement tensions of the GRS walls than the soil quality (Chapter 12). However, global stiffness (reinforcement stiffness divided by the spacing) larger than 500 kN/m^2 is recommended for use in design.

6. Secondary reinforcement layers can only be used as an alternative facing system when the backfill quality is good (ϕ_{ps} > 35 deg). Wall deflections and reinforcement tensions of wrapped face walls with secondary reinforcement layers and good quality backfill had performance very similar to the small spacing wrapped face wall.

7. Structural facing systems are able to improve both performance and internal stability of the wrapped face walls. As results in Chapter 12 indicated, wall deflection, as well as reinforcement tensions were reduced when structural facing systems were added in front of the wrapped face walls.

8. Preliminary design information such as maximum face deflection and reinforcement tension distributions can be obtained by using the prediction methods described in this chapter (Chapter 14).

9. With material properties and design geometry given, maximum face deflection of GRS walls can be predicted using Figure 14.1.1 (see Example 14.1.1). The maximum face deflection calculated in Example 14.1.1 showed an excellent agreement to the field measurement of the wall that was the basis for this example. Figure 14.1.1 can also be used to determine the required reinforcement stiffness if soil properties and design geometry are given (Example 14.1.2).

10. Example 14.2.1 shows the procedures to determine the maximum reinforcement tension inside the GRS walls using Equations 14.2.6 and 14.2.7 and design curves shown in Figures 14.2.3 and 14.2.4. Maximum reinforcement tension that was calculated in Example 14.2.1 was also found to be very close to the maximum reinforcement tension reduced from the strain gage measurement on the real wall.

11. Figure 14.3.1 shows a reinforcement tension distribution that was developed based on the working stress-strain information of an extensive parametric study. In this figure, reinforcement tension increases from 0.2 T_{max} at the top of the wall to the maximum reinforcement tension (T_{max}) at a height equal to 0.6H. The reinforcement tension remains at T_{max} between 0.6H to 0.2H, and it decreases from T_{max} to 0.2 T_{max} at bottom of the wall. As shown in Example 14.3.1 and Figure

14.3.2, the reinforcement tension distribution of the Algonquin concrete panel faced Wall 2 was able to be accurately reproduced by using Figure 14.3.1.

12. For critical cases, an extensive numerical analysis is still recommended so that complete working stress-strain information can be obtained for internal stability analyses. Determination of material properties and modeling techniques as described in Chapters 7 and 8 can be used as the "general rules" for performing the numerical analyses.

Chapter 15

Summary, Conclusions, and Recommendations for Future Research

15.1 Summary

The conventional internal stability design approach using limiting equilibrium is not appropriate for internal stability analyses of GRS retaining structures. This is because of the considerable differences of properties between the traditional steel and geosynthetic reinforcement. Present GRS wall design methods such as the tie-back wedge method tend to overestimate the internal stress levels inside the GRS walls, especially in the lower half of the wall. Previous research on this subject has not made much progress because:

1. Little information on the internal stress or strain distributions in real GRS structures was available,
2. Numerical modeling techniques for analyzing the performance of GRS walls has been problematic, and
3. Understanding of material and interface properties of GRS walls was not well developed.

This research project was an effort to improve our understanding of the internal stress-strain distribution in GRS retaining structures. The face deformations and internal stress-strain distributions of GRS retaining structures were analyzed using numerical techniques. Numerical models were first developed to simulate the field

instrumentation measurements in real walls. The same modeling techniques were then applied to develop numerical models for full scale test walls in order to predict their performance. Parametric studies were also carried out to investigate the influence of different internal stability design factors. Finally, improved techniques for analyzing the face deformations and internal stress-strain distributions as well as an improved internal stability design procedure were developed.

This research has contributed to progress in the following areas:

1. Better understanding of the material properties inside the GRS retaining structures. Material properties such as plane strain soil properties and low confining pressure soil dilation angle were carefully investigated in this research (Chapter 7).

2. Modeling techniques for working stress analyses of GRS retaining structures. Modeling techniques (Chapter 8) were developed in this research to reproduce both the external and internal working stress information of the selected case histories (Chapter 9), as well as to perform Class A predictions on the performance of three well instrumented laboratory test walls (Chapter 10). Results of these numerical modeling appeared to be successful.

3. Analytical models for analyzing the behavior of GRS. In this research, analytical models of the composite GRS modulus, lateral reinforced earth

pressure distribution (Chapter 11), and the stress-strain relationship of GRS composite element (Chapter 13) were developed in order to analyze the behavior of geosynthetic reinforced soil and the results of numerical modeling.

4. An extensive parametric study. An extensive parametric study that included more than 250 numerical models were performed in this research. Influences of design factors such as soil properties, reinforcement stiffness, and reinforcement spacing on the performance were carefully investigated. Moreover, effects of design options such as toe restraint and structural facing systems on the performance of the GRS walls were also examined in this parametric study (Chapter 12).

5. Composite approach for working stress analysis of GRS retaining structures. The developed analytical model of the GRS composite element was used to examine the reinforcing effects of the geosynthetic reinforcement to the soil, as well as to develop composite numerical models for analyzing performance of GRS retaining structures (Chapter 13).

6. Performance prediction methods and design recommendations of GRS retaining structure. Performance prediction methods developed based on the results of the parametric study and design recommendations for the internal stability design of GRS retaining structures were obtained in this research (Chapter 14).

15.2 Conclusions

15.2.1 Material Properties in GRS Retaining Structures

1. Material properties inside the GRS retaining structures were found to be different from those obtained using conventional properties tests. In order to design GRS retaining structures correctly, material properties such as plane strain strength properties of soil, low confining pressure soil dilation angles, in-soil properties of geosynthetic reinforcement, and low strain rate reinforcement stiffness need to be carefully determined.

2. The plane strain soil friction angles of rounded uniform sand such as Ottawa sand were found to be only slightly higher than triaxial friction angles. However, for angular material, the tendency that soils posses a higher friction angle under plane strain conditions than under triaxial conditions is clear. The empirical equation proposed by Lade and Lee (1976, Equation 7.1.1) was able to predict the plane strain soil friction angle within a reasonable range.

3. The tendencies that plane strain soil moduli are higher than triaxial soil moduli were clearly supported by test data presented in Chapter 7 (Tables 7.1.2 to 7.1.4). For uniform rounded material like Ottawa sand, its plane strain 1% strain secant moduli were only slightly higher than triaxial 1% strain secant moduli at low confining pressure (20 to 100kPa). For angular material, in both dense and loose

states, the plane strain 1% strain secant moduli were about twice as high as those obtained from triaxial tests at low confining pressure (20 to 100kPa).

4. Granular soils at low confining pressures possess higher dilation angles than those tested under high confining pressures. For granular materials prepared in a dense state, the low confining pressure dilation angles were as high as 40 deg. Even for sands prepared in a loose state, the low confining pressure dilation angles were 26 deg.

5. The stiffness of nonwoven geosynthetics increased when the geosynthetics were confined in soil. The increase of stiffness is controlled by the structure of the geotextile and the confining pressure. At present, because of difficulty of testing geosynthetic reinforcement in soil, the magnitude of stiffness increase of nonwoven geosynthetic reinforcement has not yet been well characterized.

6. For woven geotextiles, soil confinement seems to have less effect on its stress-strain behavior. The in-isolation stiffness of the woven geosynthetic can be used as the in-soil reinforcement stiffness.

7. Strength properties of geosynthetic reinforcement were found to be affected by the strain rate. Wide width tensile and UCD tests conducted at low strain rates to simulate actual loading rates in full scale structures have indicated that reductions in reinforcement stiffness are needed. For nonwoven geotextiles, because of the

random fabric filaments and very different index properties between different products, modulus reductions have not yet been clearly characterized. For woven reinforcement and geogrids made of polypropylene, a 50% reduction on the in-isolation modulus obtained from the wide width tensile test is recommended as the low strain rate adjustment. For woven reinforcement and geogrids made of polyester, a 20% reduction of modulus obtained from the wide width tensile test is recommended.

8. Adjustments that convert soil and geosynthetic properties obtained from conventional tests into those inside the GRS walls can be summarized as:
   8.1. Convert triaxial or direct shear soil friction angles to plane strain soil friction angles using Equations 7.1.1 and 7.1.2;
   8.2. Calculate plane strain soil modulus using the modified hyperbolic soil modulus model;
   8.3. Investigate the appropriate dilation angles of the backfill material;
   8.4. Investigate the effect of soil confinement on reinforcement tensile modulus; and
   8.5. Apply appropriate modulus reduction on reinforcement tensile modulus to account for the low strain rate that occurs during wall construction.

15.2.2 Performance Modeling of GRS Retaining Structures

1. Numerical models that were developed using material property determination

procedures described in Chapter 7 and modeling techniques described in Chapter 8 were able to reproduce both external and internal performance of GRS walls within reasonable ranges.

2. Accurate material properties are the key to a successful performance modeling of GRS walls. Results of Models RAING, ALGPC, RMC1, RMC2, and RMC3 showed better predictions of wall deflection and reinforcement strain distributions than the results of Models ALGMB1 and ALGWF1 because information of material properties of the Rainier Avenue wall, Algonquin concrete panel faced wall, and RMCC test walls were more complete.

3. For GRS walls with complicated facing systems such as modular block facing, accurate deflection predictions rely on not only correct input properties of soil and geosynthetic, but also on the correct input properties of the interfaces between blocks and reinforcement inserted between the blocks. Input properties of reinforcements inserted between blocks can be determined using connection test data, if available.

4. Modeling results also indicate that soil elements located adjacent to reinforcement layers have smaller deformation then soil elements located in between the reinforcements. Especially at the lower half of the GRS walls or at the face of a wrapped face wall where no structural facing units are used to confine the bulges, this reinforcing phenomenon becomes more obvious (Figures 9.3.7 and 9.3.8).

5. Different predictions were found between the modeling results and inclinometer measurements, especially above the locations of maximum wall deflections predicted by the numerical models (Figures 9.3.2, 9.3.6, and 9.3.7). The inclinometer measurements indicated a maximum wall deflection at the top of the wall, while the modeling results indicated a maximum deflection at about two-thirds height of the wall. Both predicted and measured results of reinforcement strain distributions verified that the deflection predictions of the numerical models and optical face survey are more reasonable than the inclinometer measurements, i.e. only small deformation occurred at top of the GRS walls. As shown in Figures 9.4.3, 9.4.6 and 9.4.7, both predicted and measured reinforcement strains in the upper reinforcement layers were smaller than those of the reinforcement layers at locations where the maximum wall deflections occurred (about two-thirds of the wall heights).

6. Results of Models ALGMB1 and ALGWF1verified that numerical models developed using modeling techniques described in Chapter 8 were able to provide reasonable working strain information of GRS walls when insufficient material properties were provided and input material properties were determined based on information from similar materials.

7. Results of Model ALGWF1 also showed that procedures used to determine the in-soil stiffness from in-isolation test data for nonwoven geosynthetics were

appropriate. The input stiffness of the nonwoven geosynthetic reinforcement was determined by multiplying the 2% strain in-isolation stiffness by five. This modification was based on the UCD test result reported by Boyle (1995).

8. Reinforcement tensions calculated using Equation 9.5.1 (the tie-back wedge method) appeared to be much higher, especially at the lower half of the wall, than those predicted by the numerical models that were able to reproduce both external and internal performance of GRS walls. This observation verifies that the conventional design method tends to over-design the reinforcement tensions, especially in the lower part of the wall. Possible reasons are that the conventional method uses a lateral earth pressure distribution without modifications for soil-reinforcement interactions and toe restraint.

9. Modeling results of the case histories presented in Chapter 9 also showed that actual locations of maximum reinforcement tensions of GRS walls occurred at heights between 0.2H to 0.5H instead of at bottom of the walls, as predicted by the tie-back method.

10. Numerical models of the RMCC laboratory test walls tended to underpredict the wall face deflection at end of the construction by only about 6 to 10mm. The most likely reason for this underestimation is that the additional movement due to the construction procedures such as soil compaction was not considered in the FLAC models.

11. Numerical models of the RMCC laboratory test walls also tended to overestimate the wall face deflection at top of the wall after surcharge was applied. This result could be improved somewhat by decreasing the contact area of the surcharge pressure. Full contact between airbag and backfill soil was assumed in the numerical models. During the tests of Walls 1 and 2, a decrease of the surcharge contact area (area between the airbag and backfill soil) behind the wall face due to the inflation of the airbag was observed by Burgess (1999). However, the actual surcharge contact area was not reported by him, so no exact decrease in surcharge contact area could be modeled.

12. Overall, the FLAC models of the RMCC test walls tended to underpredict the reinforcement strains in the lower half of the test walls. A possible reason of this underestimation is that the FLAC models did not model the toe restraint of the test wall very well.

13. Test wall Wall 2 was constructed using the same geogrids as that of Walls 1 and 3 but with every second longitudinal member of the grid removed. This process was assumed to reduce the stiffness of the geogrid by 50%. However, the actual stiffness reduction of this modified geogrid was not measured. Performance predictions of Model RMC2 could be improved by increasing the reinforcement modulus from 50% to 70% of the original modulus of this geogrid.

14. Both numerical models and post construction observations of the RMCC test walls indicated that large differential settlements occurred between the facing blocks and the backfill soil. However, the strain gage measurements did not show any strain peaks near the blocks.

15. The stiff concrete foundation of the test walls did affect both the face deflection profile and the reinforcement tension distribution, as shown in the normalized plots of Figures 10.4.1 and 10.4.2. Figure 10.4.1 indicates that the maximum face deflection of the wall with a stiff concrete foundation is located at top of the wall, while that of the wall with a soil foundation is located near the middle of the wall. Figure 10.4.2 also indicates that a stiff foundation has a similar effect on the reinforcement tension distributions. The maximum reinforcement tension of the test wall with a stiff concrete foundation occurred at a height of 0.8H, but the maximum reinforcement tension of the test wall with a soil foundation occurred at a height of 0.5H.

15.2.3 Parametric Study

1. Local failures were observed near the faces of GRS wall models with larger vertical reinforcement spacings. For wrapped face GRS walls that were designed with the same global stiffnesses but different vertical reinforcement spacings, the large spacing walls exhibited much higher face deflections than the small spacing ones (Figure 12.5.5).

2. Face deformation of GRS walls was found to be affected by both the strength properties of the backfill and the global reinforcement stiffness. Parametric analysis results shown in Section 12.5 indicated that face deflections of GRS walls increased as the soil strength properties decreased. Face deflections decreased as the global reinforcement stiffness increased. A good correlation was found between the GRS composite modulus (E_{comp}) and normalized maximum face deflection (d_{max}/H) (Figures 12.5.8 and 12.8.1).

3. Reinforcement tensions in GRS walls was also found to be affected by both the strength properties of the backfill and the global reinforcement stiffness. Parametric analysis results shown in Section 12.6 indicated that overall reinforcement tensions in the GRS walls increased as the soil strength properties decreased. Overall reinforcement tensions also increased as the global reinforcement stiffness increased. However, the reinforcement tensions started to increase when the walls were designed using very weak reinforcement because of the large strains exhibited (Figure 12.3.4).

4. Toe restraint was able to reduce the maximum face deflections and reinforcement tensions (Figures 12.7.1 to 12.7.6). Among three toe restraints (0.05H embedment, 0.1H embedment, and fixed toe), 0.1H embedment was found to be the most effective toe condition to improve the performance of GRS walls, especially for walls designed with poor quality backfill.

5. For large spacing walls, secondary reinforcement was found to be only effective for improving performance of walls with good quality backfill. Both face deflections and reinforcement tensions of GRS walls with good quality backfill could be decreased using secondary reinforcement (Figures 12.8.1, 12.8.2 and 12.8.3).

6. Structural facing systems such as modular blocks and concrete panels were able to improve the stability and reduce the deformation of GRS walls, especially walls with a large spacing. Using structural facing systems could reduce maximum face deflections (Figure 12.8.1) as well as reinforcement tensions (Figures 12.8.4 to 12.8.11) of both large and small spacing wrapped face walls.

7. Results of parametric analysis indicated that locations of the maximum overall (average) reinforcement tensions occurred between 0.25H (poor quality backfill) to 0.5H (good quality backfill). The tie-back wedge method predicts a maximum reinforcement tension at the bottom of the wall.

15.2.4 Anisotropic Model for Geosynthetic Reinforced Soil Composite Properties

1. Feasibility of analyzing GRS composite properties using the developed transversely isotropic elasticity model (Chapter 13) has been demonstrated. Different composite moduli of GRS elements were found in different principal directions using the transversely isotropic elasticity model (Figures 13.2.1 to

13.2.3); the assumption that different reinforcing mechanisms existing in different principal directions inside a GRS is further verified.

2. Results shown in Figures 13.2.1 to 13.2.3 indicated that the geosynthetics contributed to the reinforcing function in the horizontal as well as in the vertical direction. The horizontal GRS composite moduli were found to be larger than the vertical GRS composite moduli obtained from the UCD test data that was analyzed using the developed anisotropic model.

3. Numerical models developed using anisotropic GRS properties were verified to be able to provide reasonable external and internal performance information of a GRS wall. Numerical models COMPA and COMPS were able to predict quite well the field instrumentation measurements.

15.2.5 Performance Prediction and Design Recommendations of GRS Retaining Structures

1. Feasibility to use the developed analytical models of the GRS composite modulus and the lateral reinforced earth pressure distribution (Chapter 11) to analyze results of the parametric study, i.e. the influence of the design factors on the performance of the GRS walls, was demonstrated in Chapter 14. Performance prediction methods that were developed based on the analysis results were able to predict preliminary design information such as maximum face deflection and reinforcement tension distributions.

2. With material properties and design geometry given, maximum face deflection of GRS walls can be predicted using Figure 14.1.1 (Example 14.1.1). The maximum face deflection that was calculated in Example 14.1.1 showed an excellent agreement to the field measurement. Figure 14.1.1 can also be used to determine the required reinforcement stiffness if soil properties and design geometry are given (Example 14.1.2).

3. Example 14.2.1 shows the procedures to determine the maximum reinforcement tension inside the GRS walls using Equations 14.2.6 and 14.2.7 and design curves shown in Figures 14.2.3 and 14.2.4. Maximum reinforcement tension that was calculated in Example 14.2.1 was also found to be very close to the maximum reinforcement tension reduced from the strain gage measurement.

4. Figure 14.3.1 described a reinforcement tension distribution that was developed based on the working stress-strain information from an extensive parametric study summarized in Chapter 12. In this distribution, reinforcement tension increases from 0.2 T_{max} at top of the wall to the maximum reinforcement tension (T_{max}) at height equal to 0.6H. The reinforcement tension remains at T_{max} between 0.6H to 0.2H, and it decreases from T_{max} to 0.2 T_{max} at bottom of the wall. As shown in Example 14.3.1 and Figure 14.3.2, the reinforcement tension distribution of the Algonquin concrete panel faced Wall 2 was able to be accurately reproduced by using Figure 14.3.1.

5. Performance prediction methods presented in Chapter 14 were developed based on the results of the extensive parametric study performed in this research (Chapter 12). Limitations of using these methods to predict performance of the GRS walls includes the general boundary conditions, the ranges of the design factors, and geometry limits that are similar to those that were applied in the numerical models of the parametric study. Section 14.4 describes the limitations of these design curves.

15.3 Recommendations for Future Research

15.3.1 Material Properties in GRS Retaining Structures

1. More plane strain soil strength tests should be performed to further characterize the plane strain properties such as soil friction angles and elastic moduli of different type of backfill soils. The range of the confining pressure of these plane strain soil tests should cover appropriate earth pressure range that occurs inside the GRS retaining structures. A confining pressure range of 10 to 100kPa is recommended.

2. Soil dilation angles under plane strain loading condition should also be investigated, especially at low confining pressures. Plane strain soil dilation angle can be obtained by measuring the volume change during the plane strain soil tests.

3. The in-soil properties of the nonwoven geotextiles and geogrids should be investigated. More in-soil geosynthetic reinforcement tests such as UCD tests should be conducted on the nonwoven geotextile and geogrid materials. Efforts to develop relationships between the in-soil strength property modifications and material indices such as density of the nonwoven material and opening size of the geogrid are encouraged.

4. The low strain rate geosynthetic strength properties of various types of geosynthetic reinforcements should also be investigated. Relations between reinforcement stiffness reductions and strain rates or the duration of the loading for different geosynthetic reinforcements should be developed in order to understand the actual reinforcement stiffness in GRS structures.

5. Combination effects of in-soil confinement and low strain rate on the properties of the geosynthetic reinforcement should be investigated. If possible, tests of geosynthetic reinforcement materials in-soil at low strain rates should be conducted.

15.3.2 Performance Modeling of GRS Retaining Structures

1. More detailed modeling work should be performed on different structural facing systems in order to improve the working stress or strain predictions of GRS wall with structural facing systems. Numerical models of individual facing units should be developed, and the stress and strain distributions around the facing units should

be investigated. Understanding of the stress and strain distributions of the individual facing unit can then be extended to investigate their influence on the stress and strain levels inside entire GRS walls.

2. The interface elements of the FLAC program appear to be unstable during dynamic analyses. In order to extend the developed modeling techniques for dynamic analysis of GRS retaining structures, alternative modeling techniques that can reduce or replace the large number of interfaces elements in the present models should be developed. One suggestion is to model the structural facing unit by inserting structural elements into the Mohr-Coulomb material elements to avoid usage of different material elements in the same numerical model.

3. Numerical analysis utilizing computer programs other than FLAC should be performed using the property determination procedures (Chapter 7) and the modeling techniques (Chapter 8) developed in this research. This is to examine the universality of the developed property determination procedures and modeling techniques.

15.3.3 Parametric Study and Performance Prediction

1. Different reinforcement spacings were found to have very different effects on the performance of the GRS retaining structures. However, in this research, only three different reinforcement spacings (0.38m, 0.76m, and 0.6m) were investigated. Parametric study that includes more reinforcement spacings should be performed

in order to identify the reinforcement spacings that will cause the instability to occur inside the GRS retaining structures.

2. Influence of the secondary reinforcement on the working stress or strain levels were not extensively investigated in this research. Effects of the design factors such as the length and spacing of the secondary reinforcement is suggested to investigate through the parametric study.

3. In this research, effects of the surcharge were not investigated. If possible, the parametric study presented in this research should be extended to investigate the effects of surcharges with different heights and shapes. Performance prediction methods presented in this dissertation can then be modified for cases with different surcharge conditions.

4. In this research, all parametric study models were designed with vertical faces. The performance of GRS walls with batter faces needs to be investigated. Performance prediction methods presented in this dissertation are also expected to be modified for walls with different batter angles.

5. Effect of different foundations on the performance of the GRS walls was not investigated in this research because all parametric study models were designed with a good foundation. A parametric study that varies the foundation soil properties from poor soil conditions to bedrock is recommended to investigate the

influence of the foundation soil properties on the working stress levels of GRS walls.

15.3.4 Anisotropic Model for Geosynthetic Reinforced Soil Composite Properties

To improve the developed composite approach so that it can be more universally applicable, the developed transversely isotropic elasticity model for GRS elements should be calibrated with additional UCD test results. The behavior of GRS composites sampled at different horizontal strains, for example, 0.5%, 1.5%, and 2%, should be analyzed. The stress-strain distribution of GRS retaining structures can then be further analyzed using composite property models with input of moduli sampled at these horizontal strains.

References

Adib, M. (1998) "Internal Lateral Earth Pressure in Earth Walls," Ph.D. Dissertation, University of California, Berkeley, 376p.

Al-Hussaini, M.M. and Johnson, L.D. (1978) "Numerical Analysis of a Reinforced Earth Wall," Proceedings of the Symposium on Earth Reinforcement, ASCE, Pittsburgh, pp. 98-126.

Allen, T.M. and Holtz, R.D. (1991) "Design of Retaining Walls Reinforced with Geosynthetics", Proceedings of the ASCE Geotechnical Engineering Congress, Boulder, Geotechnical Special Publication No. 27, ASCE,Vol. 2, pp970-987.

Allen, T. M., Christopher, B.R., and Holtz, R.D. (1992) "Performance of a 12.6 m High Geotextile Wall in Seattle, Washington", Geosynthetic-Reinforced Soil Retaining Walls, Proceedings of the International Symposium on Geosynthetic-Reinforced Soil Retaining Walls, Denver, J.T.H. Wu, Ed., Balkema, Rotterdam, pp. 81-100.

Allen, T.M. (1999) Personal communication.

Andrawes, K.Z. and Saad, M.A. (1994) "Geogrid Reinforced Soil Walls Subjected to Controlled Lateral Deformation," Proceedings of Fifth International Conference on Geotextiles, Geomembranes, and Related Products, Singapore, Vol. 1, pp. 187-192.

Arab, R., Villard, P., and Gourc, J.P. (1998) "Large Deformations FEM Analysis of A Reinforced Earth Structure," Proceedings of Sixth International Conference on Geosynthetics, Atlanta, Vol. 2, pp597-600.

Bathurst, R.J. and Koerner R.M. (1988) "Results of Class A Predictions for the RMC Reinforced Soil Wall Trials," The Application of Polymeric Reinforcement in Soil Retaining Structures, P.M. Jarrett and A. McGown, Eds., NATO ASI Series, Series E: Applied Sciences – Vol. 147, Kluwer Academic Publishers, Boston, pp. 127-171.

Bathurst, R.J., Wawrychuk, W.F. and Jarrett, P.M. (1988) "Laboratory Investigation of Two Large-Scale Geogrid Reinforced Soil Walls," The Application of Polymeric Reinforcement in Soil Retaining Structures, P.M. Jarrett and A. McGown, Eds., NATO ASI Series, Series E: Applied Sciences –Vol. 147, Kluwer Academic Publishers, Boston, pp. 70-126.

Bathurst, R.J., Simac, M.R., Christopher, B.R., and Bonczkiewicz, C. (1993) "A Database of Results from a Geosynthetic Reinforced Modular Block Soil Retaining Wall," Proceedings of International Symposium of Soil Reinforcement, Paris, pp341-362.

Bathurst, R.J., Cai, Z., Alfaro, M., and Pelletier, M. (1997) "Seismic Design Issues for Geosynthetic Reinforced Segmental Retaining Walls," Mechanically Stabilized Backfill, Proceedings of the International Symposium on Mechanically Stabilized Backfill, J.T.H. Wu, Ed., Balkema, Rotterdam, pp. 79-97.

Bathurst, R.J. and Hatami, K. (1998a) "Seismic Response Analysis of a Geosynthetic-Reinforced Soil Retaining Wall," Geosynthetics International, I.F.A.I., Vol. 5, Nos., 1-2, pp. 127-166.

Bathurst, R.J. and Hatami, K. (1998b) "Influences of Reinforcement Stiffness, Length and Base Condition on Seismic Response Geosynthetic-Reinforced Soil Retaining Walls," Proceedings of the Sixth International Conference on Geosynthetics, Atlanta, Vol. 2, pp613-616.

Bathurst, R.J., (1999) Personal communication.

Bell, J. R., Barrett, R. K., and Ruckman, A. C. (1983) "Geotextile Earth-Reinforced Retaining Wall tests: Glenwood Canyon, Colorado," Transportation Research Record 916, pp. 59-69.

Benhamida, B., Schlosser, F., and Unterreiner, P. (1997) "Finite element modeling of a soil nailed wall: Earth pressure and arching effects," Proceedings of the Sixth International Symposium on Numerical Models in Geomechanics, Montreal, pp. 245-259.

Bolton, M.D. (1986) "The Strength and Dilatancy of Sands", Geotechnique, Vol. 36, No.1, pp. 65-78.

Boyle, S.R. (1995) "Deformation Prediction of Geosynthetic Reinforced Soil Retaining Walls," Ph.D. Dissertation, University of Washington, Seattle, 391p

Boyle, S.R., Gallagher, M, and Holtz, R.D. (1995) " Influence of Strain Rate, Specimen Length and Confinement on Measured Geotextile Properties," Geosynthetics International, I.F.A.I., Vol. 3, No. 2, pp. 205-225.

Boyle, S.R., and Holtz, R.D. (1994) "Deformation Characteristics of Geosynthetic-Reinforced Soil," Proceedings of the Fifth International Conference on Geotextiles and Geomembranes and Related Products, Singapore. Vol.1 pp. 361-364.

Broms, B.B. (1978) "Design of Fabric Reinforced Retaining Structures," Proceedings of the ASCE Symposium on Earth Reinforcement, Pittsburgh, pp283-303

Burgess, G. P. (1999) "Two Full-Scale Model Geosynthetic-Reinforced Segmental Retaining Walls," MSCE Dissertation, Royal Military College of Canada, Kingston. 207p

Chew, S.H., Schmertmann, G.R., and Mitchell, J.K. (1990) "Reinforced Soil Wall Deformations by Finite Element Method," Performance of Reinforced Soil Structures, Proceedings of International Reinforced Soil Conference, Glasgow, A. McGown, K.C, Yeo, and K.Z. Andrawes, Eds., British Geotechnical Society, pp. 35-40.

Chew, S.H. and Mitchell, J.K. (1994) "Deformation Evaluation Procedure for Reinforced Soil Walls," Proceedings of the Fifth International Conference on Geotextiles, Geomembranes and Related Products, Singapore, Vol. 1, pp. 171-176.

Chou, N.N.S. (1992) "Performance of Geosynthetic Reinforced Soil Walls," Ph.D. Dissertation, University of Colorado, Denver, 316 p.

Chou, N.N.S. and Wu, J.T.H. (1993) "Effects of Founcations on the Performance of Geosynthetic-Reinforced Soil Walls," Proceedings of Geosynthetics '93, Vancouver, Vol. 1, pp. 189-201.

Christopher, B.R., Gill, S.A., Giroud, J-P., Juan, I., Mitchell, J.K., Schlosser, F., and Dunnicliff, J. (1989) Reinforced Soil Structures, Vol. I, Design and Construction Guidelines, FHWA, Federal Highway Administration Report FHWA-RD-89-043, 287p.

Christopher, B.R., Holtz, R.D., and Allen, T.M. (1990) "Instrumentation for a 12.6 m High Geotextile-Reinforced Wall," Performance of Reinforced Soil Structures, Proceedings of International Reinforced Soil Conference, Glasgow, A. McGown, K.C, Yeo, and K.Z. Andrawes, Eds., British Geotechnical Society, pp. 73-78.

Christopher, B.R. (1993) "Deformation Response and Wall Stiffness in Relation to Reinforced Soil Wall Design," Ph.D. Dissertation, Purdue University, West Lafayette, Indiana, 354p.

Cook, R.D. and Young, W.C. (1985) Advanced Mechanics of Materials, Macmillan, 539p.

Collin, J.G. (1986) "Earth Wall Design," Ph.D. Dissertation, University of California, Berkeley, 289 p.

Duncan, J.M. and Chang, C-Y. (1970) "Nonlinear Analysis of Stress and Strain in Soil," Journal of Soil Mechanics and Foundations Division, ASCE, Vol. 96, No. SM5, pp. 1629-1653.

Duncan, J.M., Byrne, P., Wong, K.S., and Mabry, P. (1980) "Strength, Stress-Strain and Bulk Modulus Parameters for Finite Element Analyses of Stresses and Movements in Soil Masses," Geotechnical Engineering Report No. UCB/GT/80-01, University of California, Berkeley. 70p.

Ebeling, R.M., Mosher, R.L., Abraham, K., and Peters, J.F. (1993) "Soil-Structure Interaction Study of Red River Lock and Dam No. 1 Subjected to Sediment Loading," U.S. Army Corps of Engineers Technical Report ITL-93-3, 283 p.

Ebling, R.M., Peters, J.F., and Wahl, R.E. (1992a) "Prediction of Reinforced Sand Wall Performance," Geosynthetic-Reinforced Soil Retaining Walls,

Proceedings of the International Symposium on Geosynthetic-Reinforced Soil Retaining Walls, Denver, J.T.H. Wu, Ed., Balkema, Rotterdam, pp. 243-253.

Ebeling, R.M., Peters, J.F. and Mosher, R.L. (1992b) "Finite Element Analysis of Slopes with Layer Reinforcement," Stability and Performance of Slopes and Embankments- II, Berkeley, Geotechnical Special Publication No. 31, ASCE, Vol. 2, pp. 1427-1443.

El- Fermaoui, A. and Nowatzki, E. (1982) "Effect of Confining Pressure on Performance of Geotextile in Soils," Proceeding of Second International Conference on Geotextiles, Las Vegas, Vol. 3, pp. 799-804.

Fang, H.Y., Ed. (1991) Foundation Engineering Handbook, 2nd Edition, Van Norstrand Reinhold, New York. 923p

Ghinelli, A. and Sacchetti, M. (1998) "Finite Element Analysis of Instrumented Geogrid Reinforced Slopes," Proceedings of Sixth International Conference on Geosynthetics, Atlanta, Vol. 2, pp649-654.

Giroud, J.P. (1986) "From Geotextiles to Geosynthetics: a Revolution in Geotechnical Engineering," Proceedings of Third International Conference on Geotextiles, Vienna, Vol. 1, pp1-18.

Gray, D.H. and Ohashi, H (1983) "Mechanics of Fiber Reinforcement in Sand," Journal of Geotechnical Engineering, ASCE, Vol. 109, No. 3, pp. 335-353.

Harrison, W.J. and Gerrard, C.M. (1972) "Elastic Theory Applied to Reinforced Earth," Journal of the Soil Mechanics and Foundations and Division, ASCE, Vol. 98, No, SM12, pp. 1325-1345.

Hausmann, M.R. (1990) Engineering Principles of Ground Modification, McGraw-Hill, 632p.

Hausmann, M.R. (1976) "Strength of Reinforced Soil," Proceeding of Eighth Australian Road Research Board Conference, Perth, Session 13, pp. 1-3.

Hausmann, M.R., and Lee, K.L. (1976) "Strength Characteristics of Reinforced Soil," Proceedings of the International Symposium on New Horizons in Construction Materials, Lehigh, Vol. 1, pp. 165-176.

Helwany, M.B. (1992) "Finite Element Analysis of Geotextile Reinforced Retaining Walls Considering Creep," Geosynthetic-Reinforced Soil Retaining Walls, Proceedings of the International Symposium on Geosynthetic-Reinforced Soil Retaining Walls, Denver, J.T.H. Wu, Ed., Balkema, Rotterdam, pp. 179-192.

Herrmann, L.R. and Al-Yassin, Z. (1978) "Numerical Analysis of reinforced Soil Systems," Proceedings of Symposium on Earth Reinforcement, ASCE, Pittsburgh, pp. 428-457.

Ho, S.K. and Rowe, R.K. (1993) "Finite Element Analysis of Geosynthetics-Reinforced Soil Walls," Proceedings of Geosynthetics '93, Vancouver, 1993, Vol. 1, pp. 189-201.

Ho, S.K. and Rowe, R.K. (1994) "Predicted Behavior of Two Centrifugal Model Soil Walls," Journal of Geotechnical Engineering and Environmental Engineering, ASCE, Vol. 120, No. 10, pp. 1845-1873.

Holtz, R.D. (1977) "Laboratory Studies of Reinforced Earth Using a Woven Polyester Fabric," Proceedings of International Conference on the Use of Fabrics in Geotechnics, Paris, Vol. III, pp. 149-154.

Holtz, R.D., Allen, T.M., and Christopher, B.R. (1991) "Displacement of a 12.6 m High Geotextile-Reinforced Wall," Proceedings of the Tenth European Conference on Soil Mechanics and Foundation Engineering, Florence, pp. 725-728.

Holtz, R.D., Christopher, B.R., and Berg, R. (1997) Geosynthetic Engineering, BiTech Publishers, Vancouver, 452p

Holtz, R.D. and Lee, W.F. (1998) Geosynthetic Reinforced Wall Analysis, Phase II: Use of In-Soil Geosynthetic Behavior to Predict Deformation, Report No. WA-RD 452.1, Washington State Department of Transportation, 32p.

Ingold, T.S. (1982) Reinforced Earth, Thomas Telford, 141p.

Itasca Consulting Group (1993) Fast Lagrangian Analysis of Continua Version 3.4, Itasca Consulting Group, Inc., Minneapolis, Vol. I, II, III,

Jewell, R.A., Milligan, G.W.E., Sarsby, R.W., and Dubois, D. (1984) "Interaction between Soil and Geogrids," Proceedings of Symposium on Polymer Grid Reinforcement in Civil Engineering, London, Paper No. 1.3.

National Concrete Masonry Association (NCMA) (1996) Design Manual for Segmental Retaining Walls, 2nd Edition, J.G. Collin, Ed., NCMA, Herndon, 289p

Jaber, M., Collin, J.G. and Schmertmann, G.R. (1992) " Performance of Geosynthetic Reinforced Wall Performance using Finite Element Analysis," Geosynthetic-

Reinforced Soil Retaining Walls, Proceedings of the International Symposium on Geosynthetic-Reinforced Soil Retaining Walls, Denver, J.T.H. Wu, Ed., Balkema, Rotterdam, pp. 305-314.

Janbu, N (1963) "Soil Compressibility as Determined by Oedometer and Triaxial Tests," Proceeding of the Third European Conference on Soil Mechanics and Foundation Engineering, Wiesbaden, Vol. 1, pp. 19-25.

Jones, C. J.F.P. (1997) Earth Reinforcement and Soil Structures, Thomas Telford, 379p

Karpurapu, R.G. and Bathurst, R.J. (1992) "Finite Element Predictions for the Colorado Geosynthetic-Reinforced Soil Retaining Walls," Geosynthetic-Reinforced Soil Retaining Walls, Proceedings of the International Symposium on Geosynthetic-Reinforced Soil Retaining Walls, Denver, J.T.H. Wu, Ed., Balkema, Rotterdam, pp. 329-342.

Kerisel, J. (1992) "History of Retaining Wall Designs," Proceeding of Conference of Retaining Structures, Cambridge, Balkema, Rotterdam, pp. 1-16.

Lade, P.V., and Lee, K.L. (1976) "Engineering Properties of Soils," Report UCLA-ENG-7652, 145pp.

Leshchinsky, D. and Field, D.A. (1987) "In-Soil Load Elongation, Tensile Strength and Interface Friction of Non-Woven Geotextiles," Proceedings of Geosynthetics' 87, New Orleans, pp. 238-249.

Leshchinsky, D. and Boedeker, R.H. (1989) "Geosynthetic Reinforced Soil Structures," Journal of Geotechnical Engineering, ASCE, Vol. 115, No. 10, pp1459-1478.

Lee, W. F. and Holtz, R.D. (1998) "Analysis of Geosynthetic Reinforced Soil Retaining Walls using Composite Material Properties," Proceedings of The Thirteenth South East Asia Geotechnical Engineering Conference, Taipei, Vol.1, pp349-354.

Lee, W. F. (1999) "Distributions of Lateral Earth Pressure and Reinforcement Tension Inside the Geosynthetic Reinforced Soil Retaining Walls", Proceedings of Geosynthetics'99, Boston, Vol. 2, pp. 651-660.

Lee, W. F., Holtz, R.D., and Allen, T. M. (1999) "Full Scale Geosynthetic Reinforced Retaining Walls: A Numerical Parametric Study", Proceedings of Geosynthetics'99, Boston, Vol. 2 pp. 935-948.

Lindquist, D.D. (1998) "Seismic Modeling of Geosynthetic Reinforced Slopes," MSCE Dissertation, University of Washington, Seattle, 158p

Ling, H.I. and Tatsuoka, F. (1992) "Nonlinear Analysis of Reinforced Soil Structures Using Modified CANDE (M-CANDE)," Geosynthetic-Reinforced Soil Retaining Walls, Proceedings of the International Symposium on Geosynthetic-Reinforced Soil Retaining Walls, Denver, J.T.H. Wu, Ed., Balkema, Rotterdam, pp. 279-296.

Ling, H.I., Wu, J.T.H., and Tatsuoka, F. (1991) "Short-Term Strength and Deformation Characteristics of Geotextiles Under Typical Operational Conditions," Geotextiles and Geomembranes, Elsevier, Vol. 11, No. 2, pp. 185-219.

McGown, A., Andrawer, K.Z., Kabir, M.H. (1982) "Long Extension Testing of Geotextile Confined in Soil," Proceedings of Second International Conference on Geotextiles, Las Vegas, Vol. 3, pp. 793-798.

Milligan, G.W.E. and Palmeria, E.P. (1987) "Prediction of Bond between Soil and Reinforcement," Prediction and Performance in Geotechnical Engineering,

Proceedings of International Symposium, Calgary, R.C. Joshi and F.J. Griffiths, Eds., Balkema, Rotterdam, pp. 147-153.

Mitchell, J.K. and Villet, W.C.B. (1987) Reinforcement of Earth Slopes and Embankments, National Cooperative Highway Research Program Report 290, Transportation Research Board, 323p.

Mylleville B.L.J. and Rowe, R.K. (1991) "On the Design of Reinforced Embankments on Soft Brittle Clays," Proceedings of Geosynthetics' 91, New Orleans, pp. 395-408.

Naylor, D.J. (1978) "A Study of Reinforced Earth Walls Allowing Strip Slip," Proceedings of the Symposium on Earth Reinforcement, ASCE, Pittsburgh, pp. 618-643.

Naylor, D.H. and Richards, H. (1978) "Slipping Strip Analysis of Reinforced Earth," International Journal for Numerical and Analytical Methods in Geomechanics, Wiley, Vol. 2, No. 4, pp. 343-366.

Pinto, M.I.M, Pereira, R.V.C., Lopes, M.L., and Mendonca, A. (1998) "Brick-Faced Retaining Walls Reinforced with Geosynthetics – A Numerical Analysis,"

Proceedings of the Sixth International Conference on Geosynthetics, Atlanta, Vol. 2, pp. 593-596.

Porbaha, A. and Kobayashi, M. (1997) "Finite Element Analysis of Centrifuge Model Tests," Proceedings of the Sixth International Symposium on Numerical Models in Geomechanics, Montreal, pp. 245-259.

Rajagopal, K. and Bathurst R.J. (1994) "Parametric Finite Element Investigation Reinforced Soil Retaining Walls," Proceedings of the Fifth International Conference on Geotextiles, Geomembranes, and Related Products, Singapore, Vol. 1, pp. 193-196.

Riemer, M.F. (1999) "Plane Strain Testing of Sand Specimens for RMC Test Wall Modeling," Test Report, Berkeley, 4p

Romstad, K.M., Herrmann, L.R., and Shen, C.K. (1976) "Integrated Study of Reinforced Earth -- I: Theoretical Formulation," Journal of Geotechnical Engineering, ASCE, Vol. 102, No. GT5, pp. 457-472.

Rowe, R.K. and Ho, S.K. (1988) "Application of Finite Element Techniques to the Analysis of Reinforced Soil Walls," The Application of Polymeric Reinforcement in Soil Retaining Structures, P.M. Jarrett and A. McGown,

Eds., NATO ASI Series, Series E: applied Sciences – Vol. 147, Kluwer Academic Publishers, Boston, pp. 541-556.

Rowe, R. K., and Ho, S. K. (1993) "Keynote Lecture: A Review of the Behavior of Reinforced Soil Walls," Earth Reinforcement Practice, Proceedings of the International Symposium on Earth Reinforcement Practice, Fukuoka, H. Ochiai, S. Hayashi and J. Otani, Eds., Balkema, Rotterdam, pp. 801-830.

Salamon, M.D.G. (1968) "Elastic Moduli of a Stratified Rock Mass," International Journal of Rock Mechanics and Mineral Science, Pergamon Press, Vol. 5, pp. 519-527.

Sawicki, A. and Kulczykowski, M. (1994) "Pre-Failure Behaviour of Reinforced Soil," Geotextiles and Geomembranes, Elsevier, Vol. 13, No, 4, pp. 213-230.

Sawicki, A. and Lesniewska, D. (1988) "Limit Analysis of Reinforced Slopes," Geotextiles and Geomembranes, Elsevier, Vol. 7, No.3, pp. 203-220.

Sawicki, A. and Lesniewska, D. (1991) "Stability of Fabric Reinforced Cohesive Soil Slopes," Geotextiles and Geomembranes, Elsevier, Vol. 10, No.2, pp. 125-146.

Sawicki, A and Lesniewska, D. (1993) "On Modeling Visco-Elastic Behaviour of Reinforced Soil," Earth Reinforcement Practice, Proceedings of the International Symposium on Earth Reinforcement Practice, Fukuoka, H. Ochiai, S. Hayashi and J. Otani, Eds., Balkema, Rotterdam, Vol. 1, pp. 163-166.

Schlosser, F. and Elias, V. (1978) "Friction in Reinforced Earth," Proceedings of Symposium on Earth Reinforcement, ASCE, Pittsburgh, pp. 735-763.

Schloser, F. and Long, H.T. (1972) "Recent Results in French Research on Reinforced Earth," Journal of the Construction Division, ASCE, Vol. 100, No. CO3, pp.223-227

Schmertmann, G.R., Chew, S.H. and Mitchell, J.K. (1989) "Finite Element Modeling of Reinforced Soil Wall Behavior," University of California, Berkeley, Geotechnical Engineering Report No. UCB/GT/89-01, 220 p.

Seed, R.B. and Duncan, J.M. (1984) "SSCOMP: A Finite Element Analysis Program for Evaluation of Soil-Structure Interaction and Compaction Effects," Geotechnical Engineering Research Report, No. UCB/GT/84-02, University of California, Berkeley, 335p.

Simac, M.R., Christopher, B.R., and Bonczkiewicz, C. (1990) "Instrumented Field Performance of a 6m Geogrid Soil Wall," Proceedings of Fourth International Conference on Geotextiles, Geomembranes, and Related Products, The Hague, Vol. 1, pp53-59.

Shen, C.K., Romstad K.M., and Herrmann, L.R. (1976) "Integrated Study of Reinforced Earth – II: Behavior and Design," Journal of Geotechnical Engineering, ASCE, Vol. 102, No. GT6, pp. 577-590.

Shiwakoti, D.R., Pradhan, T.B.S., and Leshchinsky, D. (1998) "Performance of Geosynthetic-Reinforced Soil Structures at Limit Equilibrium State", Geosynthetics International, Vol. 5, No. 6, pp. 555-587.

Tatsuoka, F. (1993) "Keynote Lecture: Roles of Facing Rigidity in Soil Reinforcing," Earth Reinforcement Practice, Proceedings of the International Symposium on Earth Reinforcement Practice, Fukuoka, H. Ochiai, S. Hayashi and J. Otani, Eds., Balkema, Rotterdam, Vol. 2, pp. 831-870.

Tatsuoka, F., Tateyama, M., Uchimura, T., and Koseki, J. (1997) "Geosynthetic-Reinforced Soil Retaining Walls as Important Permanent Structures", Geosynthetics International, I.F.A.I., Vol. 4, No. 2, pp. 81-136

Vidal, H. (1969) "The Principle of Reinforced Earth," Highway Research Record 282, pp. 1-16.

Wood, D. M. (1990) Soil Behavior and Critical State Soil Mechanics, Cambridge University Press, New York, 462p

Wu, J.T.H. (1992a) "Predicting Performance of the Denver Walls: General Report," Geosynthetic-Reinforced Soil Retaining Walls, Proceedings of the International Symposium on Geosynthetic-Reinforced Soil Retaining Walls, Denver, J.T.H. Wu, Ed., Balkema, Rotterdam, pp. 3-20.

Wu, J.T.H. (1992b) "Construction and Instrumentation of the Denver Walls," Geosynthetic-Reinforced Soil Retaining Walls, Proceedings of the International Symposium on Geosynthetic-Reinforced Soil Retaining Walls, Denver, J.T.H. Wu, Ed., Balkema, Rotterdam, pp. 21-30.

Wu, J.T.H. (1992c) "Measured Behavior of the Denver Walls," Geosynthetic-Geosynthetic-Reinforced Soil Retaining Walls, Proceedings of the International Symposium on Geosynthetic-Reinforced Soil Retaining Walls, Denver, J.T.H. Wu, Ed., Balkema, Rotterdam, pp. 31-42.

Wu, J.T.H., Qi, X., Chou, N., Ksouri, I., Helwany, M.B., and Huang, C.C. (1992) "Comparisons of Preictions for the Denver Walls," Geosynthetic-Reinforced Soil Retaining Walls, Proceedings of the International Symposium on Geosynthetic-Reinforced Soil Retaining Walls, Denver, J.T.H. Wu, Ed., Balkema, Rotterdam, pp. 43-60.

Xi, F. (1992) "Finite Element Analysis of Geosynthetically Reinforced Walls: A Parametric Study," MSCE Dissertation, University of Delaware, Newark, 141 p.

Yogarajah, I. and Andrawes, K.Z. (1994) "Modeling Construction Effects in Polymeric Grid Reinforced Soil Walls," Proceedings of Fifth International Conference on Geotextiles, Geomembranes and Related Products, Singapore, Vol.1, pp. 177-182.

Yang, M.A. and Singh, A. (1974) "Strength and Deformation Characteristics of Reinforced Sand," National Meeting on Water Resources Engineering, ASCE, Los Angeles, Preprint 2189.

Yeo, K.C., Yogarajah, I. And Chan, A.H.C. (1992) "Prediction Analysis of Two Geosynthetic Reinforced Soil Retaining Walls Using Finite Element Method," Geosynthetic-Reinforced Soil Retaining Walls, Proceedings of the

International Symposium on Geosynthetic-Reinforced Soil Retaining Walls, Denver, J.T.H. Wu, Ed., Balkema, Rotterdam, pp. 193-204.

Zornberg, J.G. and Mitchell, J.K. (1993) "Finite Element Analysis of Geosynthetically Reinforced Soil Walls with Sloping Backfills," Geotechnical Engineering Report No. UCB/GT/93-04, Department of Civil Engineering, University of California, Berkeley, 164 p.

Appendix

Codes and Result Files of the Numerical Models

The CD disks that contains all the FLAC codes developed in this research and their result files are stored by the Geotechnical program of the University of Washington (Professor Robert D. Holtz) and Washington State Department of Transportation (Mr. Tony M. Allen).